Metabolomic responses to acute exercise and AMPK-glycogen binding disruption in mice

Belhaj, Mehdi R.

Metabolomic responses to acute exercise and AMPK-glycogen binding disruption in mice

Submitted by:

Mehdi R. Belhaj

BNutrDiet, MSc

A thesis submitted in fulfilment of the requirements for the degree of

Doctor of Philosophy

Ph.D. with Publication

Exercise and Nutrition Research Program

Mary MacKillop Institute for Health Research

Australian Catholic University

Melbourne, Victoria, Australia

November 2022

Statement of Authorship and Sources

This thesis contains no material that has been extracted in whole or in part from a thesis that I have submitted towards the award of any other degree or diploma in any other tertiary institution.

No other person's work has been used without due acknowledgment in the main text of the thesis.

All research procedures reported in the thesis received the approval of the relevant Ethics/Safety Committees (where required).

The extent of collaboration with another person or persons has been acknowledged accordingly where necessary.

Signed: 

Mehdi Belhaj Date: 18/11/2022

Acknowledgements

First and foremost, I would like to thank my Ph.D. supervisors, Dr. Nolan Hoffman, Prof. John Hawley, Dr. Jamie Whitfield and Dr. Stacey Reinke. It has been an absolute pleasure to have such great mentors and I am very grateful for the opportunity to work with all of you and learn from your expertise over the last years. I cannot thank you enough for your time, patience, guidance, and encouragement. Your inputs have been invaluable.

Thank you to all my metabolomics research collaborators from Edith Cowan University – Prof. David Broadhurst, Dr. Stacey Reinke, Mr. Thomas Dignan and Dr. Nathan Lawler for your essential contributions to my thesis. I would also like to thank my mouse research collaborators from St Vincent's Institute, Prof. Bruce Kemp and Ms. Lisa Murray-Segal for your contributions and willingness to assist and teach me. Thank you to my Ph.D. candidature milestone assessors – Dr. Andrew Govus, Dr. Hayley Abbiss, Dr. Amber Milan and A. Prof. Matthew Cooke for evaluating my Ph.D. progress and providing constructive feedback and support.

Thank you to the former and current members of the Exercise and Nutrition Research Program for the supportive and fun work atmosphere they have helped create during my Ph.D. I would like to specifically thank Dr. Natalie Janzen and Ms. Bridget Radford for always cheering me up and for making my Ph.D. journey a little easier to get through.

Lastly, I would also like to thank every member of my family for their constant support and for always believing in me, including those who have unfortunately left this world. Even long after your passing, you still live in my heart and you remain immense sources of inspiration and great models of courage, resilience, and perseverance.

Table of Contents

List of Publications from Thesis

- **Belhaj, M.R.**, Lawler, N.G., & Hoffman, N.J. (2021). Metabolomics and Lipidomics: Expanding the Molecular Landscape of Exercise Biology. *Metabolites*, 11(3): 151. https://doi.org/10.3390/metabo11030151

- **Belhaj, M.R.**, Lawler, N.G., Hawley, J.A., Broadhurst, D.I., Hoffman, N.J., & Reinke, S.N. (2022). Metabolomics reveals mouse plasma metabolite responses to acute exercise and effects of disrupting AMPK-glycogen interactions. *Front. Mol. Biosci.*, 9:957549. https://doi.org/10.3389/fmolb.2022.957549

- **Belhaj, M.R.**, Broadhurst, D.I., Dignan, T., Whitfield, J., Hawley, J.A., Reinke, S.N., & Hoffman, N.J. Metabolomic analysis of mouse skeletal muscle and liver metabolite responses to acute exercise and loss of AMPK-glycogen binding capacity. *In preparation.*

List of Conference Presentations

- "Skeletal muscle and liver metabolomic responses to acute exercise and AMPK-glycogen binding disruption". Victorian Muscle Network Symposium (2022). *Invited oral presentation.*
- "Metabolomic analysis of mouse skeletal muscle and liver responses to acute exercise and disruption of AMPK-glycogen binding". Australian Physiological Society Scientific Meeting (2022). *Invited oral presentation.*

List of Figures

List of Tables

List of Abbreviations

1-RM	One-repetition maximum
A	Alanine
AA	Arachidonic acid
ACC	Acetyl-CoA carboxylase
ACU	Australian Catholic University
AEC	Australian Ethics Committee
ADaM	Allosteric drug and metabolite
ADP	Adenosine diphosphate
AID	α-autoinhibitory domain
AMP	Adenosine monophosphate
AMPK	AMP-activated protein kinase
ANOVA	Analysis of variance
ATP	Adenosine triphosphate
BAT	Brown adipose tissue
BCA	Bicinchoninic acid
BCAA	Branched-chain amino acid
BCE	Before Common Era
cAMP	Cyclic AMP
CaMKKβ/2	Calcium/calmodulin-dependent protein kinase kinase β/2

CBM	Carbohydrate binding module
CBS	Cystathionine-β-synthase domains
CCS	Collisional cross section
CD36	Cluster of differentiation 36
CE	Capillary electrophoresis
ChREBP	Carbohydrate-responsive element binding protein
CI	Confidence interval
CIMCB	Centre for Integrative Metabolomics and Computational Biology
CoASH	Coenzyme A
COX	Cyclooxygenase
CPT1	Carnitine palmitoyltransferase-1
CREB	cAMP response element-binding protein
CTCR2	CREB-regulated transcription coactivator 2
CTD	C-terminal domain
CV	Canonical variate
CYP	Cytochrome oxidase P450
D-ratio	Dispersion ratio
Da	Daltons
DAG	Diacylglycerol
DBS	Dried blood spots

DDA	Data dependant analysis
DESI	Desorption electrospray ionisation
DHA	Docosahexaenoic acid
DHET	Dihydroxyeicosatrienoic acid
DiHDHA	DihydroxyDHA
DiHDPA	Dihydroxydocosapentaenoic acid
DiHETE	Dihydroxyeicosatetraenoic acid
DiHOME	Dihydroxyoctadecanoic acid
DIMS	Direct infusion mass spectrometry
DKI	Double knock-in
DKI-Ex	DKI mice, exercised condition
DKI-Rest	DKI mice, rested condition
DMEM	Dulbecco's Modified Eagle Medium
DMSO	Dimethyl sulfoxide
DPA	Docosapentaenoic acid
DPBS	Dulbecco's phosphate buffered saline
ECAR	Extracellular acidification rate
ECU	Edith Cowan University
EDP	Epoxydocosapentaenoic acid
eEF2	Eukaryotic elongation factor 2

eEF2K	eEF2 kinase
EEQ	Epoxyeicosatetraenoic acid
EET	Epoxyeicosatrienoic acid
EPA	Eicosapentaenoic acid
EpOME	Epoxyoctadecenoic acid
ESI	Electrospray ionisation
eV	Electronvolt
FA	Fatty acid
FAIR	Findable, Accessible, Interoperable, and Reusable
FBS	Fetal bovine serum
FC	Fold-change
FDR	False discovery rate
FFA	Free fatty acid
FIA	Flow-injection analysis
FWHM	Full width at half maximum
G	Glycine
GC	Gas chromatography
GLUT4	Glucose transporter type 4
GPAT	Glycerol-3-phosphate acyltransferase
GP-NPEA	Glycerophospho-N-palmitoylethanolamine

GS	Glycogen synthase
HCA	Hierarchical cluster analysis
HCR	High capacity running
HDAC	Histone deacetylase
HDHA	HydroxyDHA
HEPE	HydroxyEPA
HESI	Heated electrospray ionisation
HETE	Hydroxyeicosatetraenoic acid
HHTrE	Hydroxyheptadecatrienoic acid
HIIT	High-intensity interval training
HIF	Hypoxia-inducible factor
HILIC	Hydrophilic interaction liquid chromatography
HMDB	Human Metabolome Database
HMGCR	3-hydroxy-3-methylglutaryl-CoA reductase
HODE	Hydroxyoctadecadienoic acid
HpETE	Hydroperoxyeicosatetraenoic acid
HpODE	Hydroxyperoxy-octadecadienoic acid
HSL	Hormone-sensitive lipase
IF	Interstitial fluid
IMS	Ion mobility spectrometry

IMTG	Intramuscular triglycerides
IR	Insulin resistant/resistance
IS	Internal standard (or insulin sensitive; **Table 2.2**)
K	Lysine
KEGG	Kyoto Encyclopedia of Genes and Genomes
KI	Knock-in
KO	Knockout
kV	Kilovolt
LA	Linoleic acid
LC-MS	Liquid chromatography-mass spectrometry
LCR	Low capacity running
LKB1	Liver kinase B1
LNA	Linolenic acid
LOX	Lipoxygenase
LPC	Lysophosphatidylcholine
LPE	Lysophosphatidylethanolamine
LSI	Lipidomics Standards Initiative
LOX	Lipoxygenase
LT	Leukotriene
MALDI	Matrix-assisted laser desorption ionisation

MDMS-SL	Multidimensional MS-based shotgun lipidomics
MEF	Mouse embryonic fibroblast
MEGA	Mouse Engineering Garvan/ABR
MoTrPAC	Molecular Transducers of Physical Activity Consortium
MRI	Magnetic resonance imaging
MS	Mass spectrometry
MSI	Metabolomics Standard Initiative
MS/MS	Tandem mass spectrometry
mTORC1	Mammalian target of rapamycin complex 1
m/z	Mass/charge ratio
NHMRC	National Health and Medical Research Council of Australia
NIH	National Institutes of Health
NMR	Nuclear magnetic resonance
NRF2	Nuclear factor erythroid 2-related factor 2
NO	Nitric oxide
OCFA	Odd-chain fatty acid
OCR	Oxygen consumption rate
Oxo-ETE	Oxo-eicosatetraenoic acid
Oxo-ODE	Oxo-octadecadienoic acid
OXPHOS	Oxidative phosphorylation

PC	Phosphatidylcholine
PCr	Phosphocreatine
PCA	Principal component analysis
PC-CVA	Principal component – canonical variate analysis
PE(-P)	Phosphoethanolamine
PFKFB2	Phosphofructokinase-2
PG	Prostaglandin
PGC-1α	Peroxisome proliferator-activated receptor gamma coactivator 1-alpha
Pi	Inorganic phosphate
PLS-DA	Partial least square-discriminant analysis
pmol	Picomoles
ppm	Parts per million
PUFA	Polyunsaturated fatty acid
Q	Glutamine
QC	Quality control
QC-RSC	Quality control-regularised spline correction
RBC	Red blood cell
RER	Respiratory exchange ratio
RPLC	Reversed-phase liquid chromatography
rpm	Revolutions per minute

RSD	Relative standard deviation
RT	Retention time
Rv	Resolvin
S	Serine
sEH	Soluble epoxide hydrolase
SEM	Standard error of the mean
Slc22a5/ OCTN2	Solute carrier family 22 member 5/organic cation transporter novel family member 2
SM	Sphingolipid
SREBP1c	Sterol regulatory element binding protein 1c
SVI	St Vincent's Institute of Medical Research
SVI BRC	St Vincent's BioResources Centre
T	Threonine
T2DM	Type 2 diabetes mellitus
TAG	Triacylglycerol
TCA	Tricarboxylic acid
TBC1D1	TBC1 domain family member 1
TBC1D4	TBC1 domain family member 4
TG	Triglyceride
TIMS	Trapped ion mobility spectrometry
TOMC	Total observed metabolite concentration

TPWS	Total protein concentration of whole saliva
TSC2	Tuberous sclerosis complex 2
TX	Thromboxane
UHPLC	Ultra-high performance liquid chromatography
ULK1	Unc-51 like autophagy activating kinase 1
VO_2 max	Maximal oxygen consumption
W	Tryptophan
WT	Wild type
WT-Ex	WT mice, exercised condition
WT-Rest	WT mice, rested condition

Abstract

Background: Exercise is widely accepted as a potent intervention to promote whole-body metabolic health and help prevent and/or treat metabolic diseases. Exercise represents a major challenge to energy homeostasis, both at the whole-body and cellular level. Numerous molecular metabolic responses to acute exercise are activated to preserve energy homeostasis. Central to maintaining cellular energy balance is the AMP-activated protein kinase (AMPK), a heterotrimeric enzyme that senses cellular energy levels by competitively binding to adenosine mono-, di- and triphosphate (AMP, ADP and ATP, respectively). In response to energy stress, AMPK becomes activated and switches on energy-producing catabolic processes while simultaneously switching off energy-consuming anabolic processes. Through its regulatory β subunit, AMPK also binds glycogen – an important energy reserve primarily stored in liver and skeletal muscle. Although growing evidence from AMPK double knock-in (DKI) mice has highlighted physiological consequences of disrupting AMPK-glycogen binding in exercise and metabolic control, the underlying molecular pathways and mechanisms remain unclear. Metabolomics is the unbiased collection and study of small molecules (< 1500 daltons) involved in metabolic reactions to capture molecular snapshots of metabolic pathways, for example associated with given stimuli (e.g., exercise) or genotype. Therefore, metabolomic analysis of biofluids and tissues represents a promising approach to better understand the molecular metabolic responses to acute exercise and the physiological effects of disrupting AMPK-glycogen binding *in vivo*.

Methods: Plasma, gastrocnemius muscle and liver samples were collected from age-matched male WT and DKI mice with disrupted AMPK-glycogen binding at rest and immediately following 30-min submaximal treadmill running. An untargeted mass spectrometry-based metabolomic approach was utilised to determine changes in plasma and/or tissue metabolites occurring in response to acute exercise and the disruption of AMPK-glycogen interactions in

DKI mice. Complementary whole-body mouse phenotyping and real-time metabolic phenotyping assays using the Seahorse XFe24 Analyzer and Oroboros O2k high-resolution respirometer were performed to compare energy metabolism and substrate utilisation profiles in mouse embryonic fibroblast (MEF) cells and skeletal muscle from WT and DKI mice.

Results/Discussion: Relative to WT mice, DKI mice had reduced maximal running speed, concomitant with increased total body mass and adiposity. In plasma, a total of 83 metabolites were identified/annotated, with 17 metabolites significantly different in exercised versus rested mice. These included amino acids, acylcarnitines and steroid hormones. Distinct plasma metabolite profiles were observed between the rest and exercise conditions and between WT and DKI mice at rest, while metabolite profiles of both genotypes converged following exercise. These differences in metabolite profiles were primarily explained by exercise-associated increases in acylcarnitines and steroid hormones as well as decreases in amino acids and derivatives following exercise. DKI mice showed greater decreases in plasma amino acid levels following exercise versus WT. In liver and skeletal muscle, 150 and 92 metabolites were identified/annotated, respectively. Similar to the plasma metabolite responses observed across genotypes and conditions, significant overall metabolite profile shifts were observed between WT and DKI mice at rest, as well as significant metabolite profile differences between the rested and exercised conditions. Differential muscle metabolite responses to acute exercise were also observed between genotypes. Markers of mitochondrial respiration in permeabilised gastrocnemius fibres were not affected by AMPK DKI mutation, although there were reduced total ATP rate and relative contribution of glycolysis in DKI versus WT MEF cells.

Conclusion: The plasma metabolomic analyses performed in Study 1 represent the first study to map mouse plasma metabolomic changes following acute exercise in WT mice and the effects of disrupting AMPK-glycogen interactions using DKI mice. Untargeted metabolomics uncovered alterations in plasma, skeletal muscle and liver metabolite profiles between rested

and exercised mice in both genotypes, and between genotypes at rest. This study has uncovered known and previously unreported plasma metabolite responses to acute exercise in WT mice, as well as greater decreases in amino acids following exercise in DKI plasma. These mouse tissue metabolomic datasets, combined with cell and tissue respirometry data complement previous whole-body, tissue and molecular characterisation of WT and DKI mice, revealing potential metabolic pathways and novel molecular biomarkers underlying exercise's metabolic health benefits and the physiological effects of disrupting AMPK-glycogen binding in mice.

Chapter 1 – Introduction and Overview

Exercise is well accepted as a primary intervention that induces numerous metabolic health benefits [1,2]. One of the first described beneficial effects of exercise was reported over 2000 years ago by Hippocrates (460-370 BCE), who was the first physician to prescribe exercise to patients "suffering from consumption" [2]. Exercise increases energy expenditure and helps maintain energy balance by promoting the utilisation of available energy stores to meet exercise-induced increases in cellular energy requirements. However, increases in sedentary behaviour and/or decreases in time performing exercise and physical activity, combined with constant and easy access to energy-dense food, primarily in Western societies, are disturbing energy balance, contributing to energy excess. Chronic energy excess and lack of exercise and physical activity over the past decades have been associated with an increased incidence of obesity and multiple associated metabolic disorders including but not limited to insulin resistance (IR), type 2 diabetes mellitus (T2DM) and cardiovascular diseases [3]. Growing rates of obesity and these associated metabolic disorders now represent major public health and economic burdens across the world [4]. While the efficacy of exercise in combating such metabolic disorders is widely accepted and research over the last decades have led to substantial progress in the understanding of the intricate biological processes that occur in response to exercise, the breadth of molecular metabolic responses to exercise remains incompletely understood. It is therefore crucial to expand the understanding of the molecular mechanisms underlying exercise to discover novel strategies to promote energy balance and prevent and/or treat these metabolic disorders.

One of the key energy sensors required to maintain cellular energy homeostasis is the AMP-activated protein kinase (AMPK), a master regulator of energy metabolism that integrates intracellular and extracellular metabolic signals and regulates metabolic pathways to maintain adenosine triphosphate (ATP) levels – the energy currency of the cell – within a

narrow range. In response to decreased cellular energy levels induced by exercise and/or nutrient/energy deprivation (e.g. fasting), increased levels of adenosine monophosphate (AMP)/ATP and adenosine diphosphate (ADP)/ATP lead to activation of AMPK. Once activated, AMPK switches on ATP-producing catabolic pathways (e.g. glycolysis and fatty acid [FA] oxidation) and concurrently switches off ATP-consuming anabolic pathways (e.g. protein, fat and glycogen synthesis) in order to preserve cellular energy homeostasis [5]. AMPK is a heterotrimeric enzyme that contains an α catalytic subunit and two regulatory β and γ subunits. Within AMPK's β subunit lies a carbohydrate binding module (CBM) that permits AMPK to bind glycogen [6,7], an important energy reserve primarily stored in liver and skeletal muscle.

Following the discovery of AMPK's glycogen binding capacity using cell-free assay systems in 2003 [6,7], further research has helped gain a deeper understanding of the potential physiological roles of AMPK-glycogen interactions. For example, disruptions in energy homeostasis and a range of associated physiological perturbations have been observed in AMPK β knock out (KO) mouse models, including appetite dysregulation, altered skeletal muscle mitochondrial content and glucose uptake, and impaired exercise capacity [8-11]. These findings highlight the physiological importance of AMPK's β subunit, which is also thought to sense stored energy through glycogen interactions [12,13]. However, KO models resulting in deleted gene expression of the entire β subunit do not allow the investigation of the physiological consequences of specifically disrupting AMPK-glycogen interactions. Therefore, my group generated transgenic mouse models of AMPK including single knock-in (KI) and double KI (DKI) mice with mutations in amino acid residues critical for glycogen binding [14-16]. The loss of AMPK's ability to bind glycogen *in vivo* resulted in disruptions in whole-body and tissue metabolic homeostasis, including increased adiposity, impaired glucose handling and reduced maximal exercise capacity (β2 KI and DKI mice), as well as increases

in ectopic fat deposition in liver (β1 KI) and skeletal muscle (β2 KI) [14-16]. The findings in AMPK transgenic mice further reinforce the consideration of AMPK as a promising therapeutic target for the treatment of metabolic diseases such as obesity and T2DM [17,18], which have been associated with impaired AMPK activity and signalling [19-21]. However, the molecular mechanisms underlying the phenotypic consequences of disrupting AMPK-glycogen interactions in mice remain largely unknown.

To address these knowledge gaps and map the metabolic networks of acute exercise and AMPK-glycogen binding disruption, the use of metabolomics is a promising approach. Metabolomics is the study of the metabolome – the comprehensive collection of small molecules (< 1500 daltons [Da]) involved in metabolic reactions (i.e. metabolites) within a given biological system (e.g. plasma, liver, skeletal muscle, etc.) [22,23]. Studying the metabolome is appealing for numerous reasons; metabolites lie downstream to all biological layers (i.e. genome, transcriptome and proteome) and reflect the rapid and cumulative changes of all other biological layers and their interactions with the environment and stimuli such as exercise. The metabolome is therefore considered a direct readout of the phenotype and provides a snapshot of metabolic reactions in "real-time". Furthermore, the use of high-throughput mass spectrometry (MS) allows the detection of hundreds of metabolites across a wide array of metabolic pathways in a single measurement using minimal sample volumes, and can reveal changes in previously unreported metabolites using an untargeted approach [22]. Collectively, metabolomics represents a promising avenue to determine molecular biomarkers underlying exercise metabolism and the physiological consequences of disrupting AMPK-glycogen binding *in vivo*.

In this thesis, the first experimental chapter (Chapter 4 – Study 1) aimed to identify mouse plasma metabolite responses to acute treadmill running and determine the effects of disrupting AMPK-glycogen interactions on plasma metabolite profiles, both at rest and

following a single bout of submaximal exercise. Using discovery-based untargeted metabolomics, this study sought to pinpoint underlying molecular biomarkers that potentially contribute to the metabolic phenotypic effects and reduced exercise capacity previously observed in AMPK DKI mice [15,16] and reproduced in this first original research study.

Considering that the plasma metabolome may provide only limited insight into mechanistic regulation of metabolic pathways that occur within tissues, Study 2 (Chapter 6) utilised untargeted metabolomics in the primary glycogen-storing tissues (i.e. liver and skeletal muscle) to provide comprehensive and integrative insights into the complex metabolite responses to acute exercise and disrupting AMPK-glycogen interactions on energy homeostasis and exercise capacity. Complementary real-time metabolic phenotyping assays were also performed to further determine whether AMPK DKI mutations are associated with changes in metabolic pathway activation and substrate utilisation at cellular and tissue levels. **Figure 1.1** provides a brief overview of the analyses performed in this Ph.D. thesis.

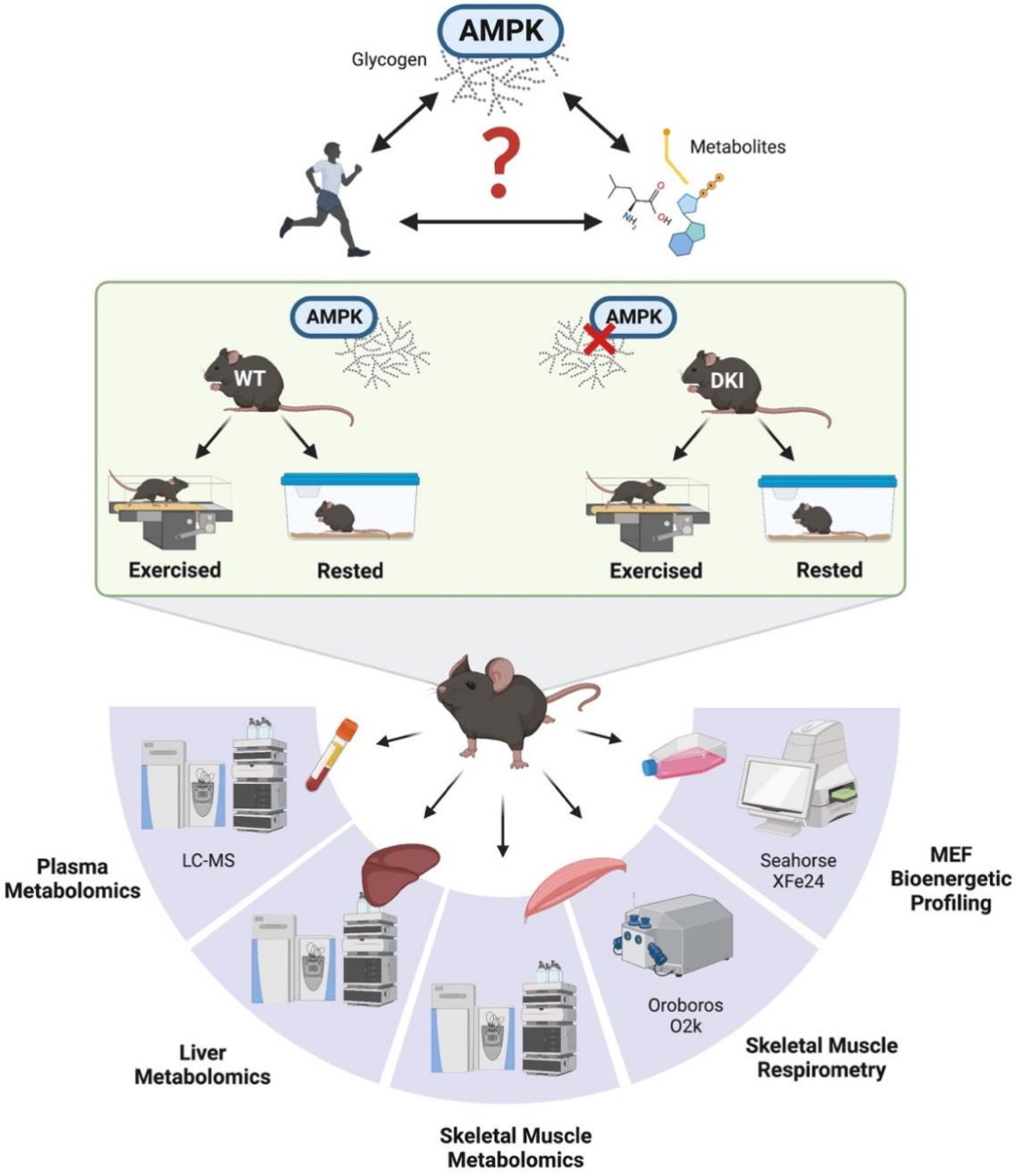

Figure 1.1 – Schematic overview of whole-body phenotyping, metabolomic and bioenergetic analyses performed in this Ph.D. thesis to characterise the consequences of disrupting AMPK-glycogen binding in the resting state and in response to a single bout of submaximal exercise. Created with BioRender.com

Chapter 2 – Literature Review

Publication statement:

Chapter 2 includes content from a review article published in ***Metabolites*** in the Special Issue titled "*10th Anniversary of Metabolites: The Changing Landscape of Metabolomics*". Additional material has been included where appropriate for the purpose of this thesis, including recent exercise metabolomics research published since 2021 and discussion of the relevance of AMPK and glycogen in exercise and metabolic health.

Belhaj, M.R., Lawler, N.G., & Hoffman, N.J. (2021). Metabolomics and Lipidomics: Expanding the Molecular Landscape of Exercise Biology. *Metabolites*, 11(3): 151. https://doi.org/10.3390/metabo11030151

Metabolomics and Lipidomics: Expanding the Molecular Landscape of Exercise Biology

Mehdi R. Belhaj [1], Nathan G. Lawler [2,3] and Nolan J. Hoffman[1,*]

[1] Exercise and Nutrition Research Program, Mary MacKillop Institute for Health Research, Australian Catholic University, Melbourne 3000, Australia; mehdi.belhaj@acu.edu.au

[2] Australian National Phenome Centre, Health Futures Institute, Murdoch University, Harry Perkins Building, Murdoch, Perth 6150, Australia; nathan.lawler@murdoch.edu.au

[3] School of Health and Medical Sciences, Edith Cowan University, Joondalup 6027, Australia

[*] Correspondence: nolan.hoffman@acu.edu.au; Tel.: +61-3-9230-8277

2.1. Abstract

Dynamic changes in circulating and tissue metabolites and lipids occur in response to exercise-induced cellular and whole-body energy demands to maintain metabolic homeostasis. The metabolome and lipidome in a given biological system provides a molecular snapshot of these rapid and complex metabolic perturbations. The application of metabolomics and lipidomics to map the metabolic responses to an acute bout of aerobic/endurance or resistance exercise has dramatically expanded over the past decade thanks to major analytical advancements, with most exercise-related studies to date focused on analysing human biofluids and tissues. Experimental and analytical considerations, as well as complementary studies using animal model systems, are warranted to help overcome challenges associated with large human interindividual variability and decipher the breadth of molecular mechanisms underlying the metabolic health-promoting effects of exercise. In this review, we provide a guide for exercise researchers regarding analytical techniques and experimental workflows commonly used in metabolomics and lipidomics. Furthermore, we discuss advancements in human and mammalian exercise research utilizing metabolomic and lipidomic approaches in the last decade, as well as highlight key technical considerations and remaining knowledge gaps to continue expanding the molecular landscape of exercise biology.

Keywords: exercise; metabolism; omics; metabolomics; metabolome; lipidomics; lipidome; mass spectrometry; nuclear magnetic resonance

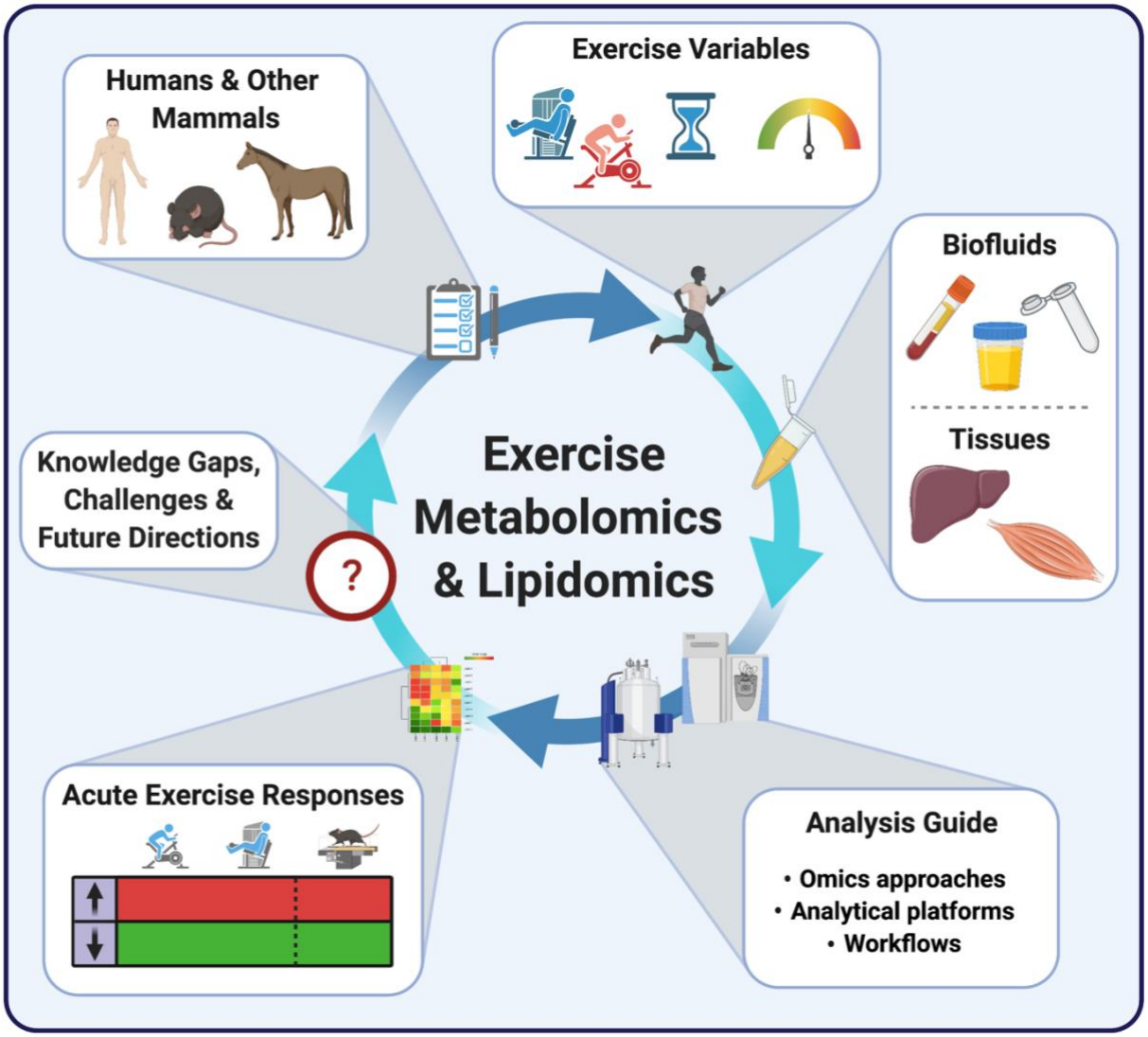

Figure 2.1 – Graphical abstract summarising the topics related to exercise, metabolomics and lipidomics that are discussed in this chapter.

2.2. Introduction

Living systems maintain metabolic homeostasis thanks to countless chemical reactions that continuously change the molecular landscape within these biological systems, including biofluids and tissues throughout the body. The term metabolism—derived from the Greek word "metabole" meaning "change"—defines all the chemical reactions that change molecules within living systems. Exercise represents a major challenge to whole-body and cellular energy homeostasis, and a multitude of molecular responses to acute exercise (i.e., a single exercise bout) are engaged to combat energy stress at the cellular and whole-body level [1]. During an intense acute exercise bout, the cellular turnover of adenosine triphosphate (ATP)—the energy "currency" of the cell—can increase 100-fold relative to the resting state, while at the whole-body level, the metabolic rate can increase up to 20-fold [24]. Given the small concentrations of readily available ATP in skeletal muscle cells (~8 mmol/kg wet weight) [25], ATP-resynthesizing pathways are rapidly activated in response to exercise to help maintain ATP concentrations within the working muscle and facilitate muscle contraction [26]. These cellular pathways responsible for ATP generation include: (1) the ATP-phosphocreatine (ATP-PCr) system whereby the breakdown of PCr produces free Cr and inorganic phosphate (Pi) that is subsequently transferred to ADP to resynthesise ATP; (2) "anaerobic" glycolysis where glucose units mainly derived from intramuscular glycogen and circulating glucose are catabolised to pyruvate and reduced to lactate, generating ATP by substrate phosphorylation; and (3) carbohydrate and lipid breakdown (glycolysis and β-oxidation, respectively) producing acetyl-CoA which subsequently enters the tricarboxylic acid (TCA) cycle in the mitochondria and produces electrons that are transferred through the electron transport chain, resulting in ATP generation [27]. The relative contribution of these different pathways and the related substrates utilised to help fuel working skeletal muscle are mainly dictated by exercise intensity and duration [24,28-30]. The metabolic perturbations provoked by exercise are however not

restricted to working muscles and engage numerous cell types and organs throughout the body to help meet the metabolic demands of exercise [1].

Although tremendous progress in the understanding of the cellular and molecular mechanisms involved in the responses to acute exercise has occurred over the past decades through traditional "reductionist" approaches, these approaches are limited to studying a biochemical pathway or molecular target of interest in isolation. As a result, further insight into the complex integrative nature of exercise-regulated molecular metabolic networks has been limited, and critical knowledge gaps remain [1,31]. Fortunately, the growing application of global "omics" approaches to unravel metabolite and lipid network responses to exercise in the last decade has marked an important turning point in this research area. These omics-based approaches have introduced new opportunities to better decipher the complexity and interconnection of exercise molecular transducers and their potential contributions to exercise's wide range of health benefits. In this review, we introduce these omics-based approaches to exercise researchers and provide a critical overview of the last decade of metabolomic and lipidomic applications, two of the most recently introduced omics-based approaches, to studying the molecular responses to acute exercise in humans and other mammalian species. Furthermore, we discuss key technical considerations, remaining knowledge gaps and hurdles associated with metabolomics and lipidomics, as well as highlight future research directions to continue expanding the molecular landscape of exercise biology (**Figure 2.1**).

2.3. Metabolomics and Lipidomics Guide for Exercise Researchers

2.3.1. What Are Metabolomics and Lipidomics?

Metabolomics is defined as the comprehensive study of metabolites present in a given biological system (e.g., biofluid, tissue) [22,23]. The metabolome—a term first coined by Oliver

and colleagues in 1998—represents the entire collection of metabolites within a biological system [32]. Metabolites are defined as low molecular weight (< 1500 daltons) chemical substrates, intermediates or end-products of enzyme-mediated reactions [22]. The study of the metabolome is also commonly referred to as "metabonomics", which was first defined as "the quantitative measurement of the dynamic multiparametric metabolic response of living systems to pathophysiological stimuli or genetic modification" [33]. This definition was later expanded to include the "particular emphasis on the elucidation of differences in population groups due to genetic modification, disease, and environmental (including nutritional) stress" [34]. Although differently defined, the terms metabolomics and metabonomics are often used interchangeably [35].

Metabolites are heterogeneous compounds that possess various physicochemical properties, but are generally classified as either hydrophilic polar molecules (e.g., amino acids, carbohydrates, organic acids and phosphorylated compounds) or hydrophobic non-polar molecules (e.g., fatty acids and membrane lipids) [36]. The human metabolome is comprised of thousands of metabolites, with the latest report from the Human Metabolome Database (HMDB) in December 2020 indicating no less than 8000 endogenous metabolites detected [37], while almost 35,000 exogenous metabolites from sources such as foods, drugs, toxins and microbes have been detected and/or expected [38].

Lipidomics, considered a subfield of metabolomics [36,39], is the study of the lipidome, i.e., the total lipid content within a cell, organ or biological system [40]. Lipids are often simply defined as hydrophobic biological substances generally soluble in organic solvents [41]. However, lipids can be more accurately characterised based on structural or biosynthetic criteria [42]. The LIPID MAPS® consortium has provided a lipid classification system including a comprehensive list of lipid categories (e.g., fatty acyls, glycerolipids, sphingolipids,

sterol lipids), classes and subclasses [42]. As of December 2020, the LIPID MAPS® Structure Database contains more than 45,000 unique lipid structures [43].

Emerging only at the start of the new millennium, metabolomics and lipidomics represent the newest applications among global omics-based approaches (i.e., genomics, transcriptomics, proteomics, phosphoproteomics). The rapidly growing fields of metabolomics and lipidomics have dramatically expanded over the past 15–20 years, thanks to major advancements in analytical instrument technologies and bioinformatic analysis platforms. As a result, there has been a substantial increase in the application of metabolomics and lipidomics across a wide range of research fields, including health and disease [44], toxicology [45], nutrition [46] and exercise physiology [47]. The growing application of these omics-based technologies therefore represents a promising avenue to continue improving our understanding of the complexity and interconnection of exercise-regulated metabolic reactions within biological systems, which were previously limited by the application of traditional reductionist approaches only studying targeted metabolite(s) of interest in isolation [22].

2.3.2. Advantages to Studying the Metabolome and Lipidome in Biological Systems

Studying the metabolome (including the lipidome) is appealing for expanding our understanding of complex biological systems in the context of exercise, as metabolites lie downstream of all other layers of biological regulation. Therefore, the metabolome reflects the cumulative changes resulting from processes involving the genome, transcriptome and the proteome, as well as their interactions with the environment (**Figure 2.2**). The metabolome thus directly reflects the phenotype of a given biological system at the molecular metabolic level [22]. Put differently, while genomics, transcriptomics and proteomics altogether provide a program of what might occur within a biological system, metabolomics provides a snapshot of phenotypic traits (i.e., phenome), revealing what is currently occurring or has happened as

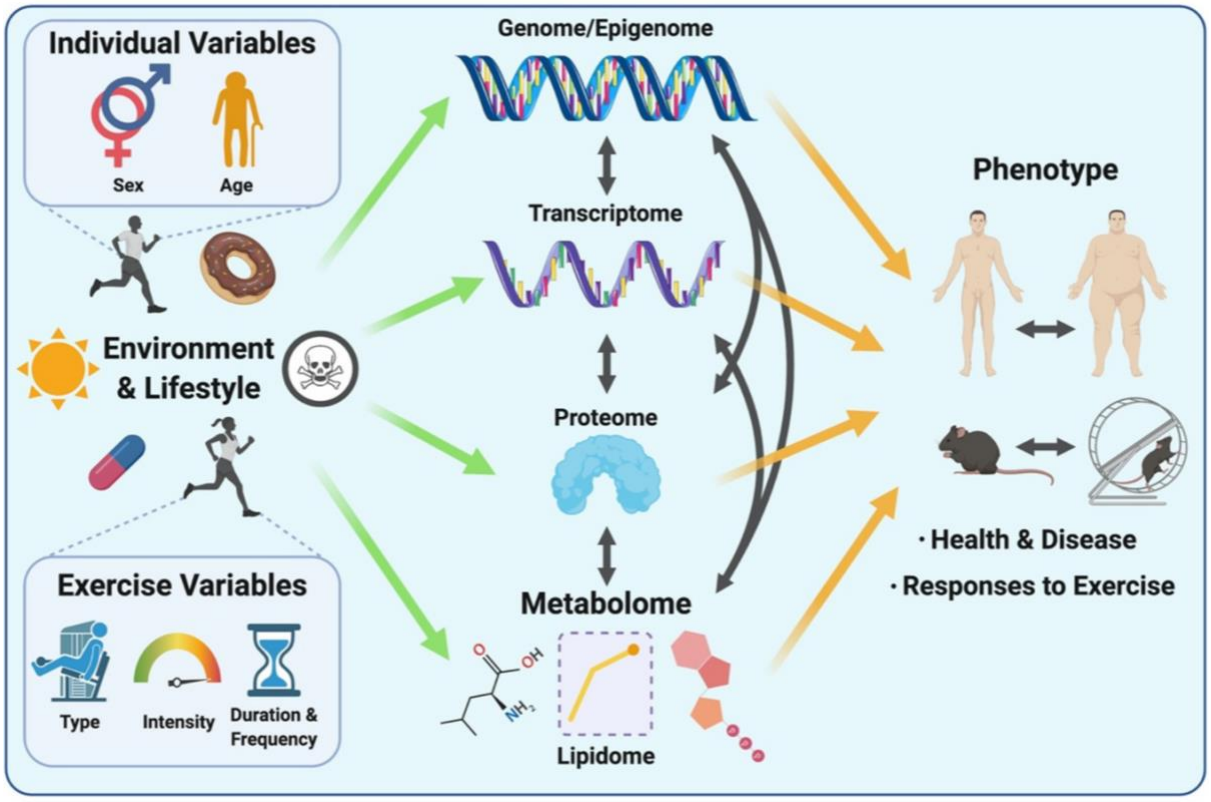

Figure 2.2 – The complex interrelations between biological layers (from the genome/epigenome, transcriptome and proteome to the metabolome) and other individual factors (sex and age, environment and lifestyle including exposure to toxins and pollutants (symbolised by skull and crossbones), medication use, dietary habits, …) and exercise variables, and how these biological networks and variables contribute to the overall phenotype. Environmental exposures and lifestyle, including diet and medication, as well as exercise and its associated variables (exercise type, intensity, duration and frequency) can affect all layers of biological regulation and lead to distinct phenotypic signatures in mammalian systems that reflect health, disease and responses to exercise. Adapted from [22].

a result of these other layers of biological regulation [48,49]. Considering rapid metabolite turnover, which can be detected in seconds versus minutes to hours for transcriptomic and proteomic responses to a stimulus such as an acute exercise bout, the metabolome serves as a rapid indicator of metabolic perturbations and chemical reactions occurring as a result of post-translational regulation (e.g., protein phosphorylation) in response to a given stimulus or environmental exposure.

Another advantage of studying the metabolome/lipidome is that the central reactions and pathways essential to energy metabolism, growth and nutrient supply are highly conserved across mammalian species, meaning that metabolite measurements obtained from other mammalian species such as rodents may be relevant and translational to humans [22,50]. In addition, the transferability of analytical methods across distinct biological systems (e.g., biofluids, tissues) makes metabolomic/lipidomic approaches attractive by dramatically reducing labour and time associated with optimisation, and providing high-throughput data at relatively low cost per sample compared with other omics-based approaches such as transcriptomics and proteomics [22]. Another advantage is the small sample volumes (typically 10–100 μL) required for compound detection, identification and quantification, which in turn makes collection of multiple samples in relatively short periods of time feasible (e.g., serial blood sampling at close intervals during/after exercise). Finally, when using an untargeted approach as detailed below, metabolomics/lipidomics permits the detection of changes in previously unknown, uncharacterised or rarely reported metabolites [51]. This approach allows for potential hypothesis generation and can facilitate retrospective data analysis to unlock potential mechanisms linked to disease or intervention strategy.

2.3.3. Types of Metabolomic and Lipidomic Approaches

Omics-based approaches such as metabolomics and lipidomics are generally described as unbiased, global experimental strategies to identify and/or quantify as many compounds as possible within a biological system. However, different approaches to investigating metabolites and/or lipids within a biological system are currently available, as briefly outlined below and reviewed elsewhere in more detail [22,52].

2.3.3.1. Untargeted Approach

This approach aims to reproducibly measure as many metabolites/lipids as possible in a given biological sample. Depending on the platform utilised, the untargeted strategy generally yields a metabolite detection coverage in the hundreds to low thousands using a combination of different separation and detection modes (described below). This approach provides semi-quantitative data, meaning that peak areas are reported for each metabolite instead of absolute concentrations. These peak areas allow the assessment of the relative abundance of detected metabolites between experimental groups. Of note, metabolite identities are usually unknown prior to data acquisition and analysis when using this approach.

2.3.3.2. Targeted Approach

As opposed to the untargeted strategy, the targeted approach aims to provide absolute concentrations of a set of known metabolites (ranging from one to 100 metabolites, typically a few dozen, depending on the number of compounds of interest) by using authentic chemical standards and calibration curves for each pre-selected metabolite. Recent developments in commercially available targeted metabolomics kits now facilitate the identification of up to 188 metabolites, and up to 1184 different lipids for lipidomics [39].

2.3.3.3. Semi-Targeted Approach

This third approach is less common. However, it is gaining popularity amongst many metabolomics research groups. This approach represents an intermediate strategy between untargeted and targeted approaches where a higher number of known metabolites (i.e., low hundreds) are investigated using a single chemical standard and ad hoc calibration curve for multiple metabolites, thus providing approximate metabolite concentrations.

The untargeted approach is primarily used as a hypothesis-generating method where the research question is generally unbiased with respect to metabolite identification. In contrast,

the targeted approach can be used as a hypothesis-testing and experimental validation method, as it provides much higher sensitivity and specificity in comparison to the untargeted approach, but with reduced metabolite coverage. Therefore, the untargeted approach permits the identification of new potential biomarkers and pathways, which can be further validated and more accurately quantified via the targeted approach. Although these approaches are complementary, the targeted strategy provides the most quantitative insights into metabolite dynamics in response to stimuli such as exercise [36].

2.3.4. Commonly Used Metabolomic and Lipidomic Analytical Platforms

Regardless of the type of metabolomic approach utilised, the main analytical platforms used in metabolomic studies are mass spectrometry (MS) and nuclear magnetic resonance (NMR) spectroscopy [36,39]. We provide a brief overview of NMR spectroscopy and MS principles below, and readers are referred to the following review articles for further details of these analytical techniques [53-56].

Briefly, NMR spectroscopy is a technique based on the interaction of an applied magnetic field with the nuclei of atoms which possess an odd number of protons or neutrons, including ^{1}H, ^{13}C, ^{15}N, conferring their magnetic properties. The magnetic orientations of these atoms, which have random directions, become aligned when a magnetic field is applied. Then, a pulse of electromagnetic radiation at a specific "resonance" frequency (dependent on the atom and magnetic field) is applied, causing nuclei "excitation" and subsequent "relaxation" when the radiation pulse stops. During relaxation, nuclei emit the radiofrequency waves absorbed during the excitation phase, thus generating radiofrequency peaks in a frequency spectrum (also called NMR spectrum) after Fourier's transformation.

NMR spectroscopy is used as a non-destructive technique and allows the measurement of chemical and physical properties of molecules, therefore helping identify and/or quantify

molecules of interest. In theory, this can be performed in solid, liquid and gas states from frozen to very high temperature materials, although researchers typically focus on only one aggregation state based on practicality and feasibility. Numerous applications using "pulse sequence" have been developed to expand the capability of NMR techniques. Pulse sequence is analogous to music scores for an orchestra to create the right harmony, which is the spectrum in NMR. Application of the right pulse sequence can enable sample information such as chemical structure, molecular shape, size and molecular aggregation to be obtained. Since NMR is non-destructive, the sample can be reused to gain more information using different pulse sequences, unless the sample condition has changed during the experiment (e.g., heat application, temperature change). The major limitation of the NMR technique is low sensitivity compared to MS, resulting in reduced metabolite coverage (typically 50–200 metabolites detected and identified) with NMR [57,58]. Compared to MS, NMR also requires more sample volume (~0.28–0.5 mL) to obtain measurements. However, advantages of NMR over MS include the ability to analyse living samples (e.g., magnetic resonance imaging) and the ease in distinguishing compounds of identical molecular weight with NMR [57].

In MS-based techniques, the compounds present in a biological sample are converted to ions (with either a positive or negative charge) through the use of an ion source. The formed ions then enter the MS instrument which detects ions and their abundance, providing a mass spectrum displaying mass-to-charge ratio (m/z) and peak intensity (i.e., ion abundance). Further information can be collected through tandem MS (MS/MS or MS^2) in which either intact "precursor" ions are fragmented into "product" ions, or ions already fragmented during MS undergo further fragmentation, providing additional structural information about a given compound detected and thus enhancing compound identification capacity. MS^2 is particularly useful for compounds with identical m/z values [54,56].

Although MS can be used as standalone instrumentation for metabolite detection and identification, i.e., direct infusion MS (DIMS), it is typically but not exclusively combined with chromatographic separation techniques such as gas chromatography (GC) and liquid chromatography (LC). Chromatography columns contain a stationary phase that interacts with the sample and uses the affinity of molecules to separate them within complex matrices. As molecules flow along the column, their different affinities for the stationary phase result in different retention times in the column and thus sequential introduction into the MS instrument, therefore enhancing sensitivity and identification capacity [54,58]. Due to major technological advances over the past two decades, LC-MS is currently the most widely used technique in metabolic profiling. Indeed, LC-MS provides high metabolite coverage, reproducibility, specificity and sensitivity [58]. Similar to LC-MS, GC-MS has a strong capacity for separation, sensitivity, selectivity and reproducibility. However, GC-MS can only be used for the separation and identification of volatile compounds and low molecular weight compounds (50–600 Da) [59], and such chemicals must be volatile or amenable to chemical derivatisation to render them volatile. Each analytical platform has its own advantages and limitations and should therefore be considered complementary rather than opposing analytical techniques to provide comprehensive metabolomic analyses. No single platform can yield detection, identification and quantification of the full range of metabolites within a given biological sample and as such, multiple separation techniques and analytical platforms may be used in combination to increase metabolite coverage [39,58]. More detailed information about specific methods, advantages and limitations regarding the use of GC-MS, LC-MS (including MS/MS) and NMR for metabolomics have been extensively reviewed elsewhere [57-59].

Lipidomics shares similar analytical techniques with metabolomics [40,60]. Although NMR spectroscopy is considered a powerful tool for lipid identification [61], the lipidomics field has predominantly applied MS-based techniques with numerous potential experimental

and sample preparation variations. The most commonly used MS techniques can be divided into two categories: (1) direct analysis from a biological matrix; and (2) analysis following lipid extraction, with or without subsequent separation [40,60].

Direct analysis from biological matrices is mainly performed by MS imaging. An appealing characteristic of this method is its ability to determine the spatial distribution of thousands of lipid species in tissue sections without any labelling [62]. The principle of MS imaging is similar to classical MS in that compounds from the sample (i.e., tissue section) are ionised, for example using matrix-assisted laser desorption ionisation (MALDI) or desorption electrospray ionisation (DESI) and analysed by MS. The main distinction between MS imaging and classical MS is that a tissue section is divided into squares or pixels with MS imaging, and compounds within each pixel are subject to ionisation and MS, pixel by pixel. Mass spectra are acquired for each pixel and specific m/z values can be individually selected to visualise their signal intensity (thus abundance) within the tissue section. By merging the different colour-coded m/z signals, spatial distribution and abundance of different lipid species can be visualised throughout the tissue [63,64]. Another interesting characteristic of MS imaging is that this approach requires minimal sample preparation (with MALDI-MS imaging) or no preparation (DESI-MS imaging) other than tissue sectioning [40].

The analysis of lipid extracts without separation is often referred to as "shotgun" lipidomics or direct infusion-based lipidomics, whereby a given lipid extract is continuously injected in the MS instrument, generally after selective ionisation by an ion source, which provides some lipid separation [40]. Despite various advantages, limitations associated with shotgun lipidomics include ambiguous identification of lipid isomers and ion suppression [65]. Ion suppression is a phenomenon that results from the presence of less ionizable/volatile compounds which affects the efficiency of droplet formation or evaporation, thus leading to a reduction in charged ions in the gas phase that enter the mass spectrometer [66]. Most

limitations of shotgun lipidomics are overcome by multidimensional MS-based shotgun lipidomics (MDMS-SL), which integrates a full mass scan (first dimension) and all MS/MS scans (second dimension) for head groups and acyl chains, thus allowing the identification of individual lipid species (including isomers) and providing accurate quantification but with relatively low throughput [40]. Lipid annotations are then based on accurate mass and fragmentation patterns, which is facilitated by reference databases [67,68]. In contrast, separation methods prior to MS analysis allow minimal ion suppression. Among these separation methods, LC-MS is the most widely used for these same reasons, among others, as detailed above [40,60,65]. Nestled between LC and MS is a very fast separation technique called ion mobility spectrometry (IMS), which is used to provide an additional dimension of separation based on ions' shape and size, known as collisional cross section (CCS). This technique is becoming particularly important for lipids as it allows the separation of isomers using trapped ion mobility spectrometry (TIMS) and a gas flow which facilitates lipid identification [69].

2.3.5. Overall Metabolomic and Lipidomic Workflow

A typical untargeted metabolomics/lipidomics workflow is composed of several experimental and analysis steps (**Figure 2.3**). The first step of this workflow is establishing the experimental question and optimizing the study design. A robust study design is crucial to ensure minimal investigator-induced variation in the biological sample and subsequent reduction of noise within the metabolomic/lipidomic dataset, which can eventually hinder confidence of data interpretation [51,52]. The following step includes performing the experimentation and the resulting sample collection, storage and preparation. These steps are also critical since many biases may be introduced, potentially altering the metabolite/lipid composition of the biological sample [70]. Consistency of experimental methods (e.g., timing of collection, materials and reagents, storage temperature) is paramount to enable acquisition

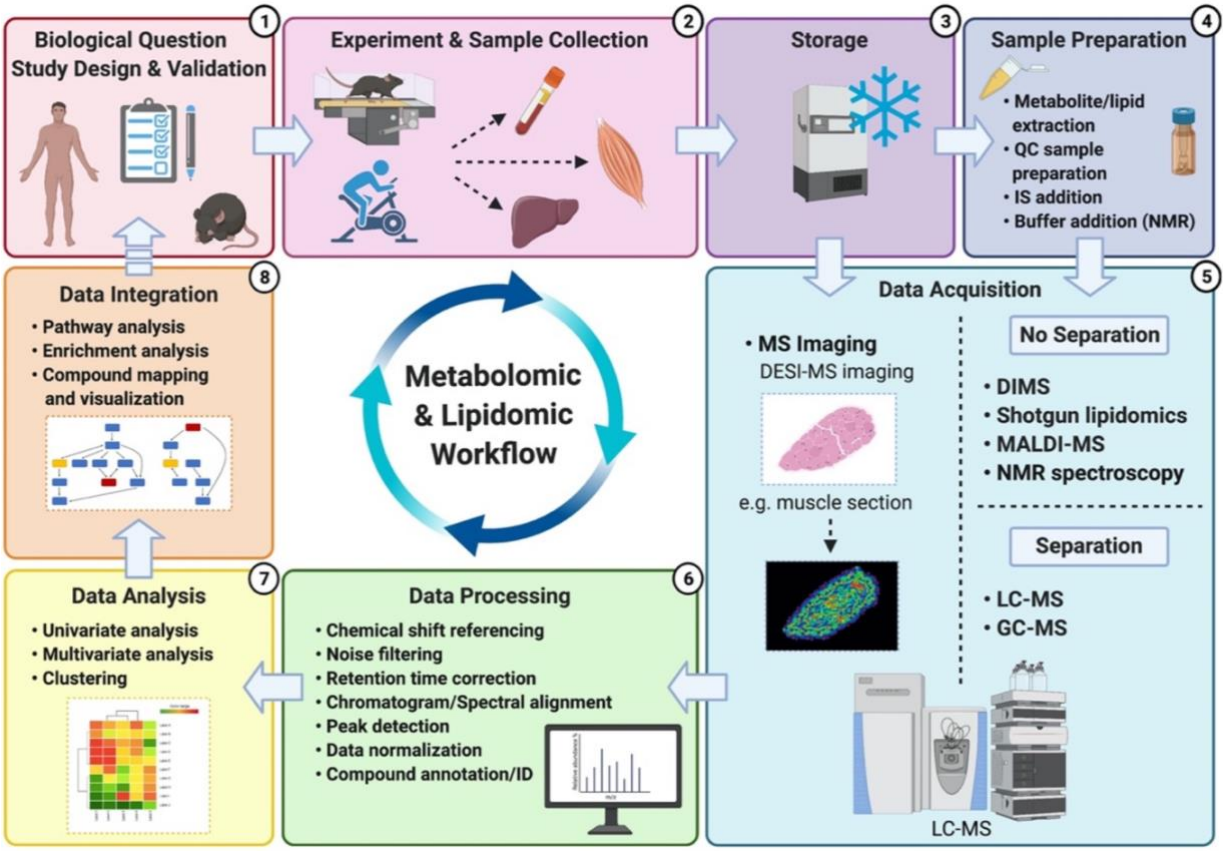

Figure 2.3 – Typical metabolomics/lipidomics workflow: (1) After establishing a given biological question, appropriate and optimised study design is a critical step to answer this biological question with minimal bias and noise (i.e., investigation-induced variability). (2) Sample collection before/during/after the experiment also requires particular attention and care to avoid introducing potential biases. Therefore, consistency of collection timing, materials and reagents is important. Metabolic reactions are rapid and must be stopped as soon as possible following collection by snap freezing or placing the sample on ice. (3) Samples are then prepared accordingly (e.g., centrifugation of whole blood to collect plasma or serum) for storage until planned sample preparation or direct data acquisition. (4) Sample preparation depends on the analytical platforms utilised and the molecular species to be extracted (e.g., lipids or other metabolites). During this step, QC samples are usually prepared and IS added to all aliquots to screen and correct platform-related shifts and enhance reproducibility. (5) Samples are analysed and data are acquired using one or multiple analytical platforms. (6) Acquired raw data are then processed through multiple steps to eventually allow accurate compound identification/annotation. (7) Multiple statistical tests are performed on the identified/annotated compounds to determine potential differences between samples and/or groups in line with the biological question and experimental design. (8) Finally, data are placed into biological context using pathway/enrichment analysis and visualisation tools, which also help inform future biological research questions and experimental designs, therefore leading back to step one of the workflow. Alternatively, targeted validation of metabolites/lipids of interest within the dataset may be performed following data integration.

of accurate and reproducible results [56]. Sample preparation methods and reagent selection will mainly depend on the sample type (e.g., blood, urine, saliva), platforms being utilised (e.g., NMR versus MS), and compounds of interest (lipid classes versus all metabolites). Whereas NMR only requires minimal and non-sophisticated sample preparation [39], MS-based platforms can require additional preparative steps for the inclusion of quality control (QC) samples and internal standards (IS) for the generation of calibration curves and accuracy check. However, both instruments will typically use QC samples within the analysis to check for reproducibility and, for MS, to monitor/correct potential shifts in mass accuracy and retention times [51,52].

Next, data acquisition refers to the detection and characterisation (e.g., m/z ratio and peak intensity in MS; and chemical shift in NMR, i.e., resonance frequency of a nucleus relative to a standard with a value of 0) of the compounds present in samples through the use of one (and sometimes several) of the analytical platforms mentioned above. Once acquired, raw peak intensity data are processed to permit further analysis.

In MS, data processing comprises many steps including conversion of raw peaks into data matrices, noise filtering, retention time correction, chromatogram alignment, peak detection, data normalisation, and eventually, compound "putative" identification by matching metabolite/lipid spectra against in-house libraries and available databases such as HMDB, METLIN or LIPID MAPS. Putatively identified compounds are then benchmarked by the investigator, and the relative levels of identification confidence are assigned and reported according to the Metabolomics Standard Initiative (MSI). The (MSI), and more recently, the Lipidomics Standards Initiative (LSI), have notably been created to standardise the confidence levels for metabolite and lipid identification [61,71]. In NMR, different steps precede compound identification/annotation including: spectral pre-processing consisting of noise reduction and baseline correction; sub-spectral selection where only areas of the spectra containing peaks are

kept; spectral alignment; spectra division into sections (i.e., bins) that can fit one or more peaks; followed by calculation of bin intensities and statistical tests to assign bins to a specific metabolite. Data normalisation, scaling and transformation are also performed prior to data analysis and interpretation [72].

Following identification (regardless of the analytical platform used), a broad range of statistical analyses is performed to determine potential differences between samples and/or experimental groups. Commonly used statistical methods include univariate and multivariate analysis, either in an unsupervised or supervised manner. ANOVA and t-test or nonparametric equivalents are widely used univariate analysis methods, whereas principal component analysis (PCA) and partial least square-discriminant analysis (PLS-DA) are common examples of unsupervised and supervised multivariate methods, respectively [73]. Briefly, the use of PCA can reveal patterns or signatures within the sample set and show sample reproducibility through clustering of quality control samples within and between batches. PLS-DA is a predictive and descriptive modelling technique used for classification between different groups of samples and optimises separation between these groups of samples [73,74]. A plethora of statistical methods are available, but there is no one size fits all approach. The choice of suitable statistical methods will depend on the biological question and study design, and consulting experienced bioinformaticians and biostatisticians prior to data collection is highly recommended to ensure appropriate data handling and analysis.

The last step of the workflow is data integration and interpretation, which allows the investigator to link detected compounds with their biological context using publicly available software tools and databases that further enable pathway and enrichment analysis, metabolite/lipid mapping and visualisation. Among these available databases, the Kyoto Encyclopedia of Genes and Genomes (KEGG), LIPID MAPS and MetaboAnalyst are widely used in applications of metabolomics and/or lipidomics [68,75]. However, it is important to note

that, as highlighted by Schwaiger *et al.*, the specifics of each step within metabolomics and lipidomics workflows can vary significantly [76]. It is also important to emphasise that data integration and interpretation is a step where the investigator's knowledge of the research field and existing principles, along with deduction skills and deep analysis of the available literature are critical to converting algorithm-generated data into biochemical and physiological insights.

2.4. Metabolomic and Lipidomic Analyses of Acute Exercise-Regulated Biological Networks

Following the introduction of metabolomic and lipidomic approaches, analytical platforms and experimental workflows above, we overview in this section metabolomic and lipidomic findings made over the last decade in the context of acute exercise. We selected 25 primary research articles and one systematic review specifically focusing on molecular metabolic responses to a single bout of exercise (i.e., acute exercise) within the first minutes/hours and up to 72 h following this single exercise bout, in healthy subjects. Articles that exclusively investigate the effects of acute exercise on the metabolome/lipidome in subjects with disease states (e.g., obese and/or insulin resistant), as well as articles investigating the effects of repeated exercise bouts (i.e., exercise training), were not included in this review. We discuss metabolomic/lipidomic findings related to both acute aerobic and acute resistance exercise bouts, with the term "endurance" used to define an aerobic exercise bout of 30 min or longer duration. As opposed to aerobic exercise which typically consists of repetitive physical activity against relatively low loads and requires the use of oxygen for energy conversion, resistance exercise consists of muscle contractions performed against relatively high loads [77,78]. Findings from both humans and other mammalian species are described, with the aim of highlighting how metabolic networks are affected by exercise in several biological fluids

and tissues (mainly skeletal muscle and liver) and setting the stage for future expansion of exercise's molecular landscape. Collectively, these findings emerge from the use of multiple analytical strategies (i.e., targeted and untargeted) and platforms, with MS-based analytical platforms predominantly being used. See supplementary **Tables 2.1 and 2.2** for further experimental details and summaries of findings from each study discussed below involving metabolomics and lipidomics, respectively.

2.4.1. Metabolomic Analyses of Acute Exercise

2.4.1.1. Humans Biofluid Analyses

An acute bout of exercise dynamically impacts the human metabolome in a range of biological fluids including blood, plasma/serum, urine and sweat, amongst others. The high variability between existing human studies in terms of age, sex, BMI, exercise type (resistance versus aerobic/endurance), modes (duration, intensity, interval versus continuous), sample types, collection time points, as well as analytical platforms used, presents challenges in distilling these large datasets into a consensus molecular metabolic signature of exercise.

Blood is considered an integrative biofluid given that it contains metabolites exchanged between organs and is therefore suitable for relatively comprehensive metabolic profiling [22]. Blood collection is minimally invasive and available in sufficient amounts for metabolomics/lipidomic purposes in humans. Compared to blood, the urinary metabolome is less comprehensive and complex (i.e., lower metabolite coverage, mostly hydrophilic compounds) since it is a filtrate of wastes from the bloodstream [79]. However, urine is an attractive biological matrix since it can be collected non-invasively in large volumes, and is under no homeostatic control mechanisms, meaning that urine may magnify some metabolite changes occurring in blood. Urine is therefore often used as a matrix for dietary intake biomarker discovery and drug or doping testing [79,80]. Similar to urine, sweat, which is made

of ~99% water, mainly contains hydrophilic compounds in addition to electrolytes. Compounds such as proteins, peptides and amino acids, but also urea, lactate and pyruvate can be found in sweat, as well as xenometabolites such as drugs and cosmetics [80]. Researchers should consider which biofluid is practical and ensure developed standard operating procedures exist in order to minimise the wide variety of artifacts which can influence metabolite measurement. The choice of a suitable biological matrix to investigate in the context of exercise will therefore come down to the nature of compounds of interest (hydrophilic and/or hydrophobic compounds), research question (e.g., comprehensive profiling versus specific submetabolome characterisation, drug and doping testing), feasibility and experimental setting (e.g., multiple sampling, required volumes, risks of contamination, sample handling, field or sport setting versus laboratory-based). Future advancements in analytical methods may promote development of technologies which can be routinely deployed to capture metabolites from biofluids such as sweat and saliva, for example in an elite sport setting, which will ultimately complement gold standard measures of metabolites from plasma and serum.

Following a qualitative systemic review of human exercise metabolomics studies by Sakaguchi *et al.* [81], Schranner *et al.* conducted a recent systematic review of human metabolomic analyses assessing metabolite trajectories following acute endurance and resistance exercise interventions with a duration ranging from 30 min to ~9 h [82]. This systematic review addressed some of these challenges by analysing a total of 27 studies meeting eligibility criteria, revealing significant changes in up to 196 metabolites in the first 24 h following a single exercise bout. These changes in metabolite concentrations were summarised in the early (0–30 min), intermediate (> 30 min–3 h) and late (> 3–24 h) stages post-exercise, and divided into classes including: carbohydrates and TCA cycle intermediates; fatty acids (FA), acylcarnitines, ketone bodies, membrane lipids; amino acids and derivatives; and nucleotides, vitamins and co-factors.

Despite some metabolite classes such as amino acids and derivatives showed mixed responses (i.e., both increased and decreased relative abundance) between exercise types (i.e., resistance versus endurance) as well as differences between endurance studies amongst the 27 studies analysed [82], other metabolites exhibited robust unidirectional changes following a single exercise bout. Among these, lactate and pyruvate—two well-documented end-products of glycolysis—expectedly increased to various extents in the early stages after both acute endurance and resistance exercise. Likewise, several components of the TCA cycle were commonly increased in blood and urine in the early and intermediate post-exercise phases. Among the observed increases in metabolite abundance following exercise, some nucleotides and their degradation products such as hypoxanthine and inosine were also commonly detected. However, the most robust changes in response to exercise involved fat metabolism. Indeed, no less than 37 FA and 17 acylcarnitines were consistently reported to be increased following acute endurance exercise. Acylcarnitines are FA bound to carnitine, an amino acid derivative which allows the transport of FA into the mitochondria where they can be oxidised and contribute to cellular energy conversion. However, acylcarnitines can also accumulate and be released by cells into the bloodstream. Most studies (predominantly endurance exercise studies) reported in this systematic review showed increased levels of several ketone bodies, along with reduced levels of ketogenic amino acids such as leucine, isoleucine and lysine, and increased levels of degradation products from these three amino acids. Conversely, membrane lipids and bile acids were mainly observed to be decreased following acute endurance exercise. Mixed responses were observed for other metabolite classes such as steroid hormones, some vitamins, cofactors and exogenous compounds in addition to amino acids and derivatives following endurance exercise.

The mixed responses observed in amino acid levels following an acute exercise bout [82] may be explained by the fact that a wide range of exercise types, durations and intensities

(**Figure 2.2**) and various biofluids with varying sample collection time points are often analysed together in such systematic reviews to compare exercise with a control resting condition. Amino acid responses can vary in multiple ways, depending on these exercise variables. For instance, if a strenuous endurance exercise bout exceeds the carbohydrate store of an individual, or if the individual's maximal FA oxidation capacity is reached, a shift towards protein catabolism and amino acid utilisation to sustain energy requirements during the prolonged exercise bout will eventually result in reduced circulating amino acid levels [83,84]. Similarly, circulating levels of amino acids can also decrease in the recovery phase following resistance exercise, characterised by an increased utilisation of amino acids for protein synthesis. Indeed, all amino acids measured in blood following acute resistance exercise in this systematic review were decreased, except for alanine which was increased. These metabolite changes during the recovery phase may not be observed following less intense and/or shorter exercise bouts. Additionally, a wide range of blood collection timings during and/or following an exercise bout may represent different fasting/feeding periods (often not controlled for in human studies) that will have a major impact on relative circulating amino acid concentrations observed between studies. Furthermore, the fact that amino acids are involved in various metabolic reactions represents another potential reason for mixed amino acid responses to different exercise stimuli. For example, amino acids are involved in protein synthesis, ATP synthesis, gluconeogenesis and ketogenesis. While these reactions will lead to reduced circulating amino acid levels, other reactions such as protein breakdown or dietary protein intake will conversely increase circulating amino acid levels. Intake of carbohydrates will impact amino acid metabolism, as increased carbohydrate availability will inhibit gluconeogenesis and ketogenesis, therefore reducing the utilisation of ketogenic and gluconeogenic amino acids to facilitate these metabolic processes [85,86]. From this seminal systematic review [82], depicting differences in metabolomic behaviours between resistance

and endurance exercise is limited given the current scarcity of studies investigating the metabolomic responses to a single bout of resistance exercise. Therefore, the only reported metabolite with a clear opposite behaviour between acute endurance versus resistance exercise reported is the ketone body acetoacetate, which is increased after endurance exercise while decreased after resistance exercise. The reader should however be aware that differential responses between exercise types, intensities and durations may also lie in the magnitude of metabolite responses rather than directionality. In summary, nutritional status, exercise types and modes represent important confounding factors between studies, introducing challenges and potentially limiting the interpretation of metabolomic responses to acute exercise. This warrants further efforts to characterise amino acid metabolism in response to different exercise types and modes, with particular attention to these common confounders.

2.4.1.1.1. Blood

Overall findings from this systematic review [82] are supported by previous work investigating the human serum metabolome in male and female athletes in response to marathon running. Stander and colleagues reported increased serum FA, ketone bodies and TCA cycle intermediates, along with decreased levels of amino acids following marathon running [84]. Increased concentrations of carbohydrates and associated metabolites, as well as elevated alpha-hydroxy acids and odd-chain fatty acids (OCFA) were also observed following acute endurance exercise [82,84]. The presence of elevated alpha-hydroxy acids and OCFA levels are indicative of an increased utilisation of α-oxidation—the process resulting in removal of the carboxyl group (the first carbon atom) in a FA— resulting in the generation of OCFA, though OCFA can also be provided through the diet (e.g., dairy products) [87]. In this study [84], FA α-oxidation was suggested as a potential alternative pathway for energy conversion when β -oxidation reaches saturation, indicated by the accumulation of 3-hydroxy acids (β-hydroxyhexanoic acid) and 3-keto acids (β-hydroxy-α, β-didehydrosebacic acid). Although the

peroxisome—the site of α-oxidation—does not contain a TCA cycle nor an electron transport system and is therefore unable to directly produce ATP, the α-oxidation of FA generates alpha-hydroxy acids which can be further subjected to β -oxidation in the peroxisome [88]. These products of the peroxisomal β oxidation could potentially be taken up by mitochondria for complete oxidation in humans, similar to what has been demonstrated in rodent skeletal muscle [89].

In contrast to some of the above findings, other studies have identified elevated serum levels of amino acids including alanine, tyrosine and phenylalanine in males following marathon running, whereas alterations of cholesterol and steroid metabolism following a marathon were consistently reported in these two studies [84,90], as elevated levels of squalene and pregnenolone are indicative of cholesterol breakdown. Pregnenolone is notably a precursor of cortisol, a known steroid stimulator of lipolysis, protein breakdown and gluconeogenesis [91]. In addition, marathon running in these males also provoked decreased serum levels of glucosamine [90]. Glucosamine is a compound involved in joint and cartilage structures, and commonly used as a dietary supplement to combat joint inflammation [92]. Next, caffeine metabolism was also shown to be increased by marathon running, indicated by increased levels of compounds including theophylline, theobromine and xanthine [90]. It is plausible that the increased levels of caffeine and associated derivatives are due to dietary caffeine intake in the hours preceding the marathon, since diets between baseline blood collection (day preceding the race) and the race day were not controlled in this study.

Metabolomic responses to exercise in blood have also been shown to be influenced by an individual's level of fitness. For instance, in a study by Schader and colleagues [93], male amateur marathon runners were divided into top (n = 18), average (n = 40) and low (n = 18) performers, based on VO_2 max (~63, 50 and 42 mL × min^{-1} × kg^{-1}, respectively) and race completion time (~175, 225 and 277 min, respectively). Blood samples from these three groups

were examined for potential differences in metabolomic responses to marathon running. Immediately post-race, the low performers exhibited a significant increase in a wide range of acylcarnitines (from short to medium- and long-chain) in plasma compared to the average and top performers groups. One possible explanation for these differences in acylcarnitine levels between top/average and low performers is that low performers may have a reduced capacity to oxidise lipids, which may in turn lead to an accumulation of acylcarnitines. Differences in arginine metabolism and urea cycle-related metabolites between low and top performers have also been reported [93]. Arginine is an amino acid central to the urea cycle, which is activated during protein breakdown when nitrogen is liberated from amino acids. Ornithine, a co-product of urea production from arginine, was shown to be lower in the top versus low marathon performance group, whereas citrulline—an alternative product of arginine metabolism—increased in the top performers group. A potential explanation for the reduced plasma levels of ornithine in top versus low performers may be the greater lactate production in these faster runners; lactate being an inhibitor of urea (and ornithine) synthesis [94]. Furthermore, it is plausible that reduced citrulline levels in low versus top runners can result from increased nitric oxide (NO) production due to longer race duration. NO has been shown to exert a negative feedback regulation of NO synthase, an enzyme that catalyses the production of citrulline and NO from arginine [95]. Another possible reason for reduced levels in citrulline observed in the low performers group may be the potential decrease in asymmetric dimethylarginine—a substrate for citrulline synthesis—that occurs during strenuous and prolonged exercise [96]. These overall differences in the urea cycle and arginine-related metabolites indicate a higher reliance on protein catabolism in low compared to top marathon performers [93]. However, given the complexity and multiple possible reactions leading to the production of arginine and urea cycle related-metabolites, further investigations are required to confirm the potential underlying mechanisms suggested above.

Another recent metabolomics analysis of plasma from young active men performing an acute time-to-exhaustion cycling trial allowed the separation of metabolomic profiles in a 20-min window, and the identification of biomarkers at the onset of fatigue [97]. One key finding from this study was that several metabolites permitted the discrimination between the pre- and post-fatigue states. In this study, Manaf *et al.* also revealed FA were among the strongest metabolomic responses to exhaustive exercise and progressively increased over time throughout the cycling trial. Particularly, robust increases in oleic and palmitic acids, as well as their carnitine-bound form, were observed while tryptophan concomitantly decreased. This supports the central fatigue hypothesis proposed by Newsholme *et al.* which suggests that increases in FA levels induce a displacement of tryptophan from albumin, resulting in enhanced availability of free tryptophan. The latter can thus enter the central nervous system to produce serotonin, a neurotransmitter associated with fatigue when it accumulates in the central nervous system [98]. This hypothesis is further supported by the observed increased levels of the end-product of serotonin metabolism, 5methoxy-3-indoleacetic acid. Other potential mechanisms implicating the aforementioned FA and acylcarnitine in the onset of fatigue have also been suggested, including inhibitory effects on adenine nucleotide translocase, responsible for the transport of ATP from the mitochondria to the other cellular compartments requiring energy [97,99].

Recently, Contrepois *et al.* investigated metabolic responses to acute aerobic exercise (i.e., ~8–12 min of treadmill running following warm-up) using multi-omics (including proteome, transcriptome, metabolome and lipidome) blood profiling [47]. The study investigated multiple biological layers before exercise and at four time points (2, 15, 30 and 60 min) following a single exercise bout. Plasma was collected from healthy older participants (i.e., average age 59 years) with wide ranges of insulin sensitivity and metabolic health status. In line with the recent systematic review discussed above [82], these metabolomic data showed

robust lipolysis and FA tissue uptake in response to exercise, indicated by large increases in various FA and acylcarnitines. However, distinct trajectories were observed depending on FA and acylcarnitine carbon chain length and the number of unsaturated bonds. While most saturated medium-chain acylcarnitine (C6:0 to C12:0) levels increased immediately post exercise to return to pre-exercise levels within 15–30 min, several monounsaturated medium- to long-chain acylcarnitines (C6:1, C8:1 and C16:1) and one saturated medium-chain acylcarnitine (C14:0) showed a more modest accumulation with exercise, but returned to pre-exercise levels after 30 to 60 min of recovery. Increased circulating levels of medium-chain acylcarnitines likely suggest incomplete FA oxidation within tissues such as skeletal muscle. Expectedly, free carnitine levels exhibited inverse trajectories, as free carnitine binds to FA to form acylcarnitines. Three main trajectories were observed for FA. While C10 and C12 FA increased two min post-exercise, C14 to C18 FA peaked at 15 min post-exercise, whereas C20 to C24 FA rapidly decreased post-exercise. In this context, the rapid drop of circulating long-chain FA likely indicates increased skeletal muscle uptake of these specific FA during exercise for subsequent oxidation. Distinctively, increased circulating levels of C10 to C18 FA in the first 15 min of recovery may potentially be explained by FA uptake and oxidation switching off more rapidly than exercise-induced lipolysis [100]. As opposed to FA, most amino acids such as glutamic acid, cystine, tryptophan, serine, threonine and glycine decreased within two min of recovery with a return to basal levels by 60 min of recovery. Alternatively, circulating BCAA levels exhibited a delayed decrease following exercise and remained reduced at 60 min of recovery. However, increases in alanine and tyrosine, in line with previous work [90], as well as increases in glutamine and proline were observed, with a return to basal levels within 60 min [47]. The precise reasons for these mixed amino acid responses in blood remain to be elucidated, although increased plasma alanine and glutamine levels indicate ammonia detoxification [47,83].

Interestingly, metabolomics analyses of blood samples have also proven useful in studying the role of liver in exercise metabolism. Indeed, Hu *et al.* recently highlighted liver-skeletal muscle crosstalk during acute exercise by analysing arterio-venous differences of metabolites in: (1) the hepato-splanchnic bed; and (2) the exercising and resting leg, in young men [101]. These data indicated only minor changes in saturated long- and very long-chain FA, whereas C6:0 and C8:0 FA, as well as TCA cycle intermediates (succinate and malate), were released by the exercising leg and taken up by the liver through the hepato-splanchnic bed. Blood analyses from the hepato-splanchnic bed therefore represent a means to study liver metabolism in humans while avoiding challenges associated with the invasive nature of liver biopsy collection.

2.4.1.1.2. Urine

Although blood is the most commonly studied biofluid in the research area of exercise metabolomics, an increasing body of work in the field of exercise involves analysis of other biofluids including urine, saliva and sweat. After blood, urine is seemingly the most commonly analysed biofluid in the context of exercise metabolomics. In humans, metabolite profiling of urine samples is appealing since it has proven to be more stable, under less homeostatic regulation than other biofluids [79], and collected non-invasively and in larger volumes compared to other biofluids. It has been suggested that the urinary metabolome can be considered complementary to the blood metabolome, since urine contains numerous end-products derived from food and drug metabolism [70]. Recent publications support the utility of urine analysis to reflect metabolomic changes following acute exercise, as analysis of urine permits confirmation of well-appreciated exercise-induced changes in metabolites related to several pathways including glycolysis (e.g., pyruvate and lactate), TCA cycle (e.g., citrate and succinate) and amino acid metabolism (e.g., alanine, taurine) [102-106]. In one of the earliest urinary metabolomic papers published, Kistner *et al.* reported that within 15–30 min following

an incremental cycling test, significant increases in urinary carnitine and novel urinary exercise-responsive metabolites could be observed; notably including increases in leucine derivatives methylsuccinate and 3-hydroxyisovalerate, and valine derivative 3-aminoisobutyrate. Increased urinary levels of these derivatives indicate branched-chain amino acid (BCAA) degradation and excretion in urine following exhaustive exercise [102]. However, an often-reported downside of metabolomic analyses in urine is that metabolite concentrations are highly influenced by hydration status and thus require normalisation for water content. Several pre-acquisition normalisation methods have been developed to address these issues. The most popular methods, each presenting advantages and drawbacks, include the assessment of relative concentration to a reference compound such as creatinine, measurement of osmolality, and the assessment of urine specific gravity (i.e., urine to pure water density ratio) [70].

2.4.1.1.3. Saliva

Saliva has gained attention over the past few years in the study of exercise metabolomic biomarkers. Like urine collection, saliva is collected non-invasively and does not require specialised laboratory facilities or skilled healthcare professionals. However, only few metabolomics-based studies investigating the effects of exercise in saliva have been conducted to date (e.g., [107-111]), and several potential pitfalls have been underscored. The salivary metabolome contains both metabolites from the body and oral bacteria, as well as ingestion-related compounds. It has also been observed that some metabolites such as lactate return to basal states much faster in saliva versus blood [112]. Similar to urine, metabolite concentrations are substantially affected by hydration status, therefore also requiring normalisation for water content. Normalisation based on total protein concentration of whole saliva (TPWS) and total observed metabolite concentration (TOMC) have been suggested to address this issue. However, normalisation for water content in metabolomics studies in saliva has not been

systematically performed to date [109]. Additional efforts are therefore needed to use saliva as a reliable source of biological information in the exercise research field.

2.4.1.1.4. Sweat

Sweat also represents an understudied biofluid in the field of exercise metabolomics, partly due to its relatively low metabolite concentrations. However, sweat metabolomics has proven useful in other contexts such as cancer diagnostics [113]. Among metabolomics-based exercise studies performed in sweat (e.g., [114-116]), in a pilot study Harshman and colleagues [115] identified dozens of metabolites following a treadmill march with 22-kg tactical gear until perceived exhaustion, either at low (4.8 km/h, 3% incline), moderate (5.1 km/h, 4% incline) or high intensity (5.6 km/h, 6% incline), in active duty military volunteers. Consistent with previous findings, amino acids were the predominant detected compounds [114,116]. However, the authors failed to observe any significant changes in metabolite concentrations between conditions, and no correlations could be drawn between metabolite concentrations and aerobic capacity (VO_2 max) or the rate of perceived fatigue. Several confounding factors and current pitfalls of sweat-based metabolomics studies have been reported, including the absence of localised sweat rate measure; normalisation methods of analyte concentrations; sweat collection devices utilised, which can also constitute a great source of interindividual and inter-study variability; and the presence of skin bacteria and cosmetics that may interact with sweat metabolites [115]. This, in combination with the frequent lack of statistical power in these human studies, limits the full potential of sweat metabolomics and questions whether sweat is a reliable biofluid for exercise biomarker discovery purposes.

2.4.1.2. Other Mammals and Tissues

Overall, metabolomics studies analysing human biofluids in the context of exercise are far more common than human studies investigating tissues. One of the main reasons for the

currently limited tissue metabolomics studies involves the more invasive nature of human tissue biopsies (e.g., skeletal muscle and liver) compared to routine blood sampling or sweat, urine and saliva collection. However, it has been demonstrated that blood and skeletal muscle metabolomes have very little overlap, thus suggesting an overall limited ability to potentially identify muscle tissue-specific metabolites from blood samples [117]. Mammalian animal models have therefore helped expand our understanding of metabolic networks affected by acute exercise by allowing easier access to metabolically active tissues such as skeletal muscle and liver.

As opposed to human studies, other mammalian studies (e.g., mice, rats) assessing the effects of a single bout of exercise on the metabolome have predominantly analysed tissues relative to biofluids. These biofluids including saliva, sweat and urine are not collected as easily and not available in sufficient volumes in small mammals such as rodents. Several metabolomics studies in rodents have analysed skeletal muscle following an acute bout of exercise. Building upon the results in human biofluids demonstrating differential responses to exercise depending on fitness level and performance, it has been shown in mouse hindlimb skeletal muscle that metabolic responses to exercise are dependent on the time of the day during which exercise is performed [118]. In a study from Sato *et al.*, mice were subjected to a treadmill running bout either in the early active phase or the early rest phase (equivalent to early morning and late evening in humans, respectively), and their hindlimb skeletal muscles were subjected to metabolomics analysis. These results suggested an increased glucose utilisation, along with increased use of other fuel sources such as lipids, amino acids and ketone bodies, when mice exercised in the early active compared to the early rest phase [118].

Furthermore, metabolomic analysis of both plasma and hindlimb skeletal muscle from rats with high and low running capacities has provided insights into substrate utilisation during and following an exhaustive running bout [119]. Following a 10-min run (i.e., exhaustion for

low-performance rats), only marginal increases in skeletal muscle long-chain acylcarnitines were observed in low-performance running rats, with very little changes observed in plasma FA. Conversely, high-performance rats exhibited significantly increased muscle levels of these long-chain acylcarnitines together with reduced plasma FA, indicating enhanced FA muscle uptake. Only following exhaustion in high-performance rats (45 min) were medium- and long-chain acylcarnitines increased both in muscle and blood. While increased long-chain acylcarnitines in muscle and blood potentially indicate that FA oxidation capacities were reached, increased circulating levels of medium-chain acylcarnitines likely indicate incomplete FA oxidation [100]. Decreased plasma and muscle levels of BCAAs in high- versus low-performance rats were also observed at 10 min, suggesting increased BCAA uptake and breakdown within the skeletal muscle. The data from this study overall showed enhanced FA and BCAA utilisation capacities in high- versus low-performance rats. While the increased FA oxidation capacities in high-performance rats are in line with findings from human marathon runners [93] described above, the amino acid results between these studies seem contradictory. However, the absence of significant changes in both plasma and muscle amino acids in low-performance rats may be due to the relatively short exercise bout (10 min) that may have been insufficient to induce protein breakdown as opposed to the 45-min run in high-performance rats. Of note, the mechanisms of exhaustion were similar between low and high capacity running rats, with exhaustion only being delayed in high capacity running rats.

In addition to rodents, tissue metabolomic responses to acute exercise have also been studied in other mammalian species. For instance, the skeletal muscle metabolome in horses was recently investigated after a single incremental exercise test to exhaustion, in both an untrained and trained status [120]. Only 31 of all identified metabolites were changed 3 h following the treadmill race in untrained horses, while 142 metabolites significantly changed in the trained horses. Regardless of training status, the predominant exercise-induced response

to acute exercise involved changes in amino acid (including BCAAs) and lipid metabolism. Nucleotides and xenometabolites also showed altered levels in horse skeletal muscle following the exercise bout. Given the increased number of metabolites significantly altered in the trained state, the authors suggested that interindividual variability can be attenuated by training. This may also reflect the enhanced ability of trained horses to run at higher intensities for a longer amount of time. However, it is important to note that post-exercise muscle biopsies were collected 3 and 24 h following the exercise test. Although food was only allowed after the 3-h post-exercise biopsy, the sample collection delay represents a limitation to this study that may have hindered observation of additional exercise-induced metabolite changes in both trained and untrained horses. Moreover, a noteworthy point raised by Zhang and colleagues [121] is that muscle biopsies do not allow distinction between extra- and intra-muscular metabolites. To do so, investigating skeletal muscle interstitial fluids is a promising, yet rarely practiced avenue in metabolomics research that has the potential to provide more accurate insights into mammalian muscle metabolism. For example, a recent study assessed both plasma and muscle interstitial fluids in rats following a short treadmill running bout at moderate intensity. Out of 299 detected metabolites, only 43% were common to both biofluids. Among the 204 metabolites changed by exercise, only 20% were shared, therefore underscoring the limited ability of circulating metabolites to reflect the full range of muscle metabolic changes induced by exercise [121]. Additional pilot data from human muscle interstitial fluid was also collected in this study and, in line with rat data, reported increased TCA cycle intermediates following exercise, possibly induced by increased FA oxidation. Likewise, increased levels of amino acids and markers of purine catabolism were observed, among others, following the exercise bout. Of note, differential FA responses were observed between rats and human data, potentially resulting from differences in sample collection timing. Taken together, these results warrant further mammalian metabolomics-based investigations in multiple tissues and/or

biofluids to potentially capture a more detailed molecular blueprint of acute exercise metabolism.

The liver, which is crucial to whole-body energy supply and maintenance of metabolic homeostasis during exercise, has also been studied using metabolomic approaches. In 2010, Huang and colleagues were the first to use metabolomics to investigate changes in liver metabolic profile induced by exhaustive treadmill running in rats [122]. Increased hepatic levels of xanthine, hypoxanthine, and creatinine—a degradation product of creatine point to increased energy conversion, while decreased hepatic levels of carbohydrates and lactate suggest glycogen depletion, to help meet exercise-induced energy requirements. Increased FA and ketone bodies further support an increased reliance on fat metabolism during prolonged exhaustive exercise. Additionally, this was accompanied by increased urea concentrations. Exhaustive exercise was associated with hepatic inflammation, as elevated levels of inflammatory precursors such as arachidonic, linoleic and oleic acids were detected and associated with the accumulation of macrophages detected by liver immunochemistry [122]. As previously discussed, Hu and colleagues who observed that FA (C6:0, C8:0) and TCA cycle intermediates (succinate and malate) were released by the exercising leg and taken up by the liver [101], conducted complementary analyses on liver transcriptome data obtained from mice following a 60-min treadmill running bout [123]. Findings indicated exercise-induced activation of HIF-, NRF2- and cAMP-dependent gene transcription, potentially indicating that metabolites released from the exercising muscle can also act as signalling molecules in the liver [101,123], although it cannot be excluded that activation of liver gene transcription may be driven by the liver's own amplified metabolism and signalling molecules. It was speculated that these circulating metabolites may be involved in metabolic adaptations to exercise, though it was acknowledged that further research is needed to validate this hypothesis [101]. Although inter-organ crosstalk during exercise is still overall poorly understood and requires further

investigations, it is important to note that feasibility of liver metabolomic investigations in humans is very limited, given the invasiveness of liver biopsy sampling. Assessing hepato-splanchnic fluxes by collecting blood from hepatic veins and peripheral arteries may help partially address this issue in future human studies [101,124].

2.4.2. Lipidomic Analyses of Acute Exercise

2.4.2.1. Humans

2.4.2.1.1. Blood Analyses

The release of vasoactive metabolites from the working skeletal muscle and vascular endothelium during exercise is well documented [125]. These numerous vasoactive substances comprise lipid species, including epoxides (also named epoxy FA) derived from arachidonic acid (AA) such as 5,6-, 8,9-, 11,12-, 14,15- epoxyeicosatrienoic acid (EET) isomers, are produced by the action of cytochrome P450 (CYP) mono-oxygenase (**Figure 2.4**) [126]. EETs can in turn induce hyperpolarisation of smooth muscle cells, leading to vascular relaxation, which has been suggested to contribute to enhanced skeletal muscle blood flow during exercise [127]. Recently, it was demonstrated that vasoactive lipids derived from the n-3 and n-6 polyunsaturated FA (PUFA) and metabolised by CYP were also released into the bloodstream following an acute maximal treadmill test using the Bruce protocol [128] in healthy adults [126]; and 12,13- epoxyoctadecenoic acids (12,13-EpOME) an epoxide originating from linoleic acid (LA)—exhibited significantly increased levels in plasma following the maximal exercise bout. Epoxides can be further metabolised to diols by soluble epoxide hydrolase (sEH) (**Figure 2.4**).

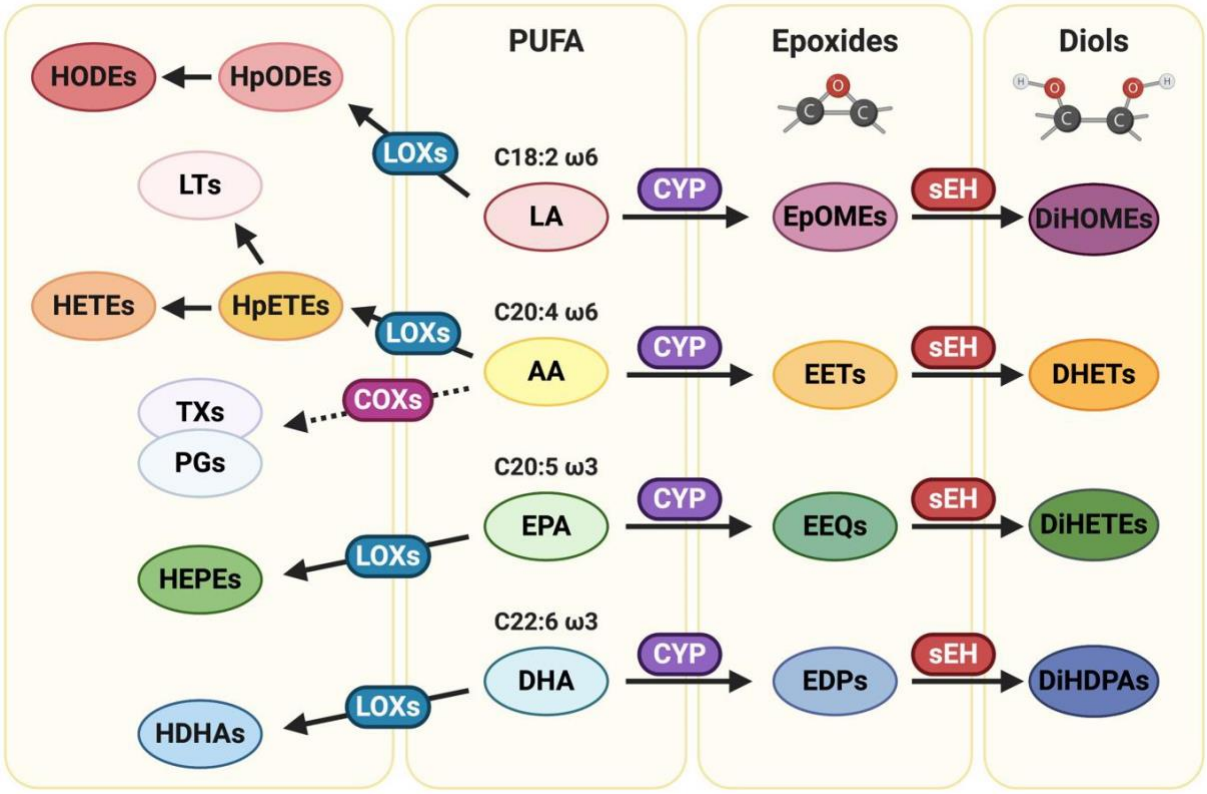

Figure 2.4 – Lipid mediators derived from polyunsaturated fatty acids (PUFA). Depending on the intervening enzymes, different lipid mediators can be generated from a given PUFA. Cytochrome P450 (CYP) mono-oxygenase converts PUFA (LA: linoleic acid; AA: arachidonic acid; EPA: eicosapentaenoic acid; and DHA: docosahexaenoic acid) to their respective epoxides (EpOMEs: epoxyoctadecenoic acids; EETs: epoxyeicosatrienoic acids; EEQs: epoxyeicosatetraenoic acids; EDPs: epoxydocosapentaenoic acids) which exist in different regioisomers. These epoxide isomers are in turn converted to their respective diols (DiHOMEs: dihydroxyctadecenoic acids; DHETs: dihydroxyeicosatrienoic acids; DiHETEs: dihydroxyeicosatetraenoic acids; DiHDPAs: dihydroxydocosapentaenoic acids) under the action of the soluble epoxide hydrolase (sEH). Conversely, PUFA can also be metabolised by lipoxygenases (LOXs) which comprise three isoforms (5-, 12- and 15-LOX). LOXs are responsible for generating hydroxyperoxy-octadecadienoic acids (HpODEs), further metabolised to hydroxy-octadecadienoic acids (HODEs), from LA. If the substrate is EPA or DHA, hydroxyEPAs (HEPEs) and hydroxyDHAs (HDHAs) will be respectively generated via LOXs. From AA, LOXs can also produce hydroperoxyeicosatetraenoic acids (HpETEs), subsequently converted to either hydroxyeicosatetraenoic acids (HETEs) or leukotrienes (LTs) from AA. Finally, COX enzymes, which exist in two isoforms (COX-1 and COX-2) are responsible for the production of prostaglandins (PGs) and thromboxanes (TXs) from AA. Dotted arrow indicates indirect reaction.

As such, increased plasma levels of diols were reported post-exercise; 5,6-dihydroxyeicosatrienoic acids (5,6-DHET), derived from AA; as well as 5,6- and 17,18-

dihydroxyeicosatetraenoic acids (5,6- and 17,18-DiHETE), derived from EPA [126]. Diols such as DHETs, although initially thought to be inactivation products of EETs, also exhibit vasodilation properties [129], potentially counteracting vasoconstrictive substances concurrently released during exercise. In contrast to EETs and DHETs, EpOMEs (especially 12,13-EpOME) have been shown to have cardiac depressant and vasoconstrictive properties [130]. The physiological roles of 5,6- and 17,18-DiHETE are largely uncharacterised, although its upstream epoxide 17,18-epoxyeicosatetraenoic acid (17,18-EEQ) is another vasodilator [131].

While no significant changes in plasma levels of other detected epoxides and diols were observed following maximal exercise in humans, Stanford and colleagues recently showed substantially increased levels of circulating 12,13-dihydroxyoctadecanoic acid (12,13-DiHOME)—the downstream product of 12,13-EpOME—after a moderate-intensity exercise bout (cycling and running at 70 and 75% VO_2 max, respectively) in healthy humans, regardless of sex, age and physical activity level [132]. In this same study, the authors also showed that exercise increases circulating 12,13-DiHOME in male mice and that this increase was negated by the surgical removal of brown adipose tissue (BAT), indicating that in mice, 12,13-DiHOME is released from BAT during exercise. Furthermore, mice injected with 12,13-DiHOME had higher skeletal muscle FA uptake compared to mice injected with vehicle control, and mouse myotubes incubated with 12,13-DiHOME displayed increased FA uptake and oxidation [132]. These lipidomic findings highlight a crosstalk between adipose tissue and skeletal muscle during acute exercise and identify potential factors that may contribute to some metabolic health benefits of exercise [132]. However, a wide range of functions have been attributed to 12,13-DiHOME including detrimental effects on both cardiac [133] and mitochondrial function [134]. The biological meaning of increased DiHOMEs thus remains unclear, warranting further investigation.

Increased plasma levels of 12,13-DiHOME and other lipid mediators have also been observed in plasma collected from trained male cyclists. In this study, cyclists completed a 75-km cycling bout at moderate intensity (~70% of VO_2 max) [135]. Increases in plasma concentrations of 9,10-DiHOME as well as 9- and 13-hydroxy-octadecadienoic acid (9- and 13-HODE) were observed. HODEs are peroxidation products of the n-6 LA (**Figure 2.4**) that have been linked to oxidative stress, inflammation, physiological and pathological states including atherosclerosis [136]. Although not associated with increased inflammation markers in this study, 9- and 13-HODE were significantly correlated with F_2-isoprostanes, indicators of oxidative stress (although in much lower abundance), supporting the inclusion of 9- and 13-HODE as oxidative stress biomarkers [135].

Gollash and colleagues have helped expand the understanding of metabolic responses to acute maximal aerobic exercise by investigating changes in lipid profiles from red blood cells (RBC), a constituent of blood largely overlooked in metabolomic/lipidomic studies [137]. RBC represents a reservoir of lipid species including epoxides which can regulate vascular capacity, as previously mentioned. Following maximal acute exercise to exhaustion (see [126]) in healthy non trained adults, venous RBC exhibited increased levels of epoxides including 9,10- and 12,13-EpOME; 5,6-EET, 11,12-EET and 14,15-EET; but also epoxides derived from docosahexaenoic acid (DHA), 16,17- and 19,20- epoxydocosapentaenoic acids (16,17- and 19,20-EDP). These two DHA-derived epoxides have shown vasodilating and cardioprotective properties [138]. All the aforementioned epoxide mediators are generated by CYP mono-oxygenase. In contrast, no changes in lipid mediators generated by lipoxygenase (LOX) and cyclooxygenase (COX) were observed (**Figure 2.4**). This suggests that CYP mono-oxygenase-derived epoxides accumulate in RBCs and may, when released, contribute to cardiovascular responses to acute exhaustive exercise [137]. However, no changes in RBC levels of the 20 quantified FA were found following the same exercise protocol [139]. The omega-3 quotient—

the percentage of EPA + DHA in FA from RBC membranes—was also unchanged. A low omega-3 quotient (or index) represents an independent risk factor for cardiovascular diseases and increased mortality [140,141]. While short duration maximal exercise was not able to elicit immediate changes in plasma and RBC FA levels (including omega-3 quotient), RBC levels of lauric acid (C12:0) significantly decreased between exhaustion and recovery, 10 min later. Lauric acid may therefore regulate cardiovascular and metabolic functions, and further research is warranted to address this possibility [139].

Efforts to characterise lipid mediators derived from COX, LOX and CYP pathways responding to acute resistance exercise have also been performed [142]. Using targeted lipidomics, 87 lipid species were detected in the serum of 16 young men who undertook a single session of high intensity resistance exercise. The resistance exercise protocol consisted of a circuit of three sets of 8–10 repetitions of leg press, bar squats and knee extension performed at 80% of individual one-repetition maximum (1-RM). Serum was collected before exercise and every 30 min within three hours post-exercise, and then at 24 h of recovery. A wide array of lipid mediators derived from COX, LOX, and CYP pathways were dynamically changed following exercise, including AA-derived metabolites such as prostaglandins (PGs), thromboxanes (TXs) and leukotrienes (LTs). PGs and TXs are formed under the action of COX enzymes while LTs are produced via LOX enzymes (**Figure 2.4**). TXs comprise TXA_2 and its metabolites TXB_2 and 12-hydroxyheptadecatrienoic acid (12S HHTrE). TXB_2 and 12S HHTrE are considered biomarkers of TXA_2 biosynthesis and are more easily detected since TXA_2 is rapidly degraded into TXB_2 or 12S HHTrE [143]. PGs comprise four primary compounds: PGD_2, PGE_2, $PGF_{2\alpha}$ and PGI_2. Likewise, PGs are also rapidly converted to primary 6 or 15-keto and secondary 13,14-dihydro-15-keto metabolites. Next, LTs are composed of LTA_4 and derivatives including LTB_4 and anti-inflammatory/pro-resolving lipoxins LXA_4 and LXB_4.

Early resistance exercise responses (0–3 h of recovery following exercise) comprised increased levels of (1) TXB_2 and 12S HHTrE; (2) PGD_2, PGE_2 and its derivative 15-keto PGE 2, 15-keto $PGF_{2\alpha}$, 6-keto $PGF_{1\alpha}$; (3) LTB_4 and derivatives LXA_4, LXB_4; (4) pro-inflammatory AA-derived 12-hydroxyeicosatetraenoic acid (12-HETE) and its by-product tetranor 12HETE, along with the anti-inflammatory 15-HETE. Early responses to resistance exercise were also marked with immediate increases in EPA-derived resolvins (RvE1) and DHA-derived 10(S),17(S)-DiHDHA (protectin D1), which are generated by LOX enzymes and exhibit anti-inflammatory properties. In contrast, LOX-mediated LA derivatives such as 9- and 13-HODE and their degradation products 9- and 13-oxo-octadecadienoic acids (9- and 13-oxo-ODE) tended to decrease in the first half hour following exercise before significantly increasing (compared to 30 min post-exercise) and peaking at 2–3 h of recovery. Similarly, CYP-mediated LA metabolite 9,10-EpOME and downstream product 9,10-DiHOME were also elevated at 2–3 h of recovery. Finally, elevations in 11,12- and 14,15-DHET-CYP-mediated metabolites of AA-were also found in the early recovery phase. Most lipid metabolites returned to basal levels within 24 h post exercise, except for a few metabolites which peaked (13,14-dihydro-15-keto PGE2, 6-keto $PGF_{1\alpha}$, 15-HETE and by-product 15-oxoETE, and protectin D1) or remained significantly elevated (12(S) HHTrE). These findings pinpoint the activation of pro-inflammatory and pro-resolving pathways following acute resistance exercise, both in the early and later stages of exercise [142].

In addition to FA-derived lipid mediators involved in pro- and anti-inflammatory/pro-resolving pathways induced by acute exercise, lipidomics has also helped recently uncover other lipid species belonging to other categories and classes and playing potential roles in exercise metabolism. Indeed, the lipidomics arm of Contrepois and colleagues' work [47] revealed large increases in circulating complex lipids within the early recovery phase (2 min post treadmill run), with a rapid return to pre-exercise levels (15–30 min post). These complex

lipids included 23 phosphatidylcholines, 20 cholesteryl esters, 15 triacylglycerols (TAGs), ten diacylglycerols (DAGs), nine ceramides and eight sphingomyelins. In addition, exercise-induced changes in TAGs appeared to depend on carbon number and unsaturation level. For instance, while plasma concentrations of most TAGs (those with shorter saturated FA in particular) decreased at 30 and 60 min of recovery, those which rapidly increased postexercise (within 2 min) mostly comprised long-chain PUFA including AA, EPA and DHA. Together with the observed early increases in ceramides and sphingomyelins, increased long-chain PUFA suggest activation of both pro- and anti-inflammatory pathways, as demonstrated in previous work [142,144]. In contrast, TAGs with shorter saturated FA may be used as a preferential substrate for energy conversion [47].

2.4.2.1.2. Tissue Analyses

Similar to the blood analyses previously described, further lipidomics analyses of skeletal muscle have uncovered inflammatory responses to acute resistance exercise. Lipidomic analyses of muscle biopsies from young active men during a single resistance exercise session indicated augmented inflammatory response in the early recovery phase [144]. Two hours post-exercise, substantial increases in skeletal muscle concentrations of various lipid mediators were observed, including COX-mediated TXs and PGs, derived from AA (**Figure 2.4**). The recovery period was also marked by increased intramuscular levels of species from the LOX pathways, including derivatives from EPA: 12-hydroxyEPA (12HEPE); DHA: 7- and 14-hydroxyDHA (7- and 14-HDHA); and AA: 5- and 12- HETE, and LTs. Finally, lipid mediators from the CYP pathway and derived from both AA (5,6-EET; 11,12- and 14,15-DHET) and LA (9,10- and 12,13-DiHOME) were also increased at this timepoint. As mentioned earlier, while a wide range of AA-derived mediators produced through COX and LOX pathways (e.g., TXs, PGs, LTs, 12-HETE) stimulate acute inflammation, several lipid mediators metabolised through the LOX and CYP pathways, (e.g., AA-derived 5-HETE, EETs

and DHETs, DHA-derived HDHAs) are potential precursors of pro-resolving mediators that inhibit inflammatory signalling. From this study and consistent with previous work from the same group conducted in serum [142], both pro-inflammatory lipid mediators and lipid markers of pro-resolving mediator biosynthesis are stimulated by resistance exercise simultaneously in skeletal muscle, 2 h post-exercise [144].

Lipidomic responses to acute resistance exercise are however influenced by an individual's age. Applying targeted lipidomics to skeletal muscle from both young (~22 years old) and older (~74 years old) healthy men who undertook a single resistance exercise bout, Rivas *et al.* observed significant differences in skeletal muscle ceramides between the two cohorts [145]. Ceramides are a subclass of sphingolipids that have emerged as potential modulators of diseases associated with lipotoxicity including IR, type 2 diabetes and cardiovascular disease [146]. Ceramides are also well-recognised activators of proinflammatory signalling [147]. In this study, a relationship was found between intramuscular ceramide levels and impaired exercise-induced anabolic signalling occurring in older men. Older men had significantly higher palmitic (C16:0) and arachidic (C20:0) ceramides levels within skeletal muscle, and a negative correlation between intramuscular C16:0 ceramide and leg lean mass was also observed. Next, blunted anabolic signalling following the exercise bout in older men was associated with increased activation of pro-inflammatory signalling compared to young men. Intramuscular levels of specific ceramides may therefore negatively impact anabolic signalling following a single bout of resistance exercise by promoting inflammation [145].

2.4.2.2. Other Mammals

2.4.2.2.1. Blood Analyses

In other mammals, to date very few studies have been performed to investigate the effects of acute exercise on the blood lipidome. To our knowledge, the only study aimed to

specifically characterise the lipidome following acute exercise in mammals to date is a pilot study performed in Thoroughbred horses [148]. Four horses (3 males and 1 female) were subjected to a supramaximal (115% VO_2 max) treadmill running bout to exhaustion. Of the 933 plasma lipid species detected, 130 were known lipids. Despite the lack of statistical power in this pilot study, 13 lipid species were changed following exercise, including seven FA and six phospholipids; three phosphatidylcholines (PCs), one lysophosphatidylcholine (LPC) and two sphingolipids (SMs). Although not reaching statistical significance, five TAGs decreased by more than 20% following exercise. While six identified phospholipids (i.e., PC (P-34:1), (P-36:2), (P-36:4); LPC (18:0); SM (d36:1) and (d42:2)), along with several FA such as LA, LNA (C18:3), and the n-6 11,14-eicosadienoic acid (C20:2), were increased by supramaximal exercise, the remaining FA (C12:0, C14:0, C17:0 and C20:0) were decreased post-exercise. The increase in plasma unsaturated FA may reflect lipolysis in the adipose tissue, reported to contain a higher ratio of unsaturated/saturated TAGs compared to plasma FA [149]. Phospholipids, which also increased immediately post-exercise, progressively decreased over time. As PCs and SMs are major components of cell membranes, the current findings may be explained by the increased cell membrane turnover due to exercise-induced lipolysis and membrane damage. Phospholipids can then be mobilised as energy substrates or for repair of cell membranes damaged during exercise [150,151]. Although this pilot study has important limitations, supramaximal exercise in Thoroughbred horses is shown to affect distinct lipid categories including FA and more complex lipids such as TAGs, SMs and PCs. In addition, these pilot findings will be useful for informing power analyses and sample size requirements in future lipidomic studies [148].

2.4.2.2.2. Tissue Analyses

As stated previously, the feasibility of investigating liver biopsy responses to exercise in humans is very low; therefore, utilizing other mammalian species has helped gain a deeper

understanding of tissue lipidomic responses to acute exercise. In 2010, Hu and colleagues were one of the first to conduct a lipidomic study to uncover molecular responses to acute treadmill running exercise in mouse liver [152]. Among 115 quantified lipid species, PCs and TAGs were the most abundant lipid classes. Almost all detected TAGs tended to increase in the liver immediately post-exercise compared to control rested mice, though statistical significance was not reached. In contrast, a clear difference in hepatic lipid profile was observed following three hours of recovery. The 21 lipid species mostly responsible for lipid profile changes were predominantly TAGs (17), with the remaining lipids being composed of three PCs and one LPC. While all four choline phospholipids decreased (PCs and LPC), all hepatic TAGs increased three hours post-exercise. The significantly increased lipid species included polyunsaturated TAGs (50:3; 54:5; 54:6; 54:7; 56:4; 58:6; and 58:10) and decreased lipids included PCs (36:1; 38:3; 40:4) and DAG (34:1). Although increased TAG concentrations in liver may have been due to refeeding post-exercise (i.e., mice had free access to food during the first two hours of recovery), the authors tested this hypothesis via a fasting/refeeding experiment and observed similar TAG levels in refed mice compared to the rested control mice, while fasted mice had significantly increased hepatic TAGs. The authors therefore concluded that increased hepatic TAGs following three hours of recovery were unlikely caused by food intake. It was rather proposed that the accumulation of TAGs in the liver may result from the large elevation in plasma FA following exercise-induced lipolysis, which may exceed oxidative capacities of the working muscle. The FA in excess may instead be delivered to the liver for transient storage. As opposed to liver, skeletal muscle total TAG content significantly declined immediately post-exercise, suggesting enhanced lipolysis for subsequent FA oxidation [152].

More recently, this same group used a similar endurance exercise protocol to study the lipidomic responses to acute exercise in both liver and hindlimb skeletal muscles (gastrocnemius and soleus) in mice [153]. Their targeted lipidomics data revealed that, while

most lipid species detected in mouse liver were unchanged by the single exercise bout, several phospholipids including five LPCs (16:0; 18:2; 20:4; 22:5 and 22:6), four lysophosphatidylethanolamines (LPEs) (16:0; 18:0; 18:1 and 20:4) and two plasmalogen phosphoethanolamines (PE-P) (P-38:4 and P-40:4) increased. The reasons for most of these changes remain to be elucidated. However, since plasmalogens are generally secreted by the liver once synthesised [154], increased hepatic levels of plasmalogens may indicate inhibited secretion with exercise. Free carnitine, acetylcarnitine and 39 acylcarnitines with carbon chain length ranging from 3–20 were also detected in liver, gastrocnemius and soleus muscles. Liver exhibited heightened concentrations of free and total carnitine following treadmill exercise, while acetylcarnitine content was reduced. The detected acylcarnitines were unchanged by the acute exercise bout. Conversely, acetylcarnitine, short-chain acylcarnitines and hydroxy-acylcarnitines were increased following exercise in both skeletal muscles, with acetylcarnitine and hydroxy-acylcarnitines showing much greater increases in soleus (61%) compared to gastrocnemius (15%) muscle. While hydroxycarnitines are intermediates of incomplete FA oxidation, acetylcarnitine is the end-product of the catabolism of all fuels including FA, pyruvate and several amino acids [100]. Higher levels of both acetylcarnitine and hydroxy-acylcarnitines following acute exercise can therefore be explained by the higher FA oxidation rate [155] and the greater carnitine uptake capacities in soleus compared to gastrocnemius muscle [156]. Next, the unchanged levels of medium- and long-chain acylcarnitines after the treadmill run may indicate that this exercise protocol was not sufficiently intense to affect muscle content of these acylcarnitines. In contrast to liver, free and total carnitine in both muscles were not affected by exercise. Increased hepatic concentrations of free and total carnitine upon acute exercise were likely due to enhanced uptake by the liver since the gene expression of the carnitine transporter Slc22a5/OCTN2 was upregulated [153]. Finally, isotope-tracing of FA and acylcarnitines showed that, consistent with previous findings [152], excess

circulating FA are taken up by the liver and incorporated into TAGs and phospholipids during recovery, highlighting tissue-specific differences in FA uptake [153].

The extensive exercise metabolomics and lipidomics literature from the past decade discussed above has helped build a strong foundation to continue expanding the molecular landscape of exercise in the next decade. **Figure 2.5** summarises the current exercise molecular landscape by overviewing the dynamic changes in metabolites and lipids that occur in response to acute aerobic and resistance exercise across species (i.e., humans and other mammals) and biological systems (i.e., blood, other biofluids, liver and skeletal muscle).

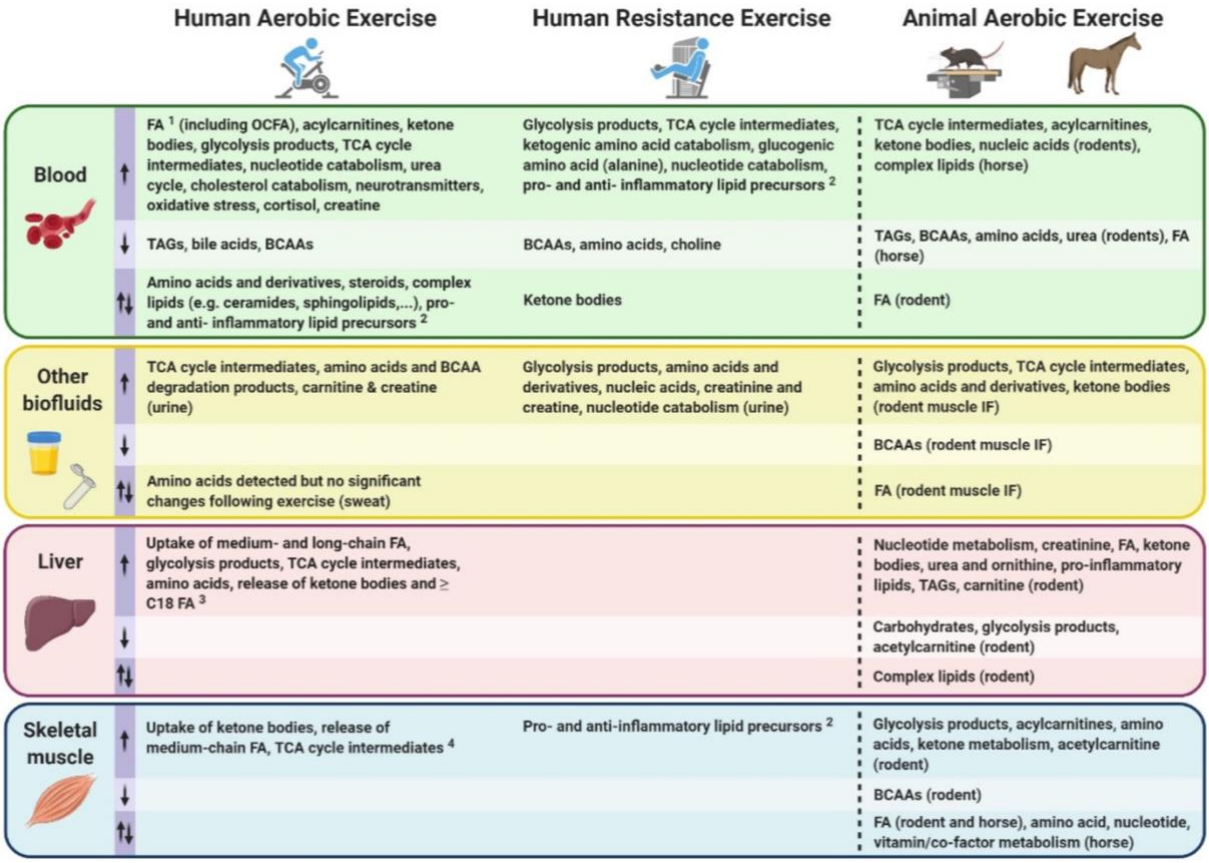

Figure 2.5 – Summary of the current exercise molecular landscape of metabolomic and lipidomic findings discussed from the past decade. Dynamic changes in metabolites and lipids (i.e., increased, decreased, or shown to be changed in both directions) occurring in response to acute aerobic and resistance exercise are summarised across various biological systems (i.e., blood and other biofluids including urine and sweat; and tissues such as liver and skeletal muscle) in humans and other mammalian species. This figure focuses on early responses (0–30 min) following an acute exercise bout except for data collected from horses within the first three hours post-exercise. Metabolomic responses can therefore show different directionality based on timing and exercise variables, as mentioned previously. BCAAs: branched-chain amino acids, FA: fatty acids, IF: interstitial fluid, OCFA: odd-chain fatty acids, TAGs: triacylglycerols, TCA: tricarboxylic acid. [1] Changes in FA levels post-exercise may depend on carbon chain length and although circulating levels of most FA have been reported to increase following an acute exercise bout, post-exercise decreases in some FA chain lengths (e.g., C20 to C24) have also been observed. [2] Directionality of specific lipid mediators in human blood and skeletal muscle are not detailed in this figure, and responses to exercise may vary depending on the specific lipid mediators within their broader classes. Refer to supplementary **Table 2.2** for information regarding the directionality of specific pro- and anti-inflammatory lipid precursors following exercise. The metabolite directionalities of human liver [3] and human skeletal muscle [4] depicted in this figure are derived from data analysing hepato-splanchnic bed and arterio-venous differences, respectively, rather than from tissue biopsies. Up arrow: increase; down arrow: decrease; bidirectional arrow: both increase and decrease.

2.5. Current Challenges and Remaining Knowledge Gaps to Continue Expanding Exercise's Molecular Landscape

2.5.1. Metabolite Identification and Annotation

To continue expanding the exercise molecular landscape in the next decade, metabolite and lipid identification/annotation still represents a main challenge and bottleneck of untargeted metabolomics and lipidomics approaches, in contrast to protein identification in proteomics, for example. Whereas proteins are composed of a finite and more manageable combination of different amino acids that can be sequenced by matching experimental peptides against in silico fragmentation spectra, metabolites (including lipid species) are a highly heterogenous group of small molecules resulting from countless different chemical structures and atomic combinations, although predominantly composed of the elements C, H, N, O, P and S [157]. Despite recent technological advances in analytical instrumentation that have enabled rapid

and simultaneous detection of thousands of metabolites from very low volumes of biological samples, a much smaller portion of these metabolites can remain after stringent data processing and cleaning processes prior to any attempt at identification/annotation [158]. These data processing and cleaning steps are essential to generate more high-confidence metabolomic and lipidomic datasets, but the overall trade-off is reduced metabolite coverage.

Next, metabolites and lipid features (such as mass-to-charge ratios and retention times) that meet quality control criteria can still correspond to numerous molecular structures. Their identification—a term used when the highest level of confidence is reached; level 1—or annotation (lower level of confidence in metabolite characterisation, levels 2 to 3) [71] notably depends on an existing reference match in currently available databases, and preferably an in-house generated database. This is important, as the vast majority of features currently fail to match any metabolite from these databases and are therefore assigned as "unknowns". These unknowns may be true unknowns (i.e., compounds for which no chemical structure, name, origin, and biological function has been described to date), but some compounds may however be assigned as unknowns because the reference is missing from the available databases. Most existing databases are still largely incomplete, and in the case of true unknown metabolites and/or lipids, extensive efforts in analytical chemistry are required to characterise their molecular structure. However, these characterisation efforts are rarely undertaken given their challenging and time-consuming nature [159]. As a result, unknowns within datasets are often disregarded, and attention is instead focused on only putatively named metabolites. In the case of compounds that are matched against a database, additional information is necessary to accurately identify and validate a single candidate since basic features such as retention time and m/z may have multiple candidates. MS^2 (and sometimes MS^n) is required to reach the highest level of confidence, as fragmentation patterns help elucidate molecular structures and distinguish metabolites with similar m/z and retention times by matching them with

fragmentation patterns of authentic chemical standards within metabolite libraries. Nevertheless, most libraries are still largely incomplete, therefore the number of authentic chemical standards available represents a current limiting factor to metabolite identification of the broader metabolome. Additionally, compounds can exhibit different levels of confidence in identification/annotation, making data integration and interpretation even more challenging since most commonly used dedicated tools (e.g., KEGG, MetaboAnalyst 3.0) require metabolite identification (i.e., level 1) to integrate the data into biological context [157].

Efforts to expand libraries with authentic standards in the next decade will help exploit the full potential of untargeted metabolomics by yielding a much higher coverage of unequivocally identified metabolites. MS^2 is however more time- and resource-consuming. In addition, validation of metabolite identification/annotation still requires extensive human intervention, since this step is usually performed manually and requires expertise in chemical structure and biochemistry. This hurdle may become a growing issue as the number of metabolites to manually validate increases with the expansion of metabolite libraries in the years to come. It is also important to note that MS^2 is not always sufficient to distinguish structural isomers—compounds with identical molecular formula but different chemical bond arrangements between atoms—and stereoisomers—compounds with identical formula and chemical bond arrangements but different spatial orientation of groups in the molecule [58,160,161]. In this case, additional separation methods (i.e., TIMS) in conjunction with MS^n may be required to validate the identification of a metabolite or lipid species. Of note, NMR represents a quicker and cheaper alternative (in terms of cost per sample) to MS^n with regard to structural elucidation [162].

2.5.2. Human Interindividual Variability and Potential Confounding Factors

One of the main challenges encountered in human exercise studies is the high interindividual variability in genetic background, sex, age, lifestyle, environmental exposure and nutritional and health status (**Figure 2.6**), which represent important confounding factors that are difficult to screen and control for in an experimental setting [22].

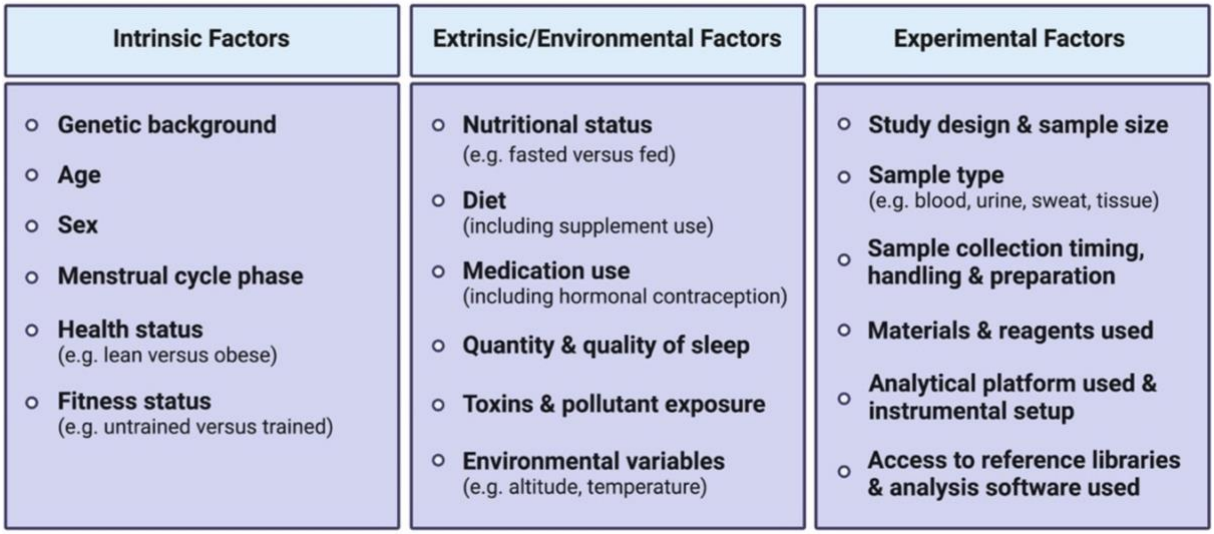

Figure 2.6 – Summary of some of the main factors responsible for variance between metabolomics/lipidomics studies, including intrinsic, extrinsic/environmental factors and experimental factors.

To overcome these challenges and account for the potential high interindividual variability amongst human participants, large-scale epidemiological studies are required [163]. Recruiting and analysing such large numbers of individuals for a given experiment will be challenging (i.e., the appropriate sample size is variable depending on effect size, but hundreds of participants are often needed in human studies), as human exercise studies are usually performed using only small sample sizes (i.e., often less than one hundred). It should also be noted that overcoming high interindividual variability may be possible in small study groups through meticulous control of the above-mentioned confounding factors although this may lead to increased cost, time and constraints. Parallel exercise interventions using animal model

systems is a complementary approach in which both genetic background and environment can be controlled to a greater extent compared to human cohorts.

Human metabolomics studies to investigate the molecular mechanisms of acute exercise are however starting to be performed at a larger scale. Indeed, a recent study investigated blood metabolic profiles of over 400 middle-aged adults, uncovering metabolic signatures associated with cardiometabolic health [164]. In addition, an ongoing initiative in the USA called The Molecular Transducers of Physical Activity Consortium (MoTrPAC) will address some of these remaining challenges in the decade ahead by examining the effects of acute and chronic exercise (including both endurance and resistance exercise) across a wide range of biological systems. This multi-site MoTrPAC initiative aims to analyse a large number of samples across pediatric, sedentary and highly active adult male and female human populations and complementary animal models using multi-omic approaches (including metabolomics/lipidomics), eventually establishing a comprehensive molecular map of exercise that will be made publicly available through the MoTrPAC Data Hub: https://motrpac-data.org [165,166].

Metabolomics/lipidomics studies in the fields of sport and exercise physiology to date have mostly been conducted using only male participants, as highlighted in a recent human exercise metabolomics review [167], with only a few recent studies investigating acute exercise metabolomic/lipidomic patterns in obese and insulin resistant women [100,168,169]. The impacts of sex and hormonal variations (i.e., menstrual cycle phases) in females on exercise-induced metabolomic and lipidomic responses are therefore poorly understood, and more studies in female participants are warranted to begin to decipher these differences. These studies should take into account and report the use of hormonal contraception (including type of hormonal contraception used) in addition to the menstrual cycle phase during which the exercise is performed. This reporting is important as substantial differences in metabolic patterns are

observed depending on menstrual cycle phase [170]. Likewise, aging is also associated with alterations in exercise-induced metabolomic responses. Therefore, continued efforts to identify new exercise-regulated biomarkers associated with aging and age-related pathologies such as muscle loss in sarcopenia may help personalise exercise interventions to prevent, delay or treat these age-related disorders [31]. As highlighted in previous sections, sampling certain tissues such as liver, which are relatively inaccessible in human exercise studies, can be more readily obtained using animal model systems. Since exercise-induced adaptations do not just involve changes in circulating, muscle and liver metabolites/lipids, animal models also provide more access to less-studied tissues (e.g., heart, brain) involved in the whole-body molecular metabolic responses to exercise.

2.5.3. Comparison and Reproducibility of Results Between Studies

Another major challenge in exercise-related metabolomics and lipidomics studies is the ability to directly compare studies between independent studies and research groups. The current lack of reproducibility and the common discrepancies observed within a given research field may in part be attributed to intrinsic and extrinsic/environmental confounding factors described in the previous section, as well as experimental factors (see **Figure 2.6**). Study designs should report or control for these factors (e.g., reporting dietary intake and timing and/or providing standardised meals at set times). Included in these experimental factors is the use of a wide variety of analytical platforms and data acquisition modes. Indeed, each analytical platform and detection mode is associated with specific sample handling, metabolite extraction and data acquisition/processing protocols and requirements. Although representing a valuable means to broaden metabolite coverage, these differences in instrumentation and analytical workflows contribute to substantial inter-study discrepancies that make reproducibility and data comparison between independent research groups a challenging and tedious process. Despite the fact that instrumentation-induced variability between studies cannot likely be

solved due to differences in equipment between research facilities, harmonisation in sample handling and data acquisition/processing protocols, along with standardised metabolite reporting are necessary to help overcome some inter-study discrepancies. This will allow more confident inter-study dataset comparisons, and subsequently improved data interpretation and biological insights. In 2007, the MSI proposed a consensus regarding minimum reporting standards for metabolite identification [71]. Similarly, the LSI also provides guidelines for lipid species annotation [171,172]. However, efforts to enforce adequate use and constant updates by the metabolomics community are necessary since, up until recently, the use of these reporting standards allowing investigators to define the level of compound identification/annotation confidence was suggested to be relatively low [161].

2.5.4. Bioinformatic Resources

To deal with the complexity and heterogeneity of metabolomics and lipidomics datasets (e.g., wide concentration range suggested to be spread over 12 orders of magnitude [159]) and the large amount of data generated by untargeted approaches, robust computational and bioinformatics resources and expertise are required. This is critical for data processing, analysis, interpretation and visualisation. Numerous open-source and commercial data processing tools are available, but the overall lack of uniformity among these tools can also hinder reproducibility of findings between independent studies and research groups. Each tool has its own characteristics, but comparison of the performances of different tools has rarely been performed. Although software packages such as XCMS Online, SIEVE™ and Compound Discoverer™ provide reproducible and consistent data processing results, they have shown differences in metabolite selection, for example as candidate biomarkers for Alzheimer's Disease [173]. Therefore, variations in data analysis among these different software packages should be carefully considered, and ideally systematic comparison of all packages utilised in untargeted metabolomics/lipidomics should be performed to help maximise data confidence,

consistency in data handling, and reliability and reproducibility of biological findings. Alternatively, utilizing multiple software packages for data handling and only considering overlapping compounds for subsequent analysis may help reduce false positive and false negative compounds in datasets [173]. In addition, data analysis code should be provided as open access, as lack of transparency and reporting standards has led to widespread concerns in the reproducibility and integrity of results. Metabolomics researchers are encouraged to share their resources to provide adequate evidence of reproducibility. Collaborative cloud computing and Jupyter Notebooks are becoming popular amongst many metabolomics research groups and seem to be favoured, as they provide added flexibility when compared to many of the online data repositories [174]. Metabolomics users are encouraged to use open-source platforms and adopt the FAIR data principles (Findable, Accessible, Interoperable, and Reusable) [175], promoting the use of open data formats, online spectral libraries and data reproducibility.

2.6. Future Directions and Potential Value for Human Performance and Exercise Metabolic Health Benefits

Untargeted metabolomics/lipidomics is a hypothesis generating method and as such, future work should also focus on following up on these generated hypotheses, notably by using targeted approaches to validate findings and provide more quantitative insight (i.e., absolute metabolite/lipid concentrations) into exercise-regulated metabolites/lipids and biochemical pathways. Although metabolite and lipid concentrations provided by these targeted approaches are crucial to enhancing the measurement accuracy of exercise-induced metabolite changes, they alone only provide a snapshot of metabolic reactions that have just occurred. Therefore, complementary analyses such as metabolic flux analysis, also called fluxomics—a method that combines stable isotope tracing of metabolites with MS or NMR spectroscopy—help depict

metabolic reaction capacities, therefore allowing more mechanistic insight into the dynamics of molecular metabolic reactions that may explain, at least partially, observed differences in metabolite concentrations between and/or within individuals over a certain time or exercise intervention [176]. In addition, the implementation of more multi-omics approaches in addition to metabolomics/lipidomics will enable researchers to gain deeper understanding of the complexity and interconnected nature of genetic, epigenetic, transcriptional, protein and post-translational networks underlying metabolomic responses to exercise [31]. Finally, repeat sampling (i.e., longitudinal tracking) is required to understand individuals at the systems level, and systems biology approaches will help revolutionise the study of exercise physiology. Moving from the traditional reactive approach, where an individual may experience fatigue through overtraining, or fail to respond to a bout of exercise conditioning, the emergence of systems biology will provide the ability to predict when an occurrence will occur. This in turn will facilitate more personalised medicine. Personalised medicine or P4 medicine (Predictive, Preventive, Personalised and Participatory) can provide new approaches for: developing personalised treatment strategies [177] that may include personalised training interventions; deepen our understanding of physiological processes; and ultimately expand our knowledge of the health continuum.

With respect to compound identification, the numerous and constantly evolving technologies in the metabolomics and lipidomics fields also provide tremendous potential for metabolomics and exercise research communities in the next decade. For example, the combination of IMS with chromatography and MS methods will help increase metabolite identification capacity. IMS-MS instruments are now available and implementation of IMS to current analytical platforms used in the field of exercise will help improve coverage of identified metabolites, therefore expanding capacity to map molecular responses to exercise. Likewise, the implementation of multidimensional approaches—where several separation

methods are combined into a single analysis [58] to enhance compound separation and structure characterisation—are expected to lead to substantial improvements in compound identification capacity in the next decade.

Advancement in technologies will also aid how omics research of human exercise and athletic performance will be taken from the "bench and into the community." Considerable interest in the use of dried blood spots (DBS and miniaturisation technologies) in human performance fields may offer several important advantages over conventional whole blood sample collection. First, sample collection is less invasive compared to venepuncture and easy to perform (e.g., finger prick for adults, and heel prick for infants). This is particularly important for maximizing participant recruitment in the context of frequent repeated blood sampling. Second, blood sampling can be performed by an individual and away from a laboratory setting, such as the home of a clinical patient following only minimal training. Third, the use of miniaturised devices allows for low volume of blood to be collected (typically 10–200 µL), compared to standard venepuncture sampling which requires a minimum of ~2 mL of whole blood. Finally, as the name implies, samples are air-dried and can be shipped by mail to laboratories at minimal expense and without the need for maintaining stable temperature environments. Such devices will benefit from discovery research, where stable and quantifiable metabolites can be selected and developed for measurement of metabolites collected via miniaturised technologies. Considerable work is already occurring with DBS and dried urine spots, and companies are now developing technologies which can provide users with live measurement of metabolite concentrations which might be useful indicators of health or fitness phenotypes. These approaches will facilitate personalised exercise interventions and provide sport and exercise scientists with data that can inform decision making, health tracking and athlete phenotypes.

In other mammalian species, recent efforts to utilise mouse genetic diversity panels and recombinant inbred mouse strains in metabolomics/lipidomics research have proven valuable tools for genetic mapping (i.e., quantitative trait loci mapping) and investigating environmental exposure, providing new insights into compound identification, as well as the molecular basis of metabolic health and disease. For example, a recent large-scale genome-lipid associated map and resource termed LipidGenie was generated by analysing liver and plasma samples from diversity outbred mice, which permitted the identification of unknown lipids from MS data by mapping molecular lipid features to genetic loci [178]. In addition, recombinant inbred mouse strains (e.g., ILSXISS) have been used to determine skeletal muscle metabolomic signatures reflective of IR across different mouse strains and diets [179]. Such determinations of molecular metabolite/lipid classifiers and predictors of metabolic disease-related phenotypes can be leveraged in future studies to help predict metabolic health status and potentially determine how an organisms' metabolism may benefit from specific diets and/or exercise interventions.

In the next decade the exercise biology and metabolism fields will continue to benefit from these ongoing efforts in the metabolomics and lipidomics research community. Metabolomics/lipidomic analyses may ultimately be capable of being performed as part of routine health checks to assess an individual's metabolic status (e.g., nutritional state, training state, pathology) and responses to a given stimuli (e.g., food intake, exercise, drug treatment) as well as predisposition to certain diseases. This will in turn enable highly tailored and personalised exercise, diet, and/or medical interventions to prevent, delay and combat metabolic disease [180].

2.7. Conclusions

The unbiased global measurement of metabolomes and lipidomes from different sources such as biological fluids and tissues are constantly improving. They represent a promising avenue to unravel the complex and interconnected metabolite and lipid networks underlying the molecular responses to exercise throughout the body. In the context of exercise biology, the application of metabolomics and lipidomics as a hypothesis-generating approach has dramatically increased the number of biological targets measured simultaneously thanks to the major technological advances over the last decade. This has allowed the measurement of hundreds to thousands of metabolites (including lipid species) in a single run and subsequently revealed biomarkers of exercise intensity, training state and exercise capacity, fatigue, among others. In summary, findings made over the past decade have revealed numerous metabolites regulated by acute aerobic/endurance and resistance exercise in various biofluids and tissues across mammalian species, including: glycolysis end-products and TCA cycle intermediates; FA, acylcarnitines and TAGs; ketone bodies; nucleotides and derivatives; amino acids and derivatives; vitamins; steroid hormones; as well as less characterised complex lipids with various functions, pro- and anti-inflammatory properties and vasoactive properties (**Figure 2.5**).

Although considered the closest reflection of an organism's metabolic phenotype, the metabolome and the lipidome alone will not be sufficient to understand to complexity of exercise's molecular landscape. Therefore, extensive efforts to integrate metabolomics and lipidomics data with other layers of biological regulation such as the genome, proteome and phosphoproteome will also be required. Importantly, expansion of metabolite and lipid databases will convert a much higher proportion of data into useful information and meaningful biological insights. In addition, continued advancements in instrumentation and analytical platforms in the metabolomics and lipidomics field will help standardise and harmonise

experimental procedures from study design, sample handling, data acquisition, processing and analysis, as well as reporting. Together these efforts in the next decade will help maximise the utility of metabolomic and lipidomic profiling in exercise biology, metabolic health and disease, and beyond.

Supplementary Materials: The following are available online at http://www.mdpi.com/2218-1989/ 11/3/151/s1, **Table 2.1**: Summary of discussed acute exercise studies in humans and other mammals using metabolomic approaches, **Table 2.2**: Summary of discussed acute exercise studies in humans and other mammals using lipidomic approaches.

Author Contributions: Conceptualisation, M.R.B., N.G.L. and N.J.H.; writing—original draft preparation, review and editing, M.R.B., N.G.L. and N.J.H.; funding acquisition, N.J.H. All authors have read and agreed to the published version of the manuscript.

Funding: This work was supported by Australian Catholic University (ACU) research funding awarded to N.J.H.

Acknowledgements: The authors acknowledge that all publications related to exercise, metabolomics and/or lipidomics could not be discussed in this review due to word limitations and the primary focus on acute exercise studies in humans and other mammals published within the last decade. All figures were created with BioRender.com.

Conflicts of Interest: The authors declare no conflict of interest.

2.8. Supplementary Materials

See following pages.

Table 2.1 – Summary of discussed acute exercise studies in humans and other mammals using metabolomic approaches

Authors & Year	Study Population	Exercise Characteristics	Analytical Platform; Biological Specimen	Study Design	Key Findings
Schranner *et al.*, 2020 [82]	27 human studies (men and women, various ages, body compositions and fitness levels)	Various types, intensities and durations	Various platforms including NMR spectroscopy, LC-MS and GC-MS (targeted and untargeted); Blood plasma and serum, urine, sweat	Systematic review following PRISMA guidelines. Search for human metabolomics studies that report metabolite concentrations before and within 24 h after endurance or resistance exercise	**196 significantly changed metabolites within 24 h after exercise in ≥ 2 out of 57 experiments: 95 lipid species, 53 amino acids and derivatives, 14 nucleotides, 13 carbohydrates, 7 TCA cycle intermediates, 6 vitamins and co-factors, 5 xenometabolites and 3 peptides** - ↑ lactate, pyruvate, TCA cycle intermediates - ↑ 37 FA, 17 acylcarnitines, and ketone bodies (endurance) - ↓ bile acids and several membrane lipids (endurance) - Mixed responses in proteinogenic and non-proteinogenic amino acids
Lewis *et al.*, 2010 [83]	25 amateur runners (aged 42 ± 9 years, men & women)	Moderate to high intensity, long duration: Marathon running (247 ± 46 min)	Targeted LC-MS; Blood plasma	Boston Marathon. Repeated measures from one cohort, blood collection before and within 10 min post-race	**88 metabolites quantified** - ↑ products of adenine nucleotides catabolism: AMP, inosine, hypoxanthine, xanthine - ↑ lipolysis (glycerol) and ketogenesis (β-hydroxybutyrate) - ↑ glycolysis products (glucose-6-phosphate, 3-phosphoglycerate, pyruvate, lactate) and TCA cycle intermediates - ↑ tryptophan metabolites: kynurenate, quinolinate, anthranilate - ↑ niacinamide (insulin sensitivity modulator) - ↓ gluconeogenic amino acids: alanine, threonine, serine, proline, valine, histidine, glutamine, asparagine
Stander *et al.*, 2018 [84]	31 amateur runners (aged 41 ± 12 years, 19 men & 12 women)	Moderate to high intensity, long duration: Marathon running (259 ± 49 min)	Untargeted 2D GC-MS; Blood serum	Druridge Bay Marathon. Repeated measures from one cohort, blood collection the day preceding the race (≥ 2h fasted) and immediately post-race	**70 metabolites identified** - ↑ glycolysis products (pyruvate), gluconeogenesis metabolites (e.g. myo-inositol, glycerol, glyceric acid) and TCA cycle intermediates - ↑ FAs, OCFAs, alpha-hydroxyacids, and ketone bodies - ↑ oxidative stress, ↑ cholesterol catabolism - ↓ amino acids
Shi *et al.*, 2020 [90]	20 amateur runners (aged 29 ± 5 years, all men)	Moderate to high intensity, long duration: Marathon running (average 160 min, all within 180 min)	Untargeted LC-MS; Blood serum	Shanghai International Marathon. Repeated measures from one cohort, blood collection 24h pre-race (fasted) and within 60 min post-race	**31 significantly changed metabolites between pre- and post-race** - ↑ glycolysis products (pyruvate), gluconeogenesis metabolites (glycerol, glyceric acid) and TCA cycle intermediates - ↑ lipolysis products: glycerol, glyceric acid, octanoic acid, quinic acid - ↑ urea and ↓ glucosamine - ↑ caffeine metabolism: xanthine, theophylline, theobromine - ↑ cortisol and ↓ testosterone - ↓ amino acids (including gluconeogenic): valine, serine, asparagine but ↑ alanine, tyrosine, phenylalanine

Table 2.1 *Cont.*

Authors & Year	Study Population	Exercise Characteristics	Analytical Platform; Biological Specimen	Study Design	Key Findings
Schader *et al.*, 2020 [93]	76 amateur runners (aged 43 ± 11 years, all men)	Moderate to high intensity, long duration: Marathon running (225 ± 43 min)	Targeted LC-MS & FIA-MS; Blood plasma	Munich Marathon. Repeated measures from 3 groups: low, average, top performers (based on VO_2 max and race time). Blood collection at 5 time points: 5 weeks and 1 week pre-race, then immediately, 24h and 72h post-race (all fasted except for immediately post-race sample, although before post-race refeeding)	**188 metabolites quantified** <u>For all cohorts immediately post-race:</u> - ↑ fat metabolism: acylcarnitines - ↑ proxy for CPT enzymes activity: ratio palmitoylcarnitine + stearoylcarnitine/free carnitine - ↑ arginine related metabolites and ↓ most amino acids ↓ phospholipids <u>Low vs top performers:</u> - Post-race acylcarnitines in low performers > top performers - Post-race arginine-related metabolites in low performers > top performers
Manaf *et al.*, 2018 [97]	18 active young men (aged 25 ± 5 years)	Moderate intensity, long duration: Time-to-exhaustion cycling test at 3mmol/L lactate (80 ± 14 min)	Untargeted LC-MS; Blood plasma	Repeated measures: blood collection 30 min pre-exercise (after a ≥ 10h overnight fast), 10 min into cycling (reference point instead of pre-exercise), before fatigue, immediately after fatigue, and 20 min post-fatigue	**80 metabolites identified with 68 significantly changed over time** - ↑ lipolysis markers and fat metabolism: glycerol, carnitine, FA including oleic, palmitic acids and their acylcarnitines, acetylcarnitine - ↓ tryptophan and ↑ serotonin (derived from tryptophan) end-product: 5-metoxy-3-indoleacetic acid Changes in alternate tryptophan metabolism compounds: ↑ indole, indole-3-lactic acid, methyl indole-3-acetate; and ↓ indole-3-acetic acid - ↑ neurotransmitters: gamma-aminobutyric acid, 2-aminobutyric acid - ↑ dopamine degradation biomarker: homovanillic acid - Mixed responses in amino acids: ↑ proline, ↓ citrulline, arginine, methionine; ↓ valine and glutamic acid with recovery; ↑ creatine
Contrepois *et al.*, 2020 [47]	36 volunteers (aged 59 ±8 years, 58% men) with a wide range of insulin sensitivities	High intensity, short duration: Incremental treadmill run to exhaustion with a target duration of 8 to 12 min	Untargeted LC-MS; Blood plasma	Repeated measures; blood collection pre-exercise, then 2, 15, 30 and 60 minutes post-exercise (fasted). 15 participants provided a fasted blood sample the next morning for inter-day variability screening. A subset of the cohort (n=14) participated in a control trial (same blood collection protocol)	**728 metabolites identified, 4 clusters of longitudinal trajectories** **Cluster 1: early ↑ post-exercise with quick return to basal levels** - Glycolysis products (pyruvate, lactate); TCA cycle intermediates (malate); fat oxidation (FA and acylcarnitines); inflammation **Cluster 2: delayed ↑ post-exercise with return to basal levels** - TCA cycle intermediates (malate, citrate, a-ketoglutarate); adenine nucleotide catabolism (hypoxanthine and xanthine); uric acid; amino acids: alanine, tyrosine, glutamine, and proline **Cluster 3: ↓ post-exercise with return to basal levels** - Amino acids (glutamic acid, cystine, tryptophan, serine, threonine, and glycine); free carnitine; FA (C20-24) **Cluster 4: ↓ post-exercise without return to basal levels** - BCAAs (valine, leucine, isoleucine) and ↑ their degradation products (branched-chain ketoacids); caffeine metabolites; bile acids

Table 2.1 *Cont.*

Authors & Year	Study Population	Exercise Characteristics	Analytical Platform; Biological Specimen	Study Design	Key Findings
Hu *et al.*, 2020 [101]	2 separate studies A) 10 young healthy men (aged 23± 1 years) B) 9 young healthy men (aged 21± 1 years)	Moderate intensity, long duration: A) 2-hour cycling at 60% VO_2max B) 2-hour continuous one-leg knee extension at 50% 1RM	Untargeted CE-MS and targeted LC-MS; Blood plasma	A) Repeated measures; plasma collected from hepato-splanchnic bed after an overnight fast before (at 0 min), during (at 60, 120 min) and after exercise (at 150, 180, 240, 300, 360 min) fasted. B) Same plasma collection characteristics but from femoral artery (one leg) and femoral vein (both legs) up to 300 min post-exercise. Note: liver transcriptomic data from male C57Bl/6N mice who ran 1h at 13m/min (14° incline) were also used [99]	**200 arterial plasma metabolites detected: 77 changed by exercise** - ↑ medium- to long-chain FA during exercise and recovery, especially unsaturated FA - ↑ ketone bodies only post-exercise - ↑ TCA cycle intermediates (succinate, malate), lactate, hypoxanthine, FA 6:0, FA 7:0 and FA 8:0 during exercise with a ↓ during recovery - ↓ most amino acids in the recovery phase **Hepato-splanchnic flux of 21 metabolites changed during exercise** - ↑ hepatic uptake of FA C6:0, C8:0, C14:0, C14:1, C16:1; TCA cycle intermediates (succinate, malate), glycolysis products (lactate and pyruvate), and amino acids arginine, glutamine and lysine - ↑ release of saturated FA of ≥ C18; β-hydroxybutyrate, hippurate, aspartate, 3-methyl-2-oxovalerate and N5-ethylglutamine **Metabolite flux from the working leg** **-** ↑ uptake of β-hydroxybutyrate - ↑ release of succinate, malate, FA C6:0 and C8:0 **↑ activation of HIF-, NRF2- and c-AMP-dependent transcription factors in mouse liver post-exercise**
Kistner *et al.*, 2020 [102]	255 healthy volunteers (aged 46 ± 17 years, 148 men and 107 women)	High intensity, short duration: Bicycle exercise to exhaustion (exercise tolerance test)	Targeted 1H NMR-spectroscopy; Urine	Repeated measures: spot urine collected (fasted) 90 min pre-exercise, then after a standardised breakfast and within 15-30 min post-exercise	**47 metabolites quantified: 37 significantly changed by exercise** **-** ↑ lactate, acetate - ↑ TCA cycle intermediates: citrate, cis-aconitate, succinate - ↑ amino acids: glycine, histidine, isoleucine, leucine, taurine, threonine, tyrosine, valine - ↑ BCAA degradation: methylsuccinate and 3-hydroxyisovalerate (leucine-derived metabolites), 3-aminoisobutyrate (valine-derived metabolite) - ↑ carnitine and creatine
Harshman *et al.*, 2018 [115]	11 active-duty military volunteers (aged 24 to 42 years, 7 men and 4 women)	Low, moderate and high intensity, short to long duration: Treadmill march with 22-kg gear (22 to 211 min)	Untargeted LC-MS; Sweat	Single sweat collection in the 3 subgroups following low (4.8 km/h, 3% incline, n=5), moderate (5.1 km/h, 4% incline, n=4) or high intensity (5.6 km/h, 6% incline, n=2) march in a control trial (same blood collection protocol)	**29 confirmed metabolites of 48 compounds tentatively identified** **-** amino acids are the most abundant metabolites in sweat - strong relationships between sweat metabolites (positive and negative) - no significant metabolites associated with exercise duration or intensity

Table 2.1 *Cont.*

Authors & Year	Study Population	Exercise Characteristics	Analytical Platform; Biological Specimen	Study Design	Key Findings
Sato *et al.*, 2019 [118]	C57Bl/6J mice (10-11 weeks of age, all male, n=6 per time point)	Low to moderate intensity, long duration: Treadmill running (60 min) at 6m/min with added 2m/min every 2 min up to 16m/min	Untargeted LC-MS & GC-MS; Skeletal muscle (*gastrocnemius* and quadriceps)	4 groups: exercise and control sedentary, both at early rest phase and early active phase. Measures at 6 time points in each group following exercise at 0, 4, 8, 12, 16 and 20 hours post-exercise	**672 metabolites detected (580 of known identity)** Exercise in early active phase: - ↓ temporal glucose metabolism - ↑ amino acid breakdown, lipid oxidation, glycolysis, ketone metabolism Exercise in early rest phase: - ↑ temporal glucose metabolism - ↓ temporal glycerol metabolism
Overmyer *et al.*, 2015 [119]	HCR and LCR rats, both bred from N:NIH colony (4.5 months of age, all male, n=4-6/group)	High intensity, short and long duration: Incremental treadmill run to exhaustion (LCR: ~10 min; HCR: ~45 min)	Targeted LC-MS & GC-MS; Blood plasma and skeletal muscle (*gastrocnemius*)	2 groups: LCR and HCR. Measures at rest (0 min) and 10 min (immediately post-exhaustion) in LCR; and at 0, 10 and 45 min (immediately post-exhaustion) in HCR	**↓ fat uptake/oxidation and amino acid utilisation during exercise in LCR vs HCR but similar mechanism of exhaustion (delayed in HCR)** Plasma - ↓ FA in LCR and HCR at 10 min - ↓ TAGs in LCR < HCR at 10 min - ↑ long-chain acylcarnitines in LCR at 10 min - Small changes in medium-chain acylcarnitines in HCR at 10 min - ↑ medium- and long-chain acylcarnitines in HCR at 45 min - ↓ BCAAs and ornithine in HCR at 10 min Skeletal muscle - Small changes in long-chain acylcarnitines in LCR but ↑ in HCR at 10 min - ↑ medium- and long-chain acylcarnitines in HCR at 45 min - ↓ BCAAs and ornithine in LCR < HCR at 10 min
Klein *et al.*, 2020 [120]	Standardbred horses (3-8 years of age, 4 male and 4 female)	High intensity (low to high), long duration: Incremental treadmill run to exhaustion (6% incline)	Untargeted LC-MS; Skeletal muscle[1] (*M. gluteus medius*)	All horses were used as both exercised and standing control in a crossover fashion. Repeated measures: 30 min pre-exercise, 3h and 24h post (food allowed after the 3h post-exercise biopsy). This protocol was repeated after a 12-week training followed by 72 hours of recovery	**545 metabolites identified** Untrained state - 31 metabolites changed 3h post (↑ 29; ↓ 2): ↑ 14 metabolites related to amino acid metabolism, other ↑ metabolites related to lipid (5), carbohydrate (3), nucleotide (3) vitamin/co-factor (1), and energy metabolism (1), 2 xenometabolites 3h post-exercise - ↓ ribose 1-phosphate and fumarate (carbohydrate and energy metabolism) - At 24h post-exercise, ↑ 1 metabolite (N-methylalanine) Trained state - ↑ 100; ↓ 42 metabolites 3h post. Metabolite changes were related to amino acid (↑ 37; ↓ 7), lipid (↑ 25; ↓ 24), xenometabolites (↑ 14), nucleotide (↑ 11; ↓ 2), carbohydrate (↑ 10; ↓ 2), and vitamin/co-factor (↑ 3; ↓ 1) metabolism - ↑ 13 and ↓ 137 metabolites 24 h vs 3h post. Metabolite changes were related to ↓ in lipid, amino acid and nucleotide metabolism - ↑ 74 other metabolites 24h post, 41 of 45 metabolites ↓ at 24 h vs 3 h in the untrained state also ↓ in the trained state

Table 2.1 *Cont.*

Authors & Year	Study Population	Exercise Characteristics	Analytical Platform; Biological Specimen	Study Design	Key Findings
Zhang *et al.*, 2019 [121]	A) Sprague Dawley rats (adult males, n=9-10/group) B) 5 healthy volunteers (aged 21-46 years, 3 men and 2 women)	Moderate intensity, short duration: A) 20-min treadmill run at 18m/min (~60% VO_2 max) B) 30-min ergometer cycling at 65% heart rate max	Untargeted GC-MS; A) Skeletal muscle (*gastrocnemius*) IF and blood plasma B) Skeletal muscle (*v. lateralis*) IF	A) All rats used as resting controls and exercise treatment (crossover with one week of interval). Blood plasma and IF collected within 10 min post-exercise B) Repeated measures, pre-exercise and during exercise (30 min into running)	**456 metabolites detected in muscle IF and plasma in rats (43% of all metabolites detected in both media, and 20% of exercise-changed metabolites present in both media)** Rat muscle IF **299 metabolites detected** - ↑ most amino acids and derivatives; ↓ isoleucine, leucine, aminomalonate - ↑ oleic acid, LA, AA, pelargonic acid, β-hydroxybutyrate ; ↓ lauric, palmitic, heptadecanoic, stearic, arachidic and lignoceric acids - ↑ fructose, mannose, lactate, citric acid, alpha-ketoglutarate, oleamide, N-acetyl-D-hexosamine and ethanolamine; ↓ glucose-6-phosphate and 3-phosphoglycerate, nicotinic acid, glycerol-alpha-phosphate Rat plasma **353 metabolites detected** - ↓ amino acids and urea; ↑ ketone: β-hydroxybutyrate - ↑ unsaturated FAs: oleic and palmitoleic acids, LA and AA, and long-chain saturated FAs palmitic and stearic acids; - ↑ fructose and lyxose; ↓ arabitol and lyxitol; ↑ cytosine and thymidine - ↑ TCA cycle intermediates (citric acid, isocitric and aconitic acids and alpha-ketoglutarate) Human muscle IF **414 metabolites detected** (including 142 also detected in rat IF). Of the metabolites changed by exercise in rat IF, 78 detected in humans and 70% changed in the same direction
Huang *et al.*, 2010 [122]	Sprague Dawley rats (6 weeks of age, all males, n=5/group)	High intensity, long duration: Incremental run to exhaustion on 10% inclined treadmill at up to 30m/min	Untargeted GC-MS; Liver	3 groups: sedentary control, exhaustive exercise and endurance training[2]. Livers collected in control group and immediately post exhaustive exercise	**55 metabolites identified** - ↑ energy consumption markers: adenosine metabolites xanthine and hypoxanthine; creatinine - ↓ carbohydrates and lactate - ↑ FA and ketone bodies - ↑ ornithine, urea - ↑ pro-inflammatory precursors: AA, LA, oleic acid

1H NMR: proton nuclear magnetic resonance; AA: arachidonic acid; BCAA: branched-chain amino acid; CE: capillary electrophoresis; CPT: carnitine palmitoyl transferase; DAG: diacylglycerol; FA: fatty acids; FIA: flow-injection analysis ; GC: gas chromatography; HCR: high running capacity; IF: interstitial fluid; LA: linoleic acid; LC: liquid chromatography; LCR: low running capacity; MS: mass spectrometry; OCFA: odd-chain fatty acid; TAG: triacylglycerol; TCA: tricarboxylic acid.

[1] Plasma BCAA concentrations were also assessed in this study but were not discussed in this review.

[2] Results from the endurance training protocol are not described since this review is focused on acute exercise only.

Table 2.2 – Summary of discussed acute exercise studies in humans and other mammals using lipidomic approaches

Authors & Year	Study Population	Exercise Characteristics	Analytical Platform; Biological Specimen	Study Design	Key Findings
Gollasch *et al.*, 2019 [126]	6 healthy volunteers (aged 38 ± 15 years, 1 woman & 5 men)	High intensity, short duration: Incremental treadmill run to exhaustion	Targeted LC-MS; Blood plasma	Bruce protocol [128]. Repeated measures; blood collection pre-exercise, during (heart rate at 150 beats per min), immediately and 10 min post-exercise	**Post-run (immediately and/or 10 min post):** - ↑ LA-derived epoxide: 12,13-EpOME - ↑ AA-derived diol: 5,6-DHET - ↑ EPA-derived diols: 5,6- DiHETE and 17,18-DiHETE - No effect on the majority of CYP and LOX lipid metabolites
Stanford *et al.*, 2018 [132]	Cohort 1: 27 healthy young and older men with various physical activity levels Cohort 2: 12 healthy young adults (29 ± 1 years, 6 men & 6 women	Moderate intensity, short duration: Cohort 1: 40 min cycling at 70% of heart rate reserve Cohort 2: 45 min treadmill running at 75% of VO_2 max	Targeted LC-MS; Blood plasma	Cohort 1: Repeated measures; blood collection following an overnight fast pre-exercise, immediately and 3h post-cycling Cohort 2: Repeated measures; blood collection following an overnight fast pre-exercise, 15 min into, immediately and 1h post-run	Cohort 1: **88 lipid mediators quantified** - ↑ LA-derived diol: 12,13-DiHOME immediately post-exercise - ↓ 13 lipids immediately post-run, including: LA-derived mediators: 9- and 13-oxoODE; 13-HODE; epoxide 9,10-EpOME - AA-derived mediators: epoxide 14,15-EET, 12-oxo-ETE, and LTB4 degradation product 12-oxo-LTB - EPA-derived mediator: 9-HEPE - DHA-derived mediator: 8-HDHA Cohort 2: - ↑ LA-derived diol: 12,13-DiHOME immediately post-exercise From both cohorts: - 12,13-DiHOME levels in active > sedentary participants before exercise - ↑ 12,13-DiHOME in active > sedentary participants immediately post-exercise
Nieman *et al.*, 2014 [135]	19 trained male cyclists (aged 38 ± 2 years)	Moderate intensity, long duration: 75-km cycling time trial (162 ± 4 min, mean intensity at 69±2 % of VO_2 max)	Untargeted GC-MS & LC-MS; Blood plasma	Repeated measures; blood collection following an overnight fast pre-exercise, immediately, 1.5h and 21h post-cycling	**Immediately and 1.5h post-cycling:** - ↑ LA, LNA, dihomo-LNA, AA, DPA, adrenate - ↑ LA-derived mediators: 9- & 13-HODE; 9,10-DiHOME; 12,13-DiHOME - ↑ oxidative stress biomarker: F2-isoprostane - Correlation of post-cycling 9- & 13-HODE with post-cycling AA; 12,13-DiHOME; F2-isoprostane, LA, dihomo-LA, adrenate
Gollasch *et al.*, 2019 [137]	6 healthy volunteers (aged 38 ± 15 years, 1 woman & 5 men)	High intensity, short duration: Incremental treadmill run to exhaustion	Targeted LC-MS; Red blood cells	Bruce protocol [128]. Repeated measures; blood collection pre-exercise, during (heart rate at 150 beats per min), immediately and 10 min post-exercise	**Immediately and 10 min post-run:** - ↑ LA-derived epoxides: 9,10- and 12,13-EpOME - ↑ AA-derived epoxides: 5,6-EET, 11,12-EET, 14,15-EET - ↑ DHA-derived epoxides: 16,17-EDP and 19,20-EDP - No significant effect on diols, LOX and COX lipid mediators
Gollasch *et al.*, 2019 [139]	6 healthy volunteers (aged 38 ± 15 years, 1 woman & 5 men)	High intensity, short duration: Incremental treadmill run to exhaustion	Targeted LC-MS; Red blood cells & blood plasma	Bruce protocol [128]. Repeated measures; blood collection pre-exercise, during (heart rate at 150 beats per min), immediately and 10 min post-exercise	**20 FAs quantified in RBCs and plasma (C12:0 to C22:6):** - No effects of exercise on RBC FA levels, including omega-3 quotient - No changes in plasma FA following exercise - ↓ RBC lauric acid (C12:0) between exhaustion and 10 min post-exercise

Table 2.2. *Cont.*

Authors & Year	Study Population	Exercise Characteristics	Analytical Platform; Biological Specimen	Study Design	Key Findings
Contrepois *et al.*, 2020 [47]	36 volunteers (aged 59 ±8 years, 58% men) with a wide range of insulin sensitivities	High intensity, short duration: Incremental treadmill run to exhaustion with a target duration of 8 to 12 min following warm-up	Semi-targeted LC-MS; Blood plasma	Repeated measures; blood collection pre-exercise, then 2, 15, 30 and 60 minutes post-exercise (fasted). 15 participants provided a fasted blood sample the next morning for inter-day variability screening. A subset of the cohort (n=14) participated in a control trial (same blood collection protocol)	**710 lipid species, 4 clusters of longitudinal trajectories** **Cluster 1: early ↑ post-exercise with quick return to basal levels** - Cholesteryl esters (n = 20), phosphatidylcholines (n = 23), DAGs (n = 10), ceramides (n = 9), and sphingomyelins (n = 8); long-chain unsaturated TAGs (including AA,EPA,DHA) markers of pro- and anti-inflammatory processes along with sphingolipids and ceramides **Cluster 4: ↓ post-exercise without return to basal levels** - Most TAGs (indicating lipolysis) especially saturated (indicating preferential use for energy conversion)
Vella *et al.*, 2019 [144]	12 young active men (aged 22 ± 1 years)	High intensity, short duration: Maximal concentric and eccentric unilateral knee extension 3x12 repetitions at 60°/s	Targeted LC-MS; Skeletal muscle (*v. lateralis*)	Repeated measures; muscle biopsies pre-exercise following an overnight fast, then 2,4 and 24h post-exercise	**84 lipid mediators detected and quantified in the resting skeletal muscle** All changes at 2h post-exercise back to basal at 4 and 24h post-exercise <u>COX pathway:</u> - ↑ AA-derived TXA2 biosynthesis markers : TXB2 and 12(S) HHTrE - ↑ AA-derived PGE2 and PGF2α - ↑ EPA-derived 15-DeoxyΔ12,14-prostaglandin J3 <u>LOX pathway:</u> - ↑ AA-derived 5-HETE; 12-HETE + degradation product tetranor 12-HETE - ↑ AA-derived LTB4 (undetectable at rest) and degradation products: 12-oxo-LTB and 20-COOH-LTB4 - ↑ EPA-derived 12-HEPE - ↑ DHA-derived 7- and 14-HDHA <u>CYP pathway:</u> - ↑ AA-derived 5,6-EET; AA-derived 11,12- and 14,15-DHET - ↑ LA-derived 9,10- and 12,13-DiHOME
Rivas *et al.*, 2012 [145]	9 healthy young men (aged 22 ± 1 years) and 10 healthy older men (aged 74 ± 2 years)	High intensity, short duration: Knee extension & leg press: 3x10 repetitions at 80% of 1-RM	Targeted LC-MS; Skeletal muscle (*v. lateralis*)	Lipidomic analysis only pre-exercise muscle biopsies following an overnight fast and standardised meals (ad-libitum) the preceding 24h (muscle biopsies immediately and 6h post-exercise (fasted) for other analyses)	**Quantification of 9 intramuscular ceramides (C14:0 to C24:1)** - No significant changes in total or unsaturated ceramides between older and younger men - Palmitic (C16:0) and arachidic (C20:0) ceramides in young men < older men

Table 2.2. *Cont.*

Authors & Year	Study Population	Exercise Characteristics	Analytical Platform; Biological Specimen	Study Design	Key Findings
Markworth *et al.*, 2013 [142]	16 healthy young men (aged 23 ± 1 years both control (n=8) and Ibuprofen (n=8) group)	High intensity, short duration: 10-min warmup followed by bar squats, leg press and knee extension. Circuit with 1-min inter-set rest and 3-min rest between different exercises 3x8-10 repetitions at 80% of 1-RM	Targeted LC-MS; Blood serum	Repeated measures; blood collection 15 min pre-exercise following an overnight fast (10h); every 30 min from 0 to 3 hours post-exercise; then 24 hours post-exercise	**87 lipid species detected and quantified** - ↑ of 29 post-exercise (especially from 1 to 3h post-exercise) - Most of lipid species were back to basal at 24h post-exercise <u>COX pathway:</u> - ↑ AA-derived TXA2 biosynthesis markers : TXB2 and 12(S) HHTrE - ↑AA-derived PGE2 and PGD2, 15-keto PGE2 and 13,14-dihydro-15-keto PG, 15-keto PGF2α , 6-keto PGF1α - ↑ EPA-derived RvE1 <u>LOX pathway:</u> - ↑ AA-derived 12-HETE + degradation product tetranor 12-HETE - ↑ AA-derived 15-HETE, 15-oxo-ETE - ↑ AA-derived LTB4 , LXA4 and LXB4 - ↑ LA-derived 9- and 13-HODE, 9- and 13-oxo-ODE - ↑ DHA-derived 10(S),17(S)-DiHDHA (protectin D1) <u>CYP pathway:</u> - ↑ AA-derived 11,12- and 14,15-DHET - ↑ LA-derived 9,10- EpOME and 9,10-DiHOME
Nolazco Sassot *et al.*, 2019 [148]	4 Thoroughbred horses (aged from 3 to 6 years, 3 male and 1 female)	High intensity, short duration: Supramaximal treadmill run (115% VO_2 max) to exhaustion	Untargeted LC-MS; Blood plasma	Repeated measures; blood collection pre-exercise following a 4-hour fast; immediately, 15 and 30 min post-exercise	**933 detected lipid species including 130 known lipids:** **13 lipid species changed by supramaximal exercise:** - ↑ 3 phosphatidylcholines: PC (p-34:1), PC (P-36:2) and PC (P-36:4) - ↑ LPC (18:0) - ↑ 2 sphingolipids: SM (d36:1) and SM (d42:2) - ↑ 3 unsaturated FAs: LA (C18:2), LNA (C18:3) and 11,14-eicosadienoic acid (C20:2) - ↓ 4 saturated FAs: C12:0, C14:0, C17:0 and C20:0
Hu *et al.*, 2010 [152]	C57Bl/6J mice (all male, aged 12-weeks) exercise group: n=8 sedentary group: n=8	Moderate intensity long duration: 60 min of treadmill running at 14 m/min and 14°incline after a 5-min warmup at 5m/min and 5° incline	Targeted LC-MS; Liver	Sedentary control group (mice stayed in their cage) and exercise group: liver collection (fed state) immediately and 3 hours post-exercise (with free access to food in the first 2 hours)	**115 lipid metabolites quantified** - No significant differences in hepatic profile between rest and exercise immediately post-exercise - 21 lipids mostly responsible (↑ 17 TAGs, ↓ 3 PCs and 1 LPC) for hepatic profile separation 3h post-exercise - ↑ polyunsaturated TAGs (50:3; 54:5; 54:6; 54:7; 56:4; 58:6; and 58:10) - ↓ PCs (36:1; 38:3; 40:4) and DAG (34:1) - ↑ 63% in total liver TAG content in the recovery phase and ↓ content in skeletal muscle immediately post-exercise and in the recovery phase

Table 2.2. *Cont.*

Authors & Year	Study Population	Exercise Characteristics	Analytical Platform; Biological Specimen	Study Design	Key Findings
Hoene *et al.*, 2016 [153]	C57Bl/6N mice (all male, aged 12-weeks, n=6) exercise and sedentary group	Moderate intensity, long duration: 60 min of treadmill running at 13 m/min and 13°incline after a 5-min warmup at 5m/min	Targeted LC-MS; Liver and skeletal muscle (*gastrocnemius* and *soleus*)	Exercised mice (fed state): liver, *gastrocnemius* and *soleus* muscle collection within 15 min post-exercise Control sedentary mice (fed state): placed 60 min in new cages without food during trial)	**199 complex lipids and 33 FA (+ 39 acylcarnitines, acetylcarnitine and free carnitine) quantified in liver, gastrocnemius and soleus muscles at rest.** **Pronounced profile differences between liver and skeletal muscle, but also between soleus and gastrocnemius:** - Liver FA, ceramides, sphingomyelins and phospholipids > than in muscle - Soleus profile more similar to liver than gastrocnemius. Total carnitine, free carnitine, acetyl- and propionylcarnitine, short-chain hydroxylated acylcarnitines in soleus >> gastrocnemius. Medium- and long-chain acylcarnitines in soleus < gastrocnemius. Total and free carnitine levels in liver more similar to gastrocnemius than soleus - Sum of short-chain acylcarnitines in liver >> soleus >> gastrocnemius **Acute exercise changed the hepatic lipid profile** - Most lipids not significantly changed by exercise in liver - ↑ liver total lysophospholipids: LPCs (16:0; 18:2; 20:4; 22:5 and 22:6), LPEs (16:0; 18:0; 18:1 and 20:4) - ↑ liver total plasmalogens: PE-P (P-38:4 and P-40:4) - ↑ liver LPC/PC and LPE/PE - ↑ free and total carnitine and ↓ acetylcarnitine (likely related to upregulation of mRNA of the carnitine transporter Slc22a5/OCTN2) **Acute exercise changed the skeletal muscle lipid profile** - Most lipids, free and total carnitine not significantly changed by exercise in skeletal muscles - ↑ acetylcarnitine (soleus > gastrocnemius), hydroxy-acylcarnitines (soleus>gastrocnemius), and short-chain acylcarnitines in both muscles **Palmitate flux differs between liver and skeletal muscles after exercise** - Excess of circulating FA taken up by the liver and incorporated in TAGs and phospholipids during recovery

1-RM: one-repetition maximum; AA: arachidonic acid; COX: cyclooxygenase; CYP: cytochrome oxidase P450 ; DAG: diacylglycerol; DHA: docosahexaenoic acid; DHET: dihydroxyeicosatrienoic acid; DiHDHA: dihydroxyDHA; DiHETE: dihydroxyeicosatetraenoic acid; DiHOME: dihydroxyoctadecanoic acid; DPA: docosapentaenoic acid; EET: epoxyeicosatrienoic acid; EDP: epoxydocosapentaenoic acid; EPA: eicosapentaenoic acid; EpOME: epoxyoctadecenoic acid; FA: fatty acids; GC: gas chromatography; HDHA: hydroxyDHA; HEPE: hydroxyEPA; HETE: hydroxyeicosatetraenoic acid; HHTrE: hydroxyheptadecatrienoic acid; HODE: hydroxyoctadecadienoic acid; IR: insulin resistant; IS: insulin sensitive; LA: linoleic acid; LC: liquid chromatography; LNA: linolenic acid; LOX: lipoxygenase; LPC: lysophosphatidylcholine; LPE: lysophosphatidylethanolamine; LT (including B, B4): leukotriene; MS: mass spectrometry; oxo-ETE: oxo-eicosatetraenoic acid; oxo-ODE: oxo-octadecadienoic acid; PC: phosphatidylcholine; PE(-P): phosphoethanolamine; PG (including D2, E2, F1α and F2α): prostaglandin; RBC: red blood cell; Rv (including E1): resolvin; SM: sphingolipid; TAG: triacylglycerol; TX (including A2 and B2): thromboxane.

2.9. Growing Trends in The Field of Exercise Metabolomics

From the early metabolomic analyses of exercise metabolism in the 2000's, an upward trend in the application of metabolomics-based approaches to study exercise has been observed [181,182]. The field of exercise metabolomics is fast-paced and constantly improving with rapid technological advancements. Since 2021, hundreds of papers have been published in the field of exercise and metabolomics in human and other mammalian species that have helped further expand understanding of exercise metabolism and its underlying adaptations and benefits for health and performance.

Growing interest in the use of metabolomics in sport, also called "sportomics", has emerged in recent years given the many appealing advantages of metabolomics, including the emergence of technologies designed to facilitate sample collection in both the laboratory and field and reduce invasiveness in sports settings [183]. Future efforts in sportomics are expected to advance comprehension of molecular mechanisms underlying fatigue [184] and recovery [185], for example, to provide more personalised, tailored approaches to monitor and enhance performance in athletic populations [186].

Furthermore, whereas most acute exercise metabolomics studies have been performed following aerobic/endurance exercise, resistance exercise studies can provide complementary insights that may benefit aspects of exercise performance [187] and help uncover distinct aerobic versus resistance exercise responses [188]. Although a large proportion of metabolites responsive to acute exercise display short-term alterations, a recent resistance exercise study revealed blood metabolite changes persisting over a week after the exercise bout [189], therefore highlighting the need for longer-term analyses of metabolomic responses to acute exercise.

A growing body of work in the field of acute exercise and metabolomics also includes analyses of numerous biofluids and tissues from other mammals including horses [190] and

rodents [191-193] with emerging trends to integrate global metabolomes from multiple tissues and biofluids within a given study. For example, a recent study by Sato *et al*. revealed time-dependent responses to exercise metabolism in seven different biological specimens, thereby expanding the understanding of the complexity and timing of exercise-regulated metabolic networks [191].

Of note, there have also been increasing interests in using metabolomic approaches in longer-term and more clinical-based investigations [182], to identify novel biomarkers of cardiorespiratory fitness [194,195], physical activity and sedentary time [196], and better understand the molecular mediators of chronic exercise and periods of exercise training on various health benefits. In the exercise metabolomics field, the last decade has witnessed increased efforts to elucidate how exercise training and different exercise variables (modality, intensity, duration, frequency, timing, etc.) can potentially prevent, delay or combat numerous diseases including obesity and T2DM, metabolic syndrome, cardiovascular and pulmonary diseases [197-200], Alzheimer's disease [201], and cancer [202]. Another large national research consortium aiming to provide a detailed map of the health-promoting molecular signals of exercise is being undertaken by the MoTrPAC group in the USA [166]. By using preclinical model systems and human clinical trials, applying multiple exercise modalities, and performing multi-omic analyses on a wide variety of biological samples, this study is expected to be the largest research study characterising the molecular links between exercise and health. The earliest preclinical MoTrPAC data from male and female rats subjected to eight weeks of endurance training are now available in preprint (https://www.biorxiv.org/content/10.1101/2022.09.21.508770v1) and identified no less than 35,000 analytes regulated by endurance training across 19 tissues . These data, combined with upcoming human clinical 'omics data, will provide tremendous insights into exercise's potential molecular mediators of health and disease prevention/treatment.

Despite the promising recent and future discoveries described above, little research has been conducted to specifically elucidate how biofluids and tissues respond to acute exercise in mice using metabolomic approaches. Likewise, the potential metabolic pathways and metabolites underlying exercise and the interactive roles of AMPK and glycogen in metabolic control and exercise in mice remain unknown.

2.10. Relevance of AMPK-Glycogen Binding in Exercise and Metabolism

2.10.1. AMPK Structure, Function and Tissue Distribution

AMPK is a highly conserved cellular energy sensor and major regulator of metabolism that plays a central role in maintaining energy homeostasis and promoting adaptations to exercise [12,203]. In response to cellular energy stress, AMPK becomes activated and inhibits the activity of energy-consuming anabolic pathways, while switching on energy-producing catabolic pathways to help restore energy homeostasis. As a serine/threonine protein kinase, AMPK phosphorylates protein substrates on serine (S) or threonine (T) amino acid residues by removing a phosphate group from adenosine triphosphate (ATP) and transferring it to either of these residues on AMPK's respective downstream targets. This phosphorylation is central to the regulation of many cellular processes and leads to a conformational change of the phosphorylated protein, resulting in its activation or inhibition. Phosphorylation is a reversible post-translational modification, as protein phosphatases can also remove this phosphate group from target proteins to regulate their activation states [204].

AMPK is a heterotrimeric complex that consists of a catalytic α subunit and two regulatory subunits, β and γ. While the α and β subunit each exist in two isoforms (α1, α2 and β1, β2), the γ subunit exists in three isoforms (γ1, γ2 and γ3). In mammals, 12 different heterotrimeric complexes have been reported with species- and tissue-specific expression

patterns [205]. An example of AMPK subunit expression patterns in mouse and human tissues such as liver and skeletal muscle is shown in **Table 2.3**.

Table 2.3 – Distribution of AMPK subunit isoforms in mouse and human liver and skeletal muscle

	Predominant AMPK Subunit Isoform Expression						
	α1	**α2**	**β1**	**β2**	**γ1**	**γ2**	**γ3**
Human Liver	**X**			**X**	**X**		
Mouse Liver	**X**		**X**		**X**		
Human Skeletal Muscle		**X**		**X**	**X**		**X**
Mouse Skeletal Muscle		**X**		**X**	**X***	**X***	**X***

*: Expression levels vary depending on skeletal muscle fibre type. Table adapted from [12,206-208].

The AMPK catalytic α subunit contains a kinase domain on its N-terminus that comprises AMPK's main regulatory phosphorylation site (T172) within the activation loop that regulates its enzymatic activity. Next to the kinase domain lies an α-autoinhibitory domain (AID) that keeps the kinase domain in its inactive conformation when AMP is absent. AID is bound by the α-linker to the C-terminal domain (CTD), which binds to the β and γ subunits [209] (**Figure 2.7**). The AMPK β subunit is a scaffolding subunit that is required for the formation of a functional AMPK heterotrimeric complex [210]. It contains a conserved subunit interaction domain on its C-terminus that links both the CTD of the α subunit and the N-terminal region of the γ subunit. At its N-terminus, the β subunit also contains a myristoylation site involved in targeting AMPK to membranes [209]. Importantly, the β subunit contains a conserved domain, the carbohydrate-binding module (CBM), that enables AMPK to bind glycogen, which is believed to allow AMPK to sense stored energy in the form of glycogen [7,13,211]. The CBM also forms an allosteric drug and metabolite binding pocket (ADaM site)

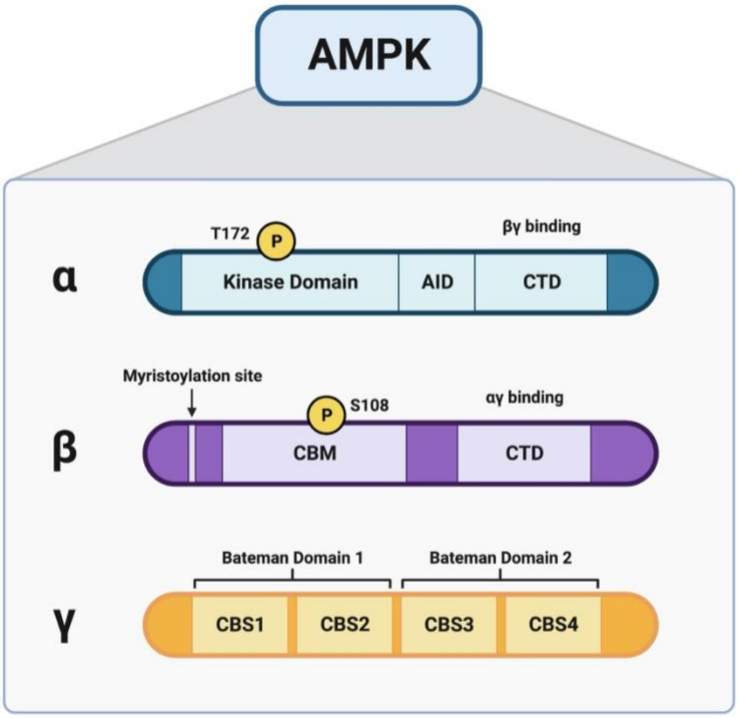

Figure 2.7 – Overview of AMPK heterotrimeric subunits and domain structure. Created with BioRender.com

in association with the kinase domain of the α subunit that allows small molecule AMPK activators (e.g., A-769662 or 991) to bind [210,212]. AMPK β phosphorylation on S108 is required for the ADaM site to stabilise, enabling AMPK to become activated by ADaM site-directed drugs [213]. The AMPK γ subunit comprises two Bateman domains that are each composed of two cystathionine β-synthase (CBS) domains. These four CBS allow AMPK to sense cellular energy levels by binding to AMP, ADP and ATP in a competitive manner [209].

2.10.2. AMPK Activation During Exercise

Activation of AMPK occurs as a result of cellular energy stress either through reduced production or increased consumption of ATP, such as states of starvation, hypoxia, and exercise [214]. Exercise represents a major stress to metabolic homeostasis and is thus a powerful activator of AMPK in skeletal muscle. The turnover of ATP, the energy "currency" of the cell, can increase 100-fold relative to the resting state while, at the whole-body level,

maximal exercise can elicit a 20-fold increase in metabolic rate [24]. This state of energy stress is characterised by a decrease in cellular adenylate charge (increased levels of adenosine mono- and diphosphate (AMP and ADP, respectively) [215]. As AMP and ADP accumulate, they bind to the CBS domains of the γ subunit, thereby changing the conformation of AMPK and promoting the phosphorylation of T172 of the catalytic α subunit by one of its two major upstream kinases, liver kinase B1 (LKB1) [216] (**Figure 2.8**). This reversible phosphorylation

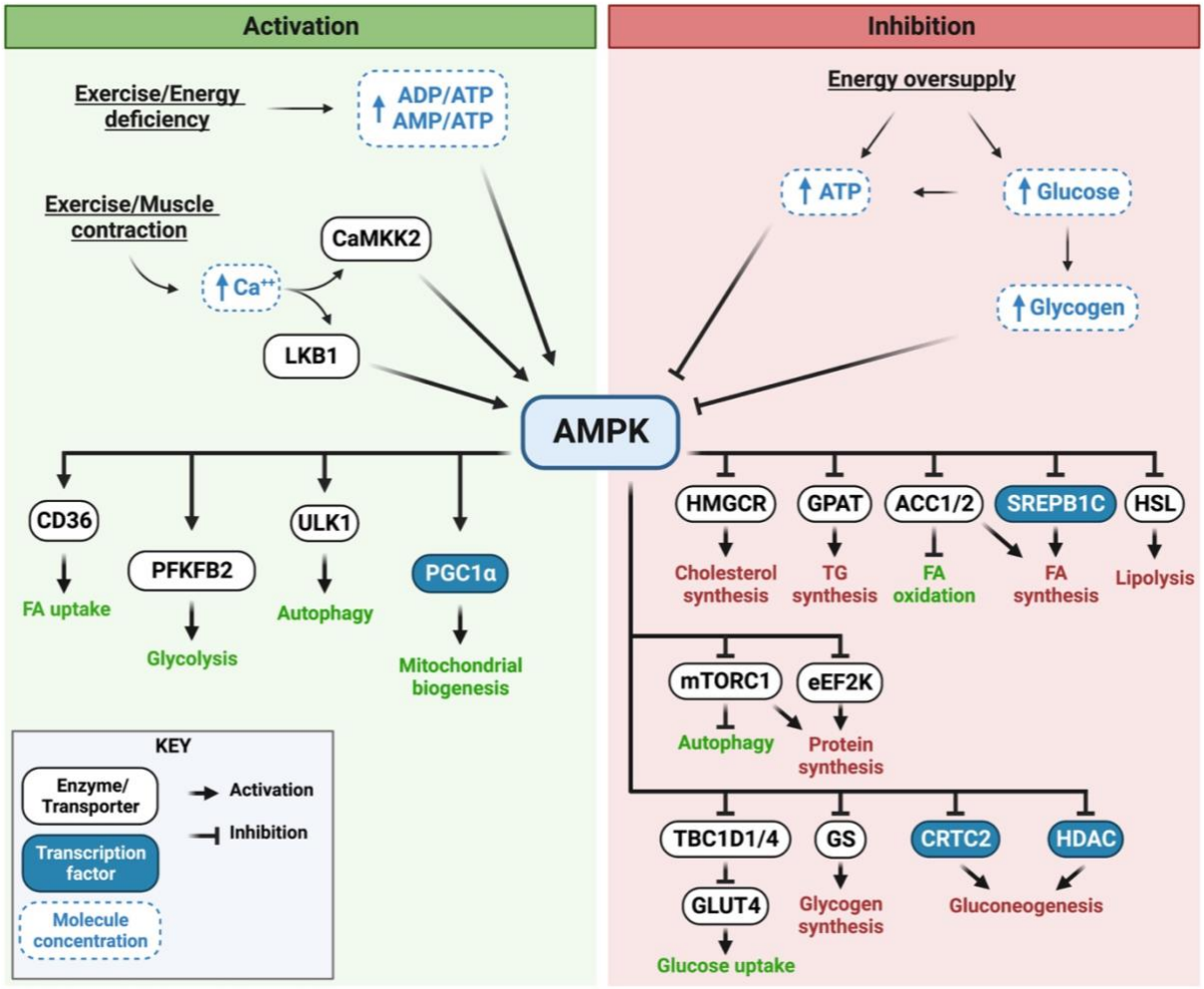

Figure 2.8 – Schematic summarising regulation of AMPK activity by some of its upstream regulators and regulation of downstream metabolic pathways through protein phosphorylation. Once activated by upstream regulators, AMPK phosphorylates numerous enzymes, resulting in their activation (green) or inhibition (red). AMPK can also promote the activation of metabolic pathways by phosphorylating negative regulators of these pathways (e.g., stimulation of glucose uptake by phosphorylating and inhibiting TBC1D1 and 4 to release GLUT4 storage vesicles to the plasma membrane). Alternatively, AMPK is able to translocate to the nucleus and regulate the activity of transcription factors. Created with BioRender.com

of T172 is required for full activation of AMPK and can enhance its activity by 50 to 100-fold [217,218]. Nucleotide binding to the γ subunit also induces a conformational change that prevents protein phosphatases from dephosphorylating AMPK at T172 [219,220]. The binding of AMP to the γ subunit promotes allosteric activation of AMPK, which can increase its activity up to 10-fold [219]. AMPK can also be activated in a nucleotide-independent manner through phosphorylation of T172 by its other major upstream kinase, Ca^{2+}/calmodulin-activated kinase kinase 2 (CAMKK2 or CAMKKβ), which becomes activated by increased intracellular levels of Ca^{2+} resulting from cellular events including muscle contraction and hormonal changes [221]. Other non-canonical mechanisms of AMPK activation have been reviewed elsewhere [17,209] and are outside the scope of this thesis.

Of note, AMPK activation is dependent on exercise intensity and duration. Activation of AMPK is observed at exercise intensities > 60% of maximal aerobic capacity [222-224], although lower intensities can also activate AMPK during prolonged exercise (e.g., 3.5 hours at 45% VO_2 max) [225]. Different AMPK heterotrimeric complexes show differential biochemical properties depending on their subunit isoforms [205], including varying sensitivity to exercise intensity or duration. For example, the α1β2γ1 complex is accountable for approximately 65% of AMPK's basal activity in human *vastus lateralis* in spite of its low expression level in this muscle (~15%) [226]. This complex exhibits little response to exercise stimuli and its activity is only increased in response to prolonged low-intensity exercise [227]. Conversely, the α2β2γ3 complex is activated in response to higher intensity exercise [227]. AMPK activation is also influenced by skeletal muscle glycogen, as commencing exercise with low glycogen levels has been associated with greater exercise-induced activation of AMPK when compared to exercising in a glycogen-replete state [223,228,229].

2.10.3. AMPK and Metabolism Regulation

Findings over the past decades have expanded the understanding of the diverse mechanisms by which AMPK regulates metabolism. As previously explained, AMPK plays a critical role in the regulation of energy homeostasis and eliciting the metabolic adaptations to exercise in tissues such as skeletal muscle. With over 60 known downstream targets including transcription factors and cofactors [230,231], AMPK can restore energy balance through regulating a wide range of metabolic pathways including glucose, lipid and protein metabolism. Some other exercise-stimulated functions of AMPK include activation of pathways underlying autophagy as well as mitochondrial biogenesis [209] (**Figure 2.8**).

2.10.3.1. Glucose Metabolism

The rate-limiting step of glucose uptake in skeletal muscle is the translocation of glucose transporter (GLUT) 4 to the plasma membrane [232]. In response to exercise-induced activation, AMPK phosphorylates Tre-BUB-CDC16 domain family member 1 (TBC1D1) and 4 (TBC1D4, also known as AS160) (**Figure 2.8**) on various residues [233-235]. This causes sequestration of TBC1D1/4 by 14-3-3 adaptor proteins and promotes translocation of GLUT4-containing vesicles to the plasma membrane facilitating glucose uptake [234]. It has also been suggested that AMPK may regulate GLUT1 through phosphorylation and the subsequent degradation of Thioredoxin-interacting protein [236].

In some tissues such as the heart, AMPK is able to regulate glycolysis by phosphorylating and activating phosphofructokinase-2 (PFKFB2), the enzyme that catalyses the conversion of fructose-6phosphate to fructose-2,6-bisphosphate [237]. The latter strongly stimulates hexokinase and phosphofructokinase, two rate-limiting enzymes of glycolysis [238]. Evidence has also shown that AMPK is able to regulate glycogen synthesis through phosphorylation of S7 on glycogen synthase (GS) (**Figure 2.8**), the rate-limiting enzyme of

glycogen synthesis [239]. Paradoxically, chronic activation of AMPK in both cardiac and skeletal muscle results in glycogen accumulation [240]. This counterintuitive accumulation of glycogen is thought to be due to an AMPK-induced stimulation of glucose uptake, leading to increased intracellular levels of glucose-6-phosphate, which allosterically activates GS, overriding the inhibitory effects of AMPK on GS [240].

2.10.3.2. Lipid Metabolism

AMPK regulates lipid metabolism by promoting FA uptake and oxidation, and by inhibiting FA synthesis. For example, AMPK activation induces FA uptake by promoting the translocation of FA transporter cluster of differentiation 36 (CD36) to the plasma membrane [19]. The most well characterised mechanism by which AMPK regulates lipid metabolism is via inhibitory phosphorylation of acetyl-CoA carboxylase (ACC) [18], which catalyses the conversion of acetyl-CoA to malonyl-CoA, an important substrate involved in FA synthesis [241]. ACC exists in two isoforms, ACC1 and ACC2, and while they exhibit different functions and subcellular localisation, both ACC isoforms are downstream targets of AMPK. Specifically, ACC1 is primarily expressed within the cytosol and is mainly involved in the promotion of FA synthesis, whereas ACC2 possesses a mitochondrial targeting sequence where it exerts inhibitory effects on the FA transporter carnitine palmitoyl transferase-1 (CPT1) through the production of malonyl-CoA [214]. Inactivation of ACC1 by phosphorylation at S79 results in reduced production of malonyl-CoA thereby inhibiting FA synthesis, whereas inactivation of ACC2 by phosphorylation at S212 promotes FA oxidation through reducing the malonyl-CoA-mediated inhibition of CPT1 [242,243]. Other downstream targets inhibited by AMPK have also been reported such as hormone-sensitive lipase (HSL), glycerol-3-phosphate acyltransferase (GPAT) and 3-hydroxy-3-methylglutaryl-CoA reductase (HMGCR), which are involved in triglyceride (TG) breakdown, TG synthesis and cholesterol synthesis, respectively [18,244,245] (**Figure 2.8**).

2.10.3.3. Protein Metabolism and Autophagy

Another critical metabolic role of AMPK within cells is the inhibition of a major and highly conserved anabolic regulatory protein, the mammalian target of rapamycin complex 1 (mTORC1) [246]. Activated AMPK phosphorylates and activates tuberous sclerosis complex 2 (TSC2) which in turn inhibits mTORC1 through the phosphorylation of S residues within the Raptor compartment of mTORC1 (**Figure 2.8**) [247]. Another well-appreciated role of AMPK is the promotion of autophagy via phosphorylation of the Unc-51 like autophagy activating kinase 1 (ULK1). AMPK appears to stimulate ULK1 in two ways; by direct phosphorylation and by inhibition of mTORC1, resulting in the release of inhibitory phosphorylation mTORC1 exerts on ULK1 [248,249]. AMPK can further inhibit protein translational elongation by phosphorylation and activation of eukaryotic elongation factor 2 (eEF2) kinase (eEF2K), which inhibits eEF2 [250]. Additional AMPK downstream targets involved in autophagy have been identified and are described in more detail elsewhere [5].

2.10.3.4. Regulation of Glucose and Lipid Metabolism through Transcriptional Control

AMPK is also able to translocate to the nucleus and regulate the transcription of genes involved in carbohydrate and lipid metabolism. Indeed, AMPK has inhibitory effects on the transcriptional induction of gluconeogenesis through phosphorylation of cAMP response element-binding protein (CREB)-regulated transcription coactivator 2 (CRTC2) and class II histone deacetylases (HDAC). This phosphorylation leads to their exclusion from the nucleus, thus preventing them from playing their crucial roles in gluconeogenesis by promoting the expression of gluconeogenic enzymes such as L-type pyruvate kinase, phosphoenolpyruvate carboxykinase and glucose-6-phosphatase [251,252]. Similarly, AMPK inhibits lipogenic pathways at the transcriptional level by inhibitory phosphorylation of several targets including a major regulator of lipid synthesis, sterol regulatory element binding protein 1c (SREBP1c)

and carbohydrate-responsive element binding protein (ChREBP), which notably promote gene expression of FA synthase and ACC1 [209,253,254].

Furthermore, AMPK activation is involved in mitochondrial biogenesis, a key skeletal muscle adaptation to endurance training [1]. Indeed, AMPK can stimulate mitochondrial biogenesis by phosphorylation and activation of the peroxisome proliferator-activated receptor gamma coactivator 1-alpha (PGC-1α) [255], an inducible transcription coactivator and key regulator of mitochondrial biogenesis (**Figure 2.8**) [256]. AMPK can also stimulate PGC-1α gene expression by phosphorylating HDAC5, leading to the release of its inhibitory effect on the myocyte enhancer factor 2, a transcription factor that promotes PGC-1α gene expression [257]. The increased expression of PGC-1α and activation of the myocyte enhancer factor 2 are associated with increased skeletal muscle oxidative capacity and improved endurance performance [258,259]. AMPK also regulates metabolic processes such as autophagy and mitophagy through transcriptional control, as reviewed elsewhere [209]. Collectively, this wide array of mechanisms by which AMPK regulates metabolism highlights its pivotal roles in metabolic homeostasis and exercise-induced metabolic adaptations.

2.10.3.5. Regulation of Energy Sensing and Metabolism via Glycogen Binding

Glycogen is a large polysaccharide synthesised from glucose through an anabolic process termed glycogen synthesis or glycogenesis. Glycogenesis involves several regulatory proteins. For example, the regulatory protein glycogenin resides in the centre of a glycogen particle and initiates glycogen synthesis [260]. The rate-limiting enzyme GS is responsible for the α-1-4 linkage of UDP-glucose donors, thereby forming the linear bonds of a glycogen particle. The presence of the UDP-glucose precursor – glucose-6-phosphate – is therefore central to activation of GS. In addition to allosterically activating GS, glucose-6-phosphate can also override the inhibitory phosphorylation of AMPK, protein kinase A and glycogen synthase

kinase 3 on GS [240,261]. Finally, glycogen branching enzyme is responsible for attaching α-1-6 branches to glycogen particles. Glycogen breakdown (also called glycogenolysis) involves two regulatory enzymes. Glycogen phosphorylase breaks down α-1-4 glycosidic bonds within glycogen particles, while glycogen debranching enzyme further degrades glycogen particles by breaking α-1-6 bonds [261].

Glycogen serves as an important energy store in mammalian species and is mainly present in liver and skeletal muscle, where it plays essential roles in the control of energy homeostasis, exercise capacity and performance [262]. Of note, while the primary function of liver glycogen is to maintain blood glucose levels, skeletal muscle glycogen is used locally as a substrate for glycolysis in order to produce energy and facilitate muscle contraction [263]. At the onset of low- to moderate-intensity exercise (< 45% and 45-75% of VO_2 max, respectively) [1], the increase in glucose uptake from the bloodstream by working skeletal muscle is associated with decreased levels of insulin and increased levels of glucagon [264]. This results in the stimulation of hepatic glucose output via the breakdown of glycogen and conversion of other energy substrates via the process of gluconeogenesis to help maintain glucose homeostasis. During high intensity exercise (> 70-75% VO_2 max), muscle glycogen becomes the primary fuel source to sustain the energetic demands of exercise [27,29,30]. Depletion of glycogen stores results in fatigue and the inability to maintain high exercise intensity [265]. Similarly, patients with glycogen storage diseases such as McArdle's disease – characterised by a deficiency in the enzyme glycogen phosphorylase [266,267] – display impaired utilisation of muscle glycogen, which is associated with exercise intolerance [265,268].

Key differences between humans and rodents exist with respect to glycogen utilisation during exercise. In humans, ~80% of glycogen is stored in skeletal muscle, which represents ~500 g of muscle glycogen on average [263]. Although liver contains a higher level of glycogen relative to muscle even after an overnight fast (~650-750 mmol × kg^{-1} dry weight in liver vs

~250-450 mmol × kg^{-1} in skeletal muscle [269]), human liver only contains a total of ~100 g glycogen due to its much smaller organ size relative to muscle [263]. The amount of muscle glycogen relative to total body mass is ~10-fold lower in mice versus humans, while the proportion of liver glycogen stores in mice is similar to humans. Therefore, mice have a greater reliance on liver-derived energy substrates in settings of increased energy demands such as exercise [265]. Therefore, limitations exist in the ability to extrapolate findings related to fuel utilisation from rodents to humans, and caution is warranted in such comparisons [265]. Further details regarding glycogen dynamics and utilisation are beyond the scope of this thesis and readers are referred to other review articles focusing on these topics [261,270]. In addition to its energy storage role, it has been suggested that glycogen may also serve regulatory functions in AMPK's control of metabolism. Indeed, Wojtaszewski and colleagues reported decreased AMPKα activity and increased GS activity in rat skeletal muscle with loaded- versus depleted-glycogen stores, regardless of the adenine nucleotides concentrations [271]. The authors also made similar observations in human skeletal muscle during exercise [223]. Together these findings suggest inhibitory effects of glycogen on AMPK activity.

The ability of AMPK β subunit isoforms to bind glycogen via the CBM was first shown *in vitro* in 2003 by Hudson *et al.* and Polekhina *et al.* [6,7]. Polekhina's experiments demonstrated that mutating the single amino acid within the β1 CBM, tryptophan (W100) or lysine (K126), to glycine (W100G) or glutamine (K126Q), respectively, disrupted glycogen binding. Subsequent experiments from McBride *et al.* (2009) demonstrated that the inhibitory effects of glycogen on AMPK could be relieved through the mutation of these critical residues [13]. Residues W100 and W133 (analogous to W98 and W133 in AMPK β2) have been shown to mediate glycogen binding within the CBM of the β1 subunit, as disrupting a single tryptophan in the pair can inhibit glycogen binding [7,13,211]. Subsequent *in vivo* experiments using whole-body AMPK β2 knock-out (KO) mice have highlighted the physiological

importance of the AMPK β subunit in exercise as these KO mice displayed reduced endurance capacity and maximal running speed relative to wild type (WT) mice [8,11]. Likewise, O'Neill *et al.* (2011) have shown that maximal running speed was also impaired in muscle-specific β1β2 double KO mice compared to control WT mice. These muscle-specific double KO mice also displayed reduced respiratory exchange ratio (RER) which indicates a greater reliance on fat oxidation (and reduced reliance on carbohydrate oxidation) for energy production [10].

Despite tremendous efforts to further understand the physiological functions of AMPK-glycogen binding, the models described above can only provide limited insight. For instance, AMPK subunit KO models, although revealing useful information about the metabolic roles of AMPK, also present some challenges. One of these challenges is that removing the expression of the entire β subunit may disturb other functions of AMPK since the β subunit serves as a scaffolding subunit that is pivotal to the stability of the αβγ heterotrimer and its removal alters AMPK activity [12]. Another challenge of deleting the expression of a specific β subunit isoform is the potential for compensatory upregulation of the other β isoform [11].

Therefore, the use of other gene editing technologies such as gene knock-in (KI) mutations using CRISPR/Cas9 have proved useful to more fully understand the interactive roles of AMPK and glycogen *in vivo* [12]. As such, recent findings from my group showed phenotypic effects of disrupting AMPK's glycogen binding capacity *in vivo*, using AMPK β1 or β2 single KI mice in which amino acid residues in either isoform CBM that mediate glycogen binding were mutated (β1 W100A KI or β2 W98A KI) [14]. These β1 W100A KI and β2 W98A KI mutations were associated with disrupted whole-body and tissue metabolism and impaired maximal running capacity in β2 W98A KI mice relative to WT mice. Considering both AMPK β1 and β2 isoforms are expressed in the majority of mouse tissues and cell types including liver and skeletal muscle [12], mice with KI mutations in both isoforms (AMPK β1 W100A/β2 W98A double knock-in; DKI) were generated to investigate the phenotypic

consequences of disrupting whole-body AMPK-glycogen interactions. DKI mice also showed impaired whole-body metabolism and changes in energy substrate utilisation patterns such as reduced fat oxidation, which was associated with increased total body and fat mass and altered tissue glycogen dynamics [15]. Furthermore, these metabolic effects were associated with reduced maximal exercise capacity in DKI mice compared to WT [16]. Despite these findings, the associated changes in metabolic pathways and molecular mechanisms underlying these phenotypic effects in DKI mice remain largely unknown and warrant further investigation using metabolomic approaches to uncover metabolites regulated by acute exercise and as a result of disrupting AMPK-glycogen interactions.

Chapter 3 – Methodology and Design

3.1. Study 1 - Metabolomics Reveals Mouse Plasma Metabolite Responses to Acute Exercise and Effects of Disrupting AMPK-Glycogen Interactions

3.1.1. Animal Models

CRISPR/Cas9 gene editing was performed by the Mouse Engineering Garvan/ABR (MEGA) Facility to generate whole-body AMPK *Prkab1*^{W100A} (β1 W100A) and *Prkab2*^{W98A} (β2 W98A) single KI mice on a C57BL/6J background [14]. Several amino acid residues within the CBM of AMPK's β subunit have been identified as being critical to AMPK-glycogen binding, including W100 and the analogous W98 residue within the β1 and β2 isoforms, respectively, as mutation of these amino acid residues has been shown to result in the disruption of AMPK-glycogen binding [7,13,211]. In these KI models, tryptophan (W) residues were mutated to alanine (A), as previously described [14]. Homozygous single KI mice with either β1 W100A or β2 W98A mutation were crossed to generate *Prkab1*^{W100A}/*Prkab*2^{W98A} DKI mice (**Figure 3.1**).

Homozygous WT mice and homozygous carriers of the KI mutations were separately bred to generate the homozygous WT and DKI mouse lines used in these thesis experiments, and WT and DKI breeders were annually backcrossed to regenerate heterozygous mice and subsequently rederive these homozygous lines to prevent potential genetic drift. Tail samples were collected for confirmatory genotyping, which was performed by TransnetYX (Cordova, TN, USA) via real-time polymerase chain reaction. Due to limited age-matched mouse cohort availability and in order to maintain sufficient female mice for breeding, only male mice were used in the present study. All metabolomics-based analyses of plasma were performed using age-matched WT and DKI male mice within an age range of 12–16 weeks.

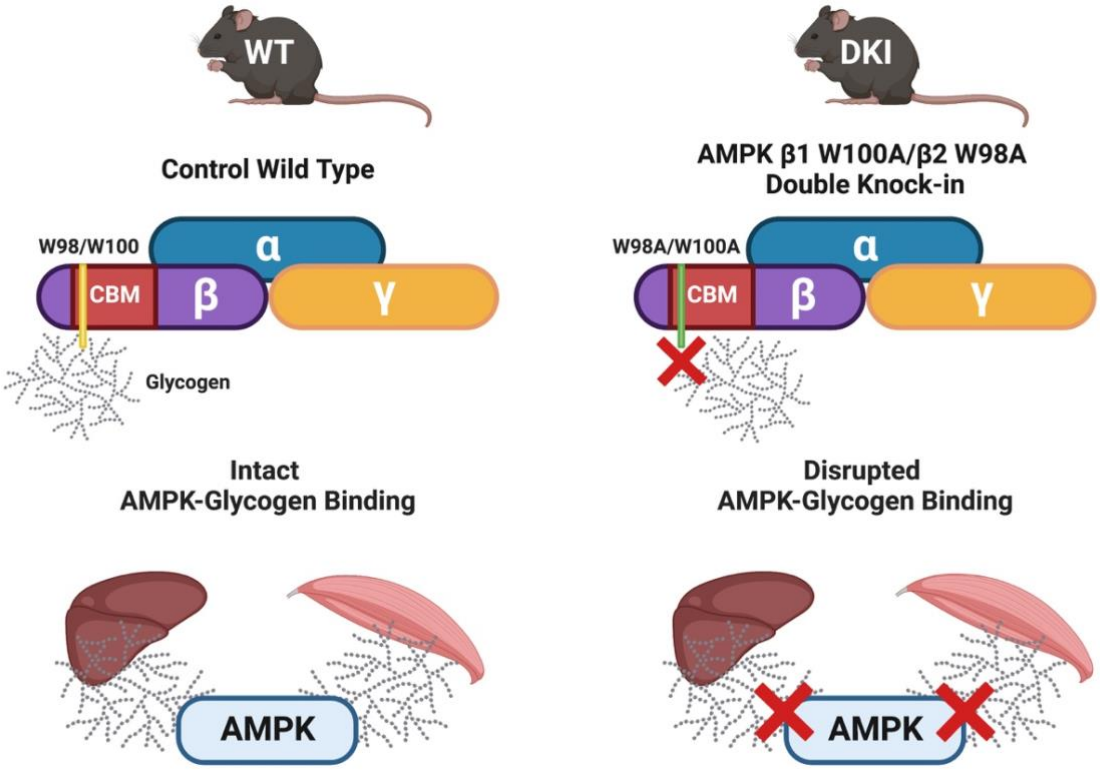

Figure 3.1 – AMPK β1 W100A/β2 W98A double knock-in (DKI) mouse model with whole-body disruption of AMPK-glycogen binding. While control wild type (WT) mice have intact AMPK-glycogen binding capacity, AMPK DKI mice with mutation of critical tryptophan residues to alanine (W100A and W98A) within the carbohydrate-binding module of each β subunit isoform have disrupted whole-body AMPK-glycogen binding. Liver and skeletal muscle represent primary tissue glycogen stores and are critical to metabolic control and responses to exercise. Created with BioRender.com.

All mouse procedures were performed under the approval of the St. Vincent's Hospital (Melbourne, Australia) Animal Ethics Committee (approval numbers 025-15 and 011-19) in accordance with NHMRC requirements and conforming to the National Institutes of Health animal research guidelines (NIH Publications No. 8023, revised 1978) and Australian codes of animal research practice (8th Edition 2013). Mice were kept in pathogen-free microisolator cages (2–5 mice per cage) on standard 12:12-h dark-light cycles with controlled temperature (21°C), humidity and bedding. Mice had ad libitum access to water and standard rodent chow diet (29% starch, 20% protein and 6% fat, Barastoc, Ridley Agriproducts, Pakenham, Australia).

3.1.2. Body Weight and Whole-Body Composition Measurements

Mouse body weights were recorded using standard laboratory scales and whole-body composition was determined by magnetic resonance imaging (MRI) using the EchoMRI Composition Analysis 3-in-1 system (EchoMRI, Houston, TX, USA). Mice were individually placed and restrained inside cylindric tubes to avoid movement during the body composition measurements (approximately 75 to 90 s). All MRI measurements were performed in the fed state between 0800 and 0900 h.

3.1.3. Maximal Running Speed Test, Acute Exercise Protocol and Plasma Sample Collection

Mice were acclimatised to the treadmill (Columbus Instruments Exer 3/6 Columbus, OH, USA) for 4 days at progressing speeds at a 0° incline (**Figure 3.2**). Manual prodding using a soft bristle brush was performed to provide encouragement when necessary during both acclimatisation and subsequent testing. On day 1, mice were placed on a stationary treadmill for 5 min; on day 2, they ran for 5 min at a rate of 5 m/min. On day 3, mice ran for 5 min at 10 m/min; and on day 4, mice ran for 5 min at each of the following speeds: 10, 12 and 15 m/min. Following a 24-h recovery period, mice were subjected to an incremental maximal exercise capacity test in which they first ran at 10 m/min for 2 min, after which the speed was increased 1 m/min every 2 min until the mouse reached exhaustion, defined as an inability to compel the mouse to continue running despite repeated manual prodding [10,11]. Mice were then randomly assigned either to the “exercised” or “rested” group.

Following two to three days of recovery, mice assigned to the exercise group completed a 30-min exercise bout at 70% of their individual maximal speed at a 0° incline, while rested mice remained in their home cage. This 70% of individual maximal running speed was used due to the mix of carbohydrate and fat energy sources expected to be utilised at this speed [272,273]. Upon completion of the rest period or exercise trial, both groups were immediately

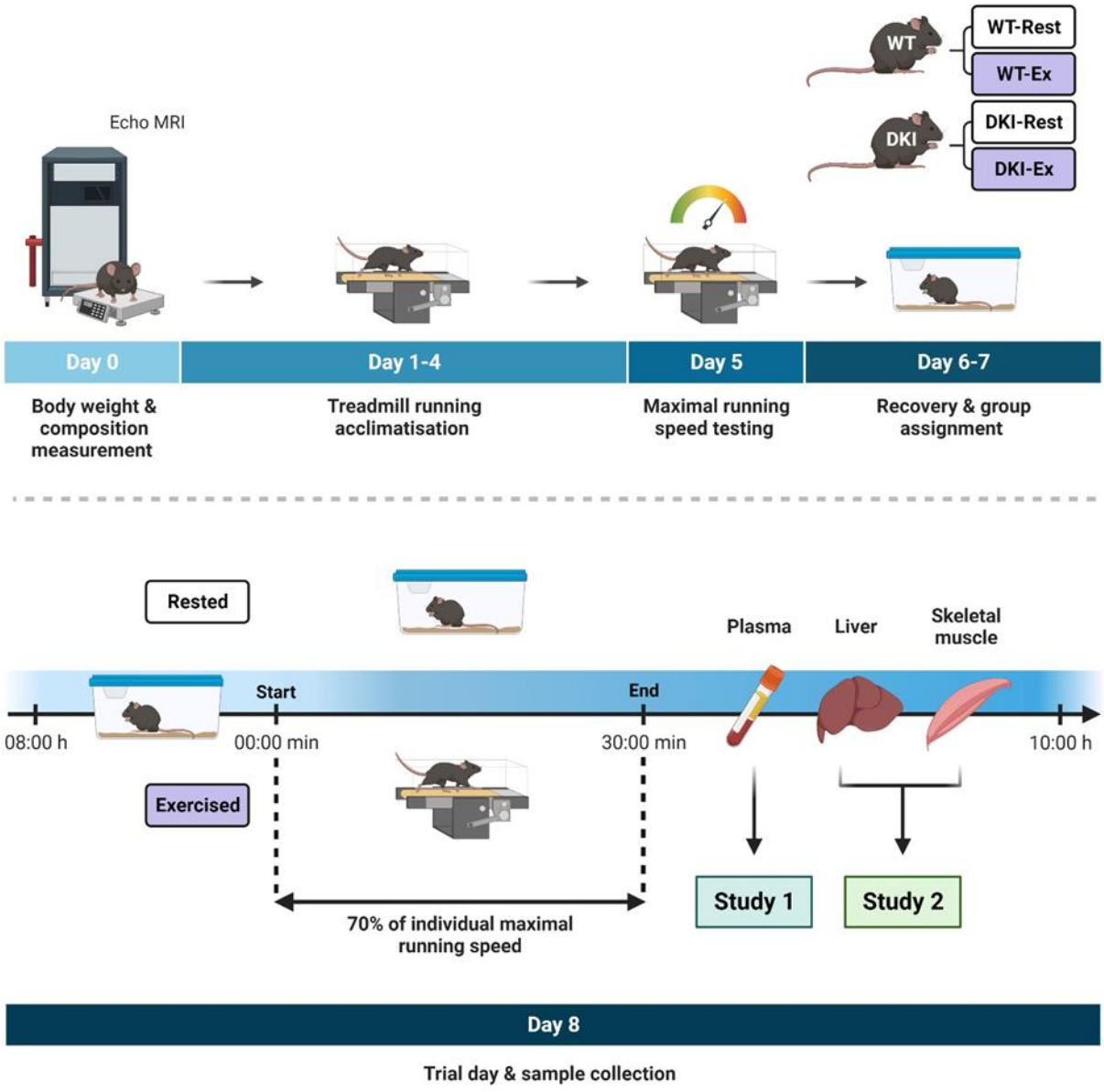

Figure 3.2 – Experimental design of Study 1 and 2 exercise trial and sample collection. Following body weight and composition measurements, mice were acclimatised to treadmill running for four days. 24 h later, maximal running speed of each mouse was determined using an incremental running test until mice reached exhaustion (i.e. inability to remain on the treadmill despite repeated manual encouragement). WT and DKI mice were randomly assigned to the rested or exercised conditions (WT-Rest, WT-Ex, DKI-Rest, DKI-Ex) and were allowed to rest for two days. On the exercise trial and sample collection day, mice from the exercised condition performed a 30-min run at 70% of their individual maximal running speed while the rested mice remained in their home cage. Immediately following exercise/rest, mice were placed in a CO_2 chamber (~10 s) and blood was collected via cardiac puncture, then immediately placed on ice and plasma was isolated via centrifugation and stored at −80°C until analyses. Liver and gastrocnemius muscles were collected and immediately snap-frozen in liquid nitrogen then stored at −80°C until analyses. n = 21 (WT) and 23 (DKI) mice. Created with BioRender.com.

placed in a CO_2 chamber for ~10 s prior to a cardiac puncture to allow collection of sufficient blood volume. Blood collections were performed in the fed state between 0800 and 1000 h in both the exercised and rested groups, corresponding to the beginning of the light phase in the animal facility. Blood was collected via cardiac puncture using a 23G needle attached to a 1 mL syringe, immediately transferred to 1.3 mL lithium-heparin coated tubes (Sarstedt, Nümbrecht, Germany), inverted 10 times and placed on ice. Tubes were then centrifuged at 2000 × g for 10 min at 4°C, with total time on ice consistent for all collected samples. Plasma supernatant was divided into 300 µL aliquots and stored at −80°C until further analysis.

3.1.4. Liquid Chromatography-Mass Spectrometry Based Metabolomics

3.1.4.1. Plasma Sample Preparation

Plasma sample preparation, data acquisition, processing and analysis were performed at the Centre for Integrative Metabolomics and Computational Biology, Edith Cowan University (Joondalup, Western Australia, Australia) according to previously established liquid chromatography-mass spectrometry (LC-MS) workflows [97]. Plasma samples were thawed on ice and each sample was separated into two 30 µL aliquots. A pooled quality control (QC) sample was prepared by mixing 50 µL of remaining plasma from each sample; the pooled sample was subsequently divided into 30 µL aliquots (**Figure 3.3**). All prepared aliquots were then frozen and stored at −80°C until day of analysis.

On the day of metabolomic data acquisition, plasma aliquots were thawed on ice, and protein precipitation was performed prior to running two liquid chromatography-based separation modes, as detailed below. For hydrophilic interaction liquid chromatography (HILIC), protein precipitation was performed by adding 90 µL of ice-cold liquid LC-MS grade acetonitrile [3:1 (v/v)] containing isotopically labelled standards of known concentration [1 ppm each: valine-d8, tryptophan-d9, taurodeoxycholic acid-d4, leucine-13C1 and sphingosine-

d9 (d18:1)] to plasma samples and pooled QC aliquots. For reversed-phase liquid chromatography (RPLC), protein precipitation was performed by adding 90 µL of ice-cold LC-MS grade methanol to each 30 µL aliquot, with identical internal standards. Samples were then mixed at 1,400 revolutions per min (rpm) for 2 min at 4°C and centrifuged (Heraeus Megafuge 8R, Thermo Fisher Scientific, Australia) for 20 min (1800 × g) at 4°C. 30 µL from each of the resulting supernatants were transferred into LC-MS vials and placed in an autosampler tray at 6°C.

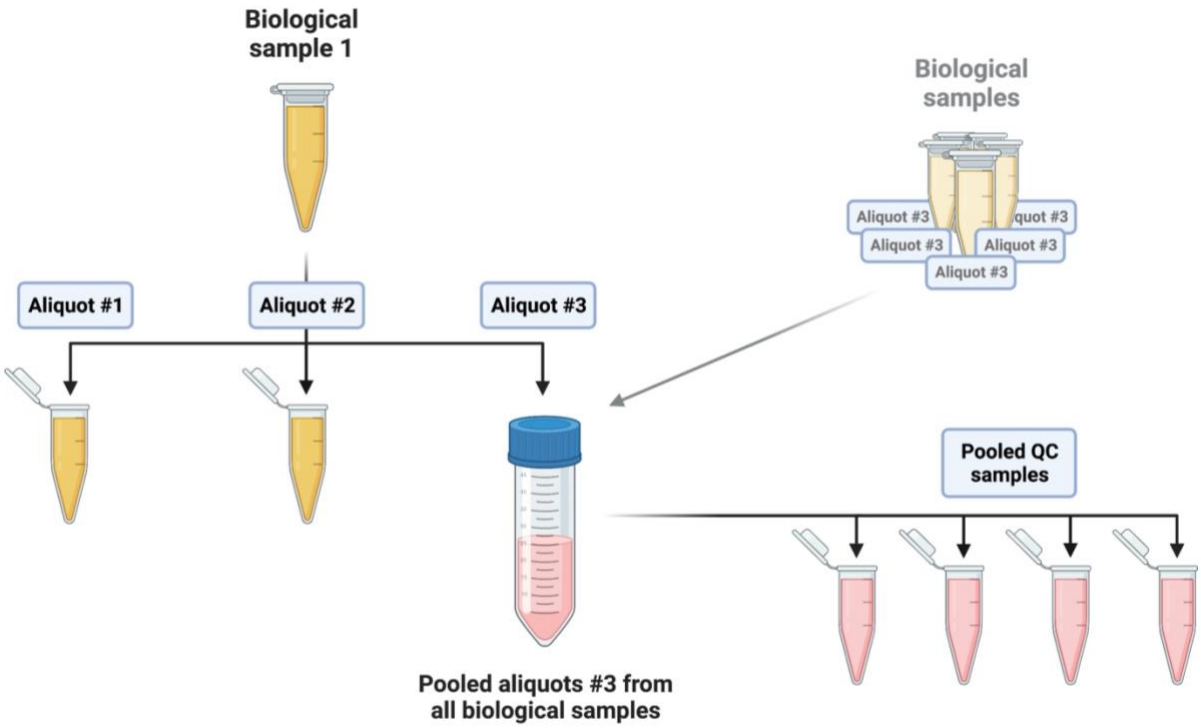

Figure 3.3 – Sample preparation procedure for pooled quality control (QC) samples was performed by adding 50 µL of each biological plasma sample (aliquots #3) in a conical tube and mixing them together before being distributed into 30 µL pooled QC sample aliquots. Created with BioRender.com.

Prior to the LC-MS run, the sample injection sequence was block randomised by group (WT-Rest, WT-Ex, DKI-Rest, DKI-Ex). LC-MS system suitability was checked using the quality assurance methods described by Broadhurst *et al.* (2018) and eight pooled QC samples were injected at the beginning of the sequence to condition the column. Pooled QC samples

were then injected following each block of eight experimental samples (i.e., every ninth injection) which were used for assessment of analytical precision as reported in [52] (**Figure 3.4**).

3.1.4.2. Metabolomic Data Acquisition: Liquid Chromatography–High Resolution Mass Spectrometry

Samples were analysed using the Dionex UltiMate 3000 platform which comprises an ultra-high performance liquid chromatography pump coupled to a heated electrospray Q Exactive Focus Orbitrap mass spectrometer (Thermo Scientific, San Jose, CA, USA). Data were acquired in full scan mode at a mass resolution of 70,000 (Full Width at Half Maximum (FWHM) at mass to charge ratio (m/z) of 200), over a scan range of m/z 70–1000. Tandem mass spectrometry (MS/MS) was performed on all QC samples using data-dependent acquisition (DDA) in "discovery" mode using the following settings: resolution = 17,500; isolation width = 3.0 m/z; stepped collision energy = 15, 30 eV. Source and ion transfer conditions were as follows: sheath gas = 35 (arbitrary units), auxiliary gas = 10 (arbitrary units), source heater 350°C, capillary temperature = 350°C, ion spray voltage = 2.5 kV (negative ion mode) and 3.0 kV (positive ion mode). The automatic gain control target was set at 3×10^{-6}.

Two chromatography-based separation methods were applied to each sample. Polar metabolites were separated by HILIC chromatography in positive mode (HILIC POS), using an ACQUITY UPLC BEH Amide column (2.1 × 100 mm, 1.7 μm; Waters, Milford, MA, USA) with a flow rate of 400 μL/ min and the following mobile phases: mobile phase A (10 mM ammonium formate in water + 50 mM formic acid) and mobile phase B (10 mM ammonium formate in 90% Acetonitrile + 50 mM formic acid). A 15-min elution gradient was applied as follows: 0 min; 100% B; 1 min 1% B; 8–9 min 60% B; 10 min 100% B through to 15 min. A 6 μL sample injection volume was applied. Non-polar metabolites were separated by RPLC on

Injection number	Sample type
1	Extraction blank 1
2	System conditioning QC sample 1
3	System conditioning QC sample 2
4	System conditioning QC sample 3
5	System conditioning QC sample 4
6	System conditioning QC sample 5
7	System conditioning QC sample 6
8	System conditioning QC sample 7
9	System conditioning QC sample 8
10	Pooled QC sample 9
11	Pooled QC sample 10
12	Biological sample 1
13	Biological sample 2
14	Biological sample 3
15	Biological sample 4
16	Biological sample 5
17	Biological sample 6
18	Biological sample 7
19	Biological sample 8
20	Pooled QC sample 11
21	Biological sample 9
22	Biological sample 10
23	Biological sample 11
24	Biological sample 12
25	Biological sample 13
26	Biological sample 14
27	Biological sample 15
28	Biological sample 16
29	Pooled QC sample 12
30	Biological sample 17
31	Biological sample 18
32	Biological sample 19
33	Biological sample 20
34	Biological sample 21
35	Biological sample 22
36	Biological sample 23
37	Biological sample 24
38	Pooled QC sample 13
39	Biological sample 25
40	Biological sample 26
41	Biological sample 27
42	Biological sample 28
43	Biological sample 29
44	Biological sample 30
45	Biological sample 31
46	Biological sample 32
47	Pooled QC sample 14
48	Biological sample 33
49	Biological sample 34
50	Biological sample 35
51	Biological sample 36
52	Biological sample 37
53	Biological sample 38
54	Biological sample 39
55	Biological sample 40
56	Pooled QC sample 15
57	Biological sample 41
58	Biological sample 42
59	Biological sample 43
60	Biological sample 44
61	Pooled QC sample 16
62	Pooled QC sample 17
63	Pooled QC sample (MS/MS acquisition 1)
64	Pooled QC sample (MS/MS acquisition 2)
65	Pooled QC sample (MS/MS acquisition 3)
66	Pooled QC sample (MS/MS acquisition 4)
67	Pooled QC sample (MS/MS acquisition 5)
68	Extraction blank 2

Figure 3.4 – Sample injection sequence for LC-MS analysis including extraction blanks, system conditioning QC samples, pooled QC samples and biological samples. Briefly, this injection sequence was used for quality assurance and system suitability (one injection of blanks at the start and end of the analytical run), conditioning of the LC column system with pooled QC samples (eight injections of conditioning QC samples at the start of the analytical run), and signal correction (two additional pooled injections of QC samples at the start and end of the run, as well as pooled QC injections every ninth injection). Another five pooled QC samples were injected into the LC-MS at the end of the run for MS/MS data acquisition. This figure was adapted from [52].

a Hypersil GOLD column (2.1 × 100 mm, 1.9 μm; Thermo Fisher Scientific, Runcorn, UK), with a flow rate 300 μL/min using the following mobile phases: mobile phase A (water + 0.1% formic acid) and mobile phase B (Acetonitrile + 0.1% formic acid). A 15-min elution gradient was applied as follows: 0 min 1% B; 1 min 1% B; 2 min 50% B; 9–10 min 99% B; 10.5 min 1% B through to 15 min. A 6 μL sample injection was applied, and samples were collected in positive and negative mode. Xcalibur software (Thermo Fisher Scientific v4.3) was used for data acquisition. Before analysis, commercially purchased calibrant solutions (negative and positive ion calibration solutions) from Thermo Fisher Scientific (San Jose, CA, USA) were used to externally calibrate the Orbitrap mass spectrometer.

3.1.4.3. Data Processing and Metabolite Identification/Annotation

Following data acquisition, spectral processing was performed (i.e., HILIC POS and C18 POS and C18 NEG) in Compound Discoverer™ 3.1 (Thermo Scientific, San Jose, CA, USA) using an untargeted metabolomics workflow. Compound Discoverer™ version 3.1 was utilised for total ion chromatograms alignment along retention times (RT) based on an adaptive curve, with a 5 ppm mass tolerance and a maximum shift of 0.5 min. Detected features with a signal-to-noise ratio > 5 and an intensity ≥ 1,000,000 in each dataset were merged into compounds according to ion adducts. Ions detected within the blanks were subtracted from the samples using the "mark background compounds" node. Online databases such as the human metabolome database (http://www.hmdb.ca), mzCloud (https://www.mzcloud.org/), and the

KEGG (http://www.genome.ad.jp/kegg/) were searched to verify and putatively annotate metabolites. Metabolite identification/annotation was also performed in Compound Discoverer™ in accordance with the Metabolomics Standard Initiative (MSI) [71]. Quality control-regularised spline correction (QC-RSC) was used to correct analytical signal drift [274]. Following standard protocols [52], metabolites with relative standard deviation (RSD) QC > 20% or a Dispersion-ratio (D-ratio) > 30% were removed from further statistical analyses based on their failure to meet acceptable measurement precision.

3.1.5. Statistical Analyses

For statistical analyses of mouse body mass, body composition and maximal running speed, *P* values were calculated using unpaired Student's t-tests (WT versus DKI) and Welch's correction was applied when applicable, with $P < 0.05$ considered statistically significant. Outlier identification was performed using the Grubb's test or the ROUT method. Statistical tests for these measures were performed using GraphPad Prism software version 8.4.3 (GraphPad Software, San Diego, CA).

For statistical analyses of the metabolomics dataset, two-way ANOVA was performed to test the null hypothesis (i.e., no differences between rested/exercised conditions and/or WT/ DKI genotypes) for each individual identified/annotated metabolite. Estimation of the false discovery rate (FDR) due to multiple comparisons was performed using the Storey FDR method [275], and *P* values < 0.05 with a FDR < 0.1 were considered statistically significant.

To assess the structured similarities between metabolite concentrations across the complete dataset, hierarchical cluster analysis (HCA) was performed using Pearson's correlation coefficient as the similarity measure, and Ward's linkage method [276]. The lowest linkages (i.e., closest metabolite clusters) within the HCA dendrogram indicate metabolites that

display the most similar responses. The resulting visualisation labelled by metabolite significance, indicates metabolites of particular interest displaying similar (correlated) changes.

To model and visualise the multivariate discrimination between the four experimental groups, all metabolites were combined into a single data matrix and applied to principal component–canonical variate analysis (PC-CVA) [277]. PC-CVA uses the (multivariate) covariance between metabolite concentration and outcome classification to test the statistical significance of the mean differences. Multivariate data is projected into a two-dimensional subspace (canonical variate axes) reflecting the combination of metabolites that best discriminate the labelled groups. Results are visualised via 1) a scores plot, with 95%, confidence intervals (CI) of the mean from each group indicating significant differences, and 2) a coefficients plot indicating the contribution importance of each metabolite to each canonical variate. Overfitting was avoided by using 5-fold cross validation to choose the optimal number of principal components to apply to the CVA model. 95% CI for the model coefficients were calculated using bootstrap resampling [278]. Prior to all statistical analyses, metabolite profiles were $\log_{10}$ transformed and scaled to unit variance (auto scaled), allowing each metabolite to be objectively compared with no bias due to large differences in metabolite concentration. Statistical analyses of the metabolomic dataset were performed using MATLAB ®package version R2021b (MathWorks, Natick, MA).

3.2. Study 2 - Metabolomic Analysis of Mouse Skeletal Muscle and Liver Metabolite Responses to Acute Exercise and Loss of AMPK-Glycogen Binding Capacity

3.2.1. Tissue Sample Collection

Since skeletal muscle and liver samples used for metabolomic analyses were derived from the same WT and DKI mice used for plasma analyses in Study 1 (as depicted in Figure

3.2), refer to sections 3.1.1. to 3.1.3. for methodological details related to the animal models, body weight, whole-body composition, maximal running speed test, and the acute exercise protocol. Following blood collection via cardiac puncture (as described for study 1), the same liver lobe was excised from each mouse and a consistent portion of mixed gastrocnemius muscle was collected and immediately snap frozen in liquid nitrogen, then stored at –80°C until further analysis. All tissue samples were collected between 0800 and 1000 h in both the exercised and rested groups, corresponding to the beginning of the light phase.

3.2.2. LC-MS Based Metabolomics

3.2.2.1. Tissue Sample Preparation

An average of 50 mg (wet weight) of liver and mixed gastrocnemius muscle from each mouse was chipped and freeze-dried overnight. Approximately 10 mg of tissue were then manually ground into fine powder with striated forceps on a glass dish and transferred to new tubes, then immediately returned to −80°C. Tissue sample preparation and LC-MS analyses were performed at the Centre for Integrative Metabolomics and Computational Biology, Edith Cowan University (Joondalup, Western Australia, Australia) according to previously described methods [175,279]. Sample preparation for LC-MS analyses was performed as follows: extraction solution was prepared using methanol:acetonitrile:water (2/2/1 (v/v)) with isotopically-labelled internal standards (valine-d8, phenylalanine-d8, caffeine-13C3, creatinine-d3, leucine-d3, sphingosine-d9, tryptophan-d5, trimethylamine N-oxide-d8, taurodeoxycholic acid-d5) at 1 ppm. Approximately 800 µL of extraction solution was added to each tissue sample (volume was corrected to the mass of each powdered tissue sample) and blank tube. Each tube was then vortexed for 10 s and placed on thermomixer agitator at 1,200 rpm for 2 min at 4°C and centrifuged (Heraeus Megafuge 8R, Thermo Fisher Scientific, Australia) for 10 min at 14000 rpm. Following agitation, 100 µL of supernatant was added to

two separate glass inserts in injection vials (one set of vials for each assay, detailed below). An additional 40 µL of remaining supernatant from each sample were combined to create a pooled QC stock solution, which was then aliquoted into 20 LC-MS vials of 60 µL each. Sample injection sequence (randomised by group; WT-Rest, WT-Ex, DKI-Rest, DKI-Ex) was identical to that of Study 1 (**Figure 3.4**). LC-MS system suitability was checked using the quality assurance methods described previously [52] and 8 pooled QC samples were injected at the beginning of the sequence to condition the column. Pooled QC samples were then injected following each block of experimental samples for assessment of analytical precision as reported in [52].

3.2.2.2. Metabolomic Data Acquisition: Liquid Chromatography–High Resolution Mass Spectrometry

- C18 Assay:

All tissue samples were analysed using an Ultra High-Pressure Liquid Chromatography pump (Dionex UltiMate 3000 RS) coupled to an Orbitrap Q-Exactive MS (Thermo Scientific, San Jose, CA, USA) fitted with a heated electrospray ionisation (HESI) probe. Metabolite separation was performed using a reversed phase Hypersil GOLD column (100 × 2.1 mm, 1.9 µm particle size; Thermo Scientific, San Jose, CA, USA) with an in-line filter. Tissue samples were analysed in positive and negative ionisation modes using 0.1% formic acid in LC-MS water (solvent A) and 0.1% formic acid in LC-MS grade acetonitrile (solvent B). The following elution gradient was utilised: isocratic at 99% solvent A for 1 min, followed by an increase to 50% solvent B (1–2 min), then a linear increase to 99% solvent B over 7 min, which was maintained at 99% solvent B for 2 min. Initial conditions were returned over 2 min and held at 100% solvent A for equilibration (3 min). The flow rate was 0.3 mL/min for positive and negative modes, the injection volume was 4 µL, and the autosampler tray was set to 6°C and

column oven temperature to 45°C. Full scans with data-dependent MS/MS were acquired with the Orbitrap mass analyser. Full scans were acquired with a resolution of 70,000 at mass-to-charge ratio (m/z) 200 over the m/z range 70–1000 with the following electrospray ionisation (ESI) conditions: source heater = 413°C (positive mode) 350°C (negative mode), sheath gas = 50 (positive mode) 35 (negative mode) (arbitrary units), auxiliary gas = 10 (arbitrary units), capillary temperature = 320°C (positive mode) 350°C (negative mode), ion spray voltage = 3.5 kV (positive mode) and 2.5 kV (negative ion mode), S-lens 50%, and automatic gain control = 1×10^{-6}. MS/MS was performed at a resolution of 17,500 at m/z 200 for each sample with the higher energy collisional dissociation energy of 20 eV. Data acquisition was performed with Xcalibur software (Thermo Scientific, San Jose, CA, USA). Prior to analysis, external calibration of the Orbitrap was carried out using ready-made calibration solutions (ESI-negative ion calibration and ESI-positive ion calibration solutions) purchased from Thermo Fisher Scientific.

- Hydrophilic Interaction Liquid Chromatography (HILIC) Assay:

Tissue samples were analysed using an Ultra High-Pressure Liquid Chromatography pump (Dionex UltiMate 3000 RS) coupled to an Orbitrap Q-Exactive MS (Thermo Scientific, San Jose, CA, USA) fitted with a HESI probe. Metabolite separation was performed on a Acquity UPLC Amide Column (100 x 2.1mm, 1.7 μm particle size; Waters, Milford, MA, USA). Sample analysis was performed using LC-MS water buffered with 10 mM ammonium formate and 50 mM formic acid for a pH of 3 (solvent A) and 90:10 LCMS acetonitrile and LC-MS grade water buffered with 10 mM ammonium formate and 50 mM formic acid (solvent B). The following elution gradient was used: isocratic at 100% solvent B for 1 min, followed by a linear increase to 40% solvent A (1–8 min), which was maintained at 40% solvent A for 1 min. Initial conditions were returned over 1 min, then held at 100% solvent B for equilibration (5 min). The flow rate was 0.4 mL/min. Injection volume was 4 μL, and the autosampler tray

was set to 6°C and column oven temperature to 45°C. Full scans with data-dependent MS/MS were acquired with the Orbitrap mass analyser. Full scan acquisition was performed at a resolution of 70,000 at mass-to-charge ratio (m/z) 200 over the m/z range 70–1000 with the following ESI conditions: source heater = 350°C, sheath gas = 35 (arbitrary units), auxiliary gas = 10 (arbitrary units), capillary temperature 350°C, ion spray voltage = 3.5 kV, S-lens 50%, and automatic gain control = 1×10^{-6}. MS/MS was performed at a resolution of 17,500 at m/z 200 for each sample with the higher energy collisional dissociation energy of 20 eV. Data acquisition was performed with Xcalibur software (Thermo Scientific, San Jose, CA, USA). Prior to analysis, external calibration of the Orbitrap was carried out using ready-made calibration solutions (ESI-negative ion calibration and ESI-positive ion calibration solutions) purchased from Thermo Fisher Scientific.

3.2.2.3. Data Processing and Metabolite Identification/Annotation

Following data acquisition, spectral processing was performed (i.e., HILIC POS and C18 POS and C18 NEG) in Compound Discoverer™ 3.1 (Thermo Scientific, San Jose, CA, USA) using an untargeted metabolomics workflow. Compound Discoverer™ version 3.1 was utilised for total ion chromatograms alignment along retention times (RT) based on an adaptive curve, with a 5 ppm mass tolerance and a maximum shift of 0.5 min. Detected features with a signal-to-noise ratio > 5 and an intensity ≥ 1,000,000 in each dataset were merged into compounds according to ion adducts. Ions detected within the blanks were subtracted from the samples using the "mark background compounds" node. Online databases such as the human metabolome database (http://www.hmdb.ca), mzCloud (https://www.mzcloud.org/), and the KEGG (http://www.genome.ad.jp/kegg/) were searched to verify and putatively annotate metabolites. Metabolite identification/annotation was also performed in Compound Discoverer™ in accordance with the MSI [71]. QC-RSC was used to correct analytical signal drift [274]. Following standard protocols [52], metabolites with RSD QC > 20% or a D-ratio >

30% were removed from further statistical analyses based on their failure to meet acceptable measurement precision.

3.2.3. Mouse Embryonic Fibroblast Isolation and Culture

Mouse embryonic fibroblasts (MEF) were derived from AMPK β1 W100A/β2 W98A DKI and control WT pregnant female breeders aged 11 to 18 weeks. Pregnant female mice were culled by cervical dislocation. Their carcass was immediately brought to the tissue culture room under the hood of the biosafety cabinet and disinfected with 70% ethanol. Following a midline incision to the abdomen, the uterus was dissected out and embryo sacs were separated with scissors and washed with Dulbecco's phosphate buffered saline (DPBS; Thermo Fisher Scientific, San Jose, CA, USA) in a Petri dish. Embryos from the same genotypes (WT or DKI) were pooled by groups of four to five and dissected out of their respective sacs with a scalpel. Head, gut, tail and limbs were cut and discarded. The remaining embryonic trunks were transferred to a new Petri dish, minced in 5 mL of pre-warmed trypsin-EDTA (Merck, Rahway, NJ, USA), and placed in a 37°C 5% CO_2 incubator for 15-20 min. Four to five minced embryonic trunks and 10 mL of growth medium – Dulbecco's Modified Eagle Medium (DMEM) high-glucose (Merck, Rahway, NJ, USA) with 10% of Fetal Bovine Serum (FBS; Thermo Fisher Scientific, San Jose, CA, USA) – were added to a Petri dish, transferred to a 50 mL conical tube and centrifuged at 500 × g for 5 min at 4°C. Supernatant was discarded and the pellet was resuspended in 6 mL of pre-warmed growth medium and eventually plated in a T25 flask.

Flasks containing cells were passaged when ~95% confluency was reached. Growth media from flasks containing cells were first discarded and cells were rinsed with 1-2 mL of pre-warmed DPBS. After discarding the DPBS, 2-3 mL of pre-warmed trypsin were added to each flask and placed in a 5% CO_2 incubator at 37°C until detachment of 95-100% of cells (~5-

8 min). 10 mL of pre-warmed growth medium were added to inactivate trypsin and any clumps of cells were dispersed by pipetting up and down and transferred to a 50 mL conical tube and centrifuged at 500 × g for 5 min at 4°C. Supernatant was discarded and the pellet was resuspended in 15 mL of pre-warmed growth medium and plated in a T75 flask. After three to four passages, MEF cells were immortalised with SV40 T antigen in collaboration with SVI, following the publicly available MEF immortalisation protocol from Heather P. Harding publicly available through Addgene at the following website: https://media.addgene.org/data/45/42/165f51de-af64-11e0-90fe-003048dd6500.pdf.

The same process was applied to freeze and store cells at –80°C, following up to three times (P_3). However, after centrifugation (500 × g for 5 min at 4°C) and disposal of supernatant, the cell pellet was resuspended in 10 mL of FBS containing 10% dimethyl sulfoxide (DMSO; Merck, Rahway, NJ, USA) and divided into 1 mL aliquots within cryovials, then stored at –80°C until analysis.

3.2.4. Seahorse XFe24 Real-Time ATP Rate Assay

Prior to performing each Real-Time ATP Rate Assay, cell count and viability were first determined by adding Trypan blue (Thermo Fisher Scientific, San Jose, CA, USA) to resuspended cells (50% v/v) and manually counting using a hemocytometer (Merck, Rahway, NJ, USA). To do so, cell vials were first thawed and transferred into a 15 mL centrifuge tube and 10 mL of pre-warmed growth medium was added. Tubes were then centrifuged at 500 rpm for 5 min at 24°C. The supernatant containing FBS with DMSO was carefully discarded and the cell pellet was resuspended with new growth medium and incubated in a 37°C and 5% CO_2 incubator. Cells at P_8-P_{14} were utilised for re-seeding in a Seahorse 24-well plate and performing the Real-Time ATP Rate Assay using the Seahorse XFe24 Analyzer (Agilent, Santa Clara, CA, USA) according to user manual's instructions [280].

The day prior to analysis, cells were harvested and resuspended to the desired concentration (i.e., cell seeding density of 20,000 cells/100 μL of growth medium) in Agilent Seahorse XFe24 Cell Culture Microplates and allowed to adhere for 60 min in a 37°C and 5% CO_2 incubator before adding another 150 μL of growth medium to each well, bringing the total volume to 250 μL per well. Cells were then placed back in the incubator overnight. The sensor cartridge was then hydrated with 1 mL of XF calibrant solution added to each well of the utility plate and placed in the 37°C non-CO_2 incubator overnight.

On the day of analysis, fresh Seahorse XF Real-Time ATP Rate Assay Medium (further referred to as "assay medium") was prepared (Seahorse XF DMEM medium, pH 7.4; Seahorse XF Glucose (1.0 M solution); Seahorse XF Pyruvate (100 mM solution); Seahorse XF L-Glutamine (200 mM solution) with 97/1/1/1 (v/v)) and warmed to 37°C. All but 50 μL of growth medium was removed from each well and cells were washed with 1 mL of assay medium. 450 μL of assay medium was then added to the wells, bringing the final volume to 500 μL per well. The plate was then placed in a 37°C non-CO_2 incubator for 60 min. XF Real-Time ATP Rate Assay injection solutions of Oligomycin (1.5 μM) and Rotenone + Antimycin A (0.5 μM) were prepared. After taking the sensor cartridge out of the incubator, injection ports A and B were loaded with Oligomycin and Rotenone + Antimycin A, respectively. Once all A and B ports were filled, the sensor cartridge and utility plate were transferred to the Seahorse XFe24 Analyzer for calibration. Following cartridge calibration, cells were washed with assay medium one more time and finally placed in the Seahorse XFe24 Analyzer for Real-Time ATP Rate Assay (**Figure 3.5**).

Following the XF Real-Time ATP Rate assay, XF assay medium was removed from all wells and 100 μL of distilled water containing 2% sodium dodecyl sulfate was added to each well and cells were detached from the plate and resuspended by repeated pipetting. Cells were

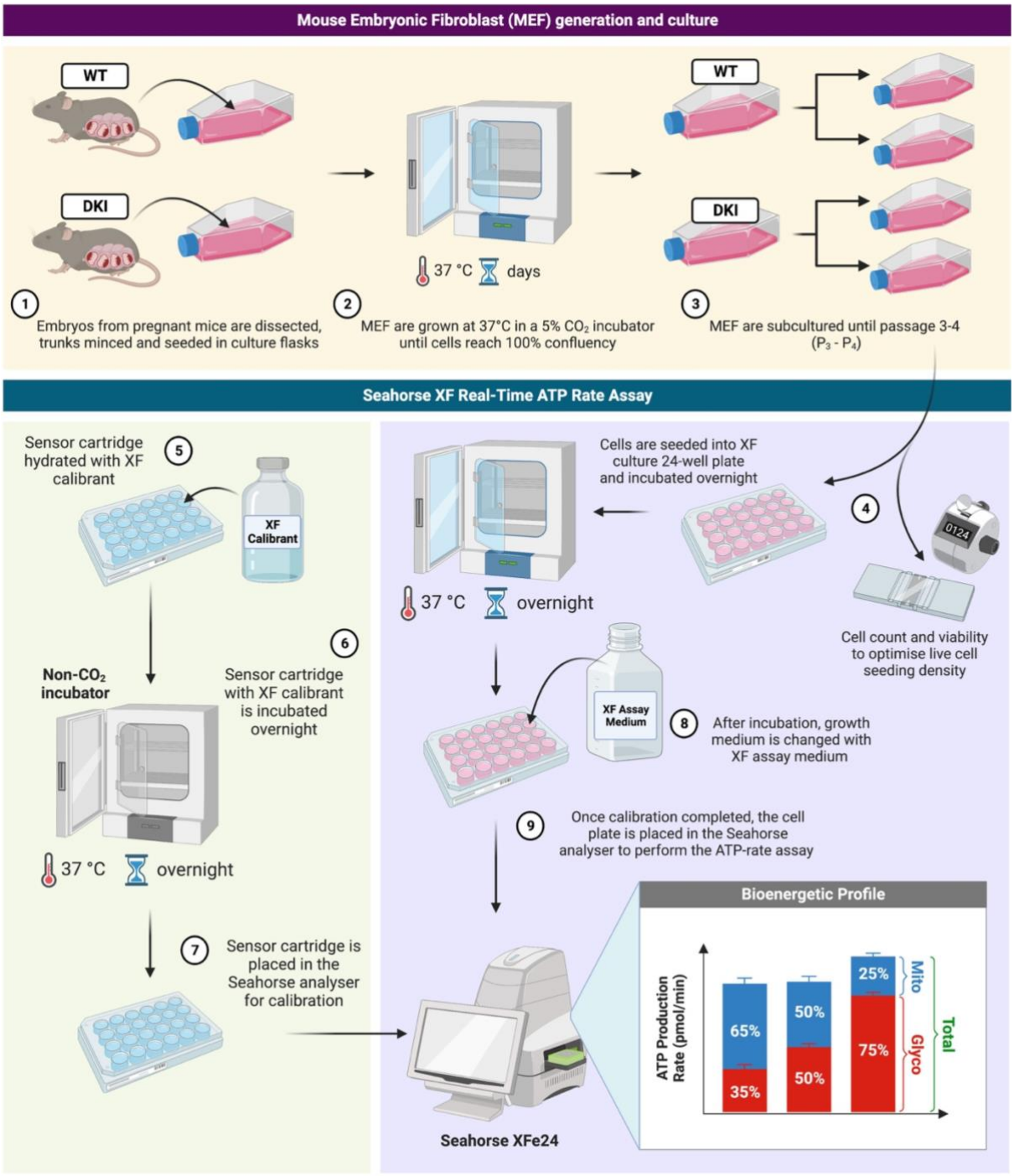

Figure 3.5 – Summary of mouse embryonic fibroblasts (MEF) generation and cell culture and overview of the Real-Time ATP Rate Assay procedure using the Seahorse XFe24 Analyzer. Created with Biorender.com

then transferred to a 96-well microplate for total protein content assessment using the Pierce™ bicinchoninic acid (BCA) Protein Assay Kit (Pierce, Rockford, Illinois, USA) according to the user manual procedure. Based on protein content, ATP rate assay values were corrected to

account for any potential differences in total protein content between WT and DKI cells in the ATP Rate assay.

3.2.5. Mitochondrial Respiration

3.2.5.1. Preparation of Permeabilised Fibres

Male WT and DKI mice aged ~15-23 weeks were culled by cervical dislocation in the fed state between 0800 h and 0900 h. Gastrocnemius muscles were collected and placed in ice-cold BIOPS solution (50 mM MES, 7.23 mM K_2EGTA, 2.77 mM CaK_2EGTA, 20 mM imidazole, 0.5 mM DTT, 20 mM taurine, 5.77 mM ATP, 15 mM PCr, and 6.56 mM $MgCl_2 \cdot H_2O$; pH 7.1). The muscle was trimmed of connective tissue and fat and separated into red and white portions. Several small muscle bundles (~2.0-5.0 mg wet weight) were prepared by separating muscle along the longitudinal axis using fine-tipped forceps under a dissecting microscope. Fibre bundles were then treated with 40 µg/mL saponin for 30 min at 4°C and subsequently washed in MiR05 respiration buffer (0.5 mM EGTA, 10 mM KH_2PO_4, 110 mM sucrose, and 1 mg/mL fatty acid-free BSA; pH 7.1) for 15 min as described previously Perry *et al*. (2012) [281].

3.2.5.2. Mitochondrial Respiration

Oxygen (O_2) consumption measurements from permeabilised muscle fibres were performed in MiR05 respiration medium using an Oxygraph-2K (Oroboros Instruments, Innsbruck, Austria) at 37°C in the presence of 25 µM blebbistatin, as described elsewhere [282]. ADP-stimulated respiration was determined from fibres prepared from red and white muscle. Titrations were initiated in the presence of 10 mM pyruvate and 5 mM malate and ADP was titrated at various concentrations. Glutamate (10 mM) and succinate (10 mM) were added to quantify maximum mitochondrial respiration. Finally, outer mitochondrial membrane integrity was determined by adding 10 µM cytochrome c, with < 10% increase in respiration indicating

outer mitochondrial membrane integrity. Experiments were performed in duplicate and data were normalised to muscle fibre bundle wet weight. The apparent K_m for ADP was determined as previously described [281].

3.2.6. Statistical Analyses

Results from this study were analysed using Student's t-test and Welch's correction was applied when applicable, with $P < 0.05$ considered statistically significant. One- or two-way ANOVA with Fisher's least significant difference as post hoc analysis were also used where applicable, with $P < 0.05$ considered statistically significant. Statistical tests for these measures were performed using GraphPad Prism software version 8.4.3 (GraphPad Software, San Diego, CA, USA).

For statistical analyses of the liver and gastrocnemius metabolomics datasets, two-way ANOVA was performed to test the null hypothesis (i.e., no differences between rested/exercised conditions and/or WT/ DKI genotypes) for each individual identified/annotated metabolite. Estimation of the FDR due to multiple comparisons was performed using the Storey FDR method [275], and P values < 0.05 with a FDR < 0.1 were considered statistically significant.

To assess the structured similarities between metabolite concentrations across the complete dataset, HCA was performed using Pearson's correlation coefficient as the similarity measure, and Ward's linkage method [276]. The lowest linkages (i.e., closest metabolite clusters) within the HCA dendrogram indicate metabolites that display the most similar responses. The resulting visualisation labelled by metabolite significance indicates metabolites of particular interest displaying similar (correlated) changes.

To model and visualise the multivariate discrimination between the four experimental groups, all metabolites were combined into a single data matrix and applied to PC-CVA [277].

PC-CVA uses the (multivariate) covariance between metabolite concentration and outcome classification to test the statistical significance of the mean differences. Multivariate data is projected into a two-dimensional subspace (canonical variate axes) reflecting the combination of metabolites that best discriminate the labelled groups. Results are visualised via: 1) a scores plot, with 95% CI of the mean from each group indicating significant differences, and 2) a coefficients plot indicating the contribution importance of each metabolite to each canonical variate. Overfitting was avoided by using 5-fold cross validation to choose the optimal number of principal components to apply to the CVA model. 95% CI for the model coefficients were calculated using bootstrap resampling [278]. Prior to all statistical analyses, metabolite profiles were $\log_{10}$ transformed and scaled to unit variance (auto scaled), allowing each metabolite to be objectively compared with no bias due to large differences in metabolite concentration. Statistical analyses of the metabolomic dataset were performed using MATLAB® package version R2021b (MathWorks, Natick, MA).

Chapter 4 – Study 1: Metabolomics Reveals Mouse Plasma Metabolite Responses to Acute Exercise and Effects of Disrupting AMPK-Glycogen Interactions

Publication statement:

The content of Chapter 4 is from an original research article published on 24 August 2022 in ***Frontiers in Molecular Biosciences*** in the Research Topic "*OMICS-Based Approaches in Sports Research Volume II*".

Belhaj, M.R., Lawler, N.G., Hawley, J.A., Broadhurst, D.I., Hoffman, N.J. & Reinke, S.N. (2022). Metabolomics reveals mouse plasma metabolite responses to acute exercise and effects of disrupting AMPK-glycogen interactions. *Front. Mol. Biosci.*, 9: 957549. https://doi.org/10.3389/fmolb.2022.957549

Metabolomics reveals mouse plasma metabolite responses to acute exercise and effects of disrupting AMPK-glycogen interactions

Mehdi R. Belhaj [1], Nathan G. Lawler [2,3], John A. Hawley [1], David I. Broadhurst [2], Nolan J. Hoffman [1,*] and Stacey N. Reinke [2,*]

[1] Exercise and Nutrition Research Program, Mary MacKillop Institute for Health Research, Australian Catholic University, Melbourne, VIC, Australia

[2] Centre for Integrative Metabolomics and Computational Biology, School of Science, Edith Cowan University, Joondalup, WA, Australia

[3] Australian National Phenome Centre and Centre for Computational and Systems Medicine, Health Futures Institute, Murdoch University, Perth, WA, Australia

[*] Correspondence: nolan.hoffman@acu.edu.au; stacey.n.reinke@ecu.edu.au

4.1. Abstract

Introduction: The AMP-activated protein kinase (AMPK) is a master regulator of energy homeostasis that becomes activated by exercise and binds glycogen, an important energy store required to meet exercise-induced energy demands. Disruption of AMPK-glycogen interactions in mice reduces exercise capacity and impairs whole-body metabolism. However, the mechanisms underlying these phenotypic effects at rest and following exercise are unknown. Furthermore, the plasma metabolite responses to an acute exercise challenge in mice remain largely uncharacterised.

Methods: Plasma samples were collected from wild type (WT) and AMPK double knock-in (DKI) mice with disrupted AMPK-glycogen binding at rest and following 30-min submaximal treadmill running. An untargeted metabolomics approach was utilised to determine the breadth of plasma metabolite changes occurring in response to acute exercise and the effects of disrupting AMPK-glycogen binding.

Results: Relative to WT mice, DKI mice had reduced maximal running speed ($P < 0.0001$) concomitant with increased body mass ($P < 0.01$) and adiposity ($P < 0.001$). A total of 83 plasma metabolites were identified/annotated, with 17 metabolites significantly different ($P < 0.05$; FDR < 0.1) in exercised (↑6; ↓11) versus rested mice, including amino acids, acylcarnitines and steroid hormones. Pantothenic acid was reduced in DKI mice versus WT. Distinct plasma metabolite profiles were observed between the rest and exercise conditions and between WT and DKI mice at rest, while metabolite profiles of both genotypes converged following exercise. These differences in metabolite profiles were primarily explained by exercise-associated increases in acylcarnitines and steroid hormones as well as decreases in amino acids and derivatives following exercise. DKI plasma showed greater decreases in amino acids following exercise versus WT.

Conclusion: This is the first study to map mouse plasma metabolomic changes following a bout of acute exercise in WT mice and the effects of disrupting AMPK-glycogen interactions in DKI mice. Untargeted metabolomics revealed alterations in metabolite profiles between rested and exercised mice in both genotypes, and between genotypes at rest. This study has uncovered known and previously unreported plasma metabolite responses to acute exercise in WT mice, as well as greater decreases in amino acids following exercise in DKI plasma. Reduced pantothenic acid levels may contribute to differences in fuel utilisation in DKI mice.

Keywords: exercise metabolism, plasma metabolite, metabolomics, AMP-activated protein kinase, glycogen, amino acids, acylcarnitines, pantothenic acid

4.2. Introduction

The benefits of exercise on metabolic health are widely appreciated. Exercise represents a substantial challenge to cellular and whole-body energy homeostasis, and a multitude of molecular metabolic responses including changes in circulating metabolites occur in response to exercise to help meet increased energy demands and preserve homeostasis [1]. One of the key regulators of energy homeostasis is the AMP-activated protein kinase (AMPK), a pivotal cellular energy sensing kinase that integrates intracellular and extracellular metabolic signals and regulates numerous downstream metabolic pathways to mobilise energy reserves and generate ATP, the energy currency of the cell [209]. Through competitive binding of ATP, ADP and AMP, AMPK senses cellular energy status. Decreases in cellular energy levels (i.e., increased AMP/ATP ratio) in response to exercise lead to activation of AMPK. Once activated, AMPK switches on catabolic pathways including glycolysis and fat oxidation, while concurrently switching off anabolic processes including fat and protein synthesis [209]. In addition, AMPK contains a carbohydrate binding module (CBM) within its β subunit (existing in two isoforms; β1 and β2) that allows AMPK to bind glycogen [6,7,211], an important energy reserve of glucose utilised during exercise [30], thereby contributing to its cellular energy sensing capacity [13].

A growing body of evidence has uncovered interactive roles of AMPK and glycogen at the molecular, cellular and physiological levels [12], including investigations using animal model systems with mutant forms of AMPK that would not be feasible to study in humans. Recent findings from our group demonstrated phenotypic effects of disrupting AMPK's glycogen binding capacity *in vivo*, using AMPK β1 or β2 single knock-in (KI) mice in which amino acid residues in either isoform CBM that mediate glycogen binding were mutated (β1 W100A KI or β2 W98A KI) [14]. These β1 W100A KI and β2 W98A KI mutations were associated with disrupted whole-body and tissue metabolism and impaired maximal running

capacity in β2 W98A KI mice relative to wild type (WT) mice. Considering both AMPK β1 and β2 isoforms are expressed in the majority of mouse tissues and cell types including liver and skeletal muscle [12], mice with KI mutations in both isoforms (AMPK β1 W100A/β2 W98A double knock-in; DKI; **Figure 3.1**) were generated to investigate the phenotypic consequences of disrupting whole-body AMPK-glycogen interactions at rest and during exercise. DKI mice displayed impaired whole-body metabolism and changes in energy substrate utilisation (i.e., reduced fat oxidation) associated with increased total body and fat mass and altered tissue glycogen dynamics [15]. Furthermore, these metabolic effects were associated with reduced maximal exercise capacity in DKI mice compared to WT [16]. Despite recent progress in the understanding of metabolic and physiological effects of disrupting AMPK-glycogen interactions, the downstream changes in metabolic pathways and molecular mechanisms underlying these effects remain largely unknown.

Discovery-based untargeted metabolomics can be used to investigate metabolic changes in response to acute exercise and in association with whole-body disruption of AMPK-glycogen binding. The metabolome reflects the cumulative changes that result from layers of biological regulation involving the genome, transcriptome and proteome, as well as their interactions with the environment and physiological stimuli such as exercise [283]. Metabolomics therefore provides a snapshot of the metabolic reactions in "real-time" [22]. Using mass spectrometry-based untargeted metabolomic approaches, metabolites across a wide range of metabolic pathways can be simultaneously identified in blood and tissue samples, requiring only minimal sample volumes. Using untargeted metabolomics, we aimed to determine plasma metabolic responses to acute treadmill running and characterise the effects of disrupting AMPK-glycogen interactions on plasma metabolite profiles both at rest and following exercise. We sought to identify underlying molecular mechanisms that may

contribute to the metabolic phenotypic effects and reduced exercise capacity observed in AMPK DKI mice.

4.3. Materials and Methods

4.3.1. Animal Models

All mouse procedures were performed under the approval of the St. Vincent's Hospital (Melbourne, Australia) Animal Ethics Committee (approval numbers 025-15 and 011-19) in accordance with NHMRC requirements and conforming to the National Institutes of Health animal research guidelines (NIH Publications No. 8023, revised 1978) and Australian codes of animal research practice (8th Edition 2013). Mice were kept in pathogen-free microisolator cages (2–5 mice per cage) on standard 12:12-h dark-light cycles with controlled temperature (21°C), humidity and bedding. Mice had ad libitum access to water and standard chow diet (29% starch 20% protein and 6% fat, Barastoc, Ridley Agriproducts, Pakenham, Australia).

CRISPR/Cas9 gene editing was performed by the Mouse Engineering Garvan/ABR (MEGA) Facility to generate whole-body AMPK Prkab1 W100A (β1 W100A) and Prkab2W98A (β2 W98A) single KI mice on a C57BL/6J background [14]. Homozygous single KI mice were crossed to generate Prkab1W100A /Prkab2 W98A DKI mice. Breeding was performed using homozygous WT mice and homozygous carriers of the DKI mutations, to generate the homozygous WT and DKI mouse lines used in the present study. Due to limited age-matched mouse cohort availability and in order to maintain sufficient female mice for breeding, only male mice were used in the present study. Tail samples were collected for confirmatory genotyping performed by TransnetYX (Cordova, TN, USA). All experiments were performed in age-matched WT and DKI male mice within an age range of 12–16 weeks,

and mice from each genotype were randomly assigned to the rested and exercised experimental groups.

4.3.2. Study Design

4.3.2.1. Treadmill Acclimatisation, Body Composition Analysis and Maximal Running Speed Testing

Prior to treadmill acclimatisation and subsequent maximal running speed testing, total body mass was determined, and body composition was analysed by magnetic resonance imaging using the EchoMRI Body Composition Analysis 3-in-1 system (EchoMRI, Houston, TX, USA). Mice were then acclimatised to treadmill running (Exer 3/6, Columbus Instruments, Columbus, OH, USA) for four consecutive days at progressing speeds at a 0° incline. Manual prodding using a soft bristle brush was performed to encourage mice when necessary during both treadmill acclimatisation and testing. On day 1, mice were placed on a stationary treadmill for 5 min. On days 2 and 3, mice ran for 5 min at 5 and 10 m/min, respectively. On day 4, mice ran for 15 min; including 5 min at 10, 12 and 15 m/min. The following day, mice underwent incremental maximal running capacity testing during which they ran for 2 min at 10 m/min, after which the speed was increased by 1 m/min every 2 min until exhaustion (i.e., when mice were unable to continue running despite repeated manual prodding). Both WT (n = 21) and DKI (n = 23) mice were then randomly assigned to either the exercised or rested control group, with a total of four experimental groups: WT rested (WT-Rest; n = 10), WT exercised (WT-Ex; n = 11), DKI rested (DKI-Rest; n = 13) and DKI exercised (DKI-Ex; n = 10).

4.3.2.2. Acute Treadmill Exercise Bout and Blood Sample Collection

Following two to 3 days of recovery after maximal running capacity testing, mice randomly assigned to the exercise group completed a single bout of running for 30 min at 70% of individual maximal speed at 0° treadmill incline, while rested control mice remained in their

home cage. This 70% of individual maximal running speed was used due to the mix of carbohydrate and fat energy sources expected to be utilised at this speed [272,273]. Upon completion of the rest period or acute exercise bout, rested and exercised mice were immediately placed in a CO_2 chamber for ~10 s prior to a cardiac puncture to allow sufficient blood volume collection. Blood collections were performed in the fed state between 0800 and 1000 h in both the exercised and rested groups, corresponding to the beginning of the light phase. Blood was collected via cardiac puncture using a 23G needle attached to a 1 mL syringe, immediately transferred to 1.3 mL lithium-heparin coated tubes (Sarstedt, Nümbrecht, Germany), inverted 10 times and placed on ice. Tubes were then centrifuged at 2000 × g for 10 min at 4°C, with total time on ice consistent for all collected samples. The resulting plasma supernatant was then divided into 300 µL aliquots and stored at −80°C until analysis.

4.3.3. Metabolomics Sample Preparation

Metabolomic analysis of mouse plasma samples was performed at the Centre for Integrative Metabolomics and Computational Biology, Edith Cowan University (Joondalup, Western Australia, Australia) according to previously established data acquisition, processing and analysis workflows [97]. Plasma samples were thawed on ice and each sample was separated into two 30 µL aliquots. A pooled quality control (QC) sample was prepared by mixing 50 µL of remaining plasma from each sample; the pooled sample was subsequently divided into 30 µL aliquots. All prepared aliquots were then frozen and stored at −80°C until analysis.

On the day of mass spectrometry-based metabolomic data acquisition, plasma aliquots were thawed on ice, and protein precipitation was performed prior to running two liquid chromatography-based separation modes, as detailed below. For hydrophilic interaction liquid chromatography (HILIC), protein precipitation was performed by adding 90 µL of ice-cold

liquid chromatography-mass spectrometry (LC-MS) grade acetonitrile [3:1 (v/v)] containing isotopically labelled standards of known concentration [1 ppm each: valine-d8, tryptophan-d9, taurodeoxycholic acid-d4, leucine-13C1 and sphingosine-d9 (d18:1)] to plasma samples and pooled QC aliquots. For reversed-phase liquid chromatography (RPLC), protein precipitation was performed by adding 90 μL of ice-cold LC-MS grade methanol to each 30 μL aliquot, with identical internal standards. Samples were then mixed at 1,400 revolutions per min (rpm) for 2 min at 4°C and centrifuged (Heraeus Megafuge 8R, Thermo Fisher Scientific, Australia) for 20 min (1800 × g) at 4°C. 30 μL from each of the resulting supernatants were transferred into LC-MS vials and placed in an autosampler tray at 6°C. Prior to the run, the sample injection sequence was block randomised by group (WT-Rest, WT-Ex, DKI-Rest, DKI-Ex). LC-MS system suitability was checked using the quality assurance methods described by Broadhurst *et al.* (2018) and eight pooled QC samples were injected at the beginning of the sequence to condition the column. Pooled QC samples were then injected following each block of eight experimental samples (i.e., every ninth injection) which were used for assessment of analytical precision as reported in [52].

4.3.4. Data Acquisition: Liquid Chromatography–High Resolution Mass Spectrometry

Samples were analysed using the Dionex UltiMate 3000™ platform which comprises an ultra-high performance liquid chromatography pump coupled to a heated electrospray Q Exactive Focus Orbitrap mass spectrometer (Thermo Scientific, San Jose, CA, USA). Data were acquired in full scan mode at a mass resolution of 70,000 [Full Width at Half Maximum (FWHM) at mass to charge ratio (m/z) of 200], over a scan range of m/z 70–1000. Tandem mass spectrometry (MS/MS) was performed on all QC samples using data-dependent acquisition (DDA) in "discovery" mode using the following settings: resolution = 17,500; isolation width = 3.0 m/z; stepped collision energy = 15, 30 eV. Source and ion transfer conditions were as follows: sheath gas = 35 (arbitrary units), auxiliary gas = 10 (arbitrary units),

source heater 350°C, capillary temperature = 350°C, ion spray voltage = 2.5 kV (negative ion mode) and 3.0 kV (positive ion mode). The automatic gain control target was set at 3×10^{-6}.

Two chromatography-based separation methods were applied to each sample. Polar metabolites were separated by HILIC chromatography in positive mode (HILIC POS), using an ACQUITY UPLC BEH Amide column (2.1 × 100 mm, 1.7 μm; Waters, Milford, MA, USA) with a flow rate of 400 μL/ min and the following mobile phases: mobile phase A (10 mM ammonium formate in water + 50 mM formic acid) and mobile phase B (10 mM ammonium formate in 90% Acetonitrile + 50 mM formic acid). A 15-min elution gradient was applied as follows: 0 min; 100% B; 1 min 1% B; 8–9 min 60% B; 10 min 100% B through to 15 min. A 6 μL sample injection volume was applied. Non-polar metabolites were separated by RPLC on a Hypersil GOLD column (2.1 × 100 mm, 1.9 μm; Thermo Fisher Scientific, Runcorn, UK), with a flow rate 300 μL/min using the following mobile phases: mobile phase A (water +0.1% formic acid) and mobile phase B (Acetonitrile +0.1% formic acid). A 15-min elution gradient was applied as follows: 0 min 1% B; 1 min 1% B; 2 min 50% B; 9–10 min 99% B; 10.5 min 1% B through to 15 min. A 6 μL sample injection was applied, and samples were collected in positive and negative mode. Xcalibur software (Thermo Fisher Scientific v4.3) was used for data acquisition. Before analysis, commercially purchased calibrant solutions (negative and positive ion calibration solutions) from Thermo Fisher Scientific (San Jose, CA, USA) were used to externally calibrate the Orbitrap mass spectrometer.

4.3.5. Data Processing

Following data acquisition, spectral processing was performed (i.e., HILIC POS and C18 POS and C18 NEG) in Compound Discoverer™ 3.1 (Thermo Scientific, San Jose, CA, USA) using an untargeted metabolomics workflow. Compound Discoverer™ version 3.1 was utilised for total ion chromatograms alignment along retention times (RT) based on an adaptive

curve, with a 5 ppm mass tolerance and a maximum shift of 0.5 min. Detected features with a signal-to-noise ratio > 5 and an intensity ≥ 1,000,000 in each dataset were merged into compounds according to ion adducts. Ions detected within the blanks were subtracted from the samples using the "mark background compounds" node.

Metabolite identification/annotation was also performed in Compound Discoverer™ in accordance with the Metabolomics Standard Initiative (MSI) levels [71]. Details on identifications/annotations can be found in Supplementary **Table S4.2**. Quality control-regularised spline correction (QC-RSC) was used to correct analytical signal drift [274]. Following standard protocols [52], metabolites with RSD QC > 20% or a Dispersion-ratio (D-ratio) > 30% were removed from further statistical analyses based on their failure to meet acceptable measurement precision. Eight haemolysed plasma samples were removed from the full sample set to prevent potential confounding effects of sample haemolysis on the metabolomic analysis.

4.3.6. Statistical Analyses

For statistical analyses of mouse body mass, body composition and maximal running speed, *P* values were calculated using unpaired Student's t-tests (WT versus DKI) and Welch's correction was applied when applicable, with $P < 0.05$ considered statistically significant. Outlier identification was performed using the Grubb's test or the ROUT method. Statistical tests for these measures were performed using GraphPad Prism software version 8.4.3 (GraphPad Software, San Diego, CA).

For statistical analyses of the metabolomics dataset, two-way ANOVA was performed to test the null hypothesis (i.e., no differences between rested/exercised conditions and/or WT/ DKI genotypes) for each individual identified/annotated metabolite. Estimation of the false

discovery rate (FDR) due to multiple comparisons was performed using the Storey FDR method [275], and P values < 0.05 with a FDR < 0.1 were considered statistically significant.

To assess the structured similarities between metabolite concentrations across the complete dataset, hierarchical cluster analysis (HCA) was performed using Pearson's correlation coefficient as the similarity measure, and Ward's linkage method [276]. The lowest linkages (i.e., closest metabolite clusters) within the HCA dendrogram indicate metabolites that display the most similar responses. The resulting visualisation labelled by metabolite significance, indicates metabolites of particular interest displaying similar (correlated) changes.

To model and visualise the multivariate discrimination between the four experimental groups, all metabolites were combined into a single data matrix and applied to principal component–canonical variate analysis (PC-CVA) [277]. PC-CVA uses the (multivariate) covariance between metabolite concentration and outcome classification to test the statistical significance of the mean differences. Multivariate data is projected into a two-dimensional subspace (canonical variate axes) reflecting the combination of metabolites that best discriminate the labelled groups. Results are visualised via: 1) a scores plot, with 95% confidence intervals (CI) of the mean from each group indicating significant differences, and 2) a coefficients plot indicating the contribution importance of each metabolite to each canonical variate. Overfitting was avoided by using 5-fold cross validation to choose the optimal number of principal components to apply to the CVA model. 95% CI for the model coefficients were calculated using bootstrap resampling [278]. Prior to all statistical analyses, metabolite profiles were $\log_{10}$ transformed and scaled to unit variance (auto scaled), allowing each metabolite to be objectively compared with no bias due to large differences in metabolite concentration. Statistical analyses of the metabolomic dataset were performed using MATLAB ®package version R2021b (MathWorks, Natick, MA).

4.4. Results

4.4.1. AMP-activated Protein Kinase Double Knock-In Mice Exhibit Increased Total Body Mass, Fat Mass and Reduced Maximal Running Speed

Compared to age-matched WT mice (n = 21), DKI mice (n = 23) with whole-body disruption of AMPK-glycogen binding (**Figure 4.1A**) displayed ~20% reduction in maximal running speed ($P < 0.0001$, **Figure 4.1B**). DKI mice had increased total body mass (~10%, $P < 0.01$, **Figure 4.1C**) associated with increased whole-body fat mass (~65%, $P < 0.001$) but no differences in lean mass (**Figures 4.1D, E**) relative to WT mice.

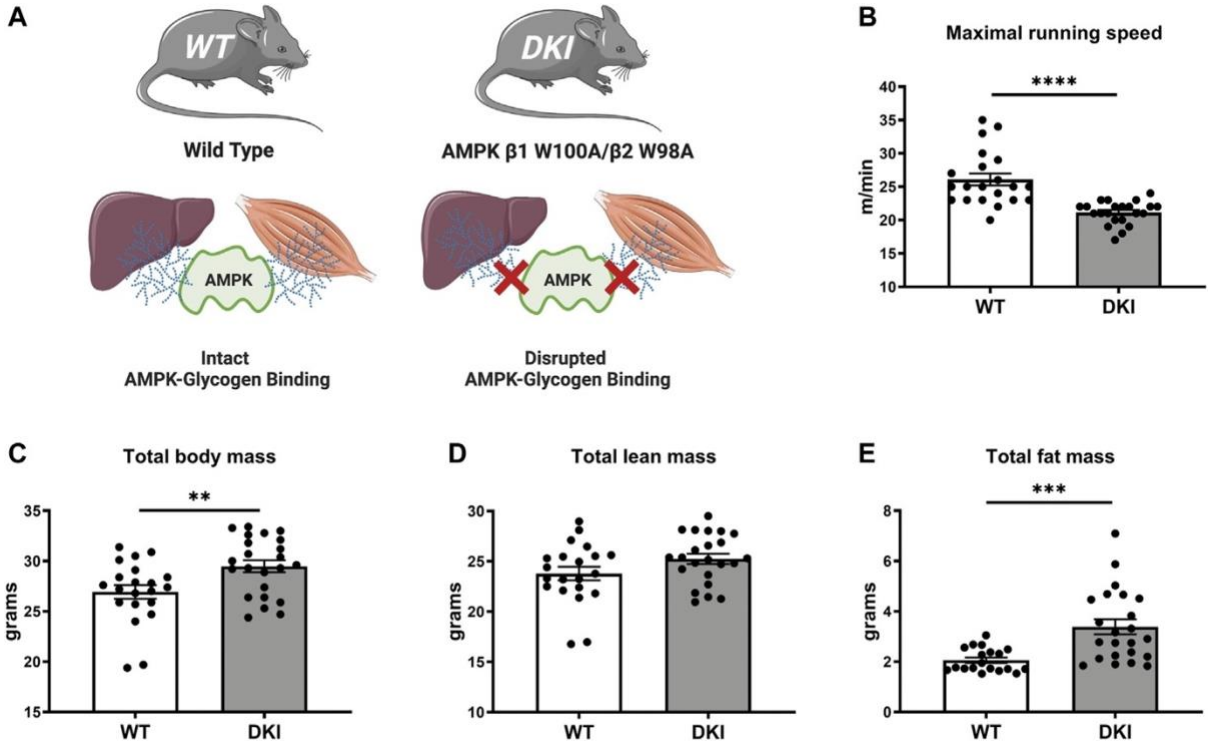

Figure 4.1 – AMPK DKI mouse model and phenotypic effects of disrupting whole-body AMPK-glycogen interactions on maximal running speed and body composition. **(A)** Schematic of WT mice with intact AMPK-glycogen binding and AMPK DKI mice in which critical tryptophan residues within the AMPK β subunit isoforms that mediate glycogen binding (β1; predominantly expressed in mouse liver; and β 2 predominantly expressed in mouse skeletal muscle) have been mutated to alanine (β1 W100A and β2 W98A, respectively), resulting in whole-body disruption of AMPK-glycogen binding; **(B)** Maximal running speed (m/min); **(C)** Total body mass (g); **(D)** Total lean mass (g); (E) Total fat mass (g). *: $P < 0.05$, **: $P < 0.01$, ****: $P < 0.0001$; values are represented as mean ± SEM; n = 21–23 mice per group.

4.4.2. Metabolomics Reveals Plasma Metabolites Affected by Acute Treadmill Exercise and/or AMP-activated Protein Kinase Double Knock-In Genotype

A total of 83 metabolites were identified/annotated following data processing and cleaning steps and according to the standard reporting guidelines from the Metabolomics Society Initiative [71]. Two-way ANOVA revealed 17 metabolites were significantly different ($P < 0.05$; FDR < 0.1) between conditions (rested versus exercised) and only one metabolite significantly different between genotypes (WT versus DKI). All identified/annotated metabolites, in addition to their molecular characteristics and respective statistical relationships are listed in **Table 4.1**. Furthermore, **Table 4.2** reports metabolite change directionality, median fold-change (FC) and 95% confidence intervals (CI) of these 17 metabolites that significantly changed between experimental groups along with their associated pathways. All metabolite information and statistics are reported in Supplementary **Tables S4.1–S4.3**.

Table 4.1 – Summary of the metabolites identified/annotated from WT and DKI mouse plasma

Column & Mode	Metabolite	Molecular Formula	Molecular Weight	RT (min)	RSD_{QC}	*P* value G	FDR G	*P* value C	FDR C	*P* value GxC	FDR GxC	MSI ID	Cluster
C18POS	alpha-Linolenic acid	C18 H30 O2	278.2241	8.27	10.918	0.911	0.454	0.657	0.658	0.429	0.519	1	A
C18NEG	C18:1 fatty acid	C18 H34 O2	282.2551	9.67	6.993	0.230	0.263	0.355	0.440	0.548	0.529	2	A
C18POS	Arachidonic acid	C20 H32 O2	304.2401	8.72	9.285	0.321	0.295	0.791	0.691	0.294	0.542	2	A
C18POS	2-Arachidonoyl glycerol	C23 H38 O4	378.2764	8.17	13.736	0.250	0.260	0.915	0.685	0.093	0.444	2	A
C18POS	Monoolein	C21 H40 O4	356.2924	8.93	10.887	0.237	0.258	0.985	0.685	0.074	0.377	2	A
HILICPOS	Lyso-PAF C16	C24 H52 N O6 P	481.3527	2.34	13.091	**0.006**	0.145	0.323	0.432	0.182	0.484	1	A
C18NEG	Bile acid (C26H45NO7S)	C26 H45 N O7 S	515.2906	3.63	3.804	**0.014**	0.222	0.846	0.702	0.356	0.483	3	A
C18NEG	Stercobilin	C33 H46 N4 O6	594.3399	4.75	8.386	0.259	0.264	0.858	0.695	0.983	0.661	2	A
C18NEG	Lithocholyltaurine	C26 H45 N O5 S	483.3010	4.61	4.708	0.185	0.271	0.952	0.675	0.381	0.497	1	A
C18POS	Taurochenodesoxycholic acid	C26 H45 N O6 S	499.2965	4.13	2.108	0.052	0.220	0.992	0.683	0.251	0.538	1	A
C18NEG	Chenodeoxycholic acid glycine conjugate	C26 H43 N O5	449.3133	4.29	4.633	0.091	0.225	0.880	0.681	0.201	0.496	1	A
C18POS	Glycocholic acid	C26 H43 N O6	465.3088	4.25	6.866	0.081	0.211	0.924	0.684	0.175	0.528	1	A
C18NEG	Glycoursodeoxycholic acid	C26 H43 N O5	449.3134	4.92	2.424	0.080	0.221	0.773	0.692	**0.048**	0.318	2	A
C18NEG	Riboflavin	C17 H20 N4 O6	376.1374	3.33	5.997	0.151	0.294	0.940	0.674	0.102	0.399	2	A
C18NEG	Oxidised glutathione	C20 H32 N6 O12 S2	612.1506	1.62	7.792	0.339	0.299	0.863	0.691	0.172	0.545	1	A
C18POS	Reduced glutathione	C10 H17 N3 O6 S	307.0836	1.30	15.021	**0.019**	0.177	0.405	0.493	0.335	0.519	1	A
C18POS	Glycylproline	C7 H12 N2 O3	172.0847	1.29	8.734	**0.015**	0.178	0.869	0.688	0.318	0.516	1	B
HILICPOS	Propionylcarnitine	C10 H19 N O4	217.1312	3.25	8.578	**0.036**	0.212	0.105	0.238	0.849	0.657	1	B
C18NEG	Bile acid (C24H40O5)	C24 H40 O5	408.2866	4.12	3.099	0.053	0.208	0.913	0.691	0.696	0.586	3	B
C18NEG	Chenodeoxycholic acid	C24 H40 O4	392.2919	4.89	7.111	0.342	0.297	0.133	0.266	0.152	0.506	1	B
C18POS	Nutriacholic acid	C24 H38 O4	390.2767	5.09	5.142	0.285	0.272	0.133	0.259	0.406	0.501	1	B

Continued

Table 4.1 – Continued

Column & Mode	Metabolite	Molecular Formula	Molecular Weight	RT (min)	RSD_{QC}	*P* value G	FDR G	*P* value C	FDR C	*P* value GxC	FDR GxC	MSI ID	Cluster
C18NEG	Deoxycholic acid	C24 H40 O4	392.2921	5.75	4.756	0.201	0.262	0.252	0.381	0.096	0.426	2	B
HILICPOS	Hypotaurine	C2 H7 N O2 S	109.0199	5.88	12.036	0.523	0.340	0.876	0.686	0.808	0.632	1	B
C18NEG	Thymidine	C10 H14 N2 O5	242.0897	2.98	5.315	0.991	0.473	0.480	0.554	0.245	0.563	2	B
HILICPOS	Acetylcarnitine	C9 H17 N O4	203.1154	4.11	11.964	0.620	0.368	0.245	0.380	0.348	0.492	1	B
HILICPOS	Bilirubin	C33 H36 N4 O6	584.2620	0.91	6.493	0.895	0.451	0.794	0.684	0.073	0.404	2	B
HILICPOS	Carnitine	C7 H15 N O3	161.1049	4.11	11.349	0.384	0.321	0.329	0.430	0.127	0.470	1	C
HILICPOS	Melatonin	C13 H16 N2 O2	232.1209	0.82	10.277	**0.041**	0.193	0.256	0.379	0.301	0.527	1	C
C18POS	Cytosine	C4 H5 N3 O	111.0435	1.30	4.534	0.454	0.322	**0.024**	**0.088**	0.963	0.661	2	C
C18POS	Cytidine	C9 H13 N3 O5	243.0853	1.29	6.709	0.515	0.345	0.983	0.690	0.925	0.655	1	C
C18POS	Kynurenic acid	C10 H7 N O3	189.0423	3.24	2.819	0.867	0.442	0.198	0.338	0.918	0.657	1	C
C18POS	Spermidine	C7 H19 N3	145.1579	0.77	7.732	0.530	0.335	0.266	0.377	0.733	0.609	1	C
HILICPOS	Stearoylethanolamide	C20 H41 N O2	327.3132	0.66	7.501	0.281	0.274	0.126	0.268	0.341	0.505	1	C
HILICPOS	Dipalmitoylphosphatidylcholine	C40 H80 N O8 P	733.5612	0.98	6.336	0.635	0.363	0.057	0.170	0.796	0.631	2	C
C18NEG	N-Acetyltyrosine	C11 H13 N O4	223.0835	3.22	8.121	0.430	0.325	0.105	0.231	0.691	0.605	1	C
C18POS	N-Acetyltryptophan	C13 H14 N2 O3	246.1002	3.66	4.804	0.552	0.344	**0.010**	**0.044**	0.547	0.536	1	C
C18POS	Progesterone	C21 H30 O2	314.2238	6.38	6.020	0.165	0.298	**1.09E-09**	**3.72E-08**	**0.030**	0.334	1	C
C18POS	Corticosterone	C21 H30 O4	346.2142	4.36	5.214	0.414	0.329	**5.11E-10**	**3.48E-08**	0.889	0.665	2	C
HILICPOS	Palmitoylcarnitine	C23 H45 N O4	399.3339	0.97	6.812	0.944	0.461	**0.001**	**0.005**	0.895	0.662	1	C
C18NEG	16-Hydroxyhexadecanoic acid	C16 H32 O3	272.2347	8.44	6.147	0.527	0.338	0.097	0.228	0.256	0.533	2	C
HILICPOS	Hexanoylcarnitine	C13 H25 N O4	259.1777	1.72	13.234	0.738	0.402	**0.024**	**0.092**	0.495	0.540	2	C
C18NEG	Hexadecanedioic acid	C16 H30 O4	286.2140	6.12	12.155	0.210	0.266	0.750	0.681	0.953	0.660	2	C
C18POS	Histamine	C5 H9 N3	111.0799	0.80	2.585	0.458	0.320	0.677	0.659	0.866	0.654	1	C

Continued

Table 4.1 – Continued

Column & Mode	Metabolite	Molecular Formula	Molecular Weight	RT (min)	RSD_{QC}	*P* value G	FDR G	*P* value C	FDR C	*P* value GxC	FDR GxC	MSI ID	Cluster
HILICPOS	Methylimidazoleacetic acid	C6 H8 N2 O2	140.0585	5.26	10.576	0.495	0.336	0.304	0.423	0.748	0.607	1	C
HILICPOS	Prolylleucine/Leucylproline	C11 H20 N2 O3	228.1468	5.10	13.965	0.357	0.304	0.503	0.571	0.977	0.663	2	D
HILICPOS	Creatine	C4 H9 N3 O2	131.0694	5.84	6.064	0.273	0.272	0.197	0.343	0.396	0.507	1	D
C18POS	Methylthioadenosine	C11 H15 N5 O3 S	297.0894	3.19	2.489	0.169	0.282	0.339	0.428	0.607	0.561	1	D
C18NEG	Fructose 6-phosphate	C6 H13 O9 P	260.0290	0.78	6.551	0.113	0.252	0.677	0.668	0.504	0.524	1	D
C18POS	Serotonin	C10 H12 N2 O	176.0949	2.92	4.198	0.141	0.287	0.713	0.674	0.642	0.586	1	D
C18NEG	12-HETE	C20 H32 O3	320.2346	6.83	5.510	0.600	0.365	0.725	0.676	0.589	0.552	1	D
C18POS	Eicosapentaenoic acid	C20 H30 O2	302.2243	6.83	6.254	0.438	0.326	0.683	0.655	0.692	0.598	2	D
HILICPOS	Hypoxanthine	C5 H4 N4 O	136.0385	3.64	10.615	0.441	0.323	0.266	0.385	0.462	0.549	1	D
HILICPOS	Adenosine	C10 H13 N5 O4	267.0961	2.25	17.382	0.577	0.355	0.192	0.345	0.574	0.548	1	D
C18NEG	Guanosine monophosphate	C10 H14 N5 O8 P	363.0571	1.27	6.942	0.170	0.275	0.507	0.557	0.694	0.592	1	D
C18POS	Adenosine monophosphate	C10 H14 N5 O7 P	347.0631	0.90	1.401	0.691	0.385	0.803	0.684	0.682	0.614	1	D
C18POS	Oleamide	C18 H35 N O	281.2714	9.16	4.790	0.236	0.263	0.433	0.508	0.738	0.606	1	E
C18POS	Hexadecanamide	C16 H33 N O	255.2559	9.23	8.763	0.167	0.290	0.556	0.591	0.484	0.555	2	E
HILICPOS	Nicotinamide 1-oxide	C6 H6 N2 O2	138.0426	2.04	4.087	0.797	0.429	0.777	0.688	0.486	0.539	2	E
C18POS	Niacinamide	C6 H6 N2 O	122.0481	1.01	11.716	0.420	0.328	0.892	0.682	0.314	0.536	1	E
HILICPOS	4-Guanidinobutyric acid	C5 H11 N3 O2	145.0851	4.47	15.185	0.854	0.444	0.072	0.195	0.175	0.506	2	E
C18NEG	Indoxyl sulfate	C8 H7 N O4 S	213.0087	3.27	4.325	0.404	0.326	0.543	0.587	0.860	0.658	1	E
C18POS	Phenylacetylglycine	C10 H11 N O3	193.0740	3.52	5.660	0.671	0.379	0.228	0.362	0.909	0.665	1	E
C18POS	2-Aminooctanoic acid	C8 H17 N O2	159.1260	3.52	3.860	0.197	0.272	0.224	0.364	0.317	0.527	1	E
C18POS	Tryptophan	C11 H12 N2 O2	204.0898	3.23	4.157	0.216	0.259	0.339	0.435	0.401	0.503	1	E
C18POS	Indole	C8 H7 N	117.0580	3.23	5.123	0.170	0.266	0.412	0.492	0.520	0.533	1	E

Continued

Table 4.1 – Continued

Column & Mode	Metabolite	Molecular Formula	Molecular Weight	RT (min)	RSD_{QC}	*P* value G	FDR G	*P* value C	FDR C	*P* value GxC	FDR GxC	MSI ID	Cluster
C18POS	Indoleacetic acid	C10 H9 N O2	175.0633	3.84	6.904	0.404	0.332	0.824	0.693	0.273	0.534	1	E
C18POS	3-Indolepropionic acid	C11 H11 N O2	189.0789	4.05	8.222	0.297	0.278	**0.030**	0.101	0.917	0.663	1	E
C18NEG	C18:2 fatty acid	C18 H32 O2	280.2398	6.34	3.507	0.424	0.325	**0.050**	0.154	0.296	0.533	3	E
C18POS	Sphingosine 1-phosphate	C18 H38 N O5 P	379.2484	5.78	2.156	0.073	0.245	**0.005**	**0.028**	0.690	0.612	1	E
C18POS	Pantothenic acid	C9 H17 N O5	219.1105	3.06	3.550	**0.001**	**0.070**	**5.50E-04**	**0.003**	0.287	0.545	1	F
C18POS	Methionine	C5 H11 N O2 S	149.0510	1.31	5.523	0.939	0.463	**3.13E-04**	**0.002**	**0.026**	0.347	1	F
C18POS	Ornithine	C5 H12 N2 O2	132.0899	0.80	1.918	0.223	0.261	**1.06E-04**	**0.001**	0.099	0.410	1	F
C18POS	Histidine	C6 H9 N3 O2	155.0695	0.81	2.298	**0.029**	0.227	**1.48E-05**	**2.02E-04**	0.266	0.537	1	F
C18POS	Phenylalanine	C9 H11 N O2	165.0789	2.96	5.817	0.726	0.400	0.084	0.205	0.327	0.519	1	F
HILICPOS	Tyrosine	C9 H11 N O3	181.0737	5.34	6.177	0.053	0.192	0.180	0.331	**0.039**	0.368	1	F
HILICPOS	Proline	C5 H9 N O2	115.0634	5.33	10.072	0.094	0.219	**0.024**	**0.096**	**0.009**	0.150	2	F
C18POS	Arginine	C6 H14 N4 O2	174.1116	0.84	3.661	0.631	0.369	**0.007**	**0.032**	**0.003**	0.198	1	F
HILICPOS	Isoleucine/Leucine	C6 H13 N O2	131.0946	4.78	6.852	0.604	0.363	**1.08E-04**	**9.19E-04**	**0.041**	0.344	1	F
C18POS	Pipecolic acid	C6 H11 N O2	129.0791	0.80	6.023	0.076	0.237	**2.70E-06**	**6.12E-05**	**0.005**	0.173	1	F
C18POS	Lysine	C6 H14 N2 O2	146.1055	0.80	3.389	0.121	0.258	**3.52E-06**	**5.99E-05**	**0.007**	0.160	1	F
C18POS	Glycerophospho-N-palmitoyl ethanolamine (GP-NPEA)	C21 H44 N O7 P	453.2853	6.82	2.864	0.244	0.260	**1.96E-04**	**0.001**	0.051	0.306	2	F
C18POS	Threonine/Homoserine	C4 H9 N O3	119.0583	0.88	2.437	0.480	0.330	0.070	0.199	**0.043**	0.314	1	F
C18POS	Testosterone	C19 H28 O2	288.2085	5.04	9.679	0.211	0.260	0.130	0.268	0.525	0.522	1	F

Table 4.1 – A total of 83 plasma metabolites were identified/annotated, including 17 metabolites significantly changed by condition (i.e., exercise versus rest) and one metabolite significantly changed by genotype (i.e., DKI versus WT) based on univariate analysis. Statistically significant values ($P < 0.05$ and/or FDR < 0.1) appear in bold text. C: condition; G: genotype; G x C: interaction between condition and genotype; FDR: false discovery rate; MSI: Metabolomics Standards Initiative; RSD_{QC}: relative standard deviation in quality control samples; RT: retention time

Table 4.2 – Summary of the 17 metabolites significantly regulated by exercise and/or genotype

	Direction	Metabolite	Pathway	Median FC & 95% CI (WT)	Median FC & 95% CI (DKI)	Cluster
Ex vs Rest	↑	Cytosine	Pyrimidines	1.11 (0.78-1.62)	1.07 (0.95-1.43)	C
		N-Acetyltryptophan	Amino acids & derivatives	1.25 (0.83-2.07)	1.60 (1.01-2.78)	C
		Progesterone	Steroid hormones	1.98 (1.13-2.39)	2.48 (1.87-3.30)	C
		Corticosterone	Steroid hormones	4.74 (2.99-15.01)	5.79 (3.92-23.90)	C
		Palmitoylcarnitine	Acylcarnitines	1.37 (0.95-1.94)	1.73 (1.31-2.94)	C
		Hexanoylcarnitine	Acylcarnitines	1.31 (0.83-2.08)	1.48 (1.01-2.01)	C
	↓	Sphingosine 1-phosphate	Sphingolipids	0.86 (0.74.-0.97)	0.90 (0.74-1.00)	E
		Pantothenic acid	Vitamins & co-factors	0.78 (0.54-1.03)	0.79 (0.72-0.88)	F
		Methionine	Amino acids & derivatives	0.90 (0.73-1.07)	0.73 (0.68-0.90)	F
		Ornithine	Amino acids & derivatives	0.75 (0.57-1.05)	0.51 (0.38-0.67)	F
		Histidine	Amino acids & derivatives	0.67 (0.50-1.00)	0.67 (0.49-0.82)	F
		Proline	Amino acids & derivatives	1.25 (0.90-1.56)	0.60 (0.48-0.83)	F
		Arginine	Amino acids & derivatives	1.02 (0.86-1.40)	0.71 (0.53-0.86)	F
		Isoleucine/leucine	Amino acids & derivatives	0.89 (0.69-1.04)	0.69 (0.54-0.80)	F
		Pipecolic acid	Amino acids & derivatives	0.83 (0.67-1.02)	0.57 (0.48-0.78)	F
		Lysine	Amino acids & derivatives	0.78 (0.68-0.93)	0.59 (0.52-0.75)	F
		GP-NPEA	Glycerophospholipids	0.96 (0.81-1.19)	0.77 (0.67-0.91)	F
	Direction	**Metabolite**	**Pathway**	**Median fold change & 95% CI (Rest)**	**Median fold change & 95% CI (Ex)**	**Cluster**
DKI vs WT	↓	Pantothenic acid	Vitamins & co-factors	0.82 (0.67-0.97)	0.83 (0.61-0.98)	F

Table 4.2 – Summary of the 17 metabolites significantly changed by exercise and/or genotype. A total of six metabolites significantly increased and 11 metabolites significantly decreased following exercise, at the univariate level. Increased metabolites primarily consisted of acylcarnitines and steroid hormones, while decreased metabolites predominantly consisted of amino acids and derivatives. Only pantothenic acid was significantly decreased in DKI versus WT mice at the univariate level. CI: confidence interval; FC: fold-change; ↑: increase; ↓: decrease.

4.4.2.1. Clustering of Correlated Metabolites

Hierarchical clustering of the 83 metabolites, based on pairwise Pearson's correlation similarity, resulted in six clusters reflecting different observed interaction between genotype and exercise. The results are displayed as a circular dendrogram (**Figure 4.2A**). The averaged z-score metabolite responses for each cluster are presented in **Figure 4.2B**. The average response for metabolites in Cluster A (16 metabolites, including fatty and bile acids) was non-significant but showed an interaction between genotype and exercise such that during rest the DKI metabolite level was greater than the WT level, but those levels converged during exercise. Cluster B (10 metabolites, including bile acids, acetylcarnitine and hypotaurine), again non-significant, showed the opposite trend (converged at rest and lower WT following exercise). Cluster C (18 metabolites, including steroid hormones and acylcarnitines), showed a significant increase in metabolite levels associated with exercise in both genotypes ($P = 2 \times 10^{-5}$). Cluster D (11 metabolites, including nucleotides and derivatives, lipid species and creatine) and Cluster E (14 metabolites, including lipid species, tryptophan and derivatives) showed similar nonsignificant trends as Cluster A and B but with the WT metabolite levels greater than DKI. Cluster F (14 metabolites, including amino acids and derivatives, pantothenic acid and testosterone) showed a significant interaction between genotype and exercise ($P = 4 \times 10^{-4}$) such that the WT metabolite levels remain constant and the DKI metabolite levels significantly decrease in association with exercise. Clusters C and F drove the metabolite profile response to exercise intervention; *P* values of all metabolite clusters are presented in Supplementary **Table S4.3**.

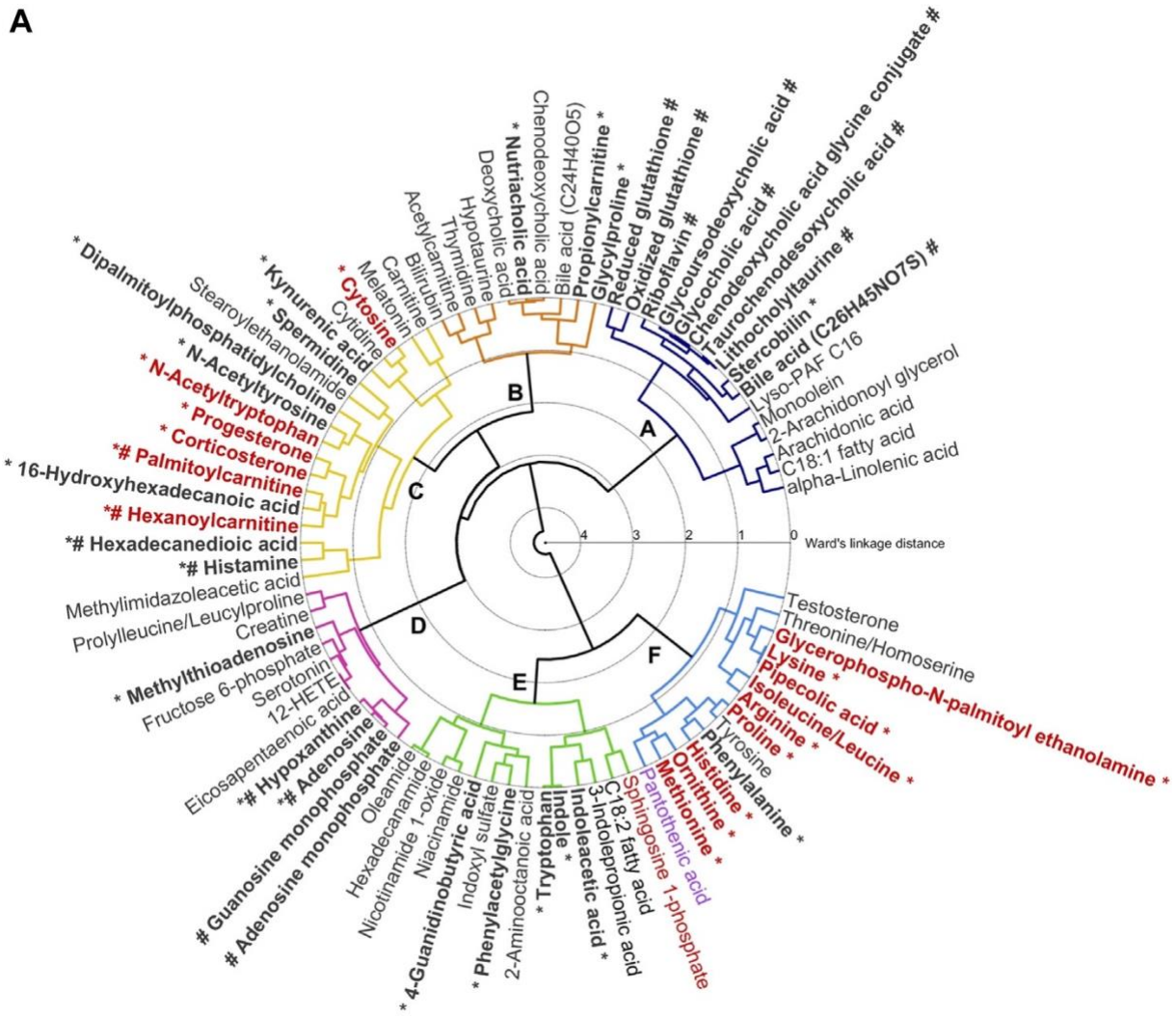

Figure 4.2A – Hierarchical Cluster Analysis (HCA) dendrogram of identified/annotated metabolites. Agglomerative clustering of individual metabolites based on pairwise correlation is shown. The lowest linkages within the HCA dendrogram indicate metabolites that display similar relative responses between the experimental groups. Six clusters were observed. Metabolite labels are coloured to reflect the results of the two-way ANOVA after filtering using a false discovery rate (FDR) of 0.1 (red = significant effect of condition only; magenta = significant effect of genotype and condition; black = no significance or FDR > 0.1). *: Metabolites that significantly ($P < 0.05$) contributed to the model along canonical variate 1 (CV1, **Figure 4.3A**); #: Metabolites that significantly ($P < 0.05$) contributed to the model along CV2.

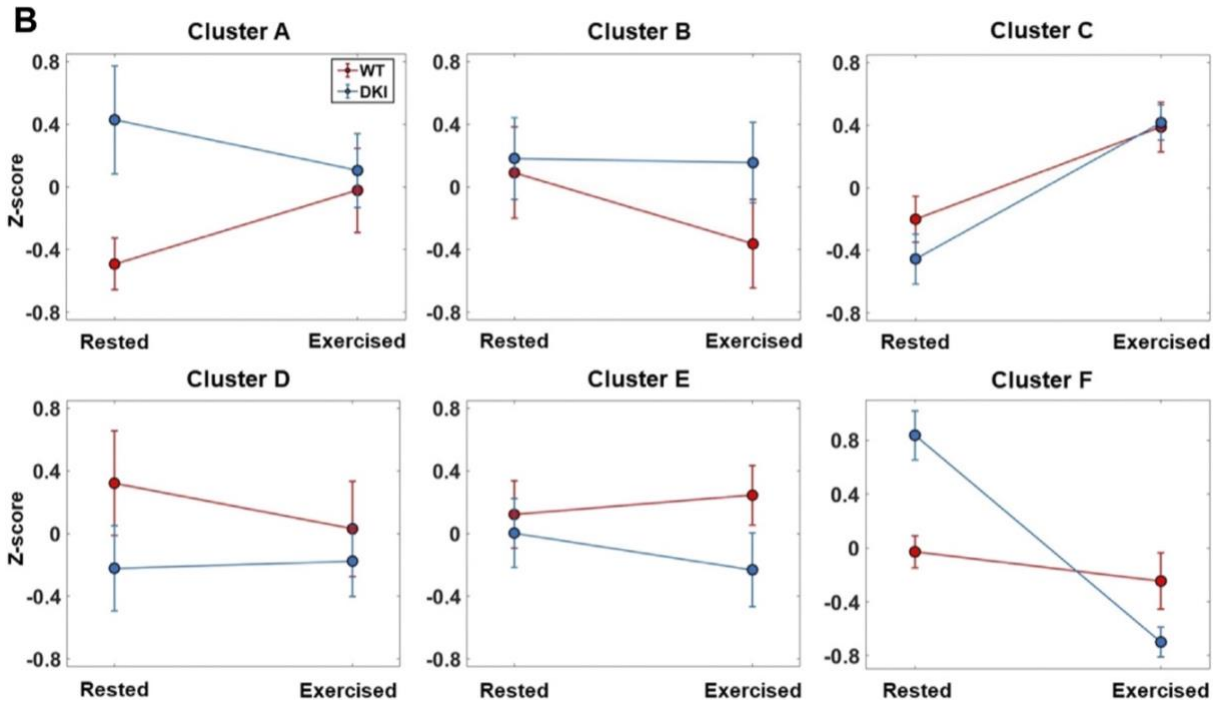

Figure 4.2B – Z-scores plot of the mean responses for each metabolite cluster. After conversion of individual metabolite $\log_{10}$ responses to a z-score, the average response of each cluster was calculated and presented here as a group error bar plot. Error bars indicate the standard error for each group mean (Red = WT; Blue = DKI). Following two-way ANOVA, only Clusters C and F showed significant differences in the averaged group metabolite response. Cluster C showed a significant effect of exercise for both genotypes ($P = 2 \times 10^{-5}$), and Cluster F showed a significant interaction between genotype and exercise ($P = 4 \times 10^{-4}$) such that the WT metabolite levels remained constant and the DKI metabolite levels significantly decreased in response to exercise.

4.4.2.2. Principal Component-Canonical Variate Analysis

PC-CVA was performed to determine between-group multivariate differences in plasma metabolite profiles with respect to condition and genotype (**Figure 4.3A**). Overall, ~65% of the total variance in the overall metabolomics dataset was explained by canonical variate (CV) 1, while CV2 explained ~3% of the total variance. The PC-CVA scores plot showed significant differences in the multivariate mean between the rested and exercised conditions for both WT and DKI, as well as significant differences between WT and DKI plasma at rest, but no significant difference between WT and DKI following exercise. CV1 particularly demonstrates a more pronounced change in metabolic profile in DKI rested versus

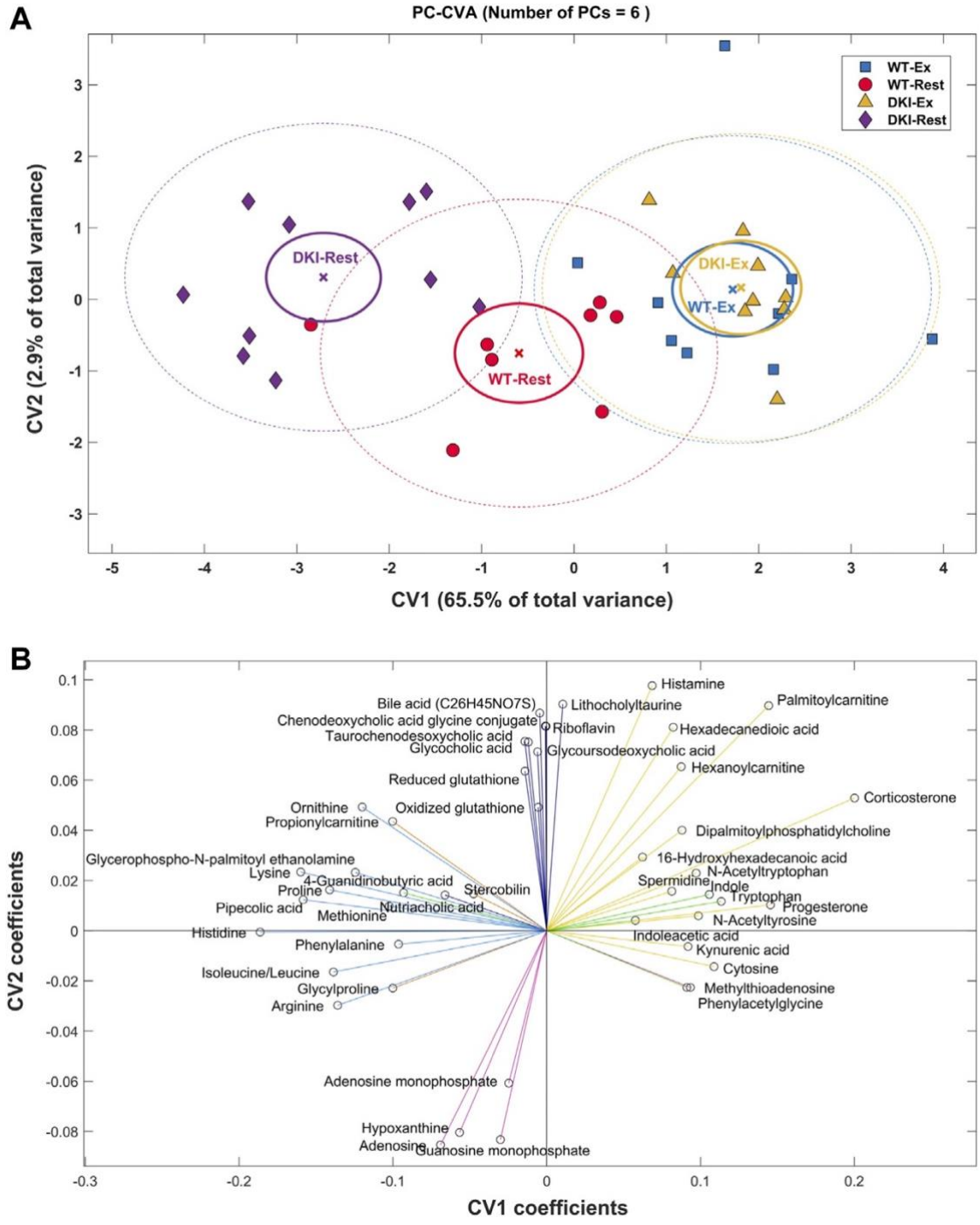

Figure 4.3 – Principal Component-Canonical Variate Analysis (PC-CVA) showing system-wide metabolite profile differences between genotypes at rest and after exercise. (**A**) Scores plot of Canonical Variate 1 (CV1) vs. Canonical Variate 2 (CV2). Each point (circle, square or triangle) represents a single sample [WT-Rest (n = 8), WT-Ex (n = 9), DKI-Rest (n = 10), DKI-Ex (n = 9)]. The mean (x) of each group is surrounded by a 95% confidence interval of the mean (full-line circles) and 95% confidence interval of membership in each sample group (dashed-line circles). Sample group means are considered significantly different when the 95% confidence interval of the means do not overlap. (**B**) The loading plot shows the influence (model coefficient value) of each metabolite that significantly ($P < 0.05$) contributes to the separation observed in the scores plot. The direction of the coefficient vector maps directly to the direction of the data points in the scores plot relative to the origin.

exercise, compared to WT rested versus exercised. The rested WT sample shows little change (sitting at the origin of the plot) relative to which the rested DKI sample are significantly different. When both genotypes are exercised their metabolic profiles change significantly but converge such that there was no significant difference between the exercised WT and DKI samples. The contribution of each metabolite (with 95% confidence intervals) to CV1 and CV2 are presented in Supplementary **Figure 4.4** (significant metabolites indicated in red).

Those metabolites observed to be significantly contributing to the model are summarised in **Figure 4.3B**. Here, the direction of each metabolite relative to the origin can be mapped to similar directions of sample groups in the scores plot (**Figure 4.3A**). As such, metabolite grouping along the x-axis are causal of differences associated with the exercise intervention (e.g., histidine to the left, reduced with exercise, and progesterone to the right, increased with exercise); whereas metabolites on the y-axis are more indicative of differences in rested genotype but no change in exercised genotype. The distribution of metabolites in **Figure 4.2B** reflect similar response clustering as the HCA results (**Figure 4.2A**). Cluster groups in **Figures 4.2A, 4.3B** are colour-matched and the significant CV coefficients are labelled to the HCA plot.

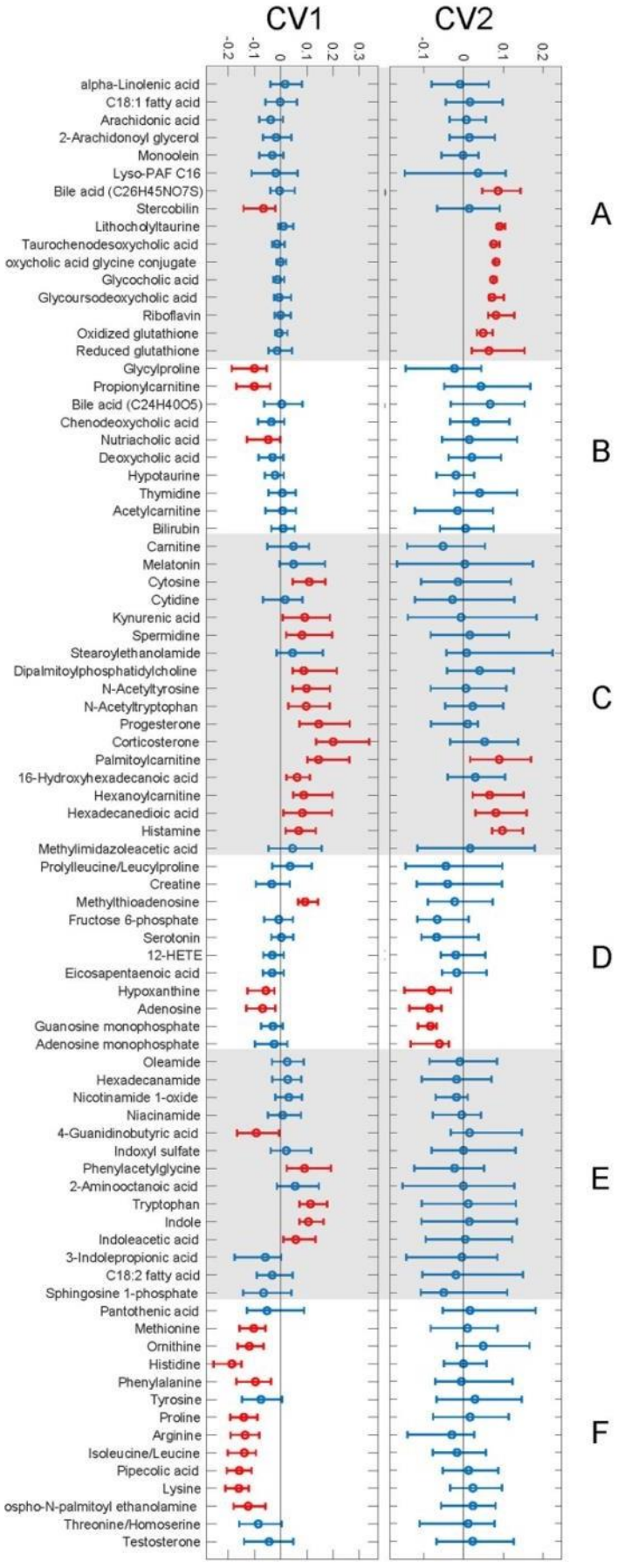
CV1
CV2
-0.2
-0.1
0
0.1
0.2
0.3
-0.1
0
0.1
0.2
alpha-Linolenic acid
C18:1 fatty acid
Arachidonic acid
2-Arachidonoyl glycerol
Monoolein
Lyso-PAF C16
Bile acid (C26H45NO7S)
Stercobilin
Lithocholyltaurine
Taurochenodesoxycholic acid
oxycholic acid glycine conjugate
Glycocholic acid
Glycoursodeoxycholic acid
Riboflavin
Oxidized glutathione
Reduced glutathione
Glycylproline
Propionylcarnitine
Bile acid (C24H40O5)
Chenodeoxycholic acid
Nutriacholic acid
Deoxycholic acid
Hypotaurine
Thymidine
Acetylcarnitine
Bilirubin
Carnitine
Melatonin
Cytosine
Cytidine
Kynurenic acid
Spermidine
Stearoylethanolamide
Dipalmitoylphosphatidylcholine
N-Acetyltyrosine
N-Acetyltryptophan
Progesterone
Corticosterone
Palmitoylcarnitine
16-Hydroxyhexadecanoic acid
Hexanoylcarnitine
Hexadecanedioic acid
Histamine
Methylimidazoleacetic acid
Prolylleucine/Leucylproline
Creatine
Methylthioadenosine
Fructose 6-phosphate
Serotonin
12-HETE
Eicosapentaenoic acid
Hypoxanthine
Adenosine
Guanosine monophosphate
Adenosine monophosphate
Oleamide
Hexadecanamide
Nicotinamide 1-oxide
Niacinamide
4-Guanidinobutyric acid
Indoxyl sulfate
Phenylacetylglycine
2-Aminooctanoic acid
Tryptophan
Indole
Indoleacetic acid
3-Indolepropionic acid
C18:2 fatty acid
Sphingosine 1-phosphate
Pantothenic acid
Methionine
Ornithine
Histidine
Phenylalanine
Tyrosine
Proline
Arginine
Isoleucine/Leucine
Pipecolic acid
Lysine
ospho-N-palmitoyl ethanolamine
Threonine/Homoserine
Testosterone
A
B
C
D
E
F

Figure 4.4 – Related to **Figure 4.3**. Loading plot showing metabolites that significantly contributed to CV1 and CV2. Data are represented as mean loading values within 95% CI. Metabolites that significantly contributed to CV1 and/or CV2 are represented by red-coloured dots and CIs, while blue dots and CIs represent metabolites that did not significantly contribute to their respective CV. Metabolites are sorted according to HCA clusters A to F (top-down). CI: confidence interval, CV: canonical variate, HCA: hierarchical cluster analysis.

4.5. Discussion

The metabolic pathways associated with the disruption of AMPK-glycogen interactions *in vivo*, despite clear phenotypic and physiological effects of the AMPK KI and DKI mutations [14-16], remain unknown. Furthermore, how an acute bout of exercise affects the plasma metabolome in widely used mouse models such as WT C57BL/6J mice, as well as the underlying metabolic pathways that contribute to these exercise-induced changes in plasma metabolite signatures has not been determined. In this study, we first reproduced the findings in AMPK DKI mice showing increased total body mass and fat mass [15] and reduced maximal running speed [16] relative to WT control mice (**Figures 4.1B–E**). We then performed metabolomics analysis on the plasma of WT and DKI mice both at rest and after acute exercise to investigate the metabolic mechanisms underlying increased adiposity and reduced exercise capacity in DKI mice. The metabolomics analyses revealed a significant mean metabolic difference between WT and DKI at rest but not after exercise, and a significant mean difference between rest and exercise in both genotypes. Cluster C metabolites (acylcarnitines, steroid hormones) increased significantly in both genotypes in association with exercise. In Cluster F (amino acids and derivatives), there was a significant interaction between genotype and exercise.

DKI mice evidenced a larger metabolome difference than the WT mice between rest and post-exercise conditions (**Figure 4.3B**). These differences support our working hypothesis

that differences in substrate utilisation and/or availability contribute to the overall phenotypic differences between DKI and WT mice. The PC-CVA CV1 scores for the rested DKI mice are further away from all exercised mice than the rested WT mice. This indicates that DKI mice may have a more "sedentary" resting metabolic phenotype compared to WT mice. This is supported by previous findings showing that DKI mice exhibit increased adiposity and total body mass, and reduced voluntary ambulatory activity versus WT mice [15].

During exercise, cellular energy demand increases. While lipids are the primary fuel source at rest and during low intensity exercise (< 50–60% VO_2 max), carbohydrates utilisation dominates at higher intensities (> 70–75% VO_2 max) [30,284]. When exercise is prolonged or under conditions of low carbohydrate availability, amino acid contribution as fuel source is increased [285]. Steroid hormones such as the glucocorticoid corticosterone increase during times of physiological energy stress, such as exercise, and promote energy store mobilisation by stimulating lipolysis, gluconeogenesis and protein breakdown [286]. Exercise-induced lipolysis leads to increased circulating levels of free fatty acids and is also associated with increased acylcarnitines [283,284]; this has also been shown in a recent investigation of rat plasma metabolomic responses to acute aerobic exercise [119]. Both WT and DKI exhibited exercise-associated increases in steroid hormones and acylcarnitines (Cluster C). While we previously showed that DKI mice have decreased levels of whole-body lipid oxidation during fasting [15] and submaximal exercise [16], the present findings reveal no differences in lipid mobilisation responses (both at rest and exercise) between the two genotypes. However, a more detailed lipid profile analysis may help establish potential differences in lipid utilisation between genotypes.

Our previous findings also showed that DKI mice had increased depletion of skeletal muscle glycogen and increased reliance on carbohydrate oxidation during exercise relative to WT mice [16]. In the present study, a significant interaction ($p = 3.53 \times 10^{-4}$) was observed

between genotype and exercise in amino acids (Cluster F), with DKI mice evidencing greater amino acid uptake and/or utilisation in DKI versus WT mice in association with exercise (**Figure 4.2B**). Together, these observations may explain the reduced maximal exercise capacity in DKI versus WT mice (**Figure 4.1B**), as increased amino acid catabolism can help sustain the energy demands of exercise when preferred fuel sources decrease [83,84], causing reduced exercise capacity. Specifically, decreased ketogenic (leucine and lysine) and glucogenic (histidine, arginine, proline, methionine) amino acids, and isoleucine (ketogenic and glucogenic) are generally reduced following exercise in blood and tissue samples from humans [47,82] and rodents [119]. Decreased amino acids may reflect increased ketogenesis and gluconeogenesis permitting continuous energy conversion when carbohydrate availability is reduced, as observed in DKI versus WT mice following exercise [16]. The precise mechanisms by which disrupting AMPK-glycogen interaction results in differential amino acid metabolism remain unclear and require further investigation.

The Cluster F metabolite pantothenic acid (vitamin B5) was significantly decreased in DKI versus WT plasma, and following exercise versus rest in both genotypes despite no interaction between genotype and exercise status. Pantothenic acid is a precursor for coenzyme A (CoASH), which is involved in numerous metabolic reactions, including energy metabolism and several steps in fatty acid oxidation [287-289]. While the mechanisms underlying decreased plasma pantothenic acid levels in DKI versus WT mice remain unclear in the present study, this may involve potential differences in gut microbiome between genotypes, as pantothenic acid is produced by gut bacteria [290,291] and changes in the gut microbiome can impair pantothenic acid production [292]. Given the influence of gut microbiota on glucose metabolism and skeletal muscle function in mice [293], further research characterizing gut microbiome composition would help determine its potential contribution to the phenotypic differences observed in DKI versus WT mice including impaired maximal running speed [**Figure 4.1B**;

[16]], increased adiposity [**Figure 4.1D**; [15]], glucose intolerance [15] and changes in whole-body and skeletal muscle fuel utilisation [15,16]. Reduced pantothenic acid availability may also be associated with reduced free CoASH [294] and/or availability of subcellular pools of CoASH in skeletal muscle. Given the numerous critical roles of CoASH in energy metabolism, CoASH has been suggested as a potential limiting factor of substrate utilisation and exercise capacity [295]. The potential contribution of decreased skeletal muscle free CoASH to the decreased whole-body rates of fat oxidation and increased rates of carbohydrate oxidation observed in DKI versus WT mice [15] remains unclear. Future research investigating CoASH species in skeletal muscle and its cytosolic and mitochondrial compartments is therefore warranted to determine their potential association with these phenotypic differences between DKI and WT mice.

A total of 17 metabolites were significantly different in association with exercise (**Table 4.2**). Although these were primarily metabolites that were expected to change with exercise (e.g., lipid species, amino acids and steroid hormones), it is worth noting two metabolites that have not been previously reported in association with exercise. N-acetyltryptophan is produced from tryptophan by the gut microbiota [296,297] and exhibited a significant increase in association with exercise in both genotypes (Cluster C, **Figure 4.2B**). While the physiological consequences of these increases are not known, recent research supports the exchange of metabolites between the bloodstream and the guts [298] and an exercise-induced bidirectional crosstalk [299]. Glycerophospho-N-palmitoylethanolamine (GP-NPEA) is a glycerophospholipid membrane constituent with signal transduction roles via palmitoylethanolamide [300]. The mechanisms underlying changes in these plasma metabolites following exercise are unclear and further investigations are required to pinpoint their potential roles in exercise metabolism.

While this study characterised plasma metabolomic responses in DKI and WT plasma at rest and in response to exercise, some limitations need to be acknowledged. First, the metabolites reported in this study were limited to those that could be identified/annotated using an in-house metabolite library or based on MS/MS spectral patterns from external databases. Accordingly, the scope of our biological interpretations remains limited. Second, this study was powered based on the detection of differences in maximal running speed and may be insufficient to detect subtle effects in some metabolic pathways. Third, mice were randomly allocated to each group in the fed state at the start of the light cycle, meaning the timing of each mouse's last food intake may have been different, therefore potentially contributing to variance in metabolite levels between mice at rest and/or following exercise at the time of sample collection. Fourth, to ensure sufficient blood volume required for metabolomic analyses could be collected via cardiac puncture, CO_2 exposure prior to euthanasia was utilised. While this CO_2 exposure could potentially impact plasma pH and metabolites, all mice were subjected to the same duration of CO_2 exposure, and we do not expect CO_2 contributed to between-group differences. Finally, metabolomics studies analysing biofluids such as plasma cannot provide comprehensive insight in terms of mechanistic regulation as, for many metabolites, little is known regarding the release and/or uptake regulation into tissues in response to a stimulus such as exercise. For example, the potential association of reduced plasma pantothenic acid levels in DKI mice with reduced skeletal muscle CoASH levels and/or rates of fat oxidation remains unclear, as we did not measure skeletal muscle metabolites in the present study. Therefore, complementary future analyses of metabolites in metabolically active tissues such as skeletal muscle will allow more comprehensive insights into how acute exercise and disruption of AMPK-glycogen binding affects tissue and circulating metabolomic signatures in mice.

4.6. Conclusion

This is the first study to map the plasma metabolomic responses to acute exercise in WT mice and simultaneously investigate the effects of disrupting AMPK-glycogen interactions on mouse plasma metabolome. Consistent with previous findings [15,16], we demonstrate that DKI mice have increased total body and fat mass, associated with reduced maximal running speed. A total of 83 mouse plasma metabolites were identified/annotated, of which 17 were significantly changed in association with acute exercise, including acylcarnitines, amino acids and steroid hormones. This study also identified/annotated previously unreported exercise-associated metabolites (e.g., GP-NPEA and N-acetyltryptophan). Metabolic differences associated with exercise were primarily explained by increased abundance of acylcarnitines and steroid hormones, and decreased abundance of amino acids. DKI mice displayed greater decrease in amino acids following exercise, potentially indicating increased utilisation versus WT mice. DKI mice also displayed decreased pantothenic acid levels, which may indicate decreased levels of tissue pantothenic acid, a precursor of CoASH involved in multiple steps of energy metabolism. Whether the observed decrease in plasma pantothenic acid is associated with decreased CoASH in skeletal muscle is unknown, and further research is warranted to determine the potential contribution to differences in substrate utilisation and exercise capacity observed in DKI versus WT mice. Future complementary investigation of the metabolome in metabolically active tissues such as skeletal muscle will provide further insights into the complex metabolite responses to acute exercise and phenotypic effects of disrupting AMPK-glycogen interactions on energy homeostasis and exercise capacity.

Data availability statement: The original contributions presented in the study are included in the article/Supplementary Material, further inquiries can be directed to the corresponding authors.

Ethics statement: The animal study was reviewed and approved by St. Vincent's Hospital (Melbourne, Australia) Animal Ethics Committee (AEC).

Author contributions: MB, NL, SR, and DB performed metabolomics experiments and data analysis. MB and NH performed mouse experimentation and sample collection. MB, NL, JH, DB, NH, and SR conceptualised the study and provided intellectual input. JH, DB, and NH. provided financial support. MB, DB, NH, and SR wrote the manuscript, and all authors edited and approved the final version.

Funding: This work was supported by Australian Catholic University research funding awarded to NH.

Acknowledgments: We are grateful to Bruce Kemp for generating and providing access to the AMPK DKI mouse model. We thank Natalie Janzen, Vicki Moshovakis and Stacey Fynch for their assistance with mouse experimentation and sample collection and Lisa Murray-Segal and the St. Vincent's BioResources Centre staff for assistance with mouse husbandry.

Conflict of interest: The authors declare that the research was conducted in the absence of any commercial or financial relationships that could be construed as a potential conflict of interest.

Publisher's note: All claims expressed in this article are solely those of the authors and do not necessarily represent those of their affiliated organisations, or those of the publisher, the editors and the reviewers. Any product that may be evaluated in this article, or claim that may be made by its manufacturer, is not guaranteed or endorsed by the publisher.

Supplementary material: The Supplementary Material for this article can be found online at:

https://www.frontiersin.org/articles/10.3389/fmolb.2022.957549/full#supplementary-material

Chapter 5 – Linking Chapter

The plasma metabolomic findings from Study 1 revealed overall metabolite differences in response to submaximal treadmill exercise and disrupting AMPK-glycogen interactions. Some of these metabolites observed to change in response to exercise are well characterised, such as acylcarnitines and steroid hormones, which are associated with exercise-stimulated fat mobilisation and energy stress. Untargeted metabolomics also detected previously unreported exercise-associated metabolites such as GP-NPEA and N-acetyltryptophan. While their precise roles in the acute exercise response remain unclear, these novel exercise-associated metabolites provide potential future research avenues to dissect their biological roles and further expand the understanding of exercise metabolism.

Easy access and low invasiveness of blood sample collections make blood metabolomics an appealing tool to capture a snapshot of systemic and extracellular responses to a given stimuli such as exercise. Several circulating metabolites are widely assessed in exercise research (e.g. blood glucose and blood lactate), and a growing body of work now utilises blood metabolomics primarily for biomarker discovery purposes [301-303]. Despite these advantages to studying the circulating/blood metabolome, some limitations remain. Indeed, it can be challenging to determine the relevance of blood metabolites in the whole-body exercise response when it is unknown what cell(s) and/or tissue(s) they are released from and whether they accurately reflect changes in respective tissue metabolite profiles. Therefore, blood metabolite profiles only provide one part of the story and limited insights into tissue-specific metabolic changes occurring during exercise that may be more biologically relevant to metabolic disease pathophysiology [304,305]. Conversely, tissues are the primary location of countless cellular metabolic reactions [306]. Although collecting tissues in human participants can be challenging given the invasive nature of collecting certain tissues such as liver, studying

specific tissue metabolomes in other mammalian species including rodents can help overcome some of these limitations.

Expanding metabolomic analyses to mouse skeletal muscle and liver tissue in Study 2 will permit the investigation of intracellular metabolic pathways regulated by AMPK within the tissues where AMPK resides and regulates its intracellular target substrates. While plasma metabolomic findings suggested potential changes in amino acid metabolism in DKI relative to WT mice following acute exercise, investigating metabolically active tissues such as skeletal muscle and liver is required to better characterise the molecular responses underpinning these potential changes in amino acid utilisation and their relationship with plasma amino acids. Disrupting AMPK-glycogen interactions is likely to result in intracellular metabolite changes, but whether these alterations are in part or fully reflected in the bloodstream remains unknown. Of note, it has been shown that blood and skeletal muscle metabolomes can demonstrate very little overlap, thus highlighting the limited ability to potentially identify muscle tissue-specific metabolites from analysing only blood samples [117]. Skeletal muscle and liver metabolomic analyses are therefore expected to enable identification of additional metabolite biomarkers of exercise and potential mechanisms underlying AMPK-glycogen binding disruption at rest and in response to acute treadmill exercise.

Chapter 6 – Study 2: Metabolomic Analysis of Mouse Skeletal Muscle and Liver Metabolite Responses to Acute Exercise and Loss of AMPK-Glycogen Binding Capacity

The present chapter is comprised of an original research manuscript currently in preparation for submission.

Metabolomic Analysis of Mouse Skeletal Muscle and Liver Metabolite Responses to Acute Exercise and Loss of AMPK-Glycogen Binding Capacity

Mehdi R. Belhaj [1], David I. Broadhurst [2], Thomas Dignan [2], Jamie Whitfield [1], John A. Hawley [1], Stacey N. Reinke [2,*] and Nolan J. Hoffman [1,*]

[1] Exercise and Nutrition Research Program, Mary MacKillop Institute for Health Research, Australian Catholic University, Melbourne, VIC, Australia

[2] Centre for Integrative Metabolomics and Computational Biology, School of Science, Edith Cowan University, Joondalup, WA, Australia

[*] Correspondence: nolan.hoffman@acu.edu.au; stacey.n.reinke@ecu.edu.au

6.1. Abstract

Introduction: Exercise elicits numerous whole-body and tissue-specific metabolic health benefits. However, the breadth of molecular mechanisms underlying these beneficial metabolic effects are not fully known. A key energy-sensing enzyme activated in response to exercise is the AMP-activated protein kinase (AMPK), a master regulator of energy metabolism that binds glycogen, a major energy reserve primarily stored in liver and skeletal muscle. My group has recently shown that disrupting glycogen binding capacity in AMPK double knock-in (DKI) mice is associated with reduced maximal running speed and impairments in whole-body and tissue metabolic homeostasis. Metabolomic analyses of plasma revealed known and novel exercise-associated metabolites and that DKI mice have increased utilisation of amino acids versus wild type (WT) mice following exercise. However, metabolomic analyses of metabolically active tissues including skeletal muscle and liver are required to better understand the molecular metabolic responses to acute treadmill exercise and potential mechanisms underlying the phenotypic effects of disrupting AMPK-glycogen binding in mice.

Methods: Gastrocnemius skeletal muscle and liver tissue samples were collected from age-matched male WT and AMPK DKI mice with disrupted AMPK-glycogen binding capacity at rest and immediately following 30-min submaximal treadmill running. An untargeted MS-based metabolomic approach was utilised to determine changes in metabolites occurring in response to acute exercise and/or disrupting AMPK-glycogen binding. Complementary real-time metabolic phenotyping assays using the Seahorse XFe24 Analyzer and Oroboros O2k respirometer were performed to compare energy metabolism and substrate utilisation profiles between genotypes in mouse embryonic fibroblasts and tissue samples obtained from WT and DKI mice.

Results: Metabolomics identified a total of 92 and 150 metabolites in skeletal muscle and liver, respectively. Similar to the plasma metabolite responses observed across genotypes and conditions, tissue metabolomic analyses indicated significant overall metabolite profile shifts between WT and DKI mice at rest, as well as significant differences in metabolite profiles between the rested and exercised conditions. In contrast to liver, an interaction effect was observed in skeletal muscle, indicating differential muscle metabolite responses to acute exercise between genotypes. Real-time metabolic phenotyping of WT and DKI mouse cell and tissue samples is currently underway to further interrogate metabolic pathways identified to be affected by AMPK-glycogen binding disruption.

Conclusion: Metabolomics has uncovered concomitant alterations in the plasma, skeletal muscle and liver metabolite profiles between rested and exercised mice in both genotypes, and between genotypes at rest. These mouse tissue metabolomic datasets complement previous whole-body, tissue and molecular characterisation of WT and DKI mice, revealing potential novel molecular biomarkers in tissues and the circulation that may contribute to exercise's metabolic health benefits and the physiological effects of disrupting AMPK-glycogen binding *in vivo*.

6.2. Introduction

Exercise has been widely appreciated for its health benefits for millennia [2]. Although decades of research in exercise biochemistry and physiology have led to tremendous progress in the understanding of the numerous and complex biological processes occurring during exercise, the breadth of molecular metabolic changes occurring in response to exercise in tissues such as liver and skeletal muscle remain incompletely understood. Exercise represents a major challenge to energy homeostasis, with adenosine triphosphate (ATP) turnover increasing up to 100-fold within cells in response to exercise [24]. Eukaryotic organisms have evolved to maintain relatively constant energy levels [5]. One of the key regulators of cellular energy homeostasis is the AMP-activated protein kinase (AMPK), a heterotrimeric enzyme able to directly sense cellular energy levels by competitively binding ATP, adenosine diphosphate (ADP) and adenosine monophosphate (AMP) [209]. During exercise, increased ATP turnover rates result in increased cellular levels of ADP and AMP relative to ATP, leading to AMPK activation. Once activated, AMPK turns off anabolic processes such as protein, glycogen and lipid synthesis and concurrently turns on catabolic pathways such as glycolysis, lipolysis and protein breakdown to help maintain energy homeostasis [209].

AMPK is also able to sense stored energy in the form of glycogen – an important energy store utilised during intense (> 70% of VO_2 max) exercise [30]. AMPK-glycogen binding is mediated by a carbohydrate binding module (CBM) within the AMPK β1 and β2 subunit isoforms [6,7]. In rodents, the β1 isoform is predominantly expressed in the liver, while the β2 isoform is predominantly expressed in skeletal muscle [12]. Research over the last two decades has shown that specific tryptophan (W) residues within the CBM are crucial for AMPK-glycogen interactions [6,7] and growing evidence has highlighted interactive roles of AMPK and glycogen at the molecular, cellular and physiological levels [12], warranting further

research into the precise *in vivo* physiological roles of AMPK-glycogen binding in metabolism and exercise.

Recently, *in vivo* mouse experiments from my group have found that whole-body knock-in mutation of these W amino acid residues to alanine (A) disrupts AMPK-glycogen interactions and is associated with a range of physiological consequences such as increased total body weight and fat mass as well as decreased maximal exercise capacity [14-16]. Nevertheless, the mechanisms underlying these phenotypic effects remain largely unknown. Discovery-based untargeted metabolomics represents a promising approach to characterise the molecular metabolic responses to stimuli such as exercise and in response to these AMPK knock-in mutations. Indeed, the metabolome is considered a reflection of the cumulative changes that occur in all upstream biological layers including the genome, transcriptome, proteome, as well as their interactions with the environment [283] and stimuli such as exercise.

An untargeted metabolomics approach was recently used to determine the molecular responses to acute exercise and the effects of AMPK-glycogen binding disruption in mouse plasma [307]. Mice with AMPK β1 (W100A)/ β2 (W98A) double knock-in (DKI) mutations to chronically disrupt whole-body AMPK-glycogen binding had significantly different overall plasma metabolic profiles at rest relative to wild type (WT) mice, but these metabolomic profiles converged following acute exercise. Of interest, AMPK DKI mice showed increased plasma amino acid levels relative to WT mice in the resting state but decreased amino acids following exercise. This interaction effect suggested an increased reliance on amino acid metabolism underlying the response to exercise in DKI versus WT mice. Additionally, DKI mice displayed decreased plasma pantothenic acid (also known as pantothenate and vitamin B5), an essential nutrient that serves as a precursor for Coenzyme A (CoASH), which is involved in multiple steps of energy metabolism [287-289]. Whether the observed reduction in plasma pantothenic acid is associated with reduced tissue levels of pantothenic acid and

CoASH remains to be determined. If this is the case, it could help explain the increased carbohydrate utilisation and reduced exercise capacity observed in DKI compared to WT mice [307]. However, only limited insight into molecular metabolic regulation in response to exercise and AMPK-glycogen binding disruption can be captured by analysing the plasma metabolome in isolation.

Therefore, in the present study I aimed to next investigate the metabolomic profile in metabolically active tissues such as liver and skeletal muscle to gain a more integrative and comprehensive understanding of the mechanistic regulation occurring in these primary glycogen-storing tissues as a result of acute treadmill exercise and disruption of AMPK-glycogen interactions *in vivo*. Similar to the plasma metabolomics study, I used an untargeted metabolomics approach, and collected liver and skeletal muscle from the same mice used for the plasma metabolomics study. Complementary cell bioenergetic measurements (i.e., glycolysis and mitochondrial ATP production) were performed using mouse embryonic fibroblasts (MEF), in addition to real-time measures of mitochondrial respiration in mouse permeabilised gastrocnemius muscle fibre bundles.

6.3. Material and Methods

6.3.1. Mouse Model

The present study utilised the AMPK DKI mouse model previously generated by my group [15] described in detail previously [307], and all tissue samples used for metabolomic analyses were collected from the same mice utilised in my recently published plasma metabolomics paper [307]. Briefly, all mouse procedures were performed under the approval of the St. Vincent's Hospital (Melbourne, Australia) Animal Ethics Committee (approval numbers 025-15 and 011-19), in accordance with all NHMRC requirements and conforming to

National Institutes of Health animal research guidelines (NIH Publications No. 8023, revised 1978) and Australian codes of animal research practice (8 th Edition 2013). All mice were kept in pathogen-free microisolator cages (2-5 mice per cage) on standard 12:12-h dark-light cycles with controlled temperature (21°C), humidity and bedding. Mice were allowed ad libitum water access and standard chow diet (29% starch 20% protein and 6% fat, Barastoc, Ridley Agriproducts, Pakenham, Australia).

The Mouse Engineering Garvan/ABR (MEGA) Facility used CRISPR/Cas9 gene editing on a C57BL/6J background to generate whole-body AMPK Prkab1 W100A (β1 W100A) and Prkab2 W98A (β2 W98A) single KI mice [14,308]. Homozygous single KI mice were subsequently bred together to generate Prkab1 W100A / Prkab2 W98A DKI mice and were compared to age-matched WT control mice. Confirmatory genotyping was performed by TransnetYX (Cordova, TN, USA) using tail samples.

6.3.2. Liver and Gastrocnemius Muscle Metabolomic Analysis

6.3.2.1. Acute Treadmill Exercise Bout and Tissue Sample Collection

Male DKI and WT mice aged 12 to 16 weeks were acclimatised to treadmill running (Exer 3/6, Columbus Instruments, Columbus, OH, USA) for four consecutive days at progressively increasing speeds. The following day, WT and DKI mice were randomly assigned to either an “exercised” or “rested” control group. Following two to three days of recovery, mice assigned to the exercised group completed a 30 min-run at 70% of their individual maximal speed at a 0° incline, while rested control mice remained in their home cage. Upon completion of the exercise bout, both rested and exercised mice were immediately euthanised in a CO_2 chamber for ~10 s. Euthanasia and sample collection were performed between 0800 and 1000 h at the start of the light cycle. Liver and skeletal muscle were

collected, immediately snap frozen in liquid nitrogen, and placed in Eppendorf tubes. Tubes were stored at −80°C until further analysis.

6.3.2.2. Tissue Sample Preparation

An average of 50 mg (wet weight) of liver and mixed gastrocnemius muscle from each mouse were chipped and freeze-dried overnight. Approximately 10 mg of tissue were then manually ground into fine powder with striated forceps on a glass dish and transferred to new tubes, then immediately returned to −80°C. Tissue sample preparation and LC-MS analyses were performed at the Centre for Integrative Metabolomics and Computational Biology, Edith Cowan University (Joondalup, Western Australia, Australia) according to previously described methods [175,279]. Sample preparation for LC-MS analyses was performed as follows: extraction solution was prepared using methanol:acetonitrile:water (2/2/1 (v/v)) with isotopically-labelled internal standards (valine-d8, phenylalanine-d8, caffeine-13C3, creatinine-d3, leucine-d3, sphingosine-d9, tryptophan-d5, trimethylamine N-oxide-d8, taurodeoxycholic acid-d5) at 1 ppm. Approximately 800 µL of extraction solution was added to each tissue sample (volume was corrected to the mass of each powdered tissue sample) and blank tube. Each tube was then vortexed for 10 s and placed on thermomixer agitator at 1,200 rpm for 2 min at 4°C and centrifuged (Heraeus Megafuge 8R, Thermo Fisher Scientific, Australia) for 10 min at 14000 rpm. Following agitation, 100 µL of supernatant was added to two separate glass inserts in injection vials (one set of vials for each assay, detailed below). An additional 40 µL of remaining supernatant from each sample were combined to create a pooled quality control (QC) stock solution, which was then aliquoted into 20 LC-MS vials of 60 µL each. Sample injection sequence (randomised by group; WT-Rest, WT-Ex, DKI-Rest, DKI-Ex) was identical to that of my mouse plasma metabolomic study [307]. LC-MS system suitability was checked using the quality assurance methods described previously [52] and 8 pooled QC samples were injected at the beginning of the sequence to condition the column.

Pooled QC samples were then injected following each block of experimental samples for assessment of analytical precision as reported in [52].

6.3.2.3. Liquid Chromatography–High Resolution Mass Spectrometry

C18 Assay:

All tissue samples were analysed using an Ultra High-Pressure Liquid Chromatography pump (Dionex UltiMate 3000 RS) coupled to an Orbitrap Q-Exactive MS (Thermo Scientific, San Jose, CA, USA) fitted with a heated electrospray ionisation (HESI) probe. Metabolite separation was performed using a reversed phase Hypersil GOLD column (100 × 2.1 mm, 1.9 μm particle size; Thermo Scientific, San Jose, CA, USA) with an in-line filter. Tissue samples were analysed in positive and negative ionisation modes using 0.1% formic acid in LC-MS water (solvent A) and 0.1% formic acid in LC-MS grade acetonitrile (solvent B). The following elution gradient was utilised: isocratic at 99% solvent A for 1 min, followed by an increase to 50% solvent B (1–2 min), then a linear increase to 99% solvent B over 7 min, which was maintained at 99% solvent B for 2 min. Initial conditions were returned over 2 min and held at 100% solvent A for equilibration (3 min). The flow rate was 0.3 mL/min for positive and negative modes, the injection volume was 4 μL, and the autosampler tray was set to 6°C and column oven temperature to 45°C. Full scans with data-dependent MS/MS were acquired with the Orbitrap mass analyser. Full scans were acquired with a resolution of 70,000 at mass-to-charge ratio (m/z) 200 over the m/z range 70–1000 with the following electrospray ionisation (ESI) conditions: source heater = 413°C (positive mode) 350°C (negative mode), sheath gas = 50 (positive mode) 35 (negative mode) (arbitrary units), auxiliary gas = 10 (arbitrary units), capillary temperature = 320°C (positive mode) 350°C (negative mode), ion spray voltage = 3.5 kV (positive mode) and 2.5 kV (negative ion mode), S-lens 50%, and automatic gain control = 1×10^{-6}. MS/MS was performed at a resolution of 17,500 at m/z 200 for each sample with the

higher energy collisional dissociation energy of 20 eV. Data acquisition was performed with Xcalibur software (Thermo Scientific, San Jose, CA, USA). Prior to analysis, external calibration of the Orbitrap was carried out using ready-made calibration solutions (ESI-negative ion calibration and ESI-positive ion calibration solutions) purchased from Thermo Fisher Scientific.

Hydrophilic Interaction Liquid Chromatography (HILIC) Assay:

Tissue samples were analysed using an Ultra High-Pressure Liquid Chromatography pump (Dionex UltiMate 3000 RS) coupled to an Orbitrap Q-Exactive MS (Thermo Scientific, San Jose, CA, USA) fitted with a HESI probe. Metabolite separation was performed on a Acquity UPLC Amide Column (100 x 2.1mm, 1.7 μm particle size; Waters, Milford, MA, USA). Sample analysis was performed using LC-MS water buffered with 10 mM ammonium formate and 50 mM formic acid for a pH of 3 (solvent A) and 90:10 LCMS acetonitrile and LC-MS grade water buffered with 10 mM ammonium formate and 50 mM formic acid (solvent B). The following elution gradient was used: isocratic at 100% solvent B for 1 min, followed by a linear increase to 40% solvent A (1–8 min), which was maintained at 40% solvent A for 1 min. Initial conditions were returned over 1 min, then held at 100% solvent B for equilibration (5 min). The flow rate was 0.4 mL/min. Injection volume was 4 μL, and the autosampler tray was set to 6°C and column oven temperature to 45°C. Full scans with data-dependent MS/MS were acquired with the Orbitrap mass analyser. Full scan acquisition was performed at a resolution of 70,000 at mass-to-charge ratio (m/z) 200 over the m/z range 70–1000 with the following ESI conditions: source heater = 350°C, sheath gas = 35 (arbitrary units), auxiliary gas = 10 (arbitrary units), capillary temperature 350°C, ion spray voltage = 3.5 kV, S-lens 50%, and automatic gain control = 1×10^{-6}. MS/MS was performed at a resolution of 17,500 at m/z 200 for each sample with the higher energy collisional dissociation energy of 20 eV. Data acquisition was performed with Xcalibur software (Thermo Scientific, San Jose, CA, USA).

Prior to analysis, external calibration of the Orbitrap was carried out using ready-made calibration solutions (ESI-negative ion calibration and ESI-positive ion calibration solutions) purchased from Thermo Fisher Scientific.

6.3.2.4. Data Processing and Metabolite Identification/Annotation

Following data acquisition, spectral processing was performed (i.e., HILIC POS and C18 POS and C18 NEG) in Compound Discoverer™ 3.1 (Thermo Scientific, San Jose, CA, USA) using an untargeted metabolomics workflow. Compound Discoverer™ version 3.1 was utilised for total ion chromatograms alignment along retention times (RT) based on an adaptive curve, with a 5 ppm mass tolerance and a maximum shift of 0.5 min. Detected features with a signal-to-noise ratio > 5 and an intensity ≥ 1,000,000 in each dataset were merged into compounds according to ion adducts. Ions detected within the blanks were subtracted from the samples using the "mark background compounds" node. Online databases such as the human metabolome database (http://www.hmdb.ca), mzCloud (https://www.mzcloud.org/), and the Kyoto Encyclopedia of Genes and Genomes (http://www.genome.ad.jp/kegg/) were searched to verify and putatively annotate metabolites. Metabolite identification/annotation was also performed in Compound Discoverer™ in accordance with the Metabolomics Standard Initiative (MSI) [71]. Quality control-regularised spline correction (QC-RSC) was used to correct analytical signal drift [274]. Following standard protocols [52], metabolites with relative standard deviation (RSD) QC > 20% or a Dispersion-ratio (D-ratio) > 30% were removed from further statistical analyses based on their failure to meet acceptable measurement precision.

6.3.3. ATP-Rate Assay in Mouse Embryonic Fibroblasts

Seahorse XFe24 Real-Time ATP Rate Assays were performed using mouse embryonic fibroblasts (MEF) derived from AMPK β1 W100A/β2 W98A DKI and control WT pregnant female breeders aged 11 to 18 weeks. MEFs were immortalised using Heather P. Harding

(Revised 11/5/03) protocol and Seahorse XFe24 measurements in MEFs were performed on cells at passages 8 to 14 (P_8-P_{14}).

Prior to performing each ATP Rate Assay, cell count and viability were first determined by adding Trypan blue (Thermo Fisher Scientific, San Jose, CA, USA) to resuspended cells (50% v/v) and manually counting using a hemocytometer (Merck, Rahway, NJ, USA). MEFs were re-seeded in a Seahorse 24-well cell culture microplate and the Real-Time ATP Rate Assay was performed using the Seahorse XFe24 Analyzer (Agilent, Santa Clara, CA, USA) according to user manual's instructions [280]. Briefly, the day prior to analysis, cells were harvested and resuspended to the desired concentration (i.e., cell seeding density of 20,000 cells/100 μL of growth medium) in Agilent Seahorse XFe24 Cell Culture Microplates and allowed to adhere for 60 min in a 37°C and 5% CO_2 incubator before adding another 150 μL to each well, bringing the total volume to 250 μL per well. Cells were then placed back in the incubator overnight. The sensor cartridge was then hydrated with 1 mL of XF calibrant solution added to each well of the utility plate and placed in the 37°C non-CO_2 incubator overnight.

On the day of analysis, fresh Seahorse XF Real-Time ATP Rate Assay Medium (further referred to as "assay medium") was prepared (Seahorse XF DMEM medium, pH 7.4; Seahorse XF Glucose (1.0 M solution); Seahorse XF Pyruvate (100 mM solution); Seahorse XF L-Glutamine (200 mM solution) with 97/1/1/1 (v/v)) and warmed to 37°C. Cells were washed with 1 mL of assay medium. The plate was then placed in a 37°C non-CO_2 incubator for 60 min. XF Real-Time ATP Rate Assay injection solutions of Oligomycin (1.5 μM) and Rotenone + Antimycin A (0.5 μM) were prepared. After taking the sensor cartridge out of the incubator, injection ports A and B were loaded with Oligomycin and Rotenone + Antimycin A, respectively. Once all A and B ports were filled, the sensor cartridge and utility plate were transferred to the Seahorse XFe24 Analyzer for calibration. Following cartridge calibration, cells were washed with assay medium one more time and finally placed in the Seahorse XFe24

Analyzer for Real-Time ATP Rate Assay. All Seahorse XFe24 data were normalised to total protein content via bicinchoninic acid (BCA) protein assay (Pierce, Rockford, Illinois, USA).

6.3.4. Mitochondrial Respiration in Skeletal Muscle Fibres

Male WT and DKI mice aged ~15-23 weeks were culled by cervical dislocation in the fed state between 0800 h and 0900 h. Gastrocnemius muscles were collected and placed in ice-cold BIOPS solution (50 mM MES, 7.23 mM K_2EGTA, 2.77 mM CaK_2EGTA, 20 mM imidazole, 0.5 mM DTT, 20 mM taurine, 5.77 mM ATP, 15 mM PCr, and 6.56 mM $MgCl_2 \cdot H_2O$; pH 7.1). Each muscle sample was trimmed of connective tissue and fat and divided into red and white muscle. Several small muscle bundles (~2.0-5.0 mg wet weight) were prepared by separating muscle along the longitudinal axis using fine-tipped forceps under a dissecting microscope. Fibre bundles were then treated with 40 µg/mL saponin for 30 min at 4°C and subsequently washed in MiR05 respiration buffer (0.5 mM EGTA, 10 mM KH_2PO_4, 110 mM sucrose, and 1 mg/mL fatty acid-free BSA; pH 7.1) for 15 min as described previously Perry *et al*. (2012) [281].

Oxygen (O_2) consumption measurements from permeabilised muscle fibres were performed in MiR05 respiration medium using an Oxygraph-2K (Oroboros Instruments, Innsbruck, Austria) at 37°C in the presence of 25 µM blebbistatin, as described elsewhere [282]. ADP-stimulated respiration was determined from fibres prepared from red and white muscle. Titrations were initiated in the presence of 10 mM pyruvate and 5 mM malate and ADP was titrated at various concentrations. Glutamate (10 mM) and succinate (10 mM) were added to quantify maximum mitochondrial respiration. Finally, outer mitochondrial membrane integrity was determined by adding 10 µM cytochrome c, with < 10% increase in respiration indicating outer mitochondrial membrane integrity. Experiments were performed in duplicate and data

were normalised to muscle fibre bundle wet weight. The apparent K_m for ADP was determined as previously described [281].

6.3.5. Statistical Analyses

Statistical analyses of metabolomics dataset was performed using two-way ANOVA to test the null hypothesis (i.e., no differences between rested/exercised conditions and/or WT/ DKI genotypes) for each individual metabolite. False discovery rate (FDR) estimation to account for multiple comparisons was performed using the Storey FDR method [275], and *P* values < 0.05 with a FDR < 0.1 were considered statistically significant.

Assessment of structured similarities between metabolite concentrations across the complete dataset was performed via hierarchical cluster analysis (HCA) using Pearson's correlation coefficient as the similarity measure, and Ward's linkage method [276]. The lowest linkages (i.e., closest metabolite clusters) within the HCA dendrogram indicate metabolites that display the most similar responses. All metabolites were combined into a single data matrix and applied to principal component–canonical variate analysis (PC-CVA) [277] to visualise the multivariate discrimination between the four experimental groups. To avoid overfitting, 5-fold cross validation was used to choose the optimal number of principal components to apply to the CVA model. 95% CI for the model coefficients were calculated using bootstrap resampling [278]. Prior to statistical analyses of the metabolomic dataset, metabolite profiles were $\log_{10}$ transformed and scaled to unit variance (auto scaled). Statistical analyses of the metabolomic dataset were performed using MATLAB ®package version R2021b (MathWorks, Natick, MA).

Additional results from this study generated in Seahorse and Oroboros O2k experiments were analysed using Student's t-test or one- or two-way ANOVA with Fisher's

least significant difference as post hoc analysis where applicable. Statistical analyses were performed using GraphPad Prism software version 8.4.3 (GraphPad Software, San Diego, CA).

6.4. Results

6.4.1. Metabolomic Analyses Reveal Metabolites Associated with Acute Submaximal Running and Loss of AMPK-Glycogen Binding Capacity in Mouse Liver

Following the standard reporting guidelines from the Metabolomics Society Initiative [71], a total of 150 metabolites were identified/annotated. Two-way ANOVA revealed 29 metabolites with significant differences ($P < 0.05$; FDR < 0.1) between conditions (rested versus exercised), whereas no significant differences were observed between genotypes (WT versus DKI). All identified/annotated liver metabolites, their molecular characteristics and respective statistical relationships are listed in **Table 6.1**.

Table 6.1 – Summary of the metabolites identified/annotated from WT and DKI mouse liver

Column & Mode	Metabolite	Molecular Formula	Molecular Weight	RT (min)	RSD_{QC}	*P* value G	FDR G	*P* value C	FDR C	*P* value GxC	FDR GxC	MSI ID	Cluster
C18POS	Lithocholyltaurine	C26 H45 N O5 S	483.3016	4.65	2.634	0.618	0.600	0.914	0.635	0.908	1	1	A
C18POS	Bile Acid (C26 H45 N O6 S)	C26 H45 N O6 S	499.2968	4.11	2.875	0.182	0.373	0.636	0.565	0.686	1	1	A
C18POS	Bile Acid (C26 H45 N O7 S)	C26 H45 N O7 S	515.2923	3.85	2.409	0.160	0.348	0.440	0.461	0.699	1	1	A
C18NEG	Taurocholic acid	C26 H45 N O7 S	515.2917	3.87	1.448	0.146	0.338	0.467	0.475	0.817	1	1	A
C18NEG	Glycocholic acid	C26 H43 N O6	465.3092	4.30	0.471	0.417	0.506	0.379	0.439	0.264	1	1	A
C18NEG	Glycodeoxycholic acid	C26 H43 N O5	449.3143	4.97	5.454	0.524	0.571	0.765	0.608	0.171	1	2	A
C18NEG	Bile Acid (C24 H40 O4)	C24 H40 O4	392.2928	5.77	4.451	**0.010**	0.182	0.704	0.593	0.918	1	1	A
C18NEG	Cholic acid	C24 H40 O5	408.2879	4.79	2.458	0.119	0.354	0.855	0.624	0.654	1	2	A
C18NEG	β-Muricholic acid	C24 H40 O5	408.2881	4.52	2.002	0.296	0.439	0.673	0.577	0.642	1	2	A
C18NEG	Bile acid (C24 H40 O5)	C24 H40 O5	408.2876	4.06	7.872	0.578	0.588	0.299	0.392	0.828	1	2	A
C18NEG	Deoxycorticosterone 21-glucoside	C27 H40 O8	492.2699	4.23	11.973	0.994	0.708	0.609	0.566	0.349	1	2	A
C18POS	O-Phosphoserine	C3 H8 N O6 P	185.0091	0.84	2.618	0.924	0.731	**0.037**	0.109	0.360	1	1	A
C18NEG	Oxidised glutathione	C20 H32 N6 O12 S2	612.1518	0.92	2.062	0.736	0.660	0.557	0.533	0.905	1	1	B
C18POS	Spermidine	C7 H19 N3	145.1580	0.75	7.827	0.383	0.493	0.803	0.619	0.624	1	1	B
HILICPOS	Nicotinamide adenine dinucleotide (NAD+)	C21 H27 N7 O14 P2	663.1097	7.77	2.423	0.253	0.422	0.874	0.633	0.347	1	2	B
HILICPOS	Trans-urocanate	C6 H6 N2 O2	138.0428	1.52	8.167	0.617	0.605	0.060	0.144	0.713	1	1	B
HILICPOS	Arginine	C6 H14 N4 O2	174.1116	7.21	4.976	0.353	0.472	0.845	0.622	0.860	1	1	B
HILICPOS	N6,N6,N6-Trimethyl-L-lysine	C9 H20 N2 O2	188.1523	6.99	2.321	0.185	0.373	0.327	0.419	0.864	1	2	B
HILICPOS	Isoputreanine	C7 H16 N2 O2	160.1211	7.05	0.596	0.906	0.739	0.812	0.611	0.581	1	1	B

Continued

Table 6.1 – Continued

Column & Mode	Metabolite	Molecular Formula	Molecular Weight	RT (min)	RSD_{QC}	*P* value G	FDR G	*P* value C	FDR C	*P* value GxC	FDR GxC	MSI ID	Cluster
C18POS	Creatine	C4 H9 N3 O2	131.0695	0.89	1.344	0.193	0.375	0.959	0.643	0.902	1	1	B
C18POS	Histamine	C5 H9 N3	111.0798	0.78	2.436	**0.016**	0.186	0.623	0.563	0.914	1	1	B
C18NEG	Biose	C12 H22 O11	342.116	0.89	7.754	**0.017**	0.181	0.170	0.262	0.862	1	1	B
C18NEG	Maltotriose	C18 H32 O16	504.1684	0.9	14.402	**0.005**	0.177	0.822	0.614	0.103	1	1	B
C18NEG	Stachyose	C24 H42 O21	666.2216	0.91	16.097	0.059	0.244	0.431	0.456	**0.021**	1	1	B
HILICPOS	Decanoylcarnitine	C17 H33 N O4	315.2407	1.27	1.369	0.542	0.568	0.134	0.228	0.708	1	1	C
HILICPOS	5'-Methylthioadenosine	C11 H15 N5 O3 S	297.0893	1.22	0.472	0.934	0.728	**0.031**	0.103	0.737	1	1	C
HILICPOS	Pipecolic acid	C6 H11 N O2	129.0789	5.4	0.934	0.478	0.549	0.082	0.175	0.876	1	1	C
C18POS	Tyrosine	C9 H11 N O3	181.0739	1.01	2.002	0.457	0.531	**0.024**	**0.090**	0.057	1	1	C
HILICPOS	Dipalmitoylphosphatidylcholine	C40 H80 N O8 P	733.562	1.14	3.674	0.332	0.479	0.062	0.146	0.741	1	2	C
HILICPOS	Guanidoacetic acid	C3 H7 N3 O2	117.0538	5.93	3.263	0.535	0.577	0.490	0.488	0.640	1	2	C
HILICPOS	Hexanoylcarnitine	C13 H25 N O4	259.1782	1.76	1.132	0.066	0.235	0.927	0.635	0.355	1	2	C
C18POS	Glucosamine	C6 H13 N O5	179.0794	0.86	4.402	0.344	0.472	0.476	0.479	0.718	1	1	C
HILICPOS	Homoarginine hydrochloride	C7 H16 N4 O2	188.1272	7.09	4.666	0.945	0.721	0.389	0.441	0.384	1	2	C
C18NEG	Aspartic acid	C4 H7 N O4	133.0374	0.87	1.820	**0.018**	0.178	**0.024**	**0.088**	0.484	1	1	C
C18NEG	Pyruvic acid	C3 H4 O3	88.01596	0.92	2.884	**0.014**	0.188	0.075	0.169	0.734	1	1	C
C18NEG	Malic acid	C4 H6 O5	134.0214	0.92	2.884	**0.014**	0.215	0.075	0.173	0.734	1	1	C
C18NEG	Cis-Aconitic acid	C6 H6 O6	174.0164	0.99	4.970	**0.023**	0.189	0.117	0.205	0.913	1	1	C
HILICPOS	Anserine	C10 H16 N4 O3	240.1222	7.31	0.705	**0.044**	0.262	0.613	0.564	0.198	1	2	C
HILICPOS	Thiamine	C12 H16 N4 O S	264.1045	4.93	2.678	0.148	0.336	0.708	0.592	0.968	1	2	C

Continued

Table 6.1 – Continued

Column & Mode	Metabolite	Molecular Formula	Molecular Weight	RT (min)	RSD_{QC}	*P* value G	FDR G	*P* value C	FDR C	*P* value GxC	FDR GxC	MSI ID	Cluster
C18POS	2-Aminooctanoic acid	C8 H17 N O2	159.1259	3.47	1.112	**0.047**	0.230	0.358	0.436	0.816	1	1	C
C18POS	Pyroglutamic acid	C5 H7 N O3	129.0427	0.85	2.370	0.549	0.569	0.513	0.506	0.669	1	1	C
C18POS	Citrulline	C6 H13 N3 O3	175.0957	0.86	6.255	0.062	0.238	0.084	0.176	0.311	1	1	D
HILICPOS	Cystathionine	C7 H14 N2 O4 S	222.0674	7.82	4.636	0.980	0.717	0.098	0.186	0.982	1	1	D
C18POS	Alanine	C3 H7 N O2	89.04776	0.84	2.050	0.992	0.716	**0.001**	**0.018**	0.803	1	1	D
HILICPOS	N-Acetyl-L-arginine	C8 H16 N4 O3	216.1221	5.88	4.036	0.742	0.660	**0.006**	**0.037**	0.376	1	2	D
HILICPOS	Imidazoleacetic acid	C5 H6 N2 O2	126.0428	5.68	11.934	0.932	0.732	**0.016**	**0.066**	0.476	1	1	D
C18NEG	Daidzein	C15 H10 O4	254.0579	3.89	3.445	0.803	0.686	**0.007**	**0.033**	0.986	1	1	D
C18NEG	Phenylpropionylglycine	C11 H13 N O3	207.0894	3.70	9.023	0.344	0.477	0.243	0.363	0.646	1	1	D
C18NEG	5-Methoxyindoleacetate	C11 H11 N O3	205.0737	3.75	3.974	0.307	0.450	0.665	0.580	0.902	1	1	D
C18POS	Phenylacetylglycine	C10 H11 N O3	193.074	3.48	6.440	0.975	0.723	0.980	0.648	0.680	1	1	D
C18NEG	Indoxyl sulfate	C8 H7 N O4 S	213.0096	3.23	4.122	0.285	0.442	0.934	0.635	0.786	1	1	D
HILICPOS	Propionylcarnitine	C10 H19 N O4	217.1312	3.27	3.405	0.201	0.377	0.051	0.135	0.519	1	1	D
HILICPOS	Acetylcholine	C7 H15 N O2	145.1101	4.40	5.142	0.834	0.701	**1.96E-04**	**0.004**	0.832	1	2	D
C18POS	Methionine	C5 H11 N O2 S	149.051	0.94	5.329	0.137	0.349	**0.033**	0.106	0.501	1	1	D
C18POS	Serine	C3 H7 N O3	105.0426	0.84	4.009	0.367	0.483	0.057	0.144	0.130	1	1	D
HILICPOS	Threonine/Homoserine	C4 H9 N O3	119.0582	6.15	1.521	0.735	0.666	0.164	0.256	0.274	1	1	D
HILICPOS	Cytidine 5′-monophosphate	C9 H14 N3 O8 P	323.0518	7.99	1.546	0.536	0.572	0.294	0.397	0.425	1	2	E
HILICPOS	Citicoline	C14 H26 N4 O11 P2	488.1075	7.90	1.358	0.161	0.345	0.876	0.630	0.567	1	2	E
HILICPOS	Adenosine monophosphate	C10 H14 N5 O7 P	347.0632	6.72	0.864	0.199	0.379	**0.010**	**0.047**	0.954	1	1	E

Continued

Table 6.1 – Continued

Column & Mode	Metabolite	Molecular Formula	Molecular Weight	RT (min)	RSD_{QC}	*P* value G	FDR G	*P* value C	FDR C	*P* value GxC	FDR GxC	MSI ID	Cluster
C18NEG	Glucosamine 6-phosphate	C6 H14 N O8 P	259.0456	0.80	1.992	0.053	0.245	0.053	0.137	0.789	1	1	E
HILICPOS	Creatine phosphate	C4 H10 N3 O5 P	211.0357	7.22	0.334	**0.046**	0.236	0.095	0.188	0.936	1	2	E
HILICPOS	Guanidinoethyl sulfonate	C3 H9 N3 O3 S	167.0363	5.40	1.508	**0.020**	0.180	0.304	0.395	0.848	1	2	E
HILICPOS	Methylimidazoleacetic acid	C6 H8 N2 O2	140.0583	4.89	7.477	**0.005**	0.139	**0.017**	**0.069**	0.195	1	1	E
HILICPOS	p-Aminobenzoic acid	C7 H7 N O2	137.0476	5.22	1.761	0.136	0.353	0.883	0.631	0.822	1	1	E
HILICPOS	Lysine	C6 H14 N2 O2	146.1054	7.35	2.007	0.819	0.694	0.371	0.441	0.688	1	1	E
C18POS	Niacinamide	C6 H6 N2 O	122.0481	0.91	2.482	0.167	0.349	0.331	0.419	0.520	1	1	E
HILICPOS	1-Methylnicotinamide	C7 H8 N2 O	136.0635	3.77	1.063	0.141	0.343	**0.002**	**0.019**	0.259	1	2	E
C18NEG	Cyclic ADP-ribose	C15 H21 N5 O13 P2	541.0605	0.92	3.719	0.907	0.734	**0.026**	**0.087**	0.091	1	2	E
C18NEG	Uridine 5'-diphosphoglucuronic acid	C15 H22 N2 O18 P2	580.0339	0.96	6.895	0.707	0.656	**0.040**	0.112	0.940	1	2	E
HILICPOS	1-Methyladenosine	C11 H15 N5 O4	281.1123	5.13	2.007	0.975	0.718	**0.001**	**0.018**	0.393	1	2	E
C18NEG	Steroid hormone (C21 H30 O4)	C21 H30 O4	346.2144	4.62	7.216	0.282	0.450	**1.98E-16**	**1.95E-14**	0.621	1	2	E
C18POS	Cortisol	C21 H30 O5	362.2096	4.10	2.358	**0.029**	0.205	**1.08E-08**	**5.31E-07**	**0.019**	1	1	E
C18NEG	Uridine diphosphate-hexose	C15 H24 N2 O17 P2	566.0553	0.80	3.440	**0.003**	0.141	**1.52E-05**	**0.001**	**0.047**	1	1	E
C18NEG	Myristyl sulfate	C14 H30 O4 S	294.1867	5.94	7.473	0.350	0.474	0.084	0.173	0.265	1	2	E
C18NEG	Hexose	C6 H12 O6	180.0633	0.87	2.244	0.225	0.400	**0.006**	**0.038**	0.131	1	1	E
HILICPOS	Carnosine	C9 H14 N4 O3	226.1065	7.37	0.548	**0.029**	0.219	0.126	0.218	0.619	1	1	E
HILICPOS	Glycerol 3-phosphate	C3 H9 O6 P	172.0135	6.65	0.534	0.057	0.246	0.657	0.578	0.836	1	1	F
C18POS	Uracil	C4 H4 N2 O2	112.0273	1.01	12.031	0.895	0.741	0.805	0.615	0.349	1	1	F
C18NEG	Uric acid	C5 H4 N4 O3	168.0282	1.27	1.013	0.454	0.532	0.830	0.615	0.884	1	1	F

Continued

Table 6.1 – Continued

Column & Mode	Metabolite	Molecular Formula	Molecular Weight	RT (min)	RSD_{QC}	*P* value G	FDR G	*P* value C	FDR C	*P* value GxC	FDR GxC	MSI ID	Cluster
C18NEG	Xanthosine	C10 H12 N4 O6	284.0756	2.90	4.018	0.247	0.419	0.554	0.535	0.870	1	2	F
C18POS	Xanthine	C5 H4 N4 O2	152.0333	1.01	1.773	0.336	0.478	0.713	0.591	0.968	1	1	F
HILICPOS	Adenosine	C10 H13 N5 O4	267.0965	2.27	2.644	0.512	0.582	0.885	0.627	0.755	1	1	F
C18NEG	Inosine	C10 H12 N4 O5	268.0807	0.94	2.676	0.290	0.442	0.551	0.537	0.932	1	1	F
C18NEG	Ribulose 5-phosphate	C5 H11 O8 P	230.0191	0.81	4.002	0.903	0.742	0.422	0.457	0.289	1	1	F
C18NEG	Inosine-5'-monophosphate (IMP)	C10 H13 N4 O8 P	348.047	0.92	0.543	0.400	0.497	0.747	0.604	0.229	1	2	F
HILICPOS	Nicotinamide	C6 H6 N2 O	122.0479	5.15	1.924	0.514	0.572	0.161	0.255	0.156	1	1	F
C18NEG	Hexose-phosphate	C6 H13 O9 P	260.0297	0.80	0.862	0.936	0.724	**0.001**	**0.011**	0.413	1	1	F
C18POS	Glucose 6-phosphate	C6 H13 O9 P	260.0301	0.79	1.020	0.709	0.653	**0.002**	**0.018**	0.755	1	1	F
C18POS	Adenine	C5 H5 N5	135.0545	0.90	3.035	0.513	0.577	**0.003**	**0.026**	0.355	1	1	F
HILICPOS	Hypoxanthine	C5 H4 N4 O	136.0384	2.19	2.498	0.553	0.568	**0.006**	**0.040**	0.465	1	1	F
HILICPOS	Guanosine monophosphate	C10 H14 N5 O8 P	363.058	7.35	4.010	0.754	0.665	**0.046**	0.125	0.891	1	1	F
C18NEG	Uridine monophosphate (UMP)	C9 H13 N2 O9 P	324.0355	0.92	3.746	0.523	0.576	0.296	0.394	0.902	1	2	F
C18NEG	Asparagine	C4 H8 N2 O3	132.0534	0.86	2.031	0.668	0.642	0.699	0.594	0.994	1	1	F
C18POS	N-acetyltryptophan	C13 H14 N2 O3	246.1006	3.64	3.140	0.096	0.294	**0.015**	**0.062**	0.561	1	1	F
HILICPOS	Tryptophan	C11 H12 N2 O2	204.0897	4.60	2.687	0.783	0.680	0.217	0.330	0.957	1	1	F
C18NEG	Gulonolactone	C6 H10 O6	178.0476	0.88	4.068	0.090	0.299	0.259	0.381	0.586	1	1	F
C18NEG	Gluconic acid	C6 H12 O7	196.0581	0.87	2.498	**0.045**	0.251	0.059	0.145	0.772	1	2	F
HILICPOS	Ergothioneine	C9 H15 N3 O2 S	229.0884	5.70	1.917	0.214	0.387	**0.006**	**0.034**	0.396	1	2	G
C18NEG	Saccharopine	C11 H20 N2 O6	276.1319	0.88	0.678	0.208	0.383	0.406	0.449	0.233	1	1	G

Continued

Table 6.1 – Continued

Column & Mode	Metabolite	Molecular Formula	Molecular Weight	RT (min)	RSD_{QC}	*P* value G	FDR G	*P* value C	FDR C	*P* value GxC	FDR GxC	MSI ID	Cluster
C18NEG	Cinnamoylglycine	C11 H11 N O3	205.0737	3.67	4.200	0.694	0.656	**0.012**	**0.052**	0.996	1	1	G
HILICPOS	Hypotaurine	C2 H7 N O2 S	109.0198	5.90	0.203	0.283	0.445	0.366	0.440	0.396	1	1	G
HILICPOS	Melatonin	C13 H16 N2 O2	232.1209	0.98	9.075	0.094	0.303	0.453	0.465	0.761	1	1	G
C18POS	Glycine	C2 H5 N O2	75.03205	0.84	3.586	0.094	0.296	0.142	0.233	0.264	1	1	G
HILICPOS	Phenylethylamine	C8 H11 N	121.0889	0.84	4.323	0.965	0.726	0.354	0.436	0.898	1	1	G
HILICPOS	Glutathione	C10 H17 N3 O6 S	307.0837	6.89	1.331	0.991	0.720	0.291	0.399	0.696	1	1	G
C18NEG	Taurine	C2 H7 N O3 S	125.0146	0.87	1.148	0.395	0.502	0.559	0.529	0.326	1	2	G
C18NEG	S-Adenosylhomocysteine	C14 H20 N6 O5 S	384.1216	1.91	0.206	0.615	0.608	0.591	0.555	0.734	1	1	G
HILICPOS	Beta-Alanine	C3 H7 N O2	89.04767	5.71	5.481	0.948	0.718	0.264	0.377	0.870	1	1	G
C18POS	Carnitine	C7 H15 N O3	161.1052	0.88	0.525	0.133	0.363	0.080	0.175	0.254	1	1	G
HILICPOS	Leucine/Isoleucine	C6 H13 N O2	131.0945	4.48	4.093	0.134	0.358	0.971	0.647	0.873	1	1	G
HILICPOS	Acetylcarnitine	C9 H17 N O4	203.1154	4.21	2.277	0.913	0.727	0.159	0.256	0.532	1	1	G
C18NEG	Benzoic acid	C7 H6 O2	122.0368	3.53	7.324	0.968	0.723	0.440	0.457	0.781	1	2	H
HILICPOS	2-Aminoisobutyric acid	C4 H9 N O2	103.0633	5.63	2.267	0.069	0.239	0.624	0.559	0.365	1	1	H
C18POS	Cytosine	C4 H5 N3 O	111.0433	3.31	4.194	0.936	0.719	0.913	0.638	0.646	1	2	H
HILICPOS	Bilirubin	C33 H36 N4 O6	584.2627	0.63	8.849	0.699	0.654	0.673	0.582	0.235	1	2	H
C18POS	Cis-4,7,10,13,16,19-Docosahexaenoic acid	C22 H32 O2	328.2400	8.29	5.613	0.295	0.443	0.393	0.440	0.510	1	2	H
C18POS	Arachidonic acid	C20 H32 O2	304.2401	8.47	10.203	0.377	0.491	0.377	0.442	0.477	1	2	H
C18POS	1-Linoleoyl glycerol	C21 H38 O4	354.277	7.96	4.787	0.130	0.376	0.263	0.382	0.529	1	2	H
HILICPOS	4-Guanidinobutyric acid	C5 H11 N3 O2	145.0851	4.47	2.343	0.233	0.401	**0.006**	**0.033**	0.361	1	2	H

Continued

Table 6.1 – Continued

Column & Mode	Metabolite	Molecular Formula	Molecular Weight	RT (min)	RSD_{QC}	*P* value G	FDR G	*P* value C	FDR C	*P* value GxC	FDR GxC	MSI ID	Cluster
HILICPOS	N-Acetylneuraminic acid	C11 H19 N O9	309.1058	6.89	4.452	0.781	0.683	0.282	0.392	0.570	1	1	H
HILICPOS	3-Methylhistidine	C7 H11 N3 O2	169.085	7.17	4.628	0.803	0.691	0.343	0.428	0.917	1	1	H
HILICPOS	Y-Glutamylcysteine	C8 H14 N2 O5 S	250.0622	6.73	1.620	0.225	0.395	0.622	0.567	0.921	1	2	H
HILICPOS	Palmitoyl sphingomyelin	C39 H79 N2 O6 P	702.5676	0.78	2.434	0.673	0.642	0.096	0.186	0.881	1	2	H
HILICPOS	N3,N4-Dimethyl-L-arginine	C8 H18 N4 O2	202.1428	6.66	2.193	0.538	0.569	**0.006**	**0.036**	0.452	1	2	H
HILICPOS	Trimethylamine N-oxide	C3 H9 N O	75.06834	2.68	1.519	0.151	0.336	**0.025**	**0.087**	0.535	1	1	H
C18POS	Cytidine	C9 H13 N3 O5	243.0855	0.90	6.038	0.145	0.344	0.762	0.611	0.391	1	1	H
HILICPOS	Proline	C5 H9 N O2	115.0633	5.33	1.898	0.342	0.480	0.729	0.594	0.208	1	2	H
HILICPOS	N-Alpha-acetyllysine	C8 H16 N2 O3	188.116	6.00	0.521	0.438	0.526	0.990	0.650	0.420	1	1	H
HILICPOS	Uridine diphosphate-N-acetylglucosamine	C17 H27 N3 O17 P2	607.0814	8.05	2.481	0.604	0.603	0.910	0.641	0.699	1	1	H
C18NEG	9(Z),11(E)-Conjugated linoleic acid	C18 H32 O2	280.2401	8.89	2.109	0.994	0.713	**0.035**	0.107	0.653	1	2	H
HILICPOS	Palmitoylcarnitine	C23 H45 N O4	399.3342	1.08	0.674	0.716	0.654	**0.005**	**0.039**	0.741	1	1	H
HILICPOS	S-Adenosylmethionine	C15 H22 N6 O5 S	398.1375	7.62	3.534	0.843	0.704	**0.002**	**0.017**	0.336	1	2	H
C18NEG	Suberic acid	C8 H14 O4	174.0892	3.37	1.674	0.445	0.528	**6.18E-05**	**0.002**	0.668	1	1	H
C18NEG	Sphingosine 1-phosphate	C18 H38 N O5 P	379.2488	5.86	3.248	0.413	0.507	0.282	0.397	0.359	1	1	H
C18NEG	ADP	C10 H15 N5 O10 P2	427.0296	0.92	6.443	**0.033**	0.221	0.714	0.587	0.811	1	1	H
C18NEG	Flavin adenine dinucleotide (FAD)	C27 H33 N9 O15 P2	785.1587	3.18	1.504	**0.002**	0.227	**0.036**	0.109	0.616	1	2	H
C18NEG	Flavin mononucleotide (FMN)	C17 H21 N4 O9 P	456.1049	3.22	1.331	**0.045**	0.241	0.092	0.184	0.098	1	2	H
HILICPOS	Pantothenic acid	C9 H17 N O5	219.1105	1.45	2.975	0.064	0.237	0.421	0.461	0.186	1	1	I
HILICPOS	Aminoadipic acid	C6 H11 N O4	161.0687	6.16	3.915	**0.006**	0.126	0.106	0.193	0.169	1	2	I

Continued

Table 6.1 – Continued

Column & Mode	Metabolite	Molecular Formula	Molecular Weight	RT (min)	RSD_{QC}	*P* value G	FDR G	*P* value C	FDR C	*P* value GxC	FDR GxC	MSI ID	Cluster
HILICPOS	Glutamine	C5 H10 N2 O3	146.0690	6.36	2.721	0.057	0.254	0.768	0.605	0.755	1	1	I
HILICPOS	Betaine	C5 H11 N O2	117.0788	4.72	1.770	0.141	0.351	0.426	0.456	0.693	1	1	I
HILICPOS	Glutamic acid	C5 H9 N O4	147.0530	6.42	1.640	0.059	0.235	0.947	0.639	0.923	1	1	I
HILICPOS	Xanthurenic acid	C10 H7 N O4	205.0370	4.10	1.934	0.396	0.497	0.807	0.612	0.386	1	2	I
HILICPOS	Stearoylethanolamide	C20 H41 N O2	327.3133	0.65	5.965	**0.043**	0.273	0.782	0.611	0.494	1	1	I
HILICPOS	1-Methylhistidine	C7 H11 N3 O2	169.0850	6.75	0.842	0.579	0.583	0.136	0.226	0.730	1	1	I
HILICPOS	Oleamide	C18 H35 N O	281.2715	0.71	1.817	0.131	0.367	0.099	0.185	0.966	1	1	I
HILICPOS	Riboflavin	C17 H20 N4 O6	376.1379	3.56	3.312	0.187	0.369	0.114	0.205	0.982	1	2	I
HILICPOS	Phenylalanine	C9 H11 N O2	165.0788	4.57	1.834	0.254	0.418	0.920	0.634	0.370	1	1	I
HILICPOS	Jasmonic acid	C12 H18 O3	210.1254	0.67	7.106	0.275	0.446	0.795	0.617	0.282	1	1	I
HILICPOS	Histidine	C6 H9 N3 O2	155.0694	7.28	2.176	0.911	0.731	0.385	0.441	0.766	1	1	I

Table 6.1 – A total of 150 liver metabolites were identified/annotated, including 29 metabolites significantly different between conditions (i.e., exercise versus rest) based on univariate analysis. Statistically significant values ($P < 0.05$ and/or FDR < 0.1) appear in bold text. C: condition; G: genotype; G x C: interaction between condition and genotype; FDR: false discovery rate; MSI: Metabolomics Standards Initiative; RSD_{QC}: relative standard deviation in quality control samples; RT: retention time

6.4.1.1. Correlated Metabolite Clusters

Hierarchical clustering of the 150 liver metabolites resulted in nine clusters reflecting differences in metabolite abundance patterns across experimental groups (WT-Rest, WT-Ex, DKI-Rest and DKI-Ex) based on pairwise Pearson's correlation similarity. The results are displayed as a circular dendrogram (**Figure 6.1A**) and averaged z-score metabolite responses for each cluster are shown in **Figure 6.1B**. The average response for metabolites in Cluster A (12 metabolites, predominantly bile acids) did not show significant differences between genotypes or conditions. Cluster B (12 metabolites, including carbohydrate species, creatine and histamine) showed a significant genotype effect ($P = 0.039$) with higher average metabolite abundance in DKI relative to WT mice. Cluster C (17 metabolites, composed of various metabolite species including amino acids, tricarboxylic acid [TCA] cycle intermediates, acylcarnitines), although not significant, showed trends for a genotype-associated decrease ($P = 0.071$) as well as an exercise-associated decrease ($P = 0.095$). In contrast, Cluster D (15 metabolites, comprising acetylcholine, amino acids and derivatives) was significantly decreased in the exercise condition ($P = 0.003$), regardless of genotype. Cluster E (20 metabolites, including creatine phosphate, adenosine monophosphate [AMP], cortisol, carnosine) showed both an exercise- and genotype-association ($P = 1.13\times 10^{-5}$ and $P = 0.01$, respectively). Cluster F (21 metabolites such as glucose-6-phosphate, xanthine and hypoxanthine) and Cluster G (14 metabolites including carnitine, acetylcarnitine and amino acids) did not show any significant associations with genotype or condition. Finally, while Cluster H (26 metabolites, including various species such as cofactors, complex lipids and amino acid derivatives) and Cluster I (13 metabolites, including vitamins and amino acids) showed trends for decreases following exercise ($P = 0.07$) and in DKI relative to WT mice ($P = 0.059$), respectively.

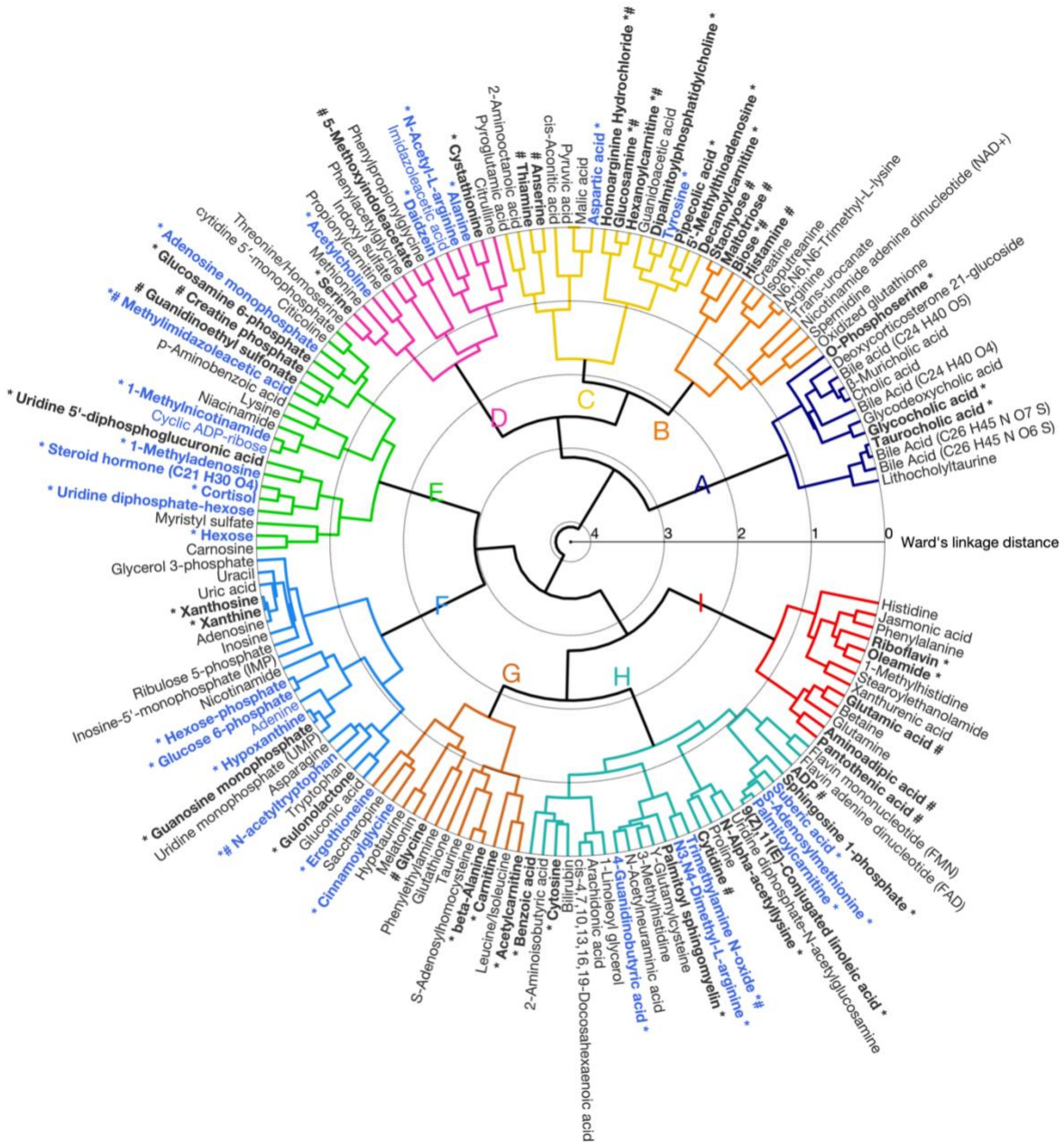

Figure 6.1A – Hierarchical Cluster Analysis (HCA) dendrogram of identified/annotated liver metabolites. Agglomerative clustering of individual metabolites based on pairwise correlation is shown. The lowest linkages within the HCA dendrogram indicate metabolites that display similar relative responses between the experimental groups. Nine clusters were observed. Metabolite labels are coloured to reflect the results of two-way ANOVA after filtering using a false discovery rate (FDR) of 0.1 (blue = significant effect of condition; black = no significance or FDR > 0.1). *: Metabolites that significantly ($P < 0.05$) contributed to the model along canonical variate 1 (CV1, **Figure 6.2**); #: Metabolites that significantly ($P < 0.05$) contributed to the model along CV2.

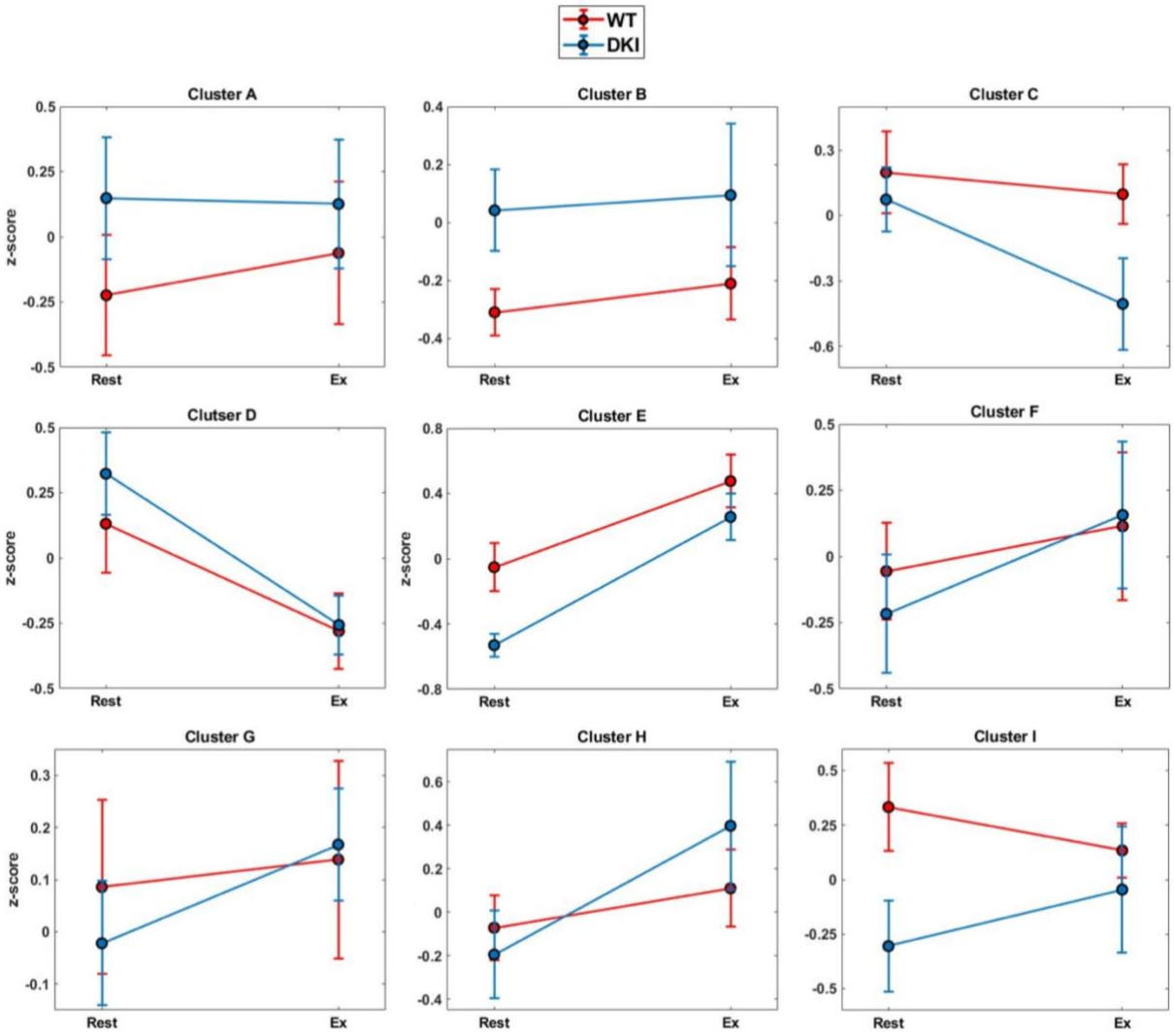

Figure 6.1B – Z-scores plot of the mean responses for each liver metabolite cluster. After conversion of individual metabolite $\log_{10}$ responses to a z-score, the average response of each cluster was calculated and presented as a group bar plot, with error bars indicating the standard error for each group mean (Red = WT; Blue = DKI). Following two-way ANOVA, Clusters B and E showed significant differences in the average group metabolite abundance between genotypes. Cluster B showed a significantly increased abundance in DKI relative to WT mice ($P = 0.039$), while Cluster E showed a significantly decreased average group metabolite abundance ($P = 0.011$) in DKI compared to WT mice. Cluster E also showed significantly increased metabolite abundance associated with exercise ($P = 1.13 \times 10^{-5}$). In contrast, Cluster D showed a significantly decreased average group metabolite abundance in response to exercise ($P = 0.003$).

6.4.1.2. Principal Component – Canonical Variate Analysis

Between-group multivariate differences in liver metabolite profiles with respect to condition and genotype were determined by performing PC-CVA (**Figure 6.2**). Canonical variate (CV1) explained > 50% of the total variance in the overall liver metabolomic dataset, whereas CV2 explained ~15% of the total variance. CV1 demonstrates significant differences in the multivariate mean between the rested and exercised conditions for both WT and DKI, while CV2 shows significant differences between WT and DKI liver metabolomes at rest and following exercise. The contribution of each metabolite (with 95% confidence intervals) to CV1 and CV2 are presented in **Figure 6.3** (significant metabolites indicated in red).

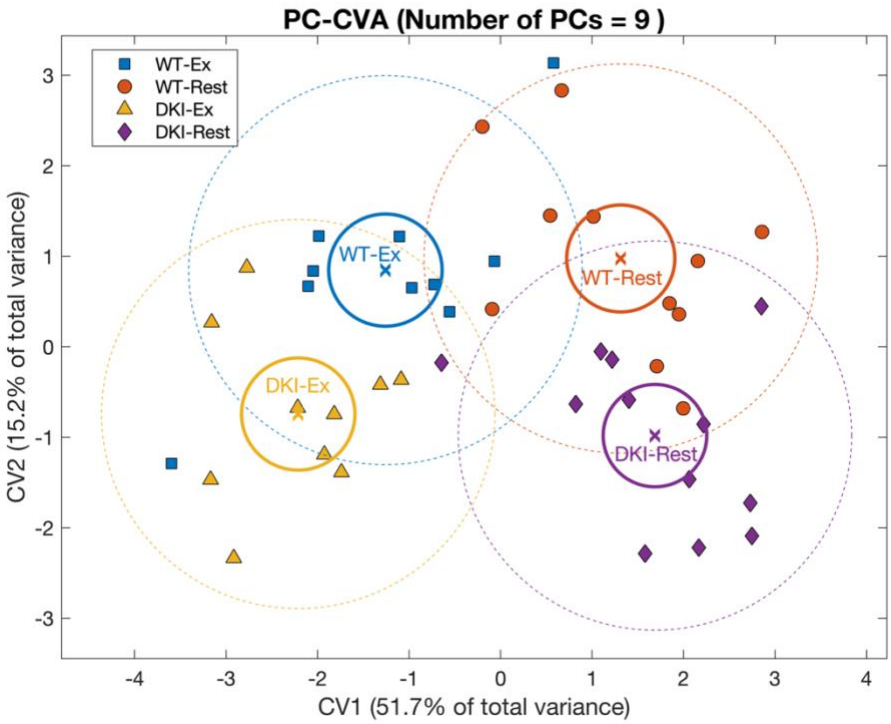

Figure 6.2 – Principal Component-Canonical Variate Analysis (PC-CVA) showing overall liver metabolite profile differences between genotypes at rest and after exercise. Scores plot of Canonical Variate 1 (CV1) versus Canonical Variate 2 (CV2). Each point (circle, square or triangle) represents a single sample [WT-Rest (n = 11), WT-Ex (n = 10), DKI-Rest (n = 12), DKI-Ex (n = 10)]. The mean (x) of each group is surrounded by a 95% confidence interval of the mean (full-line circles) and 95% confidence interval of membership in each sample group (dashed-line circles). Sample group means are considered significantly different when the 95% confidence interval of the means do not overlap.

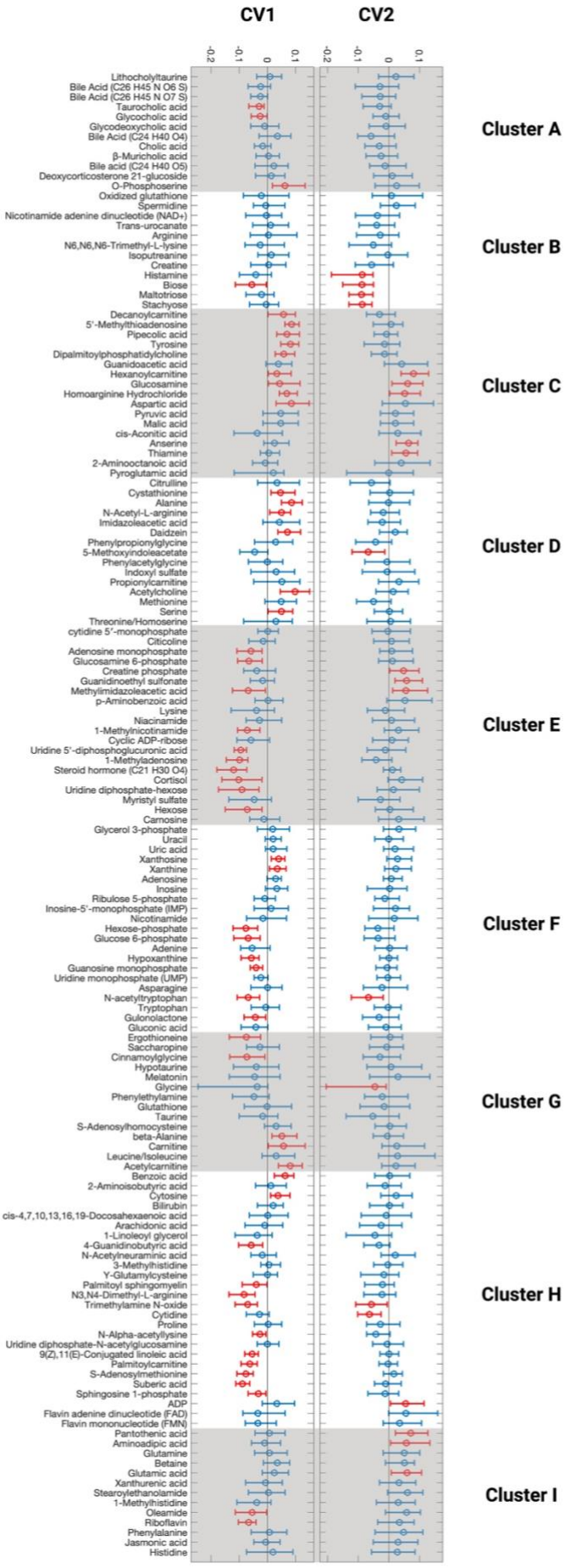
CV1
CV2
-0.2
-0.1
0
0.1
Lithocholyltaurine
Bile Acid (C26 H45 N O6 S)
Bile Acid (C26 H45 N O7 S)
Taurocholic acid
Glycocholic acid
Glycodeoxycholic acid
Bile Acid (C24 H40 O4)
Cholic acid
β-Muricholic acid
Bile acid (C24 H40 O5)
Deoxycorticosterone 21-glucoside
O-Phosphoserine
Oxidized glutathione
Spermidine
Nicotinamide adenine dinucleotide (NAD+)
Trans-urocanate
Arginine
N6,N6,N6-Trimethyl-L-lysine
Isoputreanine
Creatine
Histamine
Biose
Maltotriose
Stachyose
Decanoylcarnitine
5'-Methylthioadenosine
Pipecolic acid
Tyrosine
Dipalmitoylphosphatidylcholine
Guanidoacetic acid
Hexanoylcarnitine
Glucosamine
Homoarginine Hydrochloride
Aspartic acid
Pyruvic acid
Malic acid
cis-Aconitic acid
Anserine
Thiamine
2-Aminooctanoic acid
Pyroglutamic acid
Citrulline
Cystathionine
Alanine
N-Acetyl-L-arginine
Imidazoleacetic acid
Daidzein
Phenylpropionylglycine
5-Methoxyindoleacetate
Phenylacetylglycine
Indoxyl sulfate
Propionylcarnitine
Acetylcholine
Methionine
Serine
Threonine/Homoserine
cytidine 5'-monophosphate
Citicoline
Adenosine monophosphate
Glucosamine 6-phosphate
Creatine phosphate
Guanidinoethyl sulfonate
Methylimidazoleacetic acid
p-Aminobenzoic acid
Lysine
Niacinamide
1-Methylnicotinamide
Cyclic ADP-ribose
Uridine 5'-diphosphoglucuronic acid
1-Methyladenosine
Steroid hormone (C21 H30 O4)
Cortisol
Uridine diphosphate-hexose
Myristyl sulfate
Hexose
Carnosine
Glycerol 3-phosphate
Uracil
Uric acid
Xanthosine
Xanthine
Adenosine
Inosine
Ribulose 5-phosphate
Inosine-5'-monophosphate (IMP)
Nicotinamide
Hexose-phosphate
Glucose 6-phosphate
Adenine
Hypoxanthine
Guanosine monophosphate
Uridine monophosphate (UMP)
Asparagine
N-acetyltryptophan
Tryptophan
Gulonolactone
Gluconic acid
Ergothioneine
Saccharopine
Cinnamoylglycine
Hypotaurine
Melatonin
Glycine
Phenylethylamine
Glutathione
Taurine
S-Adenosylhomocysteine
beta-Alanine
Carnitine
Leucine/Isoleucine
Acetylcarnitine
Benzoic acid
2-Aminoisobutyric acid
Cytosine
Bilirubin
cis-4,7,10,13,16,19-Docosahexaenoic acid
Arachidonic acid
1-Linoleoyl glycerol
4-Guanidinobutyric acid
N-Acetylneuraminic acid
3-Methylhistidine
Y-Glutamylcysteine
Palmitoyl sphingomyelin
N3,N4-Dimethyl-L-arginine
Trimethylamine N-oxide
Cytidine
Proline
N-Alpha-acetyllysine
Uridine diphosphate-N-acetylglucosamine
9(Z),11(E)-Conjugated linoleic acid
Palmitoylcarnitine
S-Adenosylmethionine
Suberic acid
Sphingosine 1-phosphate
ADP
Flavin adenine dinucleotide (FAD)
Flavin mononucleotide (FMN)
Pantothenic acid
Aminoadipic acid
Glutamine
Betaine
Glutamic acid
Xanthurenic acid
Stearoylethanolamide
1-Methylhistidine
Oleamide
Riboflavin
Phenylalanine
Jasmonic acid
Histidine
Cluster A
Cluster B
Cluster C
Cluster D
Cluster E
Cluster F
Cluster G
Cluster H
Cluster I

Figure 6.3 – Related to **Figure 6.2**. Loading plot showing metabolites that significantly contributed to CV1 and CV2. Data are represented as mean loading values within 95% CI. Metabolites that significantly contributed to CV1 and/or CV2 are represented by red-coloured dots and CIs, while blue dots and CIs represent metabolites that did not significantly contribute to their respective CV. Metabolites are sorted according to HCA clusters A to I (top-down). CI: confidence interval, CV: canonical variate, HCA: hierarchical cluster analysis.

The metabolites significantly contributing to the model are presented in **Figure 6.4**. In this plot, the direction of each metabolite relative to the origin directly indicates directions of sample groups in the scores plot (**Figure 6.2**). In other words, metabolite groupings along the

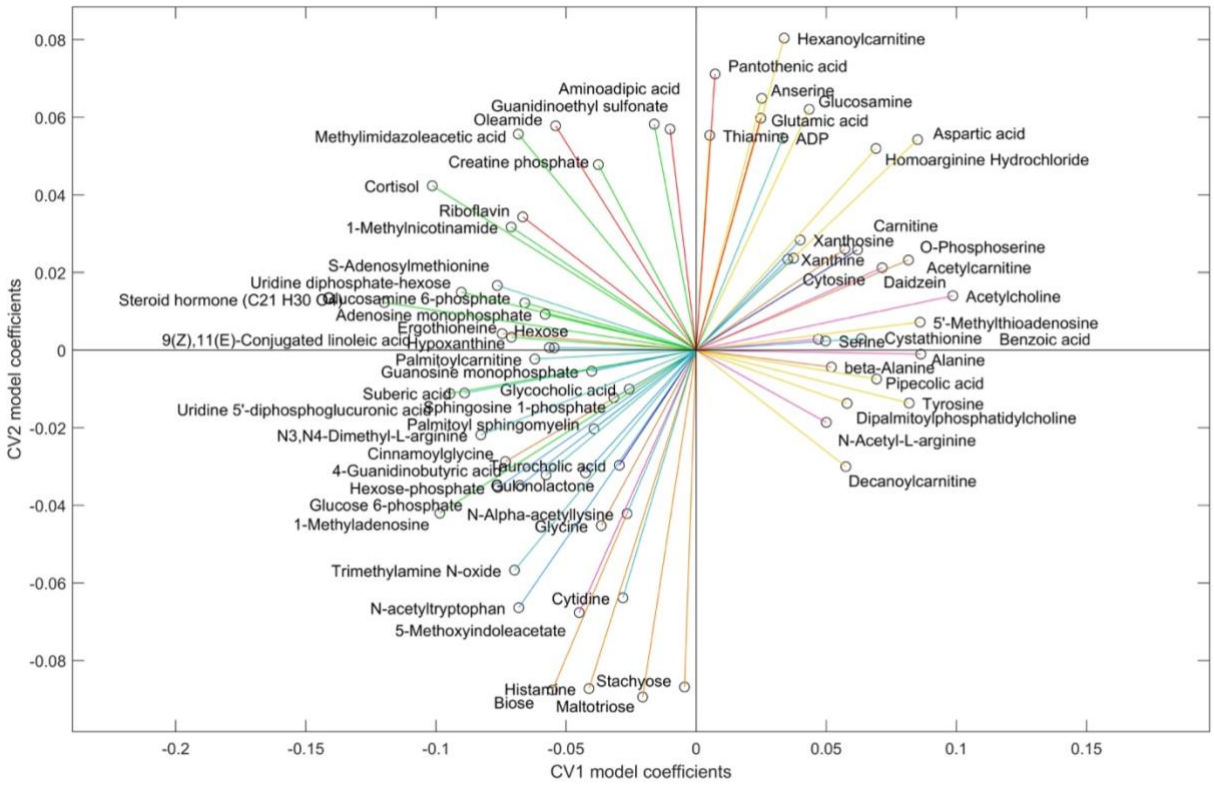

Figure 6.4 – The loading plot shows the influence (model coefficient value) of each metabolite that significantly ($P < 0.05$) contributed to the separation observed in the scores plot (**Figure 6.2**). The direction of the coefficient vector maps directly to the direction of the data points in the scores plot relative to the origin.

x-axis are causal of differences associated with the exercise intervention (e.g., palmitoylcarnitine and hypoxanthine to the left, increased with exercise; alanine and acetylcarnitine to the right, decreased with exercise); whereas metabolites on the y-axis are

indicative of genotype differences (e.g. histamine and maltotriose at the bottom, increased in DKI relative to WT liver; hexanoylcarnitine and pantothenic acid at the top, decreased in DKI liver). Cluster groups in **Figures 6.1A and 6.4** are colour-matched and the significant CV coefficients are labelled to the HCA plot.

6.4.2. Metabolomic Analyses Reveal Metabolites Associated with Acute Submaximal Running and Loss of AMPK-Glycogen Binding Capacity in Mouse Gastrocnemius Muscle

In accordance with the standard reporting guidelines from the Metabolomics Society Initiative [71], 92 gastrocnemius muscle metabolites were identified/annotated. Two-way ANOVA demonstrated 16 metabolites with significant differences ($P < 0.05$; FDR < 0.1) between conditions (rested versus exercised), whereas only one metabolite was significantly different in DKI versus WT gastrocnemius muscle. Identified/annotated gastrocnemius muscle metabolites, their molecular characteristics and respective statistical relationships are listed in **Table 6.2**.

Table 6.2 – Summary of the metabolites identified/annotated from WT and DKI mouse gastrocnemius muscle

Column & Mode	Metabolite	Molecular Formula	Molecular Weight	RT (min)	RSD_{QC}	*P* value G	FDR G	*P* value C	FDR C	*P* value GxC	FDR GxC	MSI ID	Cluster
C18NEG	Adenosine triphosphate (ATP)	C10 H16 N5 O13 P3	506.9954	1.17	6.429	0.902	0.833	0.550	0.527	0.144	0.523	2	A
C18POS	Spermidine	C7 H19 N3	145.1579	0.75	9.513	0.196	0.563	0.767	0.604	**0.020**	0.804	1	A
C18POS	Spermine	C10 H26 N4	202.2157	0.74	0.710	**0.027**	0.413	0.135	0.312	**0.023**	0.464	1	A
HILICPOS	Melatonin	C13 H16 N2 O2	232.1215	0.99	3.546	0.491	0.778	0.296	0.428	0.630	0.435	1	A
C18POS	Adenosine monophosphate	C10 H14 N5 O7 P	347.0630	1.00	2.875	0.554	0.843	0.101	0.263	0.912	0.440	1	A
HILICPOS	1-Methyladenosine	C11 H15 N5 O4	281.1125	5.09	2.922	0.883	0.835	**0.035**	0.115	0.930	0.429	2	A
HILICPOS	1-Methylhistidine	C7 H11 N3 O2	169.0853	6.70	4.518	0.732	0.847	0.178	0.370	0.914	0.436	1	A
HILICPOS	Cytosine	C4 H5 N3 O	111.0434	3.28	11.840	0.763	0.822	0.362	0.480	0.697	0.430	2	A
HILICPOS	2-Aminoisobutyric acid	C4 H9 N O2	103.0635	5.43	1.212	0.953	0.822	0.992	0.671	0.921	0.434	1	A
HILICPOS	p-Aminobenzoic acid	C7 H7 N O2	137.0479	4.86	4.435	0.931	0.850	0.306	0.433	0.148	0.495	1	A
HILICPOS	3-Hydroxyanthranilic acid	C7 H7 N O3	153.0427	1.28	3.919	0.933	0.842	0.269	0.429	0.927	0.432	1	A
HILICPOS	1-Methylnicotinamide	C7 H8 N2 O	136.0638	3.72	3.849	0.394	0.711	0.993	0.665	0.377	0.458	2	A
HILICPOS	Palmitoyl sphingomyelin	C39 H79 N2 O6 P	702.5692	1.60	5.303	0.779	0.785	0.472	0.533	0.674	0.451	2	A
HILICPOS	Pantothenic acid	C9 H17 N O5	219.1109	1.45	4.396	0.775	0.802	0.415	0.496	0.624	0.439	1	A
HILICPOS	5'-Methylthioadenosine	C11 H15 N5 O3 S	297.0901	1.20	2.768	0.776	0.793	0.117	0.280	0.825	0.447	1	A
HILICPOS	Dipalmitoylphosphatidylcholine	C40 H80 N O8 P	733.5635	0.76	2.851	0.941	0.830	0.630	0.568	0.939	0.418	2	A
C18POS	Histidine	C6 H9 N3 O2	155.0695	0.83	0.156	0.204	0.529	0.066	0.206	0.207	0.518	1	B
HILICPOS	3-Methylhistidine	C7 H11 N3 O2	169.0853	7.28	1.881	**0.018**	0.346	0.835	0.634	0.587	0.444	1	B
C18POS	Taurine	C2 H7 N O3 S	125.0147	0.86	0.784	**0.044**	0.431	0.976	0.667	0.180	0.515	2	B

Continued

Table 6.2 – Continued

Column & Mode	Metabolite	Molecular Formula	Molecular Weight	RT (min)	RSD_{QC}	*P* value G	FDR G	*P* value C	FDR C	*P* value GxC	FDR GxC	MSI ID	Cluster
C18POS	Carnosine	C9 H14 N4 O3	226.1066	0.85	0.294	0.060	0.425	0.765	0.610	0.786	0.457	1	B
HILICPOS	Creatine	C4 H9 N3 O2	131.0696	6.12	2.770	0.088	0.427	0.696	0.602	0.368	0.476	1	B
C18POS	Proline	C5 H9 N O2	115.0634	0.9	1.685	0.093	0.361	0.479	0.533	0.959	0.413	2	B
C18POS	Hydroxyproline	C5 H9 N O3	131.0583	0.86	6.750	**0.029**	0.381	0.340	0.460	0.667	0.453	2	B
C18POS	Glutathione	C10 H17 N3 O6 S	307.084	0.91	1.942	0.074	0.439	0.277	0.420	0.803	0.460	1	B
C18POS	D2-Aminooctanoic acid	C8 H17 N O2	159.1259	3.47	0.661	0.690	0.878	0.835	0.626	0.904	0.453	1	B
C18NEG	2-Hydroxycaproic acid	C6 H12 O3	132.0786	3.50	3.270	0.284	0.629	0.086	0.244	0.813	0.459	1	B
HILICPOS	Isoleucine/Leucine	C6 H13 N O2	131.0949	4.57	2.654	0.687	0.904	**3.05E-04**	**0.003**	0.133	0.669	1	B
C18POS	Carnitine	C7 H15 N O3	161.1051	0.88	1.226	0.050	0.392	**4.21E-07**	**2.65E-05**	0.712	0.426	1	C
HILICPOS	Ornithine	C5 H12 N2 O2	132.0900	7.37	1.033	0.971	0.828	**0.006**	**0.030**	0.458	0.417	1	C
HILICPOS	Gamma-Aminobutyric acid	C4 H9 N O2	103.0635	5.22	4.526	0.575	0.843	0.221	0.381	0.077	0.516	1	C
C18POS	Niacinamide	C6 H6 N2 O	122.0480	1.02	1.458	0.356	0.674	0.743	0.625	0.958	0.417	1	C
HILICPOS	Guanidinoethyl sulfonate	C3 H9 N3 O3 S	167.0365	5.36	5.833	0.083	0.461	0.934	0.653	0.435	0.459	2	C
HILICPOS	Trimethylamine N-oxide	C3 H9 N O	75.0685	2.69	4.638	0.572	0.854	0.430	0.505	0.324	0.542	1	C
C18POS	Histamine	C5 H9 N3	111.0797	0.79	0.044	0.720	0.859	0.215	0.393	0.584	0.459	1	C
HILICPOS	Isoputreanine	C7 H16 N2 O2	160.1214	7.02	2.952	0.736	0.840	0.636	0.565	0.688	0.431	1	C
HILICPOS	Arginine	C6 H14 N4 O2	174.1119	7.18	0.680	0.337	0.671	0.594	0.552	0.286	0.520	1	C
C18POS	Lysine	C6 H14 N2 O2	146.1055	0.80	11.756	0.139	0.492	0.541	0.526	0.441	0.442	1	C
C18POS	Pipecolic acid	C6 H11 N O2	129.079	0.80	5.815	0.147	0.495	0.611	0.559	0.599	0.429	1	C
C18POS	Threonine	C4 H9 N O3	119.0582	0.92	5.188	0.219	0.548	0.104	0.259	0.294	0.513	1	C

Continued

Table 6.2 – Continued

Column & Mode	Metabolite	Molecular Formula	Molecular Weight	RT (min)	RSD_{QC}	*P* value G	FDR G	*P* value C	FDR C	*P* value GxC	FDR GxC	MSI ID	Cluster
HILICPOS	N6,N6,N6-Trimethyl-L-lysine	C9 H20 N2 O2	188.1527	6.95	3.794	**4.82E-04**	**0.037**	0.750	0.623	0.372	0.466	2	C
HILICPOS	Trans-urocanate	C6 H6 N2 O2	138.0431	1.51	6.674	**0.016**	0.412	0.089	0.239	0.568	0.456	1	C
HILICPOS	Guanine	C5 H5 N5 O	151.0496	3.99	2.364	**0.038**	0.426	0.193	0.388	0.455	0.424	2	C
HILICPOS	Thiamine	C12 H16 N4 O S	264.1048	4.89	3.803	0.677	0.906	0.138	0.306	0.686	0.444	2	D
C18POS	5-Methoxyindoleacetate	C11 H11 N O3	205.0739	3.72	9.455	0.153	0.476	0.842	0.624	0.439	0.451	1	D
C18NEG	Cinnamoylglycine	C11 H11 N O3	205.0737	3.73	5.434	0.089	0.405	0.762	0.615	0.467	0.416	1	D
C18NEG	Phenylacetylglycine	C10 H11 N O3	193.0738	3.48	2.489	0.197	0.545	0.863	0.632	0.896	0.455	1	D
C18NEG	Indoxyl sulfate	C8 H7 N O4 S	213.0095	3.21	1.360	0.109	0.402	0.195	0.378	0.872	0.448	1	D
HILICPOS	Methionine	C5 H11 N O2 S	149.0512	4.94	3.812	0.940	0.839	0.239	0.402	0.550	0.450	1	E
HILICPOS	Adenine	C5 H5 N5	135.0548	7.72	4.675	**0.046**	0.395	0.540	0.534	0.225	0.502	1	E
C18POS	Glucose 6-phosphate	C6 H13 O9 P	260.0300	0.79	6.172	0.755	0.837	0.271	0.422	0.059	0.593	2	E
C18POS	Creatine phosphate	C4 H10 N3 O5 P	211.0358	1.05	7.978	0.338	0.657	0.409	0.499	0.494	0.431	2	E
HILICPOS	Glutathione oxidised	C20 H32 N6 O12 S2	612.1529	8.47	0.528	0.637	0.883	0.665	0.582	0.213	0.501	2	E
C18POS	Glycine	C2 H5 N O2	75.03197	0.84	9.872	0.772	0.810	0.151	0.323	0.905	0.448	1	E
C18POS	Bile Acid (C26 H45 N O7 S)	C26 H45 N O7 S	515.2919	3.85	0.073	0.226	0.532	0.405	0.504	0.934	0.421	1	E
C18NEG	Bile acid (C26 H45 N O6 S)	C26 H45 N O6 S	499.2973	4.18	3.741	0.398	0.702	0.384	0.487	0.817	0.449	1	E
C18NEG	Glycocholic acid	C26 H43 N O6	465.3094	4.28	4.091	0.316	0.682	0.291	0.431	0.586	0.452	1	E
HILICPOS	2-Hydroxycinnamic acid	C9 H8 O3	164.0472	5.32	4.010	0.198	0.529	0.761	0.623	0.906	0.443	1	F
HILICPOS	Tyrosine	C9 H11 N O3	181.0740	5.32	0.456	0.243	0.554	0.445	0.513	0.931	0.424	1	F
C18POS	Phenylalanine	C9 H11 N O2	165.0791	2.94	3.264	0.876	0.840	0.367	0.476	0.836	0.435	1	F

Continued

Table 6.2 – Continued

Column & Mode	Metabolite	Molecular Formula	Molecular Weight	RT (min)	RSD_{QC}	*P* value G	FDR G	*P* value C	FDR C	*P* value GxC	FDR GxC	MSI ID	Cluster
HILICPOS	Asparagine	C4 H8 N2 O3	132.0536	6.44	2.103	0.671	0.914	0.522	0.532	0.830	0.443	1	F
HILICPOS	Hypotaurine	C2 H7 N O2 S	109.0200	5.86	1.834	1.000	0.844	0.815	0.626	0.525	0.438	1	F
C18POS	Sugar alcohol (C6H14O6)	C6 H14 O6	182.0789	0.86	1.040	0.634	0.894	0.815	0.634	0.351	0.502	1	F
C18NEG	Bile acid (C24 H40 O5)	C24 H40 O5	408.2877	4.76	1.471	0.455	0.751	0.903	0.646	0.229	0.483	2	F
C18NEG	Deoxycholic acid	C24 H40 O4	392.2926	5.74	5.046	0.411	0.710	0.496	0.541	0.197	0.527	2	F
C18POS	Glutamine	C5 H10 N2 O3	146.0691	0.86	5.680	0.475	0.768	**0.023**	**0.091**	0.348	0.537	1	F
C18NEG	Pyroglutamic acid	C5 H7 N O3	129.0425	0.93	3.138	0.149	0.482	**0.032**	0.119	0.678	0.446	1	F
HILICPOS	Betaine	C5 H11 N O2	117.0791	4.69	3.210	0.726	0.854	0.946	0.654	0.755	0.445	1	F
HILICPOS	Citrulline	C6 H13 N3 O3	175.0960	6.54	0.643	0.704	0.868	0.927	0.656	0.135	0.603	1	F
C18POS	Alanine	C3 H7 N O2	89.04767	0.86	1.814	0.792	0.788	0.502	0.539	0.455	0.434	1	G
HILICPOS	Glycerol 3-phosphate	C3 H9 O6 P	172.0139	6.62	1.056	0.086	0.447	0.519	0.538	**0.033**	0.447	1	G
C18POS	Creatine monohydrate	C4 H9 N3 O2	131.0694	0.89	1.798	0.942	0.821	0.564	0.532	0.170	0.524	2	G
C18POS	Anserine	C8 H16 N2 O3	188.1161	0.91	1.866	0.765	0.814	0.708	0.604	0.074	0.594	1	G
HILICPOS	N-Acetylcadaverine	C7 H16 N2 O	144.1265	4.11	2.433	0.689	0.891	0.206	0.388	0.346	0.554	1	G
HILICPOS	Ergothioneine	C9 H15 N3 O2 S	229.0889	5.67	2.277	0.089	0.386	0.531	0.533	0.353	0.488	2	G
C18POS	Sphingosine 1-phosphate	C18 H38 N O5 P	379.2485	5.84	3.127	0.750	0.843	0.518	0.546	0.393	0.438	1	H
HILICPOS	Aspartic acid	C4 H7 N O4	133.0375	6.77	5.898	0.890	0.832	0.217	0.386	0.950	0.419	2	H
HILICPOS	Glutamic acid	C5 H9 N O4	147.0534	6.39	1.528	0.322	0.674	0.247	0.404	0.281	0.563	1	H
C18POS	Phosphoserine	C3 H8 N O6 P	185.0089	0.85	0.737	0.577	0.829	0.314	0.434	0.284	0.543	1	H
HILICPOS	Palmitoylcarnitine	C23 H45 N O4	399.3352	0.72	4.467	0.756	0.827	**0.023**	**0.096**	0.391	0.448	1	H

Continued

Table 6.2 – Continued

Column & Mode	Metabolite	Molecular Formula	Molecular Weight	RT (min)	RSD_{QC}	*P* value G	FDR G	*P* value C	FDR C	*P* value GxC	FDR GxC	MSI ID	Cluster
C18POS	Decanoylcarnitine	C17 H33 N O4	315.2415	5.03	2.328	0.073	0.474	**2.28E-04**	**0.003**	0.594	0.441	1	H
C18POS	Hexanoylcarnitine	C13 H25 N O4	259.1786	3.7	4.698	0.090	0.369	**7.66E-05**	**0.002**	0.430	0.466	2	H
C18POS	Acetylcarnitine	C9 H17 N O4	203.1157	0.92	3.373	1.000	0.835	0.072	0.214	0.350	0.520	1	H
C18POS	Propionylcarnitine	C10 H19 N O4	217.1315	1.41	3.401	0.716	0.869	**0.035**	0.120	0.140	0.563	1	H
C18POS	Tryptophan	C11 H12 N2 O2	204.0901	3.19	2.013	0.809	0.795	**4.03E-04**	**0.004**	0.359	0.480	1	H
HILICPOS	S-Adenosylmethionine	C15 H22 N6 O5 S	398.1381	7.58	1.170	0.417	0.703	**0.010**	**0.043**	0.511	0.436	2	H
C18NEG	D-Ribulose 5-phosphate	C5 H11 O8 P	230.0188	0.79	4.838	0.696	0.871	**3.83E-05**	**0.001**	0.097	0.553	1	H
HILICPOS	Citicoline	C14 H26 N4 O11 P2	488.1081	7.86	3.003	0.869	0.843	**0.002**	**0.009**	0.377	0.445	2	H
C18POS	Adenosine	C10 H13 N5 O4	267.0967	1.02	5.060	0.172	0.512	**1.13E-04**	**0.002**	0.595	0.434	1	H
C18NEG	Xanthine	C5 H4 N4 O2	152.0332	1.01	5.299	0.333	0.680	**0.001**	**0.005**	0.444	0.434	1	H
C18POS	Hypoxanthine	C5 H4 N4 O	136.0384	1.02	6.369	0.366	0.676	**0.001**	**0.004**	0.687	0.437	1	H
C18NEG	Inosine	C10 H12 N4 O5	268.0805	0.92	2.479	0.221	0.535	**0.001**	**0.004**	0.835	0.440	1	H
HILICPOS	Inosine-5'-monophosphate (IMP)	C10 H13 N4 O8 P	348.0477	6.93	0.916	0.516	0.800	**0.008**	**0.036**	0.817	0.455	2	H

Table 6.2 – A total of 92 gastrocnemius muscle metabolites were identified/annotated, including 16 metabolites that were significantly changed by condition (i.e., exercise versus rest) and one metabolite significantly associated with genotype (i.e. DKI versus WT) based on univariate analysis. Statistically significant values ($P < 0.05$ and/or FDR < 0.1) appear in bold text. C: condition; G: genotype; G x C: interaction between condition and genotype; FDR: false discovery rate; MSI: Metabolomics Standards Initiative; RSD_{QC}: relative standard deviation in quality control samples; RT: retention time

6.4.2.1. Correlated Metabolite Clusters

A total of eight metabolite clusters were identified from the hierarchical clustering of the 92 identified/annotated gastrocnemius muscle metabolites. Circular dendrogram and averaged z-score metabolite responses for each cluster are shown in **Figure 6.5A** and **6.5B**, respectively. Cluster A (16 metabolites, including ATP, AMP and melatonin) did not show significant differences between genotypes or conditions. Cluster B (11 metabolites, primarily amino acids and derivatives) was significantly increased in DKI relative to WT mice ($P < 0.01$). Cluster C (15 metabolites, mainly composed of carnitine, ornithine and several amino acids), Cluster D (5 metabolites, including thiamine and glycine derivatives), Cluster E (9 metabolites, including bile acids, oxidised glutathione and glucose-6-phosphate) and Cluster F (12 metabolites including deoxycholic acid, hypotaurine and citrulline) did not show significant associations with either genotype or condition. In contrast, Cluster G (6 metabolites including alanine, glycerol-3-phosphate and creatine monohydrate) showed a significant interaction effect between genotype and condition ($P < 0.05$). While these metabolites were decreased following exercise in WT mice, the opposite trend in these metabolites was observed in DKI mice. Finally, Cluster H (18 metabolites, including various several carnitine species, adenosine, inosine and hypoxanthine) was significantly increased in the exercise condition ($P = 3.58 \times 10^{-4}$), regardless of genotype.

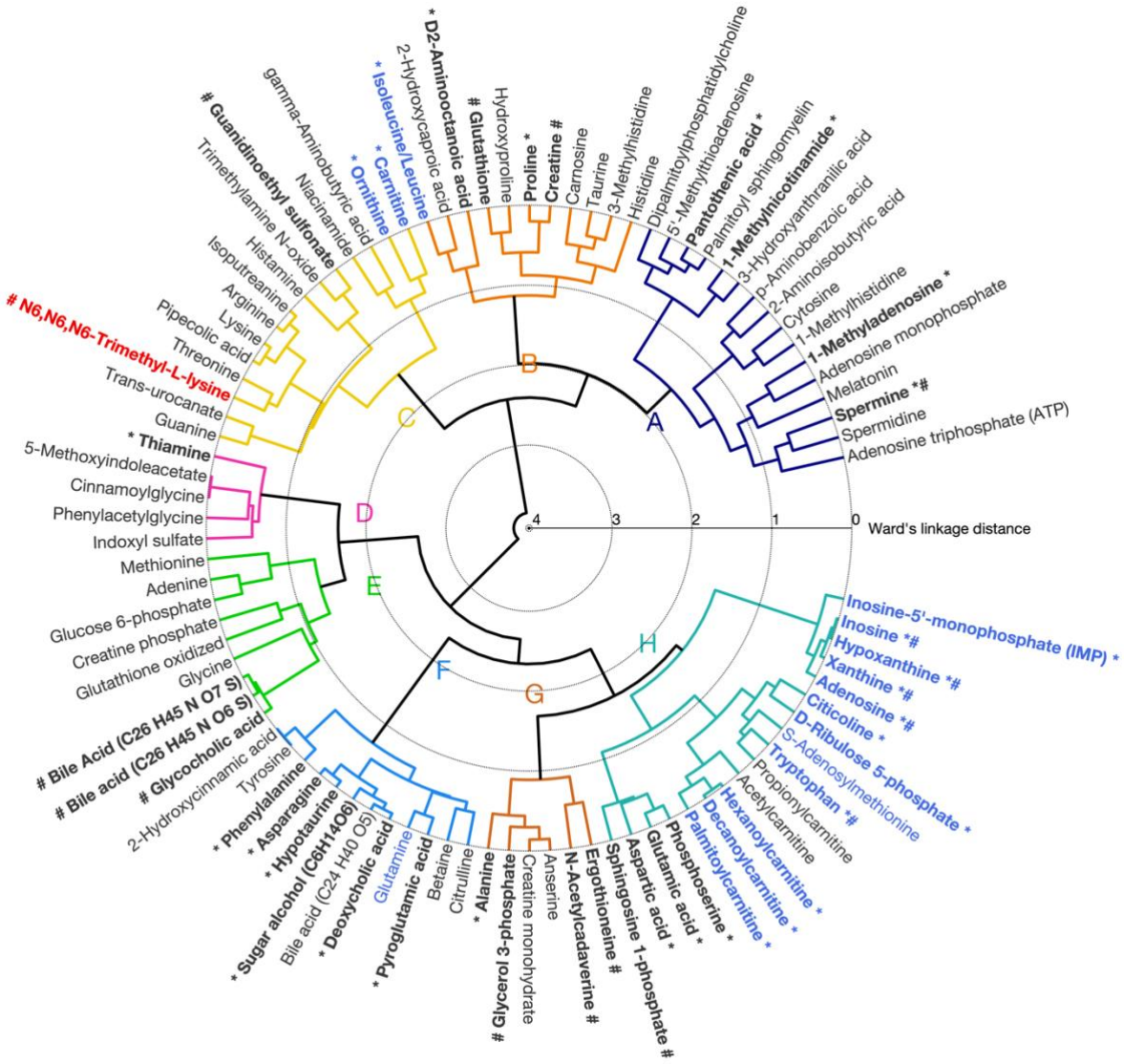

Figure 6.5A – Hierarchical Cluster Analysis (HCA) dendrogram of identified/annotated gastrocnemius muscle metabolites. Agglomerative clustering of individual metabolites based on pairwise correlation is shown. The lowest linkages within the HCA dendrogram indicate metabolites that display similar relative responses between the experimental groups. Eight clusters were observed. Metabolite labels are coloured to reflect the results of the two-way ANOVA after filtering using a false discovery rate (FDR) of 0.1 (blue = significant effect of condition; red = significant genotype effect; black = no significance or FDR > 0.1). *: Metabolites that significantly (P < 0.05) contributed to the model along canonical variate 1 (CV1, **Figure 6.7**); #: Metabolites that significantly (P < 0.05) contributed to the model along CV2.

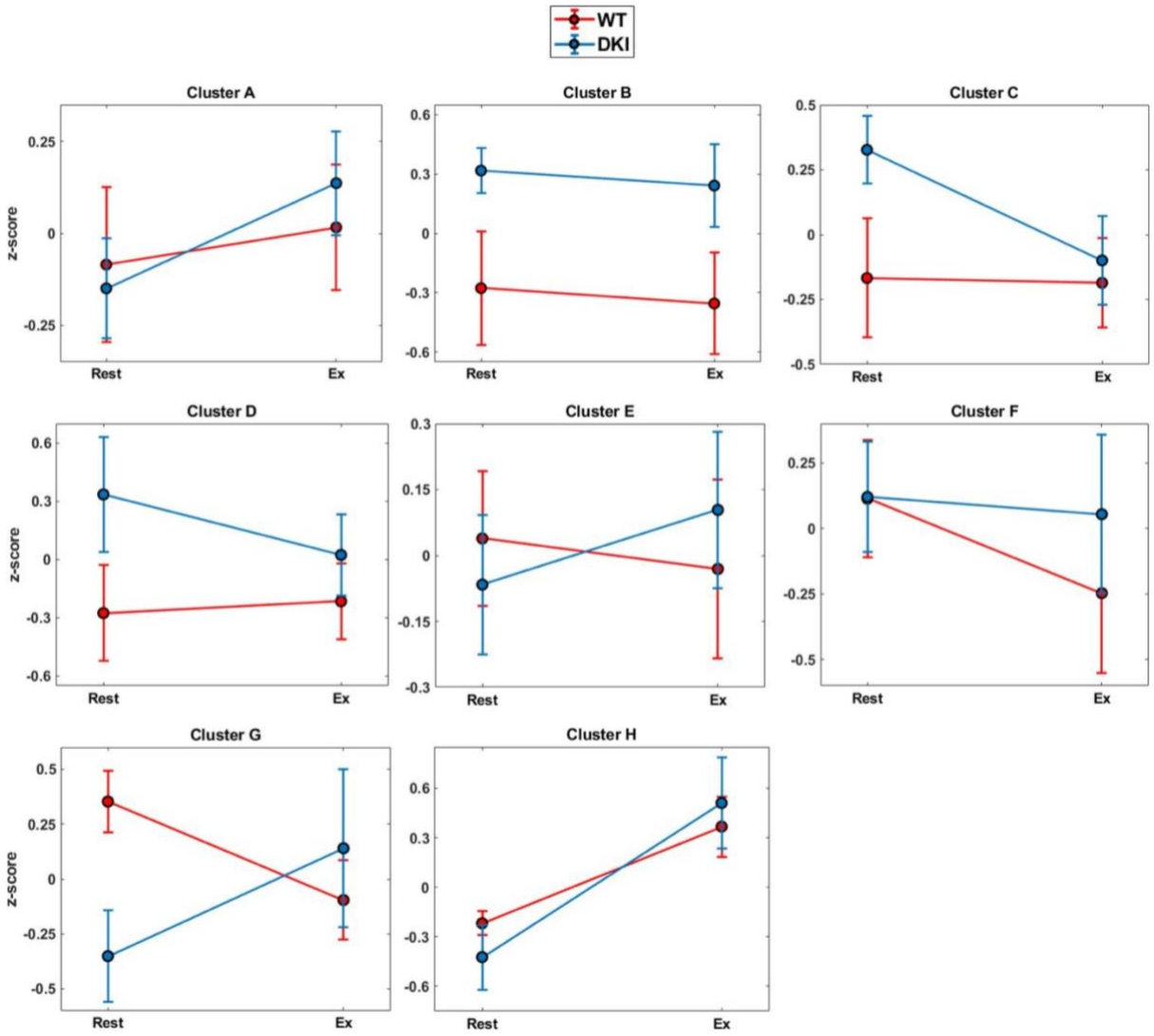

Figure 6.5B – Z-scores plot of the mean responses for each gastrocnemius muscle metabolite cluster. After conversion of individual metabolite $\log_{10}$ responses to a z-score, the average response of each cluster was calculated and presented here as a group bar plot with error bars indicating the standard error for each group mean (Red = WT; Blue = DKI). Following two-way ANOVA, Cluster B showed a significantly increase in abundance in DKI relative to WT mice ($P < 0.01$), independent of condition. Cluster B metabolites showed no significant association with exercise. Conversely, Cluster G demonstrated a significant interaction between genotype and condition ($P = 0.046$), with opposite metabolite trajectories observed between DKI and WT mice following exercise. Cluster G metabolites were decreased after exercise in WT mice while they were increased in DKI mice. Cluster H showed significantly increased metabolite abundance associated with exercise ($P = 3.58 \times 10^{-4}$) in both genotypes.

6.4.2.2. Principal Component – Canonical Variate Analysis

PC-CVA was applied to the gastrocnemius muscle metabolomic dataset to identify between-group multivariate differences in overall metabolite profiles with respect to condition and genotype (**Figure 6.6**). Canonical variate (CV1) explained ~58% of the total variance in the overall muscle dataset, whereas CV2 explained ~13% of the total variance. CV1 demonstrates significant muscle metabolome differences in the multivariate mean between the rested and exercised conditions for both WT and DKI, while CV2 shows significant differences between WT and DKI muscle metabolomes at rest, but not following exercise. The contribution of each metabolite (with 95% confidence intervals) to CV1 and CV2 is presented in **Figure 6.7** (significant metabolites indicated in red).

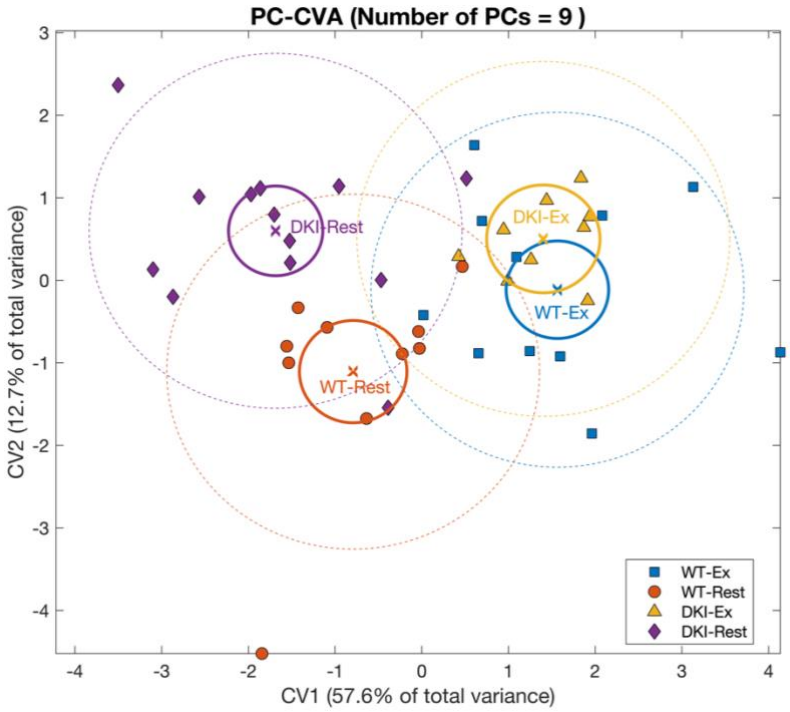

Figure 6.6 – Principal Component-Canonical Variate Analysis (PC-CVA) showing overall gastrocnemius muscle metabolite profile differences between genotypes at rest, and between conditions (exercise versus rest). Scores plot of Canonical Variate 1 (CV1) versus Canonical Variate 2 (CV2). Each point (circle, square or triangle) represents a single sample [WT-Rest (n = 10), WT-Ex (n = 11), DKI-Rest (n = 13), DKI-Ex (n = 10)]. The mean (x) of each group is surrounded by a 95% confidence interval of the mean (full-line circles) and 95% confidence interval of membership in each sample group (dashed-line circles). Sample group means are considered significantly different when the 95% confidence interval of the means do not overlap.

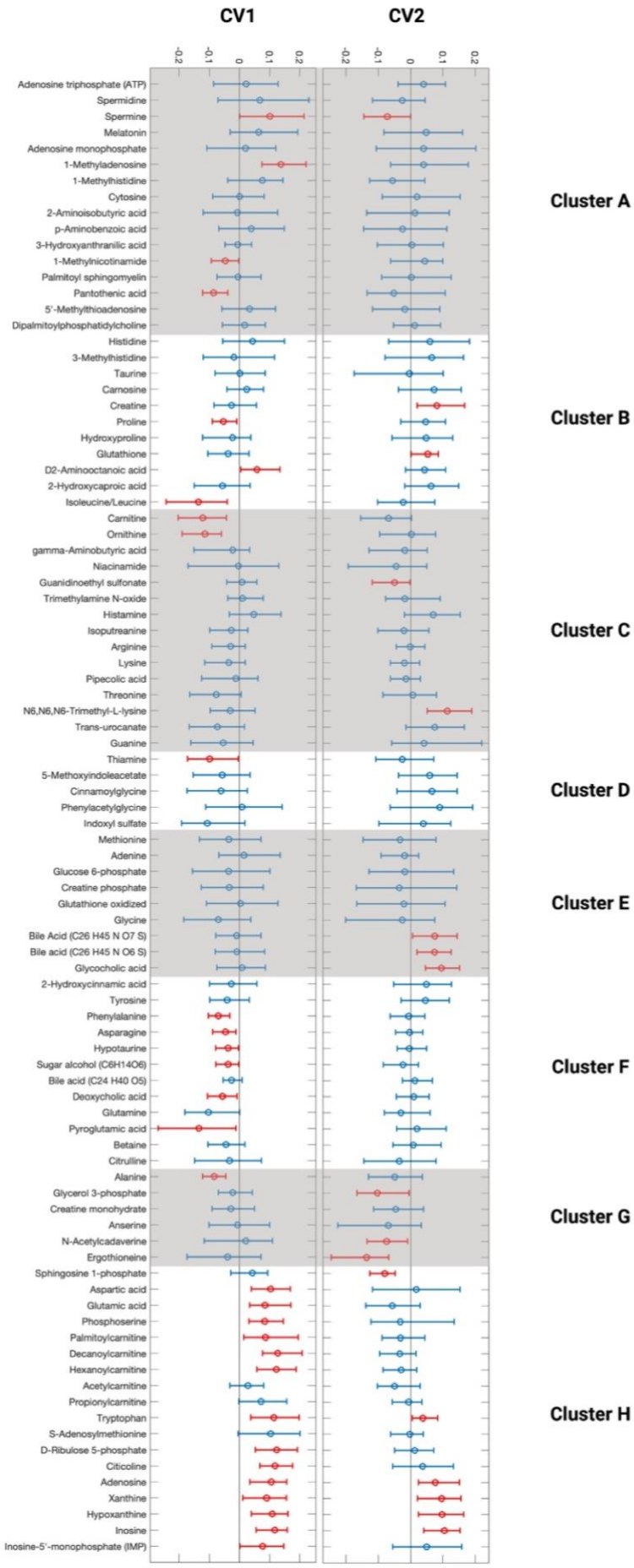
CV1
CV2
-0.2
-0.1
0
0.1
0.2
Adenosine triphosphate (ATP)
Spermidine
Spermine
Melatonin
Adenosine monophosphate
1-Methyladenosine
1-Methylhistidine
Cytosine
2-Aminoisobutyric acid
p-Aminobenzoic acid
3-Hydroxyanthranilic acid
1-Methylnicotinamide
Palmitoyl sphingomyelin
Pantothenic acid
5'-Methylthioadenosine
Dipalmitoylphosphatidylcholine
Histidine
3-Methylhistidine
Taurine
Carnosine
Creatine
Proline
Hydroxyproline
Glutathione
D2-Aminooctanoic acid
2-Hydroxycaproic acid
Isoleucine/Leucine
Carnitine
Ornithine
gamma-Aminobutyric acid
Niacinamide
Guanidinoethyl sulfonate
Trimethylamine N-oxide
Histamine
Isoputreanine
Arginine
Lysine
Pipecolic acid
Threonine
N6,N6,N6-Trimethyl-L-lysine
Trans-urocanate
Guanine
Thiamine
5-Methoxyindoleacetate
Cinnamoylglycine
Phenylacetylglycine
Indoxyl sulfate
Methionine
Adenine
Glucose 6-phosphate
Creatine phosphate
Glutathione oxidized
Glycine
Bile Acid (C26 H45 N O7 S)
Bile acid (C26 H45 N O6 S)
Glycocholic acid
2-Hydroxycinnamic acid
Tyrosine
Phenylalanine
Asparagine
Hypotaurine
Sugar alcohol (C6H14O6)
Bile acid (C24 H40 O5)
Deoxycholic acid
Glutamine
Pyroglutamic acid
Betaine
Citrulline
Alanine
Glycerol 3-phosphate
Creatine monohydrate
Anserine
N-Acetylcadaverine
Ergothioneine
Sphingosine 1-phosphate
Aspartic acid
Glutamic acid
Phosphoserine
Palmitoylcarnitine
Decanoylcarnitine
Hexanoylcarnitine
Acetylcarnitine
Propionylcarnitine
Tryptophan
S-Adenosylmethionine
D-Ribulose 5-phosphate
Citicoline
Adenosine
Xanthine
Hypoxanthine
Inosine
Inosine-5'-monophosphate (IMP)
Cluster A
Cluster B
Cluster C
Cluster D
Cluster E
Cluster F
Cluster G
Cluster H

Figure 6.7 – Related to **Figure 6.6** Loading plot showing metabolites that significantly contributed to CV1 and CV2. Data are represented as mean loading values within 95% CI. Metabolites that significantly contributed to CV1 and/or CV2 are represented by red-coloured dots and CIs, while blue dots and CIs represent metabolites that did not significantly contribute to their respective CV. Metabolites are sorted according to HCA clusters A to H (top-down). CI: confidence interval, CV: canonical variate, HCA: hierarchical cluster analysis.

The metabolites that contribute significantly to the model are depicted in **Figure 6.8**. Similar to the liver loading plot (**Figure 6.4**), the direction of each metabolite relative to the origin directly indicates the direction of sample groups in the scores plot (**Figure 6.6**). In this

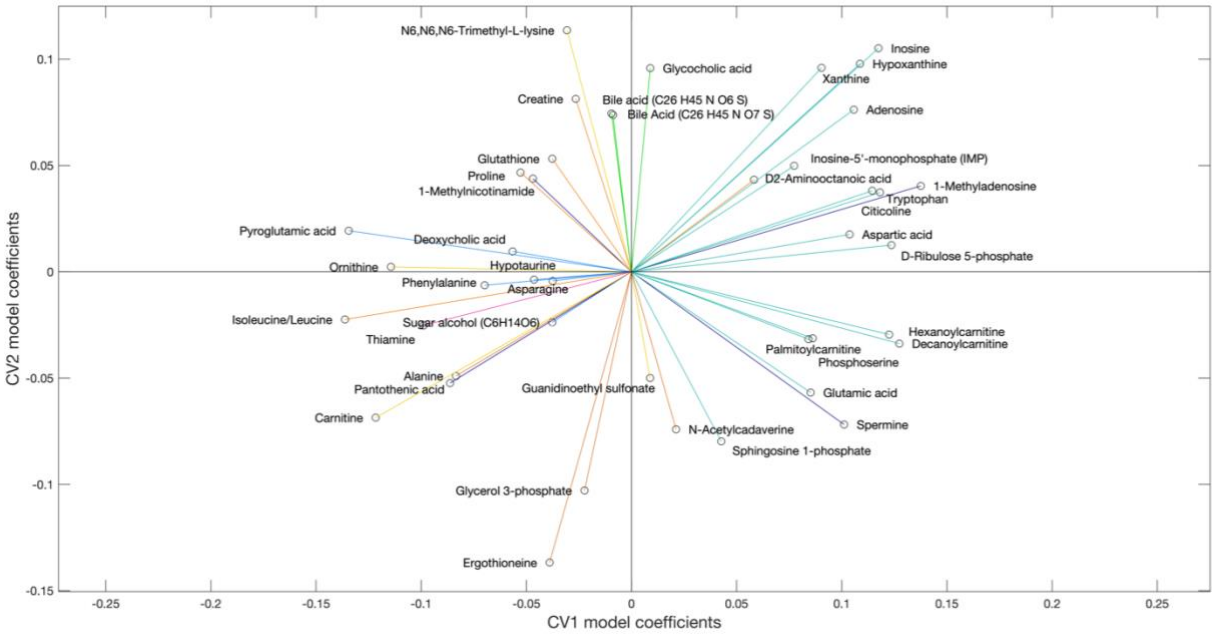

Figure 6.8 – The loading plot shows the influence (model coefficient value) of each metabolite that significantly ($P < 0.05$) contributed to the separation observed in the scores plot (**Figure 6.6**). The direction of the coefficient vector maps directly to the direction of the data points in the scores plot relative to the origin.

muscle dataset, metabolite groupings along the x-axis are causal of differences associated with the exercise intervention (e.g., inosine-5'-monophosphate [IMP] and hexanoylcarnitine to the right, increased with exercise; ornithine and isoleucine/leucine to the left, decreased with exercise); whereas metabolites on the y-axis demonstrate genotype differences (e.g. N6, N6, N6-trimethyl-L-lysine at the top, increased in DKI relative to WT gastrocnemius; glycerol-3-

phosphate and ergothioneine at the bottom, decreased in DKI gastrocnemius). Cluster groups in **Figures 6.5A and 6.8** are colour-matched and the significant CV coefficients are labelled in the HCA plot.

6.4.3. DKI Mouse Embryonic Fibroblasts Have Reduced ATP Production Rate and Increased Reliance on Mitochondrial Respiration

To provide further insights into the shift in substrate utilisation previously observed in DKI mice showing decreased levels of whole-body fat utilisation with a concomitant increase in carbohydrate oxidation [15,16], real-time ATP Rate Assays were performed with the Seahorse XFe24 using MEF cells obtained from WT and DKI mice. DKI MEF cells displayed significantly reduced rates of total ATP coming from both glycolysis (glycoATP, $P < 0.0001$, **Figure 6.9A**) and mitochondrial respiration (mitoATP, $P < 0.0001$, **Figure 6.9BA**) versus WT, therefore resulting in decreased total ATP production rate (**Figure 6.9C**). The relative contribution of glycolysis and oxidative phosphorylation (OXPHOS) to total ATP production was also assessed (**Figure 6.9D**) and indicated significantly decreased contribution of glycolysis (~5%; $P < 0.03$) to total ATP production compared to WT MEF cells.

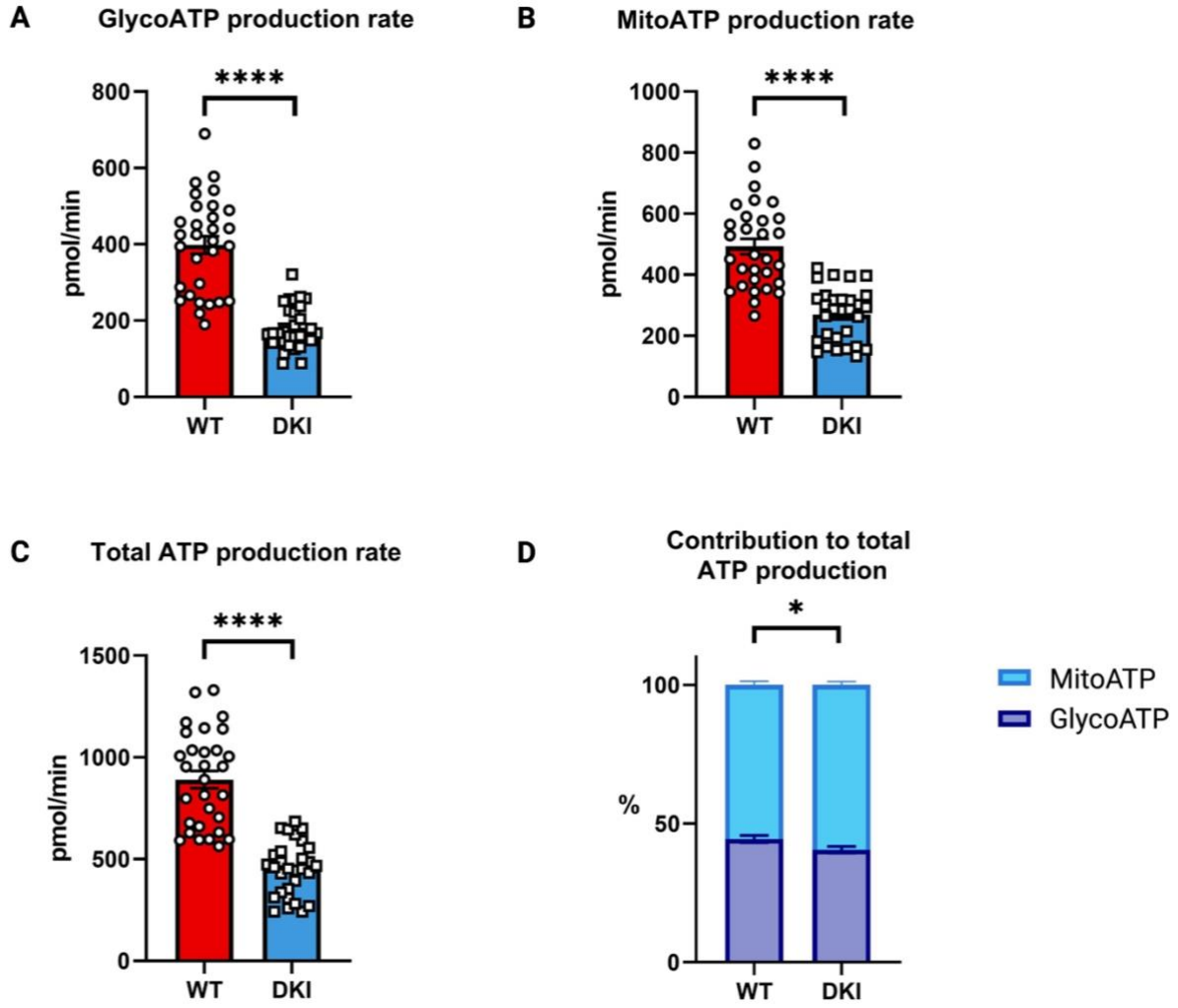

Figure 6.9 – Bioenergetic profile of WT and DKI mouse embryonic fibroblasts (MEF). **A)** GlycoATP is the energy produced from glycolysis through the measurement of the extracellular acidification rate (ECAR), expressed in picomoles (pmol) per min; **B)** MitoATP is the energy produced from oxidative phosphorylation (OXPHOS) and obtained by measuring oxygen consumption rate (OCR); **C)** Total ATP production rate is the sum of glycoATP and mitoATP; **D)** The observed relative contributions from glycolysis and OXPHOS to total ATP production are expressed as a percentage of total ATP production. *: $P < 0.05$, ****: $P < 0.0001$; values are represented as mean ± SEM; n = 30 cell measurements per group.

6.4.4. Mitochondrial Respiration in Permeabilised Red and White Gastrocnemius Muscle Fibres Are Not Different Between WT and DKI Mice

Given the changes in the bioenergetic profile in DKI MEF cells, I next examined whether DKI mice would display altered skeletal muscle mitochondrial respiratory function versus WT. There were no genotypic differences in maximal respiration when ADP was titrated in either red (**Figure 6.10A**) or white (**Figure 6.10D**) muscle, nor were there any differences in ADP sensitivity as assessed by the apparent K_m (**Figure 6.10B** and **E**), or overall

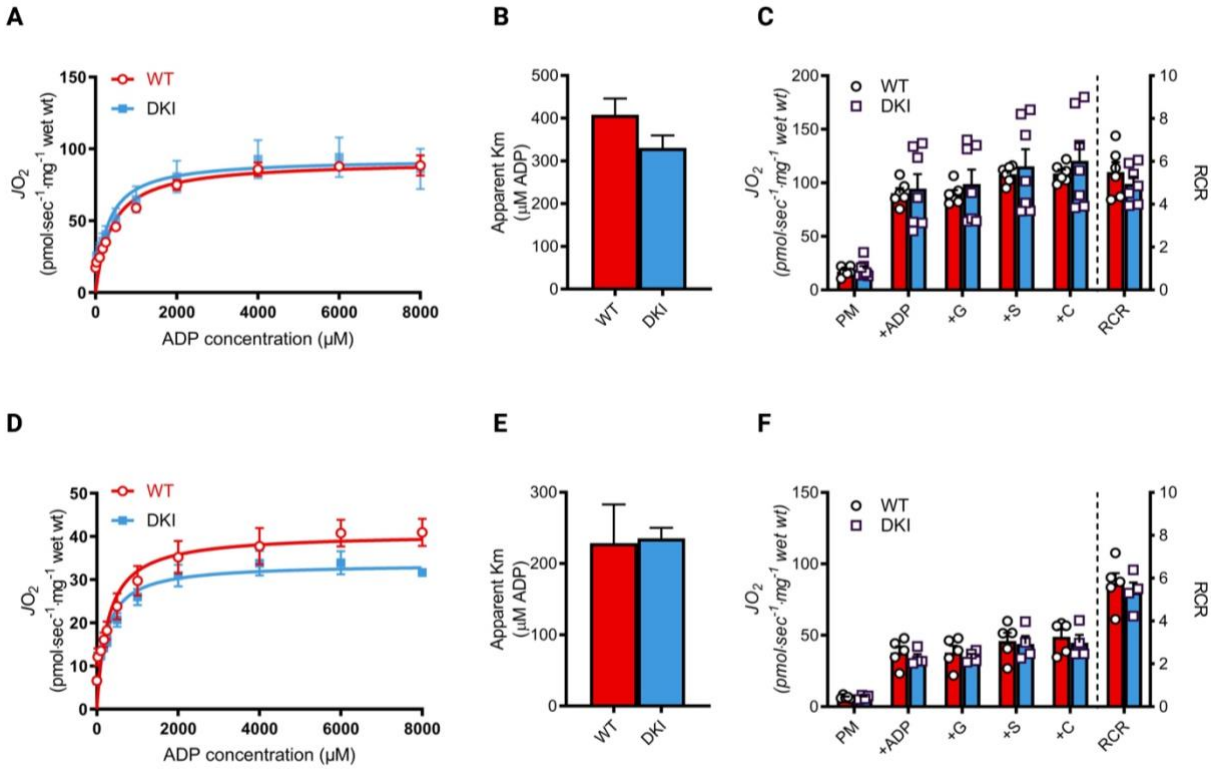

Figure 6.10 – Mitochondrial bioenergetics. **A** and **D)** ADP titration in the presence of pyruvate and malate in the respiration media. JO_2 indicates mitochondrial flux of oxygen. **B** and **E)** Apparent K_m as a reflexion of ADP sensitivity. **C** and **F)** Mitochondrial capacity of permeabilised gastrocnemius fibres. PM: pyruvate 10 mM + malate 2 mM without ADP (leak); +ADP: PM + 5 mM ADP; +G: state III maximal complex 1 linked, addition of 10 mM glutamate to the previous; + S: max complex 1 and 2 linked, addition of 10 mM succinate to the previous; +C: addition of 10 μM cytochrome *c* to assess mitochondrial membrane integrity. RCR: respiratory control ratio (coupling efficiency). Panels A, B and C represent red gastrocnemius muscle data while panels D, E and F represent white gastrocnemius muscle data. Values are expressed as means ± SEM. n = 5-7 permeabilised fibres per genotype and muscle type (i.e. red and white gastrocnemius).

mitochondrial flux (**Figure 6.10C** and **F**) when providing saturating substrates for complex I (pyruvate, malate, glutamate) or complex II (succinate).

6.5. Discussion

Research from my group over the past five years has highlighted the phenotypic consequences of disrupting AMPK-glycogen binding *in vivo*, using transgenic mouse models with whole-body AMPK β isoform-specific KI and DKI mutations [14-16]. The molecular mechanisms underlying the whole-body phenotypic differences with respect to exercise capacity and metabolic control (e.g., reduced maximal running speed, increased adiposity, greater reliance on carbohydrate utilisation and reduced fat oxidation) as a result of disrupting AMPK-glycogen interactions however remain unclear.

To address some of these knowledge gaps, LC-MS based untargeted metabolomics was first performed in plasma from WT and DKI male mice, at rest and following a single bout of treadmill running (30 min at 70% of individual maximal running speed) [307]. Exercise was associated with significantly distinct overall metabolite profiles versus rest. Furthermore, DKI plasma showed overall metabolite profile differences versus WT at rest, but not following exercise. From the 83 identified/annotated plasma metabolites, one metabolite cluster (including markers of fat mobilisation and cellular energy stress) contributed to the exercise-associated metabolite profile, while another cluster primarily containing amino acids and derivatives showed significant interaction between genotype (WT versus DKI) and condition (rest versus exercise), suggesting potential distinct patterns of the utilisation of amino acids and their derivatives [307]. This metabolomics study identified known and uncharacterised plasma metabolite responses to acute exercise, as well as potential molecular biomarkers underlying the phenotype associated with AMPK-glycogen binding disruption.

To expand the understanding of such molecular biomarkers, untargeted metabolomics was then performed in the primary glycogen-storing tissues, liver and skeletal muscle. In the present study, liver and gastrocnemius muscles were collected from the same mice utilised in the previous metabolomics analyses of plasma.

In liver, metabolomic analyses revealed significant mean differences in overall metabolite profiles between WT and DKI mice, and between rested and exercised conditions (**Figure 6.2**). Three metabolite clusters were associated with DKI mutation and/or exercise (**Figure 6.1B**).

Cluster B metabolites, including histamine and several carbohydrate species, showed increased mean abundance in DKI versus WT liver (P = 0.039) and were amongst the most potent drivers of overall metabolite profile genotypic differences (**Figure 6.4**). Histamine regulates numerous physiological and pathophysiological processes. While increased skeletal muscle histamine has been reported as a physiological response to exercise [309], increased hepatic levels of histamine have also been associated with the progression of pathophysiological conditions including liver disease [310]. Whether increased hepatic levels of histamine observed in DKI mice is associated with increased inflammation and impaired liver health remains uncertain, but it would be plausible given the close relationship between increased levels of adiposity and inflammation, including liver inflammation [311].

Cluster D metabolites including alanine, acetylcholine, serine and cystathionine were on average significantly decreased with exercise (P = 0.003) as shown in **Figure 6.1B**. Recent work from Olsen *et al.* (2020) in male cyclists have demonstrated increased circulating levels of glutathione – a downstream product of cystathionine and a major systemic antioxidant – in response to exhaustive exercise [312]. Decreased hepatic levels of cystathionine and its

component serine may therefore suggest enhanced hepatic production and release of glutathione into the bloodstream to combat exercise-induced oxidative stress [313-315].

Cluster E metabolites were significantly increased in association with exercise ($P = 1.13 \times 10^{-5}$) and significantly reduced abundance in DKI versus WT mouse liver ($P = 0.011$) as indicated in **Figure 6.1B**. Metabolites such as AMP and cortisol contributed to exercise-associated metabolite profile separation while metabolites including methylimidazoleacetic acid and creatine phosphate contributed to genotype metabolite profile separation (**Figures 6.3** and **6.4**). Increased AMP and steroid hormone cortisol levels likely indicate increased exercise-induced ATP-turnover [316]. As a catabolic hormone, cortisol stimulates mobilisation of energy stores by promoting lipolysis, gluconeogenesis and protein breakdown [286]. Although corticosterone is well established to be the main glucocorticoid hormone produced in rodents, cortisol can also be found in rodents at lower concentrations and can increase following exposure to various stress-inducing stimuli [317-319]. Methylimidazoleacetic acid is the main end-product of histamine catabolism [320]. Reduced methylimidazoleacetic acid levels in DKI liver may therefore suggest decreased levels of histamine catabolism, given the increased hepatic histamine observed in DKI versus WT liver. Creatine phosphate, also named phosphocreatine (PCr), is an essential component of mitochondrial function and the ATP-PCr system that serves as a source of phosphate for ATP resynthesis that can be rapidly mobilised during high ATP turnover (e.g. during short and intense/explosive exercise) and acts as a cellular energy buffer [321]. Of relevance, recent metabolomic analyses from Maqdasy *et al.* discovered that excess adiposity/obesity was associated with perturbations in phosphocreatine/creatine ratio in white adipose tissue samples from individuals with obesity [322]. Increased phosphocreatine/creatine ratio associated with obesity reportedly resulted in changes in the ATP/ADP ratio and attenuated AMPK activity [322]. In the present study, while no changes in hepatic creatine were observed, the significant contribution of PCr to genotype

differences (CV2) indicating decreased abundance versus WT suggests a potential hepatic decrease in the DKI phosphocreatine/creatine ratio. This observation contrasts the findings from Maqdasy and colleagues [322], therefore warranting further investigations of phosphocreatine/creatine metabolism.

In gastrocnemius muscle, significant mean differences in overall metabolite profiles were also observed between rested and exercised conditions, and between genotypes at rest, but not following exercise (**Figure 6.6**). Strikingly, these overall metabolite profile differences in gastrocnemius muscle display similar patterns to those observed in my plasma metabolomic study demonstrating an interaction between condition and genotype and convergence of DKI and WT overall metabolite profiles following acute exercise [307]. Similar to observations in the liver, three metabolite clusters were associated with DKI mutation and/or exercise.

Cluster B mean metabolite abundance was increased in DKI versus WT ($P < 0.01$, **Figure 6.5B**) with glutathione and creatine as the main drivers of genotype differences (**Figures 6.7 and 6.8**). Increased intramuscular glutathione in DKI relative to WT mice may potentially indicate an adaptive response to increased oxidative stress. In contrast to observations of creatine and PCr in the liver, no changes in intramuscular PCr levels were observed across conditions and genotypes, whereas increased abundance in muscle creatine contributed to genotype overall profile differences, demonstrating changes in phosphocreatine/creatine ratio that are in line with Maqdasy *et al.* findings [322].

Cluster G displayed a significant interaction effect between genotype and condition ($P = 0.046$) with opposite mean metabolite abundance changes following exercise in DKI versus WT gastrocnemius muscle (**Figure 6.5B**). Glycerol-3-phosphate was the predominant endogenous metabolite driving DKI versus WT overall metabolite profiles within Cluster G. These metabolites were on average decreased following acute exercise in WT gastrocnemius

muscle but increased in DKI muscle. Glycerol-3-phosphate is an intermediate metabolite at the intersection of several energy metabolism pathways including glycolysis, gluconeogenesis, and glycerolipid (e.g., TG) and FA utilisation, as well as energy metabolism via the electron transport chain, recently reviewed elsewhere [323]. Given the numerous metabolic pathways involving glycerol-3-phosphate, measuring additional sets of metabolites related to these metabolic pathways in future studies would help reveal the potential reasons for this metabolite's observed interaction between genotypes and conditions.

Finally, Cluster H metabolite mean abundance was significantly increased in association with exercise ($P = 3.58 \times 10^{-4}$) with no genotype differences (**Figure 6.5B**). From the 18 metabolites within cluster H, 14 significantly contributed to exercise-associated differences in overall metabolite profiles and supported univariate analyses (**Figures 6.5A** and **6.7**). Cluster H included long-, medium- and short-chain acylcarnitines, amino acids, as well as several metabolites of purine metabolism such as adenosine, inosine monophosphate (IMP), inosine, xanthine and hypoxanthine. Exercise-induced increase in purine metabolism is a well-established response to energy stress and biomarker of increased ATP turnover supported by previous findings from Zhang and colleagues (2019) who demonstrated increased purine metabolites, as well as amino acids and TCA cycle intermediates in interstitial fluids of rat skeletal muscle following a single bout of exercise [121]. Likewise, increased intramuscular levels of fatty acylcarnitines in response to exercise is well documented and has been reviewed recently [283]. In line with recent metabolomic findings in plasma [283], the present skeletal muscle fatty acylcarnitine profile does not suggest differences in fat utilisation in DKI versus WT mice in response to acute submaximal exercise, as previously reported at the whole-body level by Janzen *et al*. [15,16]. However, a more targeted analysis and/or identification of more breadth of metabolites underlying substrate utilisation may help establish potential differences underlying potential whole-body changes in fat oxidation between genotypes.

These skeletal muscle and liver metabolomic results extend previous plasma metabolome findings and provide additional insight into the metabolic networks responsive to exercise and disrupting AMPK-glycogen interactions *in vivo*. Real-time ATP Rate Assays in MEF cells and measurements of mitochondrial bioenergetics from permeabilised white and red gastrocnemius muscle fibres were performed to gain understanding of potential cell- and tissue-specific mechanisms underlying the DKI phenotype observed at the whole-body level [15,16]. No changes in gastrocnemius mitochondrial bioenergetics (ADP sensitivity, mitochondrial capacity, coupling efficiency) were found between WT and DKI mice (**Figure 6.10**). These findings complement previous measures of skeletal muscle mitochondrial content in DKI and WT which indicated no differences between genotypes [16]. In contrast, it appears that AMPK DKI mutation even in MEF cells is associated with perturbations in energy metabolism, as observed by significantly decreased total, glycolytic and mitochondrial ATP production rates relative to WT MEF cells (**Figure 6.9A-C**). Furthermore, a small but significant shift in the relative contribution to total ATP production was found, with DKI mice showing increased relative contribution of mitochondrial respiration to total ATP production (**Figure 6.9D**). However, whether these genotype differences are also observed in other cell types and tissues and throughout the lifespan of mice with intact versus chronically disrupted AMPK-glycogen interactions remains unknown and warrants further investigations.

Some limitations associated with this study need to be acknowledged. Despite numerous advantages, untargeted metabolomics still faces some hurdles that have been described in the previous plasma metabolomic analysis [307] and reviewed elsewhere [283]. Briefly, the metabolites reported in the present study were limited to the metabolite references available through in-house metabolite library and external databases, therefore limiting the scope of some biological interpretations. This study used a sample size based on power to detect differences in maximal running speed between genotypes and may therefore be

insufficient to detect subtle effects in some specific metabolic pathways. Furthermore, muscle samples were collected from mice in the fed state. Therefore, the timing of each mouse's last food intake may have been different, potentially contributing to increased variance in metabolite levels observed between mice. To ensure sufficient blood volume collection for plasma metabolomic analyses in my previous study, CO_2 exposure prior to euthanasia was utilised and may have potentially impacted plasma pH and metabolite concentrations, in both plasma and tissues. However, all mice were subjected to the same duration of CO_2 exposure, therefore minimising likelihood of between-group differences. With respect to cell bioenergetics, the ATP Rate Assay results provide some complementary insight to previous whole-body and tissue findings by determining the relative contribution of glycolysis and mitochondrial respiration to total ATP production and revealed genotype differences in MEFs. However, it is unknown whether these changes are consistent over time and in different cell types. The relative contribution of carbohydrate and fat oxidation to total mitochondrial respiration also cannot be determined using the Seahorse XFe24 Real-Time ATP Rate Assay. The media used in this assay contains no fatty acids and the contribution of MEF intracellular fat oxidation to ATP production remains unknown. Comparing the lipid profiles of DKI and WT MEFs in future experiments will provide more insights into potential underlying genotypic differences in lipid content and fatty acid oxidation capacity.

6.6. Conclusion

This study extends previous plasma metabolomic findings showing WT mouse plasma responses to acute exercise and how disrupting AMPK-glycogen binding alters the plasma metabolome. In the present study, a total of 92 and 150 metabolites were identified/annotated in gastrocnemius muscle and liver, respectively, using untargeted MS-based metabolomics.

Similar to the plasma metabolite responses across genotypes and conditions, metabolomic analyses indicated significant overall metabolite profile shifts between WT and DKI mice at rest and significant differences between rested and exercised conditions. In contrast to liver, an interaction effect was observed in skeletal muscle, suggesting differential muscle metabolite responses to acute exercise between genotypes. Tissue metabolomics has helped expand knowledge of the metabolites associated with exercise and with the disruption of AMPK-glycogen binding, revealing potential novel molecular biomarkers that may contribute to exercise's metabolic health benefits and the physiological effects of disrupting AMPK-glycogen binding *in vivo*. Complementary bioenergetic analyses in cells and permeabilised fibres further characterised the mouse DKI phenotype and has revealed potential future directions to further pinpoint possible mechanisms underlying the phenotypic effects on metabolic control and exercise capacity.

Chapter 7 – General Discussion and Concluding Remarks

7.1. Introduction

The discovery of AMPK's β subunit isoforms' ability to bind glycogen via the CBM was first shown *in vitro* in 2003 in independent studies by Hudson *et al.* and Polekhina *et al.* [6,7]. Given the limited physiological insights that can be provided by these *in vitro* models, subsequent *in vivo* experiments used whole-body AMPK β2 KO mice to start addressing these knowledge gaps and highlighting the physiological consequences of deleting the AMPK β subunit in these mice [8,11]. AMPK β2 KO mice displayed reduced endurance capacity and maximal running speed relative to WT mice [8,11]. Similarly, O'Neill *et al.* (2011) demonstrated decreased maximal running speed in muscle-specific β1β2 double KO mice compared to control WT mice. These muscle-specific double KO mice also displayed reduced RER, indicating a shift in substrate utilisation (i.e., greater reliance on fat oxidation relative to carbohydrate oxidation) underlying energy production [10]. Several limitations to these AMPK KO mouse models however remained, as described in chapter 2, and AMPK β subunit KI models were then generated to overcome some of the challenges associated with KO models and more specifically investigate the interactive roles of AMPK and glycogen *in vivo*.

Recent work from my group using AMPK β1 or β2 single KI mice with disrupted AMPK-glycogen binding in either β isoform showed phenotypic effects of disrupting AMPK's glycogen binding capacity *in vivo* [14]. These β1 W100A KI and β2 W98A KI displayed whole-body, tissue and/or cellular metabolic perturbations and impaired maximal running capacity in β2 W98A KI mice relative to WT mice. Although certain tissues predominantly express either the β1 (e.g. mouse liver) or β2 (e.g. mouse skeletal muscle) isoform, both AMPK β1 and β2 isoforms are detectable in the majority of mouse tissues including liver and skeletal muscle [12], and compensatory upregulation in expression of the non-mutated isoform can potentially

complicate interpretation of data from such models. Therefore, my group generated mice with KI mutations in both isoforms (AMPK β1 W100A/β2 W98A DKI) to investigate more specifically the phenotypic consequences of chronically disrupting whole-body AMPK-glycogen interactions. Early findings from this DKI mouse model demonstrated impairments in whole-body metabolism and changes in patterns of substrate utilisation such as reduced rates of fat oxidation, which was associated with increased total body and fat mass and altered tissue glycogen dynamics. Furthermore, these metabolic effects translated to reduced maximal exercise capacity in DKI relative to WT mice [15,16]. However, the molecular metabolic pathways underlying these phenotypic effects in DKI mice and how disrupting AMPK-glycogen interactions affects metabolic control and metabolic responses to exercise remain poorly understood. Additionally, little research to date has been conducted to map the breadth of metabolites associated with acute treadmill exercise in mouse tissues and the bloodstream.

Using an untargeted metabolomic approach across mouse plasma, liver and gastrocnemius skeletal muscle, the overall aim of this thesis was to capture snapshots of metabolic pathways responsive to acute exercise and whole-body disruption of AMPK-glycogen binding *in vivo*, and to determine whether disrupting AMPK-glycogen interactions affect responses to acute exercise. The research projects included in this thesis first confirmed the DKI phenotype previously demonstrated by my group, including increased total body mass and adiposity and impaired maximal running speed in DKI versus WT mice. Plasma, liver and gastrocnemius muscle metabolomic analysis revealed both known and novel metabolites associated with acute exercise. Furthermore, a distinct DKI overall metabolite profile phenotype was observed across all three biological specimens in the rested state, also revealing differential responses to acute exercise in plasma and skeletal muscle between WT and DKI mice. While additional bioenergetic measures in white and red skeletal muscle fibres showed no changes in mitochondrial characteristics between genotypes, significant perturbations in

energy metabolism and underlying metabolic pathways were discovered through metabolomic approaches and analysis of DKI versus WT MEF cells.

7.2. Effects of AMPK-Glycogen Binding Disruption on Body Mass, Adiposity and Exercise Capacity

7.2.1. AMPK DKI Mice Have Increased Body Mass and Adiposity

Some of the most well characterised roles of AMPK in energy homeostasis and pathways involved in substrate utilisation have been described in Chapter 2 and recently reviewed in detail [5,209]. While a growing body of evidence has established a negative correlation between AMPK activity and increased adiposity/obesity [19,20,324], less is known about the physiological importance of AMPK-glycogen interactions for whole-body, tissue and cellular energy homeostasis. Of note was that, while DKI mice showed some phenotypic aspects similar to β2 single KI mice, such as increased adiposity and impaired exercise capacity, they more closely reflected β1 single KI phenotype in terms of substrate utilisation patterns [14]. These findings suggest potential differences between β1 and β2, potentially indicating a role of the β1 isoform and glycogen interactions in energy substrate selection.

Although increased adiposity possibly resulted from increased food intake/hyperphagia in DKI versus WT mice, as demonstrated by Janzen *et al.* [15], the precise cause(s) for this observation remains unknown. The hypothesis that increased food intake in DKI mice was related to dysregulation of appetite/satiety hormones was partially explored by quantifying circulating leptin levels. Leptin is an anorexigenic hormone which exerts a critical role in body mass maintenance by stimulating satiety, suppressing appetite and reducing food intake [325]. Leptin resistance leads to increased circulating leptin concentrations and has been linked to the development of obesity [326]. However, no genotype differences in circulating leptin levels

were observed in DKI mice [15]. Whether other endocrine hormones regulating the orexigenic-anorexigenic axis are altered by DKI mutation has not been investigated and warrants further research to determine the potential links between increased total body and/or fat mass and increased food intake in these mutant mice.

7.2.2. AMPK DKI Mice Have Impaired Maximal Running Speed

Exercise is characterised by increased cellular and tissue energy demands. Lipids are the primary fuel source for skeletal muscle and other insulin-sensitive tissues, at rest and during low intensity exercise (< 50–60% VO_2 max). Rates of FA oxidation continue to increase with exercise intensity until maximal rates of oxidation are reached (~70-75% VO_2 max). Beyond that exercise intensity, FA oxidation decreases, and carbohydrate-based fuels become the predominant energy source for contracting muscles [30,284]. Although substrate utilisation was not directly assessed as part of this thesis, it is plausible that impaired maximal running speed in DKI mice may have resulted from increased carbohydrate utilisation and increased glycogen depletion in skeletal muscle, as previously observed in DKI mice following an incremental maximal running bout [16]. Hence, it is possible that preferred utilisation of carbohydrate as an energy source may lead to early depletion of skeletal muscle glycogen stores and premature fatigue in the incremental running speed test in DKI mice. Furthermore, DKI mutation in this previous study was linked to diminished skeletal muscle levels of AMPK α and β2 content, both known to be associated with exercise capacity in mice [10,11,327], regardless of relative levels of downstream AMPK signalling [16]. Of note, data in the metabolomics and mitochondrial experiments in this thesis were only collected using gastrocnemius muscle, and it is possible that DKI mutation may have had different effects in other muscles and/or fibre types, and different tissues such as adipose tissue. Impaired fat oxidation in adipose tissue may also potentially result in increased carbohydrate utilisation and reflect the observed changes in DKI versus WT whole-body substrate utilisation.

Another possible explanation for genotype differences in substrate utilisation and reduced maximal running speed during an incremental test [15,16,307] is the possibility of a genotype-related switch in muscle fibre types. White/fast-twitch muscle fibres (type II) are characterised by low mitochondrial content, high glycolytic capacities and high fatigability. In contrast, red/slow-twitch muscle fibres (type I) have relatively high resistance to fatigue, high mitochondrial content, and hence high oxidative capacities [328]. As such, an increased proportion of type II fibres in DKI may help explain increased whole-body reliance on carbohydrate utilisation given the lower mitochondrial content of white muscle fibres. Therefore, increased proportion of more rapidly fatigable white muscle fibres in DKI mice may cause the premature exhaustion observed in DKI versus WT mice during an incremental maximal running test [16,307]. Assessing potential differences in muscle fibre type between DKI and WT mice is warranted in future studies to help elucidate the biological mechanisms underlying these phenotypic differences.

Exercise capacity in DKI and WT mice in this thesis was only determined via maximal running speed tests, and additional running time to exhaustion tests were performed in Janzen *et al.* (2022) [16]. Complementary measures of muscle function in future research will help uncover additional mechanisms underlying potential differences in muscle function and gait (e.g., hanging wire tests, rotarod challenge, gait analysis) between WT and DKI mice.

7.3. Plasma, Liver and Skeletal Muscle Metabolite Responses to Acute Exercise and Effects of AMPK-Glycogen Binding Disruption

In this thesis, the use of LC-MS-based untargeted metabolomics allowed the detection, identification or annotation of a total of 325 metabolites across blood plasma (83 metabolites), liver (150 metabolites) and gastrocnemius muscle (92 metabolites), representing coverage

across a wide array of metabolic pathways. Among these datasets, both known and previously unreported exercise-associated metabolites (e.g., GP-NPEA and N-acetyltryptophan) were revealed. While univariate analyses identified 17, 29 and 16 metabolites significantly associated with exercise, respectively, two metabolites (one plasma and one gastrocnemius muscle metabolite) were significantly different between genotypes based on univariate analyses. Collectively, the relatively large differences in overall metabolite profile responses between rest and acute exercise compared to WT and DKI genotypes suggests that exercise elicits a greater perturbation to overall metabolism compared to DKI mutation. Exercise is well-known to represent a major challenge to whole-body metabolic homeostasis and induce a wide range of responses in cells to cope with the associated cellular perturbations in energy homeostasis in tissues such as skeletal muscle and liver [1].

Multivariate analyses allow for a deeper understanding of metabolite response patterns in high-dimension datasets such as omics datasets, notably by estimating correlated covariance between multiple metabolites [277]. In the present thesis, multivariate analyses revealed significant differences in overall metabolite profiles between rest and acute exercise in plasma, liver and gastrocnemius muscle. The multivariate analyses also indicated greater condition-associated separations of overall metabolites profiles compared to genotype-associated separations in all three biological specimens, thus supporting the univariate analyses showing more metabolites significantly associated with exercise than with DKI mutation. Furthermore, plasma and gastrocnemius muscle overall metabolite profiles demonstrated similar patterns. While genotype differences were observed at rest in both of these samples, they were no longer observed following exercise as the overall metabolite profiles converged, hence indicating an interaction between genotype and condition. In contrast, liver overall metabolite profiles only displayed main effects of genotype and condition, but no significant interactions. Collectively,

this suggests that exercise-associated changes in plasma metabolites more closely reflect metabolite changes occurring within gastrocnemius muscle.

7.3.1. Plasma Metabolome

In plasma, exercise was linked to increased abundance of lipid species, fatty acylcarnitines and steroid hormones, which represent commonly reported biomarkers of energy stress and fat mobilisation in response to the demands of an acute exercise challenge [283,284,286]. From the present plasma data, lipid species do not appear to be differently altered between genotypes but a more detailed profile of plasma lipid species is required to fully answer this question. For example, Contrepois *et al*. recently demonstrated, using lipidomic analyses, complex and dynamic changes in lipid species following exercise, depending on carbon chain length and number of unsaturated bonds [47]. Exercise was also associated with reduced plasma levels of several amino acids and their derivatives, which is typically observed when the availability of preferred carbohydrate and lipid-based fuel sources decreases [83,84]. Interestingly, plasma amino acids displayed a significant interaction between genotype and exercise, indicating a greater decrease following exercise compared to WT, possibly suggesting an increased amino acid uptake or oxidation. However, this is probably not due to reduced substrate availability, since this was not observed by Janzen *et al.* in DKI mice subjected to a submaximal exercise bout similar to the exercise bouts used in this thesis [16]. The precise reasons for the greater decrease in plasma amino acids in DKI mice therefore remain unclear. In addition, interpretation of changes in amino acids in a given sample can prove difficult given the multiple metabolic pathways amino acids are involved in, including protein synthesis, TCA cycle, keto- and gluconeogenesis, for example [283].

7.3.2. Liver Metabolome

In liver, while univariate analyses did not detect any metabolite differences between genotypes, multivariate analyses did identify different trajectories of metabolite clusters with discriminant mean abundances between genotypes. One of the most robust contributors to increased liver metabolite abundance in DKI versus WT liver was histamine, which is implicated in several physiological and pathophysiological processes. Increased abundance of hepatic histamine may suggest a pro-inflammatory state in DKI liver, which can be observed with increased adiposity [311]. Of note, the metabolite cluster with reduced abundance in DKI versus WT liver contained methylimidazoleacetic acid, the main end-product of histamine catabolism [320]. Increased histamine and reduced methylimidazoleacetic acid levels in liver may indicate a decreased histamine catabolism. More detailed analyses of this metabolic pathway and associated physiological measures are required to characterise histamine metabolism and whether the present findings are associated with perturbations in hepatic function and metabolic health in DKI mice.

Multivariate analyses also identified metabolite clusters with exercise-associated differences compared to the rested state in liver metabolite profiles, including reduced abundance of metabolites such as cystathionine and several amino acids including serine, while clusters with increased mean abundance following exercise were also observed and included metabolites such as AMP and cortisol. Given the role of cystathionine and serine in the production of glutathione, an important systemic antioxidant, their reduced abundance following exercise may indicate increased conversion to glutathione to combat exercise-induced oxidative stress [313-315]. Conversely, the identified metabolite cluster with an exercise-associated increase in abundance included AMP and cortisol, likely indicating increased exercise-induced ATP-turnover and energy stress [316], as observed in plasma which also displayed increased steroid hormones such as corticosterone following exercise [307].

7.3.3. Gastrocnemius Muscle Metabolome

Similar to the observed exercise responses in plasma, univariate analyses of the gastrocnemius metabolome demonstrated significant increases in lipid species, reflecting potential fat mobilisation/uptake/oxidation within muscle [283]. Similar to plasma, the identified muscle lipid species did not suggest any differences in fat utilisation between DKI and WT mice. However, a more detailed lipid profile analysis is required to verify whether other lipid species not detected within these datasets show potential differences or not between conditions and/or genotypes. In addition, increased purines such as AMP, IMP, inosine, xanthine and hypoxanthine also reflected increased energy turnover with exercise [121]. These responses were similar in both WT and DKI mice. Multivariate analyses supported these findings and identified potential other metabolic pathways influenced by exercise and/or genotype. Several amino acids and derivatives, including glutathione, showed increased mean abundance in DKI relative WT gastrocnemius muscle which, again, potentially indicates an adaptative response to changes in redox status/oxidative stress [312]. Finally, multivariate analyses revealed a significant interaction effect between genotype and condition with opposite mean metabolite abundance changes following exercise in DKI (increase) versus WT (decrease). One of these metabolites differently changed with exercise depending on genotype was glycerol-3-phosphate, an intermediate metabolite implicated in several energy metabolism pathways including carbohydrate and lipid metabolism [323]. Given the numerous metabolic pathways involving glycerol-3-phosphate, measuring additional metabolites related to these metabolic pathways will be needed to pinpoint the potential reasons for this interaction observed between genotypes and conditions.

7.3.4. Limitations and Future Directions

These metabolomic data provide novel insight into the metabolic networks associated with acute exercise and DKI mutation in plasma and the main glycogen-storing tissues liver and skeletal muscle, leading to hypothesis generation and future avenues for follow-up research projects. It is however important to bear in mind that these interpretations are limited to a subset of metabolites that were capable of being detected with sufficient accuracy and that could be identified or annotated with confidence, following the guidelines proposed by the Metabolomics Standard Initiative [71]. With no less than 200,000 endogenous metabolites identifiable according to the Human Metabolome database (https://hmdb.ca/statistics), a higher number of metabolites would be expected to be responsive to exercise and DKI mutation, potentially revealing additional metabolites and molecular biomarkers associated with the DKI versus WT mouse phenotypes observed in this thesis.

Another limitation related to untargeted metabolomics in this study is that limited interpretation of metabolite changes is possible when additional metabolites belonging to the related metabolic pathways are not also included in the dataset. For instance, metabolites such as amino acids are involved in numerous metabolic pathways, making the interpretation of their relative abundances difficult. Furthermore, the unbiased nature of data acquisition in untargeted metabolomic approaches did not allow the detection and identification/annotation of sufficient metabolites belonging to the lipid and carbohydrate pathways to confirm impaired levels of fat oxidation and/or increased reliance on carbohydrate oxidation in response to a submaximal treadmill running bout. Recent technological advances now permit targeted metabolomics/lipidomic assays to yield > 1000 lipid metabolites [39]. Future work to identify and quantify a wider coverage of amino acids and derivatives is necessary for greater in-depth coverage and improved understanding of their potential roles in exercise and AMPK-glycogen binding disruption. Performing targeted metabolomics of amino acid, glucose and lipid

metabolites involved in the main pathways of energy production or utilising more dynamic analytical methods such as metabolic flux analyses would help gain a more comprehensive understanding of the changing pathways and metabolites within the present metabolomics datasets.

7.4. Effects of AMPK-Glycogen Binding Disruption on Mitochondrial Capacity and Substrate Utilisation in MEF Cells

7.4.1. Mitochondrial Capacity Is Not Different Between WT and DKI MEF Cells

Findings from Janzen *et al*. (2022) revealed that DKI mice with disrupted AMPK-glycogen binding capacity had reduced whole-body rates of fat oxidation and increased rates of carbohydrate oxidation [15,16]. While the untargeted metabolomic results in this thesis do not suggest specific differences in fat or carbohydrate utilisation between DKI and WT mice, only a small subset of lipid and carbohydrate species were identified and annotated, providing limited information regarding the utilisation of these two major fuel sources. It was therefore hypothesised that shifts in fuel utilisation were the result of impaired skeletal muscle mitochondrial capacity, since previous findings from DKI mice had suggested no changes in mitochondrial protein content versus WT [16]. Neither red nor white gastrocnemius fibres displayed changes in mitochondrial capacity. Therefore, it is possible that increased carbohydrate utilisation and decreased fat oxidation levels observed at the whole-body level may reflect an increased proportion of white glycolytic fibres and a decreased proportion of red oxidative fibres within muscles such as gastrocnemius and/or quadriceps. Analyses assessing skeletal muscle composition of these fibre types in future projects will help test this hypothesis.

7.4.2. MEF Cells with DKI Mutation Have Increased Relative Contribution of Mitochondrial Respiration to Total ATP Production

To assess whether shifts in substrate utilisation was also observed in other cell types and determine the contribution of glycolysis and mitochondrial respiration to total ATP production, WT and DKI MEF cells were analysed using the Seahorse XFe24 Real-Time ATP Rate Assay. In contrast to the *in vivo* findings from the gastrocnemius muscle from adult mice, DKI MEF cells displayed a small but significant decrease in the contribution of glycolysis to total ATP production rate. In addition, total ATP production rate was significantly reduced in DKI versus WT MEF cells, but the explanation for such observation remains unclear. While MEF cells are considered as a powerful system to study gene function and mutations such as DKI in mice, fibroblasts are heterogeneous cells with diverse activities [329]. Whether changes in MEF cells as a result of DKI mutation can predict/reflect changes in cell types such as hepatocytes or skeletal muscle cells in adult mice is unknown. The Seahorse XFe24 Analyzer is however compatible with many cell types and tissues and potential future experiments using the Seahorse XFe24 Analyzer to analyse primary hepatocytes and/or liver and skeletal muscle tissue sections could help provide more accurate characterisation of tissue-specific changes in metabolic pathways.

7.5. Conclusion

Throughout this thesis, the analyses performed have addressed important knowledge gaps with respect to the metabolite responses to acute exercise and disrupting AMPK-glycogen binding *in vivo*. The results from the experiments conducted for this thesis confirmed the DKI mouse phenotype, including increased total body mass and adiposity, as well as reduced maximal running speed. Second, the use of untargeted metabolomics from WT and DKI mouse

plasma, liver and gastrocnemius muscle collected at rest and following a single bout of submaximal treadmill exercise identified and annotated a total of 325 metabolites and included a large diversity of metabolite species spread across a wide array of metabolic pathways. These metabolomic analyses revealed differences in metabolite profiles associated with acute exercise and/or AMPK-glycogen binding disruption and reported known and novel metabolites to add to the growing body of literature regarding the molecular metabolic responses to exercise. Differential metabolite responses to exercise depending on mouse genotype were also revealed, including potential differences in amino acid metabolism and other pathways underlying substrate utilisation and energy metabolism. Complementary bioenergetic measures in permeabilised gastrocnemius muscle fibres showed no changes in mitochondrial characteristics between genotypes but demonstrated perturbations in energy metabolism patterns in MEFs from DKI mice. The metabolomics datasets generated in this thesis have also identified potential directions for future research to keep advancing the field of exercise metabolism and improving the understanding of the importance of AMPK's interactive roles in exercise and metabolic health.

References

1. Hawley, J.A.; Hargreaves, M.; Joyner, M.J.; Zierath, J.R. Integrative biology of exercise. *Cell* **2014**, *159*, 738-749, doi:10.1016/j.cell.2014.10.029.
2. Tipton, C.M. The history of "Exercise Is Medicine" in ancient civilizations. *Adv Physiol Educ* **2014**, *38*, 109-117, doi:10.1152/advan.00136.2013.
3. Strasser, B. Physical activity in obesity and metabolic syndrome. *Ann N Y Acad Sci* **2013**, *1281*, 141-159, doi:10.1111/j.1749-6632.2012.06785.x.
4. Okunogbe, A.; Nugent, R.; Spencer, G.; Ralston, J.; Wilding, J. Economic impacts of overweight and obesity: current and future estimates for eight countries. *BMJ Glob Health* **2021**, *6*, doi:10.1136/bmjgh-2021-006351.
5. Trefts, E.; Shaw, R.J. AMPK: restoring metabolic homeostasis over space and time. *Mol Cell* **2021**, *81*, 3677-3690, doi:10.1016/j.molcel.2021.08.015.
6. Hudson, E.R.; Pan, D.A.; James, J.; Lucocq, J.M.; Hawley, S.A.; Green, K.A.; Baba, O.; Terashima, T.; Hardie, D.G. A novel domain in AMP-activated protein kinase causes glycogen storage bodies similar to those seen in hereditary cardiac arrhythmias. *Curr Biol* **2003**, *13*, 861-866, doi:10.1016/s0960-9822(03)00249-5.
7. Polekhina, G.; Gupta, A.; Michell, B.J.; van Denderen, B.; Murthy, S.; Feil, S.C.; Jennings, I.G.; Campbell, D.J.; Witters, L.A.; Parker, M.W.; et al. AMPK beta subunit targets metabolic stress sensing to glycogen. *Curr Biol* **2003**, *13*, 867-871, doi:10.1016/s0960-9822(03)00292-6.
8. Dasgupta, B.; Ju, J.S.; Sasaki, Y.; Liu, X.; Jung, S.R.; Higashida, K.; Lindquist, D.; Milbrandt, J. The AMPK beta2 subunit is required for energy homeostasis during metabolic stress. *Mol Cell Biol* **2012**, *32*, 2837-2848, doi:10.1128/MCB.05853-11.
9. Dzamko, N.; van Denderen, B.J.; Hevener, A.L.; Jorgensen, S.B.; Honeyman, J.; Galic, S.; Chen, Z.P.; Watt, M.J.; Campbell, D.J.; Steinberg, G.R.; et al. AMPK beta1 deletion reduces appetite, preventing obesity and hepatic insulin resistance. *J Biol Chem* **2010**, *285*, 115-122, doi:10.1074/jbc.M109.056762.
10. O'Neill, H.M.; Maarbjerg, S.J.; Crane, J.D.; Jeppesen, J.; Jorgensen, S.B.; Schertzer, J.D.; Shyroka, O.; Kiens, B.; van Denderen, B.J.; Tarnopolsky, M.A.; et al. AMP-activated protein kinase (AMPK) beta1beta2 muscle null mice reveal an essential role for AMPK in maintaining mitochondrial content and glucose uptake during exercise. *Proc Natl Acad Sci U S A* **2011**, *108*, 16092-16097, doi:10.1073/pnas.1105062108.

11. Steinberg, G.R.; O'Neill, H.M.; Dzamko, N.L.; Galic, S.; Naim, T.; Koopman, R.; Jorgensen, S.B.; Honeyman, J.; Hewitt, K.; Chen, Z.P.; et al. Whole body deletion of AMP-activated protein kinase {beta}2 reduces muscle AMPK activity and exercise capacity. *J Biol Chem* **2010**, *285*, 37198-37209, doi:10.1074/jbc.M110.102434.
12. Janzen, N.R.; Whitfield, J.; Hoffman, N.J. Interactive Roles for AMPK and Glycogen from Cellular Energy Sensing to Exercise Metabolism. *Int J Mol Sci* **2018**, *19*, doi:10.3390/ijms19113344.
13. McBride, A.; Ghilagaber, S.; Nikolaev, A.; Hardie, D.G. The glycogen-binding domain on the AMPK beta subunit allows the kinase to act as a glycogen sensor. *Cell Metab* **2009**, *9*, 23-34, doi:10.1016/j.cmet.2008.11.008.
14. Hoffman, N.J.; Whitfield, J.; Janzen, N.R.; Belhaj, M.R.; Galic, S.; Murray-Segal, L.; Smiles, W.J.; Ling, N.X.Y.; Dite, T.A.; Scott, J.W.; et al. Genetic loss of AMPK-glycogen binding destabilises AMPK and disrupts metabolism. *Mol Metab* **2020**, *41*, 101048, doi:10.1016/j.molmet.2020.101048.
15. Janzen, N.R.; Whitfield, J.; Murray-Segal, L.; Kemp, B.E.; Hawley, J.A.; Hoffman, N.J. Mice with Whole-Body Disruption of AMPK-Glycogen Binding Have Increased Adiposity, Reduced Fat Oxidation and Altered Tissue Glycogen Dynamics. *Int J Mol Sci* **2021**, *22*, doi:10.3390/ijms22179616.
16. Janzen, N.R.; Whitfield, J.; Murray-Segal, L.; Kemp, B.E.; Hawley, J.A.; Hoffman, N.J. Disrupting AMPK-Glycogen Binding in Mice Increases Carbohydrate Utilization and Reduces Exercise Capacity. *Frontiers in Physiology* **2022**, *13*, doi:10.3389/fphys.2022.859246.
17. Hardie, D.G.; Lin, S.C. AMP-activated protein kinase - not just an energy sensor. *F1000Res* **2017**, *6*, 1724, doi:10.12688/f1000research.11960.1.
18. Steinberg, G.R.; Kemp, B.E. AMPK in Health and Disease. *Physiol Rev* **2009**, *89*, 1025-1078, doi:10.1152/physrev.00011.2008.
19. Jeon, S.M. Regulation and function of AMPK in physiology and diseases. *Exp Mol Med* **2016**, *48*, e245, doi:10.1038/emm.2016.81.
20. Sriwijitkamol, A.; Coletta, D.K.; Wajcberg, E.; Balbontin, G.B.; Reyna, S.M.; Barrientes, J.; Eagan, P.A.; Jenkinson, C.P.; Cersosimo, E.; DeFronzo, R.A.; et al. Effect of acute exercise on AMPK signaling in skeletal muscle of subjects with type 2 diabetes: a time-course and dose-response study. *Diabetes* **2007**, *56*, 836-848, doi:10.2337/db06-1119.

21. Witters, L.A.; Kemp, B.E. Insulin activation of acetyl-CoA carboxylase accompanied by inhibition of the 5'-AMP-activated protein kinase. *J Biol Chem* **1992**, *267*, 2864-2867.
22. Dunn, W.B.; Broadhurst, D.I.; Atherton, H.J.; Goodacre, R.; Griffin, J.L. Systems level studies of mammalian metabolomes: the roles of mass spectrometry and nuclear magnetic resonance spectroscopy. *Chem Soc Rev* **2011**, *40*, 387-426, doi:10.1039/b906712b.
23. Fiehn, O. Metabolomics--the link between genotypes and phenotypes. *Plant Mol Biol* **2002**, *48*, 155-171.
24. Gaitanos, G.C.; Williams, C.; Boobis, L.H.; Brooks, S. Human muscle metabolism during intermittent maximal exercise. *J Appl Physiol (1985)* **1993**, *75*, 712-719, doi:10.1152/jappl.1993.75.2.712.
25. Baker, J.S.; McCormick, M.C.; Robergs, R.A. Interaction among Skeletal Muscle Metabolic Energy Systems during Intense Exercise. *Journal of Nutrition and Metabolism* **2010**, *2010*, 905612, doi:10.1155/2010/905612.
26. Dunn, J.; Grider, M.H. Physiology, Adenosine Triphosphate (ATP). In *StatPearls*; Treasure Island (FL), 2020.
27. Egan, B.; Zierath, J.R. Exercise metabolism and the molecular regulation of skeletal muscle adaptation. *Cell Metab* **2013**, *17*, 162-184, doi:10.1016/j.cmet.2012.12.012.
28. Parolin, M.L.; Chesley, A.; Matsos, M.P.; Spriet, L.L.; Jones, N.L.; Heigenhauser, G.J. Regulation of skeletal muscle glycogen phosphorylase and PDH during maximal intermittent exercise. *Am J Physiol* **1999**, *277*, E890-900, doi:10.1152/ajpendo.1999.277.5.E890.
29. Romijn, J.A.; Coyle, E.F.; Sidossis, L.S.; Gastaldelli, A.; Horowitz, J.F.; Endert, E.; Wolfe, R.R. Regulation of endogenous fat and carbohydrate metabolism in relation to exercise intensity and duration. *Am J Physiol* **1993**, *265*, E380-391, doi:10.1152/ajpendo.1993.265.3.E380.
30. van Loon, L.J.; Greenhaff, P.L.; Constantin-Teodosiu, D.; Saris, W.H.; Wagenmakers, A.J. The effects of increasing exercise intensity on muscle fuel utilisation in humans. *J Physiol* **2001**, *536*, 295-304, doi:10.1111/j.1469-7793.2001.00295.x.
31. Hoffman, N.J. Omics and Exercise: Global Approaches for Mapping Exercise Biological Networks. *Cold Spring Harb Perspect Med* **2017**, *7*, doi:10.1101/cshperspect.a029884.

32. Oliver, S.G.; Winson, M.K.; Kell, D.B.; Baganz, F. Systematic functional analysis of the yeast genome. *Trends Biotechnol* **1998**, *16*, 373-378, doi:10.1016/s0167-7799(98)01214-1.
33. Nicholson, J.K.; Lindon, J.C.; Holmes, E. 'Metabonomics': understanding the metabolic responses of living systems to pathophysiological stimuli via multivariate statistical analysis of biological NMR spectroscopic data. *Xenobiotica* **1999**, *29*, 1181-1189, doi:10.1080/004982599238047.
34. Ramsden, J. Metabolomics and Metabonomics. 2009; pp. 1-6.
35. Nicholson, J.K.; Lindon, J.C. Systems biology: Metabonomics. *Nature* **2008**, *455*, 1054-1056, doi:10.1038/4551054a.
36. Au, A. Metabolomics and Lipidomics of Ischemic Stroke. *Adv Clin Chem* **2018**, *85*, 31-69, doi:10.1016/bs.acc.2018.02.002.
37. Human Metabolome Database. Available online: https://hmdb.ca/metabolites?utf8=✓&quantified=1&detected=1&endogenous=1&filter=true (accessed on 15th of December).
38. Human Metabolome Database. Available online: https://hmdb.ca/metabolites?utf8=✓&filter=true&quantified=1&detected=1&expected=1&predicted=1&exogenous=1&food=1&plant=1&microbial=1&toxin=1&cosmetic=1&drug=1&drug_metabolite=1&filter=true (accessed on 16th of December).
39. Amberg, A.; Riefke, B.; Schlotterbeck, G.; Ross, A.; Senn, H.; Dieterle, F.; Keck, M. NMR and MS Methods for Metabolomics. *Methods Mol Biol* **2017**, *1641*, 229-258, doi:10.1007/978-1-4939-7172-5_13.
40. Wang, J.; Wang, C.; Han, X. Tutorial on lipidomics. *Anal Chim Acta* **2019**, *1061*, 28-41, doi:10.1016/j.aca.2019.01.043.
41. Smith, A. *Oxford Dictionary of Biochemistry and Molecular Biology*, 2nd ed.; Oxford University Press: Oxford (UK), 2000.
42. Fahy, E.; Subramaniam, S.; Brown, H.A.; Glass, C.K.; Merrill, A.H., Jr.; Murphy, R.C.; Raetz, C.R.; Russell, D.W.; Seyama, Y.; Shaw, W.; et al. A comprehensive classification system for lipids. *J Lipid Res* **2005**, *46*, 839-861, doi:10.1194/jlr.E400004-JLR200.
43. LIPID MAPS® Lipidomics Gateway. Available online: http://www.lipidmaps.org/resources/databases/index.php (accessed on 15th of December).

44. Shah, S.H.; Kraus, W.E.; Newgard, C.B. Metabolomic profiling for the identification of novel biomarkers and mechanisms related to common cardiovascular diseases: form and function. *Circulation* **2012**, *126*, 1110-1120, doi:10.1161/CIRCULATIONAHA.111.060368.
45. Chen, C.; Fan, Z.; Xu, H.; Tan, X.; Zhu, M. Metabolomics-based parallel discovery of xenobiotics and induced endogenous metabolic dysregulation in clinical toxicology. *Biomed Chromatogr* **2019**, *33*, e4413, doi:10.1002/bmc.4413.
46. Sato, S.; Parr, E.B.; Devlin, B.L.; Hawley, J.A.; Sassone-Corsi, P. Human metabolomics reveal daily variations under nutritional challenges specific to serum and skeletal muscle. *Mol Metab* **2018**, *16*, 1-11, doi:10.1016/j.molmet.2018.06.008.
47. Contrepois, K.; Wu, S.; Moneghetti, K.J.; Hornburg, D.; Ahadi, S.; Tsai, M.S.; Metwally, A.A.; Wei, E.; Lee-McMullen, B.; Quijada, J.V.; et al. Molecular Choreography of Acute Exercise. *Cell* **2020**, *181*, 1112-1130 e1116, doi:10.1016/j.cell.2020.04.043.
48. Riekeberg, E.; Powers, R. New frontiers in metabolomics: from measurement to insight. *F1000Res* **2017**, *6*, 1148, doi:10.12688/f1000research.11495.1.
49. Sinclair, K.; Dudley, E. Metabolomics and Biomarker Discovery. *Adv Exp Med Biol* **2019**, *1140*, 613-633, doi:10.1007/978-3-030-15950-4_37.
50. Peregrin-Alvarez, J.M.; Sanford, C.; Parkinson, J. The conservation and evolutionary modularity of metabolism. *Genome Biol* **2009**, *10*, R63, doi:10.1186/gb-2009-10-6-r63.
51. Dunn, W.B.; Wilson, I.D.; Nicholls, A.W.; Broadhurst, D. The importance of experimental design and QC samples in large-scale and MS-driven untargeted metabolomic studies of humans. *Bioanalysis* **2012**, *4*, 2249-2264, doi:10.4155/bio.12.204.
52. Broadhurst, D.; Goodacre, R.; Reinke, S.N.; Kuligowski, J.; Wilson, I.D.; Lewis, M.R.; Dunn, W.B. Guidelines and considerations for the use of system suitability and quality control samples in mass spectrometry assays applied in untargeted clinical metabolomic studies. *Metabolomics* **2018**, *14*, 72, doi:10.1007/s11306-018-1367-3.
53. Mlynarik, V. Introduction to nuclear magnetic resonance. *Anal Biochem* **2017**, *529*, 4-9, doi:10.1016/j.ab.2016.05.006.
54. Pitt, J.J. Principles and applications of liquid chromatography-mass spectrometry in clinical biochemistry. *Clin Biochem Rev* **2009**, *30*, 19-34.
55. Tognarelli, J.M.; Dawood, M.; Shariff, M.I.; Grover, V.P.; Crossey, M.M.; Cox, I.J.; Taylor-Robinson, S.D.; McPhail, M.J. Magnetic Resonance Spectroscopy: Principles

and Techniques: Lessons for Clinicians. *J Clin Exp Hepatol* **2015**, *5*, 320-328, doi:10.1016/j.jceh.2015.10.006.

56. Zhou, B.; Xiao, J.F.; Tuli, L.; Ressom, H.W. LC-MS-based metabolomics. *Mol Biosyst* **2012**, *8*, 470-481, doi:10.1039/c1mb05350g.
57. Emwas, A.H.; Roy, R.; McKay, R.T.; Tenori, L.; Saccenti, E.; Gowda, G.A.N.; Raftery, D.; Alahmari, F.; Jaremko, L.; Jaremko, M.; et al. NMR Spectroscopy for Metabolomics Research. *Metabolites* **2019**, *9*, doi:10.3390/metabo9070123.
58. Gika, H.; Virgiliou, C.; Theodoridis, G.; Plumb, R.S.; Wilson, I.D. Untargeted LC/MS-based metabolic phenotyping (metabonomics/metabolomics): The state of the art. *J Chromatogr B Analyt Technol Biomed Life Sci* **2019**, *1117*, 136-147, doi:10.1016/j.jchromb.2019.04.009.
59. Beale, D.J.; Pinu, F.R.; Kouremenos, K.A.; Poojary, M.M.; Narayana, V.K.; Boughton, B.A.; Kanojia, K.; Dayalan, S.; Jones, O.A.H.; Dias, D.A. Review of recent developments in GC-MS approaches to metabolomics-based research. *Metabolomics* **2018**, *14*, 152, doi:10.1007/s11306-018-1449-2.
60. Jurowski, K.; Kochan, K.; Walczak, J.; Baranska, M.; Piekoszewski, W.; Buszewski, B. Analytical Techniques in Lipidomics: State of the Art. *Crit Rev Anal Chem* **2017**, *47*, 418-437, doi:10.1080/10408347.2017.1310613.
61. O'Donnell, V.B.; Ekroos, K.; Liebisch, G.; Wakelam, M. Lipidomics: Current state of the art in a fast moving field. *Wiley Interdiscip Rev Syst Biol Med* **2020**, *12*, e1466, doi:10.1002/wsbm.1466.
62. Buchberger, A.R.; DeLaney, K.; Johnson, J.; Li, L. Mass Spectrometry Imaging: A Review of Emerging Advancements and Future Insights. *Anal Chem* **2018**, *90*, 240-265, doi:10.1021/acs.analchem.7b04733.
63. Caprioli, R.M. Imaging Mass Spectrometry: A Perspective. *J Biomol Tech* **2019**, *30*, 7-11, doi:10.7171/jbt.19-3001-002.
64. Murayama, C.; Kimura, Y.; Setou, M. Imaging mass spectrometry: principle and application. *Biophys Rev* **2009**, *1*, 131, doi:10.1007/s12551-009-0015-6.
65. Hu, C.; Duan, Q.; Han, X. Strategies to Improve/Eliminate the Limitations in Shotgun Lipidomics. *Proteomics* **2020**, e1900070, doi:10.1002/pmic.201900070.
66. Annesley, T.M. Ion suppression in mass spectrometry. *Clin Chem* **2003**, *49*, 1041-1044, doi:10.1373/49.7.1041.
67. Hartler, J.; Triebl, A.; Ziegl, A.; Trötzmüller, M.; Rechberger, G.N.; Zeleznik, O.A.; Zierler, K.A.; Torta, F.; Cazenave-Gassiot, A.; Wenk, M.R.; et al. Deciphering lipid

structures based on platform-independent decision rules. *Nature Methods* **2017**, *14*, 1171-1174, doi:10.1038/nmeth.4470.

68. Sud, M.; Fahy, E.; Cotter, D.; Brown, A.; Dennis, E.A.; Glass, C.K.; Merrill, A.H., Jr.; Murphy, R.C.; Raetz, C.R.; Russell, D.W.; et al. LMSD: LIPID MAPS structure database. *Nucleic Acids Res* **2007**, *35*, D527-532, doi:10.1093/nar/gkl838.
69. Hernandez-Mesa, M.; Ropartz, D.; Garcia-Campana, A.M.; Rogniaux, H.; Dervilly-Pinel, G.; Le Bizec, B. Ion Mobility Spectrometry in Food Analysis: Principles, Current Applications and Future Trends. *Molecules* **2019**, *24*, doi:10.3390/molecules24152706.
70. Bi, H.; Guo, Z.; Jia, X.; Liu, H.; Ma, L.; Xue, L. The key points in the pre-analytical procedures of blood and urine samples in metabolomics studies. *Metabolomics* **2020**, *16*, 68, doi:10.1007/s11306-020-01666-2.
71. Sumner, L.W.; Amberg, A.; Barrett, D.; Beale, M.H.; Beger, R.; Daykin, C.A.; Fan, T.W.; Fiehn, O.; Goodacre, R.; Griffin, J.L.; et al. Proposed minimum reporting standards for chemical analysis Chemical Analysis Working Group (CAWG) Metabolomics Standards Initiative (MSI). *Metabolomics* **2007**, *3*, 211-221, doi:10.1007/s11306-007-0082-2.
72. Emwas, A.H.; Saccenti, E.; Gao, X.; McKay, R.T.; Dos Santos, V.; Roy, R.; Wishart, D.S. Recommended strategies for spectral processing and post-processing of 1D (1)H-NMR data of biofluids with a particular focus on urine. *Metabolomics* **2018**, *14*, 31, doi:10.1007/s11306-018-1321-4.
73. Gromski, P.S.; Muhamadali, H.; Ellis, D.I.; Xu, Y.; Correa, E.; Turner, M.L.; Goodacre, R. A tutorial review: Metabolomics and partial least squares-discriminant analysis--a marriage of convenience or a shotgun wedding. *Anal Chim Acta* **2015**, *879*, 10-23, doi:10.1016/j.aca.2015.02.012.
74. Lee, L.C.; Liong, C.Y.; Jemain, A.A. Partial least squares-discriminant analysis (PLS-DA) for classification of high-dimensional (HD) data: a review of contemporary practice strategies and knowledge gaps. *Analyst* **2018**, *143*, 3526-3539, doi:10.1039/c8an00599k.
75. Cambiaghi, A.; Ferrario, M.; Masseroli, M. Analysis of metabolomic data: tools, current strategies and future challenges for omics data integration. *Brief Bioinform* **2017**, *18*, 498-510, doi:10.1093/bib/bbw031.
76. Schwaiger, M.; Schoeny, H.; El Abiead, Y.; Hermann, G.; Rampler, E.; Koellensperger, G. Merging metabolomics and lipidomics into one analytical run. *Analyst* **2018**, *144*, 220-229, doi:10.1039/c8an01219a.

77. Hughes, D.C.; Ellefsen, S.; Baar, K. Adaptations to Endurance and Strength Training. *Cold Spring Harb Perspect Med* **2018**, *8*, doi:10.1101/cshperspect.a029769.
78. Millstein, R. Aerobic Exercise. In *Encyclopedia of Behavioral Medicine*, Gellman, M.D., Turner, J.R., Eds.; Springer New York: New York, NY, 2013; pp. 48-49.
79. Wu, J.Q.; Gao, Y.H. Physiological conditions can be reflected in human urine proteome and metabolome. *Expert Rev Proteomic* **2015**, *12*, 623-636, doi:10.1586/14789450.2015.1094380.
80. Mena-Bravo, A.; Luque de Castro, M.D. Sweat: a sample with limited present applications and promising future in metabolomics. *J Pharm Biomed Anal* **2014**, *90*, 139-147, doi:10.1016/j.jpba.2013.10.048.
81. Sakaguchi, C.A.; Nieman, D.C.; Signini, E.F.; Abreu, R.M.; Catai, A.M. Metabolomics-Based Studies Assessing Exercise-Induced Alterations of the Human Metabolome: A Systematic Review. *Metabolites* **2019**, *9*, doi:10.3390/metabo9080164.
82. Schranner, D.; Kastenmuller, G.; Schonfelder, M.; Romisch-Margl, W.; Wackerhage, H. Metabolite Concentration Changes in Humans After a Bout of Exercise: a Systematic Review of Exercise Metabolomics Studies. *Sports Med Open* **2020**, *6*, 11, doi:10.1186/s40798-020-0238-4.
83. Lewis, G.D.; Farrell, L.; Wood, M.J.; Martinovic, M.; Arany, Z.; Rowe, G.C.; Souza, A.; Cheng, S.; McCabe, E.L.; Yang, E.; et al. Metabolic signatures of exercise in human plasma. *Sci Transl Med* **2010**, *2*, 33ra37, doi:10.1126/scitranslmed.3001006.
84. Stander, Z.; Luies, L.; Mienie, L.J.; Keane, K.M.; Howatson, G.; Clifford, T.; Stevenson, E.J.; Loots, D.T. The altered human serum metabolome induced by a marathon. *Metabolomics* **2018**, *14*, 150, doi:10.1007/s11306-018-1447-4.
85. Evans, M.; Cogan, K.E.; Egan, B. Metabolism of ketone bodies during exercise and training: physiological basis for exogenous supplementation. *J Physiol* **2017**, *595*, 2857-2871, doi:10.1113/JP273185.
86. Krug, S.; Kastenmuller, G.; Stuckler, F.; Rist, M.J.; Skurk, T.; Sailer, M.; Raffler, J.; Romisch-Margl, W.; Adamski, J.; Prehn, C.; et al. The dynamic range of the human metabolome revealed by challenges. *FASEB J* **2012**, *26*, 2607-2619, doi:10.1096/fj.11-198093.
87. Jenkins, B.J.; Seyssel, K.; Chiu, S.; Pan, P.H.; Lin, S.Y.; Stanley, E.; Ament, Z.; West, J.A.; Summerhill, K.; Griffin, J.L.; et al. Odd Chain Fatty Acids; New Insights of the Relationship Between the Gut Microbiota, Dietary Intake, Biosynthesis and Glucose Intolerance. *Sci Rep* **2017**, *7*, 44845, doi:10.1038/srep44845.

88. Jenkins, B.; West, J.A.; Koulman, A. A review of odd-chain fatty acid metabolism and the role of pentadecanoic Acid (c15:0) and heptadecanoic Acid (c17:0) in health and disease. *Molecules* **2015**, *20*, 2425-2444, doi:10.3390/molecules20022425.
89. Noland, R.C.; Woodlief, T.L.; Whitfield, B.R.; Manning, S.M.; Evans, J.R.; Dudek, R.W.; Lust, R.M.; Cortright, R.N. Peroxisomal-mitochondrial oxidation in a rodent model of obesity-associated insulin resistance. *Am J Physiol Endocrinol Metab* **2007**, *293*, E986-E1001, doi:10.1152/ajpendo.00399.2006.
90. Shi, R.; Zhang, J.; Fang, B.; Tian, X.; Feng, Y.; Cheng, Z.; Fu, Z.; Zhang, J.; Wu, J. Runners' metabolomic changes following marathon. *Nutr Metab (Lond)* **2020**, *17*, 19, doi:10.1186/s12986-020-00436-0.
91. Thau, L.; Gandhi, J.; Sharma, S. Physiology, Cortisol. In *StatPearls*; Treasure Island (FL), 2020.
92. Henrotin, Y.; Marty, M.; Mobasheri, A. What is the current status of chondroitin sulfate and glucosamine for the treatment of knee osteoarthritis? *Maturitas* **2014**, *78*, 184-187, doi:10.1016/j.maturitas.2014.04.015.
93. Schader, J.F.; Haid, M.; Cecil, A.; Schoenfeld, J.; Halle, M.; Pfeufer, A.; Prehn, C.; Adamski, J.; Nieman, D.C.; Scherr, J. Metabolite Shifts Induced by Marathon Race Competition Differ between Athletes Based on Level of Fitness and Performance: A Substudy of the Enzy-MagIC Study. *Metabolites* **2020**, *10*, doi:10.3390/metabo10030087.
94. Metz, R.; Salter, J.M.; Brunet, G. Effect of pyruvate and other substrates on urea synthesis in rat liver slices. *Metabolism* **1968**, *17*, 158-167, doi:10.1016/0026-0495(68)90143-1.
95. Kopincova, J.; Puzserova, A.; Bernatova, I. Biochemical aspects of nitric oxide synthase feedback regulation by nitric oxide. *Interdiscip Toxicol* **2011**, *4*, 63-68, doi:10.2478/v10102-011-0012-z.
96. Riccioni, G.; Scotti, L.; Guagnano, M.T.; Bosco, G.; Bucciarelli, V.; Di Ilio, E.; Speranza, L.; Martini, F.; Bucciarelli, T. Physical exercise reduces synthesis of ADMA, SDMA, and L-Arg. *Front Biosci (Elite Ed)* **2015**, *7*, 417-422.
97. Manaf, F.A.; Lawler, N.; Peiffer, J.J.; Maker, G.L.; Boyce, M.C.; Fairchild, T.J.; Broadhurst, D. Characterizing the plasma metabolome during and following a maximal exercise cycling test. *J Appl Physiol (1985)* **2018**, doi:10.1152/japplphysiol.00499.2018.

98. Newsholme, E.A.; Blomstrand, E. Tryptophan, 5-hydroxytryptamine and a possible explanation for central fatigue. *Adv Exp Med Biol* **1995**, *384*, 315-320, doi:10.1007/978-1-4899-1016-5_25.
99. Bell, F.P. Inhibition of adenine nucleotide translocase by oleoylcarnitine, oleoylcoa and oleate in isolated arterial mitochondria. *Atherosclerosis* **1980**, *37*, 21-32, doi:10.1016/0021-9150(80)90090-8.
100. Zhang, J.; Light, A.R.; Hoppel, C.L.; Campbell, C.; Chandler, C.J.; Burnett, D.J.; Souza, E.C.; Casazza, G.A.; Hughen, R.W.; Keim, N.L.; et al. Acylcarnitines as markers of exercise-associated fuel partitioning, xenometabolism, and potential signals to muscle afferent neurons. *Exp Physiol* **2017**, *102*, 48-69, doi:10.1113/EP086019.
101. Hu, C.X.; Hoene, M.; Plomgaard, P.; Hansen, J.S.; Zhao, X.J.; Li, J.; Wang, X.L.; Clemmesen, J.O.; Secher, N.H.; Haring, H.U.; et al. Muscle-Liver Substrate Fluxes in Exercising Humans and Potential Effects on Hepatic Metabolism. *J Clin Endocr Metab* **2020**, *105*, doi:10.1210/clinem/dgz266.
102. Kistner, S.; Rist, M.J.; Doring, M.; Dorr, C.; Neumann, R.; Hartel, S.; Bub, A. An NMR-Based Approach to Identify Urinary Metabolites Associated with Acute Physical Exercise and Cardiorespiratory Fitness in Healthy Humans-Results of the KarMeN Study. *Metabolites* **2020**, *10*, doi:10.3390/metabo10050212.
103. Mukherjee, K.; Edgett, B.A.; Burrows, H.W.; Castro, C.; Griffin, J.L.; Schwertani, A.G.; Gurd, B.J.; Funk, C.D. Whole blood transcriptomics and urinary metabolomics to define adaptive biochemical pathways of high-intensity exercise in 50-60 year old masters athletes. *PLoS One* **2014**, *9*, e92031, doi:10.1371/journal.pone.0092031.
104. Pechlivanis, A.; Kostidis, S.; Saraslanidis, P.; Petridou, A.; Tsalis, G.; Mougios, V.; Gika, H.G.; Mikros, E.; Theodoridis, G.A. (1)H NMR-based metabonomic investigation of the effect of two different exercise sessions on the metabolic fingerprint of human urine. *J Proteome Res* **2010**, *9*, 6405-6416, doi:10.1021/pr100684t.
105. Pechlivanis, A.; Papaioannou, K.G.; Tsalis, G.; Saraslanidis, P.; Mougios, V.; Theodoridis, G.A. Monitoring the Response of the Human Urinary Metabolome to Brief Maximal Exercise by a Combination of RP-UPLC-MS and (1)H NMR Spectroscopy. *J Proteome Res* **2015**, *14*, 4610-4622, doi:10.1021/acs.jproteome.5b00470.
106. Siopi, A.; Deda, O.; Manou, V.; Kellis, S.; Kosmidis, I.; Komninou, D.; Raikos, N.; Christoulas, K.; Theodoridis, G.A.; Mougios, V. Effects of Different Exercise Modes

on the Urinary Metabolic Fingerprint of Men with and without Metabolic Syndrome. *Metabolites* **2017**, *7*, doi:10.3390/metabo7010005.

107. Akazawa, N.; Kobayashi, N.; Nakamura, Y.; Kumagai, H.; Choi, Y.; Maeda, S. Effect of sleep efficiency on salivary metabolite profile and cognitive function during exercise in volleyball athletes. *Eur J Appl Physiol* **2019**, *119*, 2215-2223, doi:10.1007/s00421-019-04205-7.
108. McBride, E.M.; Lawrence, R.J.; McGee, K.; Mach, P.M.; Demond, P.S.; Busch, M.W.; Ramsay, J.W.; Hussey, E.K.; Glaros, T.; Dhummakupt, E.S. Rapid liquid chromatography tandem mass spectrometry method for targeted quantitation of human performance metabolites in saliva. *J Chromatogr A* **2019**, *1601*, 205-213, doi:10.1016/j.chroma.2019.04.071.
109. Pitti, E.; Petrella, G.; Di Marino, S.; Summa, V.; Perrone, M.; D'Ottavio, S.; Bernardini, A.; Cicero, D.O. Salivary Metabolome and Soccer Match: Challenges for Understanding Exercise induced Changes. *Metabolites* **2019**, *9*, doi:10.3390/metabo9070141.
110. Ra, S.G.; Maeda, S.; Higashino, R.; Imai, T.; Miyakawa, S. Metabolomics of salivary fatigue markers in soccer players after consecutive games. *Appl Physiol Nutr Metab* **2014**, *39*, 1120-1126, doi:10.1139/apnm-2013-0546.
111. Santone, C.; Dinallo, V.; Paci, M.; D'Ottavio, S.; Barbato, G.; Bernardini, S. Saliva metabolomics by NMR for the evaluation of sport performance. *J Pharm Biomed Anal* **2014**, *88*, 441-446, doi:10.1016/j.jpba.2013.09.021.
112. Tekus, E.; Kaj, M.; Szabo, E.; Szenasi, N.L.; Kerepesi, I.; Figler, M.; Gabriel, R.; Wilhelm, M. Comparison of blood and saliva lactate level after maximum intensity exercise. *Acta Biol Hung* **2012**, *63 Suppl 1*, 89-98, doi:10.1556/ABiol.63.2012.Suppl.1.9.
113. Delgado-Povedano, M.D.; Calderon-Santiago, M.; Priego-Capote, F.; Jurado-Gamez, B.; de Castro, M.D.L. Recent advances in human sweat metabolomics for lung cancer screening. *Metabolomics* **2016**, *12*, doi:10.1007/s11306-016-1116-4.
114. Delgado-Povedano, M.M.; Calderon-Santiago, M.; Luque de Castro, M.D.; Priego-Capote, F. Metabolomics analysis of human sweat collected after moderate exercise. *Talanta* **2018**, *177*, 47-65, doi:10.1016/j.talanta.2017.09.028.
115. Harshman, S.W.; Pitsch, R.L.; Smith, Z.K.; O'Connor, M.L.; Geier, B.A.; Qualley, A.V.; Schaeublin, N.M.; Fischer, M.V.; Eckerle, J.J.; Strang, A.J.; et al. The proteomic and metabolomic characterization of exercise-induced sweat for human performance

monitoring: A pilot investigation. *PLoS One* **2018**, *13*, e0203133, doi:10.1371/journal.pone.0203133.

116. Hooton, K.; Han, W.; Li, L. Comprehensive and Quantitative Profiling of the Human Sweat Submetabolome Using High-Performance Chemical Isotope Labeling LC-MS. *Anal Chem* **2016**, *88*, 7378-7386, doi:10.1021/acs.analchem.6b01930.
117. Fazelzadeh, P.; Hangelbroek, R.W.; Tieland, M.; de Groot, L.C.; Verdijk, L.B.; van Loon, L.J.; Smilde, A.K.; Alves, R.D.; Vervoort, J.; Muller, M.; et al. The Muscle Metabolome Differs between Healthy and Frail Older Adults. *J Proteome Res* **2016**, *15*, 499-509, doi:10.1021/acs.jproteome.5b00840.
118. Sato, S.; Basse, A.L.; Schonke, M.; Chen, S.; Samad, M.; Altintas, A.; Laker, R.C.; Dalbram, E.; Barres, R.; Baldi, P.; et al. Time of Exercise Specifies the Impact on Muscle Metabolic Pathways and Systemic Energy Homeostasis. *Cell Metab* **2019**, *30*, 92-110 e114, doi:10.1016/j.cmet.2019.03.013.
119. Overmyer, K.A.; Evans, C.R.; Qi, N.R.; Minogue, C.E.; Carson, J.J.; Chermside-Scabbo, C.J.; Koch, L.G.; Britton, S.L.; Pagliarini, D.J.; Coon, J.J.; et al. Maximal oxidative capacity during exercise is associated with skeletal muscle fuel selection and dynamic changes in mitochondrial protein acetylation. *Cell Metab* **2015**, *21*, 468-478, doi:10.1016/j.cmet.2015.02.007.
120. Klein, D.J.; McKeever, K.H.; Mirek, E.T.; Anthony, T.G. Metabolomic Response of Equine Skeletal Muscle to Acute Fatiguing Exercise and Training. *Front Physiol* **2020**, *11*, 110, doi:10.3389/fphys.2020.00110.
121. Zhang, J.; Bhattacharyya, S.; Hickner, R.C.; Light, A.R.; Lambert, C.J.; Gale, B.K.; Fiehn, O.; Adams, S.H. Skeletal muscle interstitial fluid metabolomics at rest and associated with an exercise bout: application in rats and humans. *Am J Physiol Endocrinol Metab* **2019**, *316*, E43-E53, doi:10.1152/ajpendo.00156.2018.
122. Huang, C.C.; Lin, W.T.; Hsu, F.L.; Tsai, P.W.; Hou, C.C. Metabolomics investigation of exercise-modulated changes in metabolism in rat liver after exhaustive and endurance exercises. *Eur J Appl Physiol* **2010**, *108*, 557-566, doi:10.1007/s00421-009-1247-7.
123. Hoene, M.; Irmler, M.; Beckers, J.; Hrabe de Angelis, M.; Haring, H.U.; Weigert, C. A Vitamin E-Enriched Antioxidant Diet Interferes with the Acute Adaptation of the Liver to Physical Exercise in Mice. *Nutrients* **2018**, *10*, doi:10.3390/nu10050547.
124. Sobhi, H.F.; Zhao, X.; Plomgaard, P.; Hoene, M.; Hansen, J.S.; Karus, B.; Niess, A.M.; Haring, H.U.; Lehmann, R.; Adams, S.H.; et al. Identification and regulation of the

xenometabolite derivatives cis- and trans-3,4-methylene-heptanoylcarnitine in plasma and skeletal muscle of exercising humans. *Am J Physiol Endocrinol Metab* **2020**, *318*, E701-E709, doi:10.1152/ajpendo.00510.2019.

125. Clifford, P.S.; Hellsten, Y. Vasodilatory mechanisms in contracting skeletal muscle. *J Appl Physiol (1985)* **2004**, *97*, 393-403, doi:10.1152/japplphysiol.00179.2004.
126. Gollasch, B.; Dogan, I.; Rothe, M.; Gollasch, M.; Luft, F.C. Maximal exercise and plasma cytochrome P450 and lipoxygenase mediators: a lipidomics study. *Physiol Rep* **2019**, *7*, e14165, doi:10.14814/phy2.14165.
127. Spector, A.A. Arachidonic acid cytochrome P450 epoxygenase pathway. *J Lipid Res* **2009**, *50 Suppl*, S52-56, doi:10.1194/jlr.R800038-JLR200.
128. Bruce, R.A.; Cooper, M.N.; Gey, G.O.; Fisher, L.D.; Peterson, D.R. Variations in responses to maximal exercise in health and in cardiovascular disease. *Angiology* **1973**, *24*, 691-702, doi:10.1177/000331977302401105.
129. Hercule, H.C.; Schunck, W.H.; Gross, V.; Seringer, J.; Leung, F.P.; Weldon, S.M.; da Costa Goncalves, A.; Huang, Y.; Luft, F.C.; Gollasch, M. Interaction between P450 eicosanoids and nitric oxide in the control of arterial tone in mice. *Arterioscler Thromb Vasc Biol* **2009**, *29*, 54-60, doi:10.1161/ATVBAHA.108.171298.
130. Siegfried, M.R.; Aoki, N.; Lefer, A.M.; Elisseou, E.M.; Zipkin, R.E. Direct cardiovascular actions of two metabolites of linoleic acid. *Life Sci* **1990**, *46*, 427-433, doi:10.1016/0024-3205(90)90086-7.
131. Hercule, H.C.; Salanova, B.; Essin, K.; Honeck, H.; Falck, J.R.; Sausbier, M.; Ruth, P.; Schunck, W.H.; Luft, F.C.; Gollasch, M. The vasodilator 17,18-epoxyeicosatetraenoic acid targets the pore-forming BK alpha channel subunit in rodents. *Exp Physiol* **2007**, *92*, 1067-1076, doi:10.1113/expphysiol.2007.038166.
132. Stanford, K.I.; Lynes, M.D.; Takahashi, H.; Baer, L.A.; Arts, P.J.; May, F.J.; Lehnig, A.C.; Middelbeek, R.J.W.; Richard, J.J.; So, K.; et al. 12,13-diHOME: An Exercise-Induced Lipokine that Increases Skeletal Muscle Fatty Acid Uptake. *Cell Metab* **2018**, *27*, 1111-1120 e1113, doi:10.1016/j.cmet.2018.03.020.
133. Bannehr, M.; Lohr, L.; Gelep, J.; Haverkamp, W.; Schunck, W.H.; Gollasch, M.; Wutzler, A. Linoleic Acid Metabolite DiHOME Decreases Post-ischemic Cardiac Recovery in Murine Hearts. *Cardiovasc Toxicol* **2019**, *19*, 365-371, doi:10.1007/s12012-019-09508-x.
134. Sisemore, M.F.; Zheng, J.; Yang, J.C.; Thompson, D.A.; Plopper, C.G.; Cortopassi, G.A.; Hammock, B.D. Cellular characterization of leukotoxin diol-induced

mitochondrial dysfunction. *Arch Biochem Biophys* **2001**, *392*, 32-37, doi:10.1006/abbi.2001.2434.

135. Nieman, D.C.; Shanely, R.A.; Luo, B.; Meaney, M.P.; Dew, D.A.; Pappan, K.L. Metabolomics approach to assessing plasma 13- and 9-hydroxy-octadecadienoic acid and linoleic acid metabolite responses to 75-km cycling. *Am J Physiol Regul Integr Comp Physiol* **2014**, *307*, R68-74, doi:10.1152/ajpregu.00092.2014.
136. Vangaveti, V.; Baune, B.T.; Kennedy, R.L. Hydroxyoctadecadienoic acids: novel regulators of macrophage differentiation and atherogenesis. *Ther Adv Endocrinol Metab* **2010**, *1*, 51-60, doi:10.1177/2042018810375656.
137. Gollasch, B.; Wu, G.; Dogan, I.; Rothe, M.; Gollasch, M.; Luft, F.C. Maximal exercise and erythrocyte epoxy fatty acids: a lipidomics study. *Physiol Rep* **2019**, *7*, e14275, doi:10.14814/phy2.14275.
138. Schunck, W.H.; Konkel, A.; Fischer, R.; Weylandt, K.H. Therapeutic potential of omega-3 fatty acid-derived epoxyeicosanoids in cardiovascular and inflammatory diseases. *Pharmacol Ther* **2018**, *183*, 177-204, doi:10.1016/j.pharmthera.2017.10.016.
139. Gollasch, B.; Dogan, I.; Rothe, M.; Gollasch, M.; Luft, F.C. Maximal exercise and erythrocyte fatty-acid status: a lipidomics study. *Physiol Rep* **2019**, *7*, e14040, doi:10.14814/phy2.14040.
140. Thuppal, S.V.; von Schacky, C.; Harris, W.S.; Sherif, K.D.; Denby, N.; Steinbaum, S.R.; Haycock, B.; Bailey, R.L. Discrepancy between Knowledge and Perceptions of Dietary Omega-3 Fatty Acid Intake Compared with the Omega-3 Index. *Nutrients* **2017**, *9*, doi:10.3390/nu9090930.
141. von Schacky, C. Omega-3 fatty acids in cardiovascular disease--an uphill battle. *Prostaglandins Leukot Essent Fatty Acids* **2015**, *92*, 41-47, doi:10.1016/j.plefa.2014.05.004.
142. Markworth, J.F.; Vella, L.; Lingard, B.S.; Tull, D.L.; Rupasinghe, T.W.; Sinclair, A.J.; Maddipati, K.R.; Cameron-Smith, D. Human inflammatory and resolving lipid mediator responses to resistance exercise and ibuprofen treatment. *Am J Physiol Regul Integr Comp Physiol* **2013**, *305*, R1281-1296, doi:10.1152/ajpregu.00128.2013.
143. Nakahata, N. Thromboxane A2: physiology/pathophysiology, cellular signal transduction and pharmacology. *Pharmacol Ther* **2008**, *118*, 18-35, doi:10.1016/j.pharmthera.2008.01.001.
144. Vella, L.; Markworth, J.F.; Farnfield, M.M.; Maddipati, K.R.; Russell, A.P.; Cameron-Smith, D. Intramuscular inflammatory and resolving lipid profile responses to an acute

bout of resistance exercise in men. *Physiol Rep* **2019**, *7*, e14108, doi:10.14814/phy2.14108.

145. Rivas, D.A.; Morris, E.P.; Haran, P.H.; Pasha, E.P.; Morais Mda, S.; Dolnikowski, G.G.; Phillips, E.M.; Fielding, R.A. Increased ceramide content and NFkappaB signaling may contribute to the attenuation of anabolic signaling after resistance exercise in aged males. *J Appl Physiol (1985)* **2012**, *113*, 1727-1736, doi:10.1152/japplphysiol.00412.2012.
146. Summers, S.A.; Nelson, D.H. A role for sphingolipids in producing the common features of type 2 diabetes, metabolic syndrome X, and Cushing's syndrome. *Diabetes* **2005**, *54*, 591-602, doi:10.2337/diabetes.54.3.591.
147. Engin, A.B. What Is Lipotoxicity? *Adv Exp Med Biol* **2017**, *960*, 197-220, doi:10.1007/978-3-319-48382-5_8.
148. Sassot, L.N.; Villarino, N.F.; Dasgupta, N.; Morrison, J.J.; Bayly, W.M.; Gang, D.; Sanz, M.G. The lipidome of Thoroughbred racehorses before and after supramaximal exercise. *Equine Veterinary Journal* **2019**, *51*, 696-700, doi:10.1111/evj.13064.
149. Nikolaidis, M.G.; Mougios, V. Effects of exercise on the fatty-acid composition of blood and tissue lipids. *Sports Med* **2004**, *34*, 1051-1076, doi:10.2165/00007256-200434150-00004.
150. Le Moyec, L.; Robert, C.; Triba, M.N.; Billat, V.L.; Mata, X.; Schibler, L.; Barrey, E. Protein catabolism and high lipid metabolism associated with long-distance exercise are revealed by plasma NMR metabolomics in endurance horses. *PLoS One* **2014**, *9*, e90730, doi:10.1371/journal.pone.0090730.
151. Mach, N.; Ramayo-Caldas, Y.; Clark, A.; Moroldo, M.; Robert, C.; Barrey, E.; Lopez, J.M.; Le Moyec, L. Understanding the response to endurance exercise using a systems biology approach: combining blood metabolomics, transcriptomics and miRNomics in horses. *BMC Genomics* **2017**, *18*, 187, doi:10.1186/s12864-017-3571-3.
152. Hu, C.; Hoene, M.; Zhao, X.; Haring, H.U.; Schleicher, E.; Lehmann, R.; Han, X.; Xu, G.; Weigert, C. Lipidomics analysis reveals efficient storage of hepatic triacylglycerides enriched in unsaturated fatty acids after one bout of exercise in mice. *PLoS One* **2010**, *5*, e13318, doi:10.1371/journal.pone.0013318.
153. Hoene, M.; Li, J.; Li, Y.; Runge, H.; Zhao, X.; Haring, H.U.; Lehmann, R.; Xu, G.; Weigert, C. Muscle and liver-specific alterations in lipid and acylcarnitine metabolism after a single bout of exercise in mice. *Sci Rep* **2016**, *6*, 22218, doi:10.1038/srep22218.

154. Vance, J.E. Lipoproteins secreted by cultured rat hepatocytes contain the antioxidant 1-alk-1-enyl-2-acylglycerophosphoethanolamine. *Biochim Biophys Acta* **1990**, *1045*, 128-134, doi:10.1016/0005-2760(90)90141-j.

155. Minokoshi, Y.; Kim, Y.B.; Peroni, O.D.; Fryer, L.G.; Muller, C.; Carling, D.; Kahn, B.B. Leptin stimulates fatty-acid oxidation by activating AMP-activated protein kinase. *Nature* **2002**, *415*, 339-343, doi:10.1038/415339a.

156. Furuichi, Y.; Sugiura, T.; Kato, Y.; Shimada, Y.; Masuda, K. OCTN2 is associated with carnitine transport capacity of rat skeletal muscles. *Acta Physiol (Oxf)* **2010**, *200*, 57-64, doi:10.1111/j.1748-1716.2010.02101.x.

157. Schrimpe-Rutledge, A.C.; Codreanu, S.G.; Sherrod, S.D.; McLean, J.A. Untargeted Metabolomics Strategies-Challenges and Emerging Directions. *J Am Soc Mass Spectrom* **2016**, *27*, 1897-1905, doi:10.1007/s13361-016-1469-y.

158. Dias, D.A.; Jones, O.A.; Beale, D.J.; Boughton, B.A.; Benheim, D.; Kouremenos, K.A.; Wolfender, J.L.; Wishart, D.S. Current and Future Perspectives on the Structural Identification of Small Molecules in Biological Systems. *Metabolites* **2016**, *6*, doi:10.3390/metabo6040046.

159. Viant, M.R.; Kurland, I.J.; Jones, M.R.; Dunn, W.B. How close are we to complete annotation of metabolomes? *Curr Opin Chem Biol* **2017**, *36*, 64-69, doi:10.1016/j.cbpa.2017.01.001.

160. Dunn, W.B.; Erban, A.; Weber, R.J.M.; Creek, D.J.; Brown, M.; Breitling, R.; Hankemeier, T.; Goodacre, R.; Neumann, S.; Kopka, J.; et al. Mass appeal: metabolite identification in mass spectrometry-focused untargeted metabolomics. *Metabolomics* **2013**, *9*, 44-66, doi:10.1007/s11306-012-0434-4.

161. Salek, R.M.; Steinbeck, C.; Viant, M.R.; Goodacre, R.; Dunn, W.B. The role of reporting standards for metabolite annotation and identification in metabolomic studies. *Gigascience* **2013**, *2*, 13, doi:10.1186/2047-217X-2-13.

162. Miggiels, P.; Wouters, B.; van Westen, G.J.P.; Dubbelman, A.C.; Hankemeier, T. Novel technologies for metabolomics: More for less. *Trac-Trend Anal Chem* **2019**, *120*, doi:ARTN 115323 10.1016/j.trac.2018.11.021.

163. Broadhurst, D.I.; Kell, D.B. Statistical strategies for avoiding false discoveries in metabolomics and related experiments. *Metabolomics* **2006**, *2*, 171-196, doi:10.1007/s11306-006-0037-z.

164. Nayor, M.; Shah, R.V.; Miller, P.E.; Blodgett, J.B.; Tanguay, M.; Pico, A.R.; Murthy, V.L.; Malhotra, R.; Houstis, N.E.; Deik, A.; et al. Metabolic Architecture of Acute Exercise Response in Middle-Aged Adults in the Community. *Circulation* **2020**, *142*, 1905-1924, doi:10.1161/CIRCULATIONAHA.120.050281.

165. MoTrPAC Data Hub. Available online: https://motrpac-data.org (accessed on 15th of December).

166. Sanford, J.A.; Nogiec, C.D.; Lindholm, M.E.; Adkins, J.N.; Amar, D.; Dasari, S.; Drugan, J.K.; Fernandez, F.M.; Radom-Aizik, S.; Schenk, S.; et al. Molecular Transducers of Physical Activity Consortium (MoTrPAC): Mapping the Dynamic Responses to Exercise. *Cell* **2020**, *181*, 1464-1474, doi:10.1016/j.cell.2020.06.004.

167. Kelly, R.S.; Kelly, M.P.; Kelly, P. Metabolomics, physical activity, exercise and health: A review of the current evidence. *Biochim Biophys Acta Mol Basis Dis* **2020**, *1866*, 165936, doi:10.1016/j.bbadis.2020.165936.

168. Grapov, D.; Fiehn, O.; Campbell, C.; Chandler, C.J.; Burnett, D.J.; Souza, E.C.; Casazza, G.A.; Keim, N.L.; Hunter, G.R.; Fernandez, J.R.; et al. Impact of a weight loss and fitness intervention on exercise-associated plasma oxylipin patterns in obese, insulin-resistant, sedentary women. *Physiol Rep* **2020**, *8*, e14547, doi:10.14814/phy2.14547.

169. Grapov, D.; Fiehn, O.; Campbell, C.; Chandler, C.J.; Burnett, D.J.; Souza, E.C.; Casazza, G.A.; Keim, N.L.; Newman, J.W.; Hunter, G.R.; et al. Exercise plasma metabolomics and xenometabolomics in obese, sedentary, insulin-resistant women: impact of a fitness and weight loss intervention. *Am J Physiol Endocrinol Metab* **2019**, *317*, E999-E1014, doi:10.1152/ajpendo.00091.2019.

170. Draper, C.F.; Duisters, K.; Weger, B.; Chakrabarti, A.; Harms, A.C.; Brennan, L.; Hankemeier, T.; Goulet, L.; Konz, T.; Martin, F.P.; et al. Menstrual cycle rhythmicity: metabolic patterns in healthy women. *Sci Rep* **2018**, *8*, 14568, doi:10.1038/s41598-018-32647-0.

171. Liebisch, G.; Vizcaino, J.A.; Kofeler, H.; Trotzmuller, M.; Griffiths, W.J.; Schmitz, G.; Spener, F.; Wakelam, M.J. Shorthand notation for lipid structures derived from mass spectrometry. *J Lipid Res* **2013**, *54*, 1523-1530, doi:10.1194/jlr.M033506.

172. Pauling, J.K.; Hermansson, M.; Hartler, J.; Christiansen, K.; Gallego, S.F.; Peng, B.; Ahrends, R.; Ejsing, C.S. Proposal for a common nomenclature for fragment ions in mass spectra of lipids. *PLoS One* **2017**, *12*, e0188394, doi:10.1371/journal.pone.0188394.

173. Hao, L.; Wang, J.; Page, D.; Asthana, S.; Zetterberg, H.; Carlsson, C.; Okonkwo, O.C.; Li, L. Comparative Evaluation of MS-based Metabolomics Software and Its Application to Preclinical Alzheimer's Disease. *Sci Rep* **2018**, *8*, 9291, doi:10.1038/s41598-018-27031-x.

174. Mendez, K.M.; Pritchard, L.; Reinke, S.N.; Broadhurst, D.I. Toward collaborative open data science in metabolomics using Jupyter Notebooks and cloud computing. *Metabolomics* **2019**, *15*, 125, doi:10.1007/s11306-019-1588-0.

175. Wilkinson, D.J.; Rodriguez-Blanco, G.; Dunn, W.B.; Phillips, B.E.; Williams, J.P.; Greenhaff, P.L.; Smith, K.; Gallagher, I.J.; Atherton, P.J. Untargeted metabolomics for uncovering biological markers of human skeletal muscle ageing. *Aging (Albany NY)* **2020**, *12*, 12517-12533, doi:10.18632/aging.103513.

176. Xu, J.; Martien, J.; Gilbertson, C.; Ma, J.; Amador-Noguez, D.; Park, J.O. Metabolic flux analysis and fluxomics-driven determination of reaction free energy using multiple isotopes. *Curr Opin Biotechnol* **2020**, *64*, 151-160, doi:10.1016/j.copbio.2020.02.018.

177. Li, B.; He, X.; Jia, W.; Li, H. Novel Applications of Metabolomics in Personalized Medicine: A Mini-Review. *Molecules* **2017**, *22*, doi:10.3390/molecules22071173.

178. Linke, V.; Overmyer, K.A.; Miller, I.J.; Brademan, D.R.; Hutchins, P.D.; Trujillo, E.A.; Reddy, T.R.; Russell, J.D.; Cushing, E.M.; Schueler, K.L.; et al. A large-scale genome-lipid association map guides lipid identification. *Nat Metab* **2020**, *2*, 1149-1162, doi:10.1038/s42255-020-00278-3.

179. Stockli, J.; Fisher-Wellman, K.H.; Chaudhuri, R.; Zeng, X.Y.; Fazakerley, D.J.; Meoli, C.C.; Thomas, K.C.; Hoffman, N.J.; Mangiafico, S.P.; Xirouchaki, C.E.; et al. Metabolomic analysis of insulin resistance across different mouse strains and diets. *J Biol Chem* **2017**, *292*, 19135-19145, doi:10.1074/jbc.M117.818351.

180. Trivedi, D.K.; Hollywood, K.A.; Goodacre, R. Metabolomics for the masses: The future of metabolomics in a personalized world. *New Horiz Transl Med* **2017**, *3*, 294-305, doi:10.1016/j.nhtm.2017.06.001.

181. Lv, Z.; Gong, Z.G.; Xu, Y.J. Research in the Field of Exercise and Metabolomics: A Bibliometric and Visual Analysis. *Metabolites* **2022**, *12*, doi:10.3390/metabo12060542.

182. Khoramipour, K.; Sandbakk, O.; Keshteli, A.H.; Gaeini, A.A.; Wishart, D.S.; Chamari, K. Metabolomics in Exercise and Sports: A Systematic Review. *Sports Med* **2022**, *52*, 547-583, doi:10.1007/s40279-021-01582-y.

183. Bongiovanni, T.; Lacome, M.; Fanos, V.; Martera, G.; Cione, E.; Cannataro, R. Metabolomics in Team-Sport Athletes: Current Knowledge, Challenges, and Future Perspectives. *Proteomes* **2022**, *10*, doi:10.3390/proteomes10030027.

184. Chen, Y.; Wang, X. Analysis of Metabonomic Characteristics after Exercise Fatigue Based on NMR. *Contrast Media Mol Imaging* **2022**, *2022*, 9041293, doi:10.1155/2022/9041293.

185. Hudson, J.F.; Phelan, M.M.; Owens, D.J.; Morton, J.P.; Close, G.L.; Stewart, C.E. "Fuel for the Damage Induced": Untargeted Metabolomics in Elite Rugby Union Match Play. *Metabolites* **2021**, *11*, doi:10.3390/metabo11080544.

186. Pintus, R.; Bongiovanni, T.; Corbu, S.; Francavilla, V.C.; Dess, I.A.; Noto, A.; Corsello, G.; Finco, G.; Fanos, V.; Cesare Marincola, F. Sportomics in professional soccer players: metabolomics results during preseason. *J Sports Med Phys Fitness* **2021**, *61*, 324-330, doi:10.23736/S0022-4707.20.11200-3.

187. Gehlert, S.; Weinisch, P.; Romisch-Margl, W.; Jaspers, R.T.; Artati, A.; Adamski, J.; Dyar, K.A.; Aussieker, T.; Jacko, D.; Bloch, W.; et al. Effects of Acute and Chronic Resistance Exercise on the Skeletal Muscle Metabolome. *Metabolites* **2022**, *12*, doi:10.3390/metabo12050445.

188. Pellegrino, J.K.; Anthony, T.G.; Gillies, P.; Arent, S.M. The exercise metabolome: acute aerobic and anaerobic signatures. *J Int Soc Sports Nutr* **2022**, *19*, 603-622, doi:10.1080/15502783.2022.2115858.

189. Dunnwald, T.; Paglia, G.; Weiss, G.; Denti, V.; Faulhaber, M.; Schobersberger, W.; Wackerhage, H. High Intensity Concentric-Eccentric Exercise Under Hypoxia Changes the Blood Metabolome of Trained Athletes. *Front Physiol* **2022**, *13*, 904618, doi:10.3389/fphys.2022.904618.

190. Park, J.W.; Kim, K.H.; Kim, S.; So, J.R.; Cho, B.W.; Song, K.D. Comparative metabolomic analysis in horses and functional analysis of branched chain (alpha) keto acid dehydrogenase complex in equine myoblasts under exercise stress. *J Anim Sci Technol* **2022**, *64*, 800-811, doi:10.5187/jast.2022.e45.

191. Sato, S.; Dyar, K.A.; Treebak, J.T.; Jepsen, S.L.; Ehrlich, A.M.; Ashcroft, S.P.; Trost, K.; Kunzke, T.; Prade, V.M.; Small, L.; et al. Atlas of exercise metabolism reveals time-dependent signatures of metabolic homeostasis. *Cell Metab* **2022**, *34*, 329-345 e328, doi:10.1016/j.cmet.2021.12.016.

192. Liu, X.; Han, Y.; Zhou, S.; Tian, J.; Qin, X.; Ji, C.; Zhao, W.; Chen, A. Serum metabolomic responses to aerobic exercise in rats under chronic unpredictable mild stress. *Sci Rep* **2022**, *12*, 4888, doi:10.1038/s41598-022-09102-2.

193. Wu, L.; Wang, J.; Cao, X.; Tian, Y.; Li, J. Effect of acute high-intensity exercise on myocardium metabolic profiles in rat and human study via metabolomics approach. *Sci Rep* **2022**, *12*, 6791, doi:10.1038/s41598-022-10976-5.

194. Shah, R.V.; Miller, P.; Colangelo, L.A.; Chernofsky, A.; Houstis, N.E.; Malhotra, R.; Velagaleti, R.S.; Jacobs, D.R., Jr.; Gabriel, K.P.; Reis, J.P.; et al. Blood-Based Fingerprint of Cardiorespiratory Fitness and Long-Term Health Outcomes in Young Adulthood. *J Am Heart Assoc* **2022**, *11*, e026670, doi:10.1161/JAHA.122.026670.

195. Nayor, M.; Chernofsky, A.; Miller, P.E.; Spartano, N.L.; Murthy, V.L.; Malhotra, R.; Houstis, N.E.; Murabito, J.M.; Clish, C.B.; Larson, M.G.; et al. Integrative Analysis of Circulating Metabolite Levels That Correlate With Physical Activity and Cardiorespiratory Fitness. *Circ Genom Precis Med* **2022**, *15*, e003592, doi:10.1161/CIRCGEN.121.003592.

196. Vaara, J.P.; Kyrolainen, H.; Vasankari, T.; Kainulainen, H.; Raitanen, J.; Kujala, U.M. Accelerometer-Based Sedentary Time, Physical Activity, and Serum Metabolome in Young Men. *Metabolites* **2022**, *12*, doi:10.3390/metabo12080700.

197. Du, Y.; Wu, J.; Tian, Y.; Zhang, L.; Zhao, P.; Li, J. Serum metabolomics using ultra-high performance liquid chromatography-Q-Exactive tandem mass spectrometry reveals the mechanism of action of exercise training on chronic obstructive pulmonary disease rats. *Biomed Chromatogr* **2022**, e5507, doi:10.1002/bmc.5507.

198. Savikj, M.; Stocks, B.; Sato, S.; Caidahl, K.; Krook, A.; Deshmukh, A.S.; Zierath, J.R.; Wallberg-Henriksson, H. Exercise timing influences multi-tissue metabolome and skeletal muscle proteome profiles in type 2 diabetic patients - A randomized crossover trial. *Metabolism* **2022**, *135*, 155268, doi:10.1016/j.metabol.2022.155268.

199. Zheng, M.; Liu, C.; Lv, Y.; Mi, J.; Qiu, D.; He, L.; Zhao, L. Comparisons of High Intensity Interval Training and Continuous Training on Metabolomic Alteration and Cardiac Function in Male Adolescent Rats. *Front Physiol* **2022**, *13*, 900661, doi:10.3389/fphys.2022.900661.

200. Moholdt, T.; Parr, E.B.; Devlin, B.L.; Debik, J.; Giskeodegard, G.; Hawley, J.A. The effect of morning vs evening exercise training on glycaemic control and serum metabolites in overweight/obese men: a randomised trial. *Diabetologia* **2021**, *64*, 2061-2076, doi:10.1007/s00125-021-05477-5.

201. Gaitan, J.M.; Moon, H.Y.; Stremlau, M.; Dubal, D.B.; Cook, D.B.; Okonkwo, O.C.; van Praag, H. Effects of Aerobic Exercise Training on Systemic Biomarkers and Cognition in Late Middle-Aged Adults at Risk for Alzheimer's Disease. *Front Endocrinol (Lausanne)* **2021**, *12*, 660181, doi:10.3389/fendo.2021.660181.
202. Qi, J.; Spinelli, J.J.; Dummer, T.J.B.; Bhatti, P.; Playdon, M.C.; Levitt, J.O.; Hauner, B.; Moore, S.C.; Murphy, R.A. Metabolomics and cancer preventive behaviors in the BC Generations Project. *Sci Rep* **2021**, *11*, 12094, doi:10.1038/s41598-021-91753-8.
203. Aschenbach, W.G.; Sakamoto, K.; Goodyear, L.J. 5' adenosine monophosphate-activated protein kinase, metabolism and exercise. *Sports Med* **2004**, *34*, 91-103, doi:10.2165/00007256-200434020-00003.
204. Humphrey, S.J.; James, D.E.; Mann, M. Protein Phosphorylation: A Major Switch Mechanism for Metabolic Regulation. *Trends Endocrinol Metab* **2015**, *26*, 676-687, doi:10.1016/j.tem.2015.09.013.
205. Ross, F.A.; MacKintosh, C.; Hardie, D.G. AMP-activated protein kinase: a cellular energy sensor that comes in 12 flavours. *FEBS J* **2016**, *283*, 2987-3001, doi:10.1111/febs.13698.
206. Mahlapuu, M.; Johansson, C.; Lindgren, K.; Hjalm, G.; Barnes, B.R.; Krook, A.; Zierath, J.R.; Andersson, L.; Marklund, S. Expression profiling of the gamma-subunit isoforms of AMP-activated protein kinase suggests a major role for gamma3 in white skeletal muscle. *Am J Physiol Endocrinol Metab* **2004**, *286*, E194-200, doi:10.1152/ajpendo.00147.2003.
207. Uhlen, M.; Fagerberg, L.; Hallstrom, B.M.; Lindskog, C.; Oksvold, P.; Mardinoglu, A.; Sivertsson, A.; Kampf, C.; Sjostedt, E.; Asplund, A.; et al. Proteomics. Tissue-based map of the human proteome. *Science* **2015**, *347*, 1260419, doi:10.1126/science.1260419.
208. Wu, J.; Puppala, D.; Feng, X.; Monetti, M.; Lapworth, A.L.; Geoghegan, K.F. Chemoproteomic analysis of intertissue and interspecies isoform diversity of AMP-activated protein kinase (AMPK). *J Biol Chem* **2013**, *288*, 35904-35912, doi:10.1074/jbc.M113.508747.
209. Garcia, D.; Shaw, R.J. AMPK: Mechanisms of Cellular Energy Sensing and Restoration of Metabolic Balance. *Mol Cell* **2017**, *66*, 789-800, doi:10.1016/j.molcel.2017.05.032.

210. Xiao, B.; Sanders, M.J.; Carmena, D.; Bright, N.J.; Haire, L.F.; Underwood, E.; Patel, B.R.; Heath, R.B.; Walker, P.A.; Hallen, S.; et al. Structural basis of AMPK regulation by small molecule activators. *Nat Commun* **2013**, *4*, 3017, doi:10.1038/ncomms4017.

211. Polekhina, G.; Gupta, A.; van Denderen, B.J.; Feil, S.C.; Kemp, B.E.; Stapleton, D.; Parker, M.W. Structural basis for glycogen recognition by AMP-activated protein kinase. *Structure* **2005**, *13*, 1453-1462, doi:10.1016/j.str.2005.07.008.

212. Cool, B.; Zinker, B.; Chiou, W.; Kifle, L.; Cao, N.; Perham, M.; Dickinson, R.; Adler, A.; Gagne, G.; Iyengar, R.; et al. Identification and characterization of a small molecule AMPK activator that treats key components of type 2 diabetes and the metabolic syndrome. *Cell Metab* **2006**, *3*, 403-416, doi:10.1016/j.cmet.2006.05.005.

213. Dite, T.A.; Ling, N.X.Y.; Scott, J.W.; Hoque, A.; Galic, S.; Parker, B.L.; Ngoei, K.R.W.; Langendorf, C.G.; O'Brien, M.T.; Kundu, M.; et al. The autophagy initiator ULK1 sensitizes AMPK to allosteric drugs. *Nat Commun* **2017**, *8*, 571, doi:10.1038/s41467-017-00628-y.

214. Hardie, D.G. AMP-activated protein kinase as a drug target. *Annu Rev Pharmacol Toxicol* **2007**, *47*, 185-210, doi:10.1146/annurev.pharmtox.47.120505.105304.

215. Oakhill, J.S.; Steel, R.; Chen, Z.P.; Scott, J.W.; Ling, N.; Tam, S.; Kemp, B.E. AMPK is a direct adenylate charge-regulated protein kinase. *Science* **2011**, *332*, 1433-1435, doi:10.1126/science.1200094.

216. Hawley, S.A.; Boudeau, J.; Reid, J.L.; Mustard, K.J.; Udd, L.; Makela, T.P.; Alessi, D.R.; Hardie, D.G. Complexes between the LKB1 tumor suppressor, STRAD alpha/beta and MO25 alpha/beta are upstream kinases in the AMP-activated protein kinase cascade. *J Biol* **2003**, *2*, 28, doi:10.1186/1475-4924-2-28.

217. Hawley, S.A.; Davison, M.; Woods, A.; Davies, S.P.; Beri, R.K.; Carling, D.; Hardie, D.G. Characterization of the AMP-activated protein kinase kinase from rat liver and identification of threonine 172 as the major site at which it phosphorylates AMP-activated protein kinase. *J Biol Chem* **1996**, *271*, 27879-27887, doi:10.1074/jbc.271.44.27879.

218. Suter, M.; Riek, U.; Tuerk, R.; Schlattner, U.; Wallimann, T.; Neumann, D. Dissecting the role of 5'-AMP for allosteric stimulation, activation, and deactivation of AMP-activated protein kinase. *J Biol Chem* **2006**, *281*, 32207-32216, doi:10.1074/jbc.M606357200.

219. Gowans, G.J.; Hawley, S.A.; Ross, F.A.; Hardie, D.G. AMP is a true physiological regulator of AMP-activated protein kinase by both allosteric activation and enhancing net phosphorylation. *Cell Metab* **2013**, *18*, 556-566, doi:10.1016/j.cmet.2013.08.019.

220. Xiao, B.; Sanders, M.J.; Underwood, E.; Heath, R.; Mayer, F.V.; Carmena, D.; Jing, C.; Walker, P.A.; Eccleston, J.F.; Haire, L.F.; et al. Structure of mammalian AMPK and its regulation by ADP. *Nature* **2011**, *472*, 230-233, doi:10.1038/nature09932.

221. Hawley, S.A.; Pan, D.A.; Mustard, K.J.; Ross, L.; Bain, J.; Edelman, A.M.; Frenguelli, B.G.; Hardie, D.G. Calmodulin-dependent protein kinase kinase-beta is an alternative upstream kinase for AMP-activated protein kinase. *Cell Metab* **2005**, *2*, 9-19, doi:10.1016/j.cmet.2005.05.009.

222. Chen, Z.P.; Stephens, T.J.; Murthy, S.; Canny, B.J.; Hargreaves, M.; Witters, L.A.; Kemp, B.E.; McConell, G.K. Effect of exercise intensity on skeletal muscle AMPK signaling in humans. *Diabetes* **2003**, *52*, 2205-2212, doi:10.2337/diabetes.52.9.2205.

223. Wojtaszewski, J.F.; MacDonald, C.; Nielsen, J.N.; Hellsten, Y.; Hardie, D.G.; Kemp, B.E.; Kiens, B.; Richter, E.A. Regulation of 5'AMP-activated protein kinase activity and substrate utilization in exercising human skeletal muscle. *Am J Physiol Endocrinol Metab* **2003**, *284*, E813-822, doi:10.1152/ajpendo.00436.2002.

224. Wojtaszewski, J.F.; Nielsen, P.; Hansen, B.F.; Richter, E.A.; Kiens, B. Isoform-specific and exercise intensity-dependent activation of 5'-AMP-activated protein kinase in human skeletal muscle. *J Physiol* **2000**, *528 Pt 1*, 221-226, doi:10.1111/j.1469-7793.2000.t01-1-00221.x.

225. Wojtaszewski, J.F.; Mourtzakis, M.; Hillig, T.; Saltin, B.; Pilegaard, H. Dissociation of AMPK activity and ACCbeta phosphorylation in human muscle during prolonged exercise. *Biochem Biophys Res Commun* **2002**, *298*, 309-316, doi:10.1016/s0006-291x(02)02465-8.

226. Kjobsted, R.; Hingst, J.R.; Fentz, J.; Foretz, M.; Sanz, M.N.; Pehmoller, C.; Shum, M.; Marette, A.; Mounier, R.; Treebak, J.T.; et al. AMPK in skeletal muscle function and metabolism. *FASEB J* **2018**, *32*, 1741-1777, doi:10.1096/fj.201700442R.

227. Birk, J.B.; Wojtaszewski, J.F. Predominant alpha2/beta2/gamma3 AMPK activation during exercise in human skeletal muscle. *J Physiol* **2006**, *577*, 1021-1032, doi:10.1113/jphysiol.2006.120972.

228. Steinberg, G.R.; Watt, M.J.; McGee, S.L.; Chan, S.; Hargreaves, M.; Febbraio, M.A.; Stapleton, D.; Kemp, B.E. Reduced glycogen availability is associated with increased AMPKalpha2 activity, nuclear AMPKalpha2 protein abundance, and GLUT4 mRNA

expression in contracting human skeletal muscle. *Appl Physiol Nutr Metab* **2006**, *31*, 302-312, doi:10.1139/h06-003.

229. Yeo, W.K.; Paton, C.D.; Garnham, A.P.; Burke, L.M.; Carey, A.L.; Hawley, J.A. Skeletal muscle adaptation and performance responses to once a day versus twice every second day endurance training regimens. *J Appl Physiol (1985)* **2008**, *105*, 1462-1470, doi:10.1152/japplphysiol.90882.2008.
230. Hardie, D.G.; Schaffer, B.E.; Brunet, A. AMPK: An Energy-Sensing Pathway with Multiple Inputs and Outputs. *Trends Cell Biol* **2016**, *26*, 190-201, doi:10.1016/j.tcb.2015.10.013.
231. Mouchiroud, L.; Eichner, L.J.; Shaw, R.J.; Auwerx, J. Transcriptional coregulators: fine-tuning metabolism. *Cell Metab* **2014**, *20*, 26-40, doi:10.1016/j.cmet.2014.03.027.
232. Holloszy, J.O.; Hansen, P.A. Regulation of glucose transport into skeletal muscle. *Rev Physiol Biochem Pharmacol* **1996**, *128*, 99-193, doi:10.1007/3-540-61343-9_8.
233. Treebak, J.T.; Pehmoller, C.; Kristensen, J.M.; Kjobsted, R.; Birk, J.B.; Schjerling, P.; Richter, E.A.; Goodyear, L.J.; Wojtaszewski, J.F. Acute exercise and physiological insulin induce distinct phosphorylation signatures on TBC1D1 and TBC1D4 proteins in human skeletal muscle. *J Physiol* **2014**, *592*, 351-375, doi:10.1113/jphysiol.2013.266338.
234. Vichaiwong, K.; Purohit, S.; An, D.; Toyoda, T.; Jessen, N.; Hirshman, M.F.; Goodyear, L.J. Contraction regulates site-specific phosphorylation of TBC1D1 in skeletal muscle. *Biochem J* **2010**, *431*, 311-320, doi:10.1042/BJ20101100.
235. Whitfield, J.; Paglialunga, S.; Smith, B.K.; Miotto, P.M.; Simnett, G.; Robson, H.L.; Jain, S.S.; Herbst, E.A.F.; Desjardins, E.M.; Dyck, D.J.; et al. Ablating the protein TBC1D1 impairs contraction-induced sarcolemmal glucose transporter 4 redistribution but not insulin-mediated responses in rats. *J Biol Chem* **2017**, *292*, 16653-16664, doi:10.1074/jbc.M117.806786.
236. Wu, N.; Zheng, B.; Shaywitz, A.; Dagon, Y.; Tower, C.; Bellinger, G.; Shen, C.H.; Wen, J.; Asara, J.; McGraw, T.E.; et al. AMPK-dependent degradation of TXNIP upon energy stress leads to enhanced glucose uptake via GLUT1. *Mol Cell* **2013**, *49*, 1167-1175, doi:10.1016/j.molcel.2013.01.035.
237. Marsin, A.S.; Bertrand, L.; Rider, M.H.; Deprez, J.; Beauloye, C.; Vincent, M.F.; Van den Berghe, G.; Carling, D.; Hue, L. Phosphorylation and activation of heart PFK-2 by AMPK has a role in the stimulation of glycolysis during ischaemia. *Curr Biol* **2000**, *10*, 1247-1255, doi:10.1016/s0960-9822(00)00742-9.

238. Hue, L.; Rider, M.H. Role of fructose 2,6-bisphosphate in the control of glycolysis in mammalian tissues. *Biochem J* **1987**, *245*, 313-324, doi:10.1042/bj2450313.

239. Jorgensen, S.B.; Nielsen, J.N.; Birk, J.B.; Olsen, G.S.; Viollet, B.; Andreelli, F.; Schjerling, P.; Vaulont, S.; Hardie, D.G.; Hansen, B.F.; et al. The alpha2-5'AMP-activated protein kinase is a site 2 glycogen synthase kinase in skeletal muscle and is responsive to glucose loading. *Diabetes* **2004**, *53*, 3074-3081, doi:10.2337/diabetes.53.12.3074.

240. Hunter, R.W.; Treebak, J.T.; Wojtaszewski, J.F.; Sakamoto, K. Molecular mechanism by which AMP-activated protein kinase activation promotes glycogen accumulation in muscle. *Diabetes* **2011**, *60*, 766-774, doi:10.2337/db10-1148.

241. McGarry, J.D.; Mannaerts, G.P.; Foster, D.W. A possible role for malonyl-CoA in the regulation of hepatic fatty acid oxidation and ketogenesis. *J Clin Invest* **1977**, *60*, 265-270, doi:10.1172/JCI108764.

242. Fullerton, M.D.; Galic, S.; Marcinko, K.; Sikkema, S.; Pulinilkunnil, T.; Chen, Z.P.; O'Neill, H.M.; Ford, R.J.; Palanivel, R.; O'Brien, M.; et al. Single phosphorylation sites in Acc1 and Acc2 regulate lipid homeostasis and the insulin-sensitizing effects of metformin. *Nat Med* **2013**, *19*, 1649-1654, doi:10.1038/nm.3372.

243. Munday, M.R.; Campbell, D.G.; Carling, D.; Hardie, D.G. Identification by amino acid sequencing of three major regulatory phosphorylation sites on rat acetyl-CoA carboxylase. *Eur J Biochem* **1988**, *175*, 331-338, doi:10.1111/j.1432-1033.1988.tb14201.x.

244. Clarke, P.R.; Hardie, D.G. Regulation of HMG-CoA reductase: identification of the site phosphorylated by the AMP-activated protein kinase in vitro and in intact rat liver. *EMBO J* **1990**, *9*, 2439-2446, doi:10.1002/j.1460-2075.1990.tb07420.x.

245. Kim, S.J.; Tang, T.; Abbott, M.; Viscarra, J.A.; Wang, Y.; Sul, H.S. AMPK Phosphorylates Desnutrin/ATGL and Hormone-Sensitive Lipase To Regulate Lipolysis and Fatty Acid Oxidation within Adipose Tissue. *Mol Cell Biol* **2016**, *36*, 1961-1976, doi:10.1128/MCB.00244-16.

246. Gonzalez, A.; Hall, M.N.; Lin, S.C.; Hardie, D.G. AMPK and TOR: The Yin and Yang of Cellular Nutrient Sensing and Growth Control. *Cell Metab* **2020**, *31*, 472-492, doi:10.1016/j.cmet.2020.01.015.

247. Gwinn, D.M.; Shackelford, D.B.; Egan, D.F.; Mihaylova, M.M.; Mery, A.; Vasquez, D.S.; Turk, B.E.; Shaw, R.J. AMPK phosphorylation of raptor mediates a metabolic checkpoint. *Mol Cell* **2008**, *30*, 214-226, doi:10.1016/j.molcel.2008.03.003.

248. Kim, J.; Kundu, M.; Viollet, B.; Guan, K.L. AMPK and mTOR regulate autophagy through direct phosphorylation of Ulk1. *Nat Cell Biol* **2011**, *13*, 132-141, doi:10.1038/ncb2152.

249. Russell, R.C.; Tian, Y.; Yuan, H.; Park, H.W.; Chang, Y.Y.; Kim, J.; Kim, H.; Neufeld, T.P.; Dillin, A.; Guan, K.L. ULK1 induces autophagy by phosphorylating Beclin-1 and activating VPS34 lipid kinase. *Nat Cell Biol* **2013**, *15*, 741-750, doi:10.1038/ncb2757.

250. Leprivier, G.; Remke, M.; Rotblat, B.; Dubuc, A.; Mateo, A.R.; Kool, M.; Agnihotri, S.; El-Naggar, A.; Yu, B.; Somasekharan, S.P.; et al. The eEF2 kinase confers resistance to nutrient deprivation by blocking translation elongation. *Cell* **2013**, *153*, 1064-1079, doi:10.1016/j.cell.2013.04.055.

251. Koo, S.H.; Flechner, L.; Qi, L.; Zhang, X.; Screaton, R.A.; Jeffries, S.; Hedrick, S.; Xu, W.; Boussouar, F.; Brindle, P.; et al. The CREB coactivator TORC2 is a key regulator of fasting glucose metabolism. *Nature* **2005**, *437*, 1109-1111, doi:10.1038/nature03967.

252. Mihaylova, M.M.; Vasquez, D.S.; Ravnskjaer, K.; Denechaud, P.D.; Yu, R.T.; Alvarez, J.G.; Downes, M.; Evans, R.M.; Montminy, M.; Shaw, R.J. Class IIa histone deacetylases are hormone-activated regulators of FOXO and mammalian glucose homeostasis. *Cell* **2011**, *145*, 607-621, doi:10.1016/j.cell.2011.03.043.

253. Dentin, R.; Pegorier, J.P.; Benhamed, F.; Foufelle, F.; Ferre, P.; Fauveau, V.; Magnuson, M.A.; Girard, J.; Postic, C. Hepatic glucokinase is required for the synergistic action of ChREBP and SREBP-1c on glycolytic and lipogenic gene expression. *J Biol Chem* **2004**, *279*, 20314-20326, doi:10.1074/jbc.M312475200.

254. Li, Y.; Xu, S.; Mihaylova, M.M.; Zheng, B.; Hou, X.; Jiang, B.; Park, O.; Luo, Z.; Lefai, E.; Shyy, J.Y.; et al. AMPK phosphorylates and inhibits SREBP activity to attenuate hepatic steatosis and atherosclerosis in diet-induced insulin-resistant mice. *Cell Metab* **2011**, *13*, 376-388, doi:10.1016/j.cmet.2011.03.009.

255. Jager, S.; Handschin, C.; St-Pierre, J.; Spiegelman, B.M. AMP-activated protein kinase (AMPK) action in skeletal muscle via direct phosphorylation of PGC-1alpha. *Proc Natl Acad Sci U S A* **2007**, *104*, 12017-12022, doi:10.1073/pnas.0705070104.

256. Lin, J.; Handschin, C.; Spiegelman, B.M. Metabolic control through the PGC-1 family of transcription coactivators. *Cell Metab* **2005**, *1*, 361-370, doi:10.1016/j.cmet.2005.05.004.

257. McGee, S.L.; Hargreaves, M. AMPK-mediated regulation of transcription in skeletal muscle. *Clin Sci (Lond)* **2010**, *118*, 507-518, doi:10.1042/CS20090533.

258. Calvo, J.A.; Daniels, T.G.; Wang, X.; Paul, A.; Lin, J.; Spiegelman, B.M.; Stevenson, S.C.; Rangwala, S.M. Muscle-specific expression of PPARgamma coactivator-1alpha improves exercise performance and increases peak oxygen uptake. *J Appl Physiol (1985)* **2008**, *104*, 1304-1312, doi:10.1152/japplphysiol.01231.2007.

259. Potthoff, M.J.; Wu, H.; Arnold, M.A.; Shelton, J.M.; Backs, J.; McAnally, J.; Richardson, J.A.; Bassel-Duby, R.; Olson, E.N. Histone deacetylase degradation and MEF2 activation promote the formation of slow-twitch myofibers. *J Clin Invest* **2007**, *117*, 2459-2467, doi:10.1172/JCI31960.

260. Alonso, M.D.; Lomako, J.; Lomako, W.M.; Whelan, W.J. A new look at the biogenesis of glycogen. *FASEB J* **1995**, *9*, 1126-1137, doi:10.1096/fasebj.9.12.7672505.

261. Roach, P.J.; Depaoli-Roach, A.A.; Hurley, T.D.; Tagliabracci, V.S. Glycogen and its metabolism: some new developments and old themes. *Biochem J* **2012**, *441*, 763-787, doi:10.1042/BJ20111416.

262. Bergstrom, J.; Hermansen, L.; Hultman, E.; Saltin, B. Diet, muscle glycogen and physical performance. *Acta Physiol Scand* **1967**, *71*, 140-150, doi:10.1111/j.1748-1716.1967.tb03720.x.

263. Jensen, J.; Rustad, P.I.; Kolnes, A.J.; Lai, Y.C. The role of skeletal muscle glycogen breakdown for regulation of insulin sensitivity by exercise. *Front Physiol* **2011**, *2*, 112, doi:10.3389/fphys.2011.00112.

264. Wasserman, D.H. Four grams of glucose. *Am J Physiol Endocrinol Metab* **2009**, *296*, E11-21, doi:10.1152/ajpendo.90563.2008.

265. Pederson, B.A.; Cope, C.R.; Schroeder, J.M.; Smith, M.W.; Irimia, J.M.; Thurberg, B.L.; DePaoli-Roach, A.A.; Roach, P.J. Exercise capacity of mice genetically lacking muscle glycogen synthase: in mice, muscle glycogen is not essential for exercise. *J Biol Chem* **2005**, *280*, 17260-17265, doi:10.1074/jbc.M410448200.

266. Martin, M.A.; Rubio, J.C.; Wevers, R.A.; Van Engelen, B.G.; Steenbergen, G.C.; Van Diggelen, O.P.; De Visser, M.; De Die-Smulders, C.; Blazquez, A.; Andreu, A.L.; et al. Molecular analysis of myophosphorylase deficiency in Dutch patients with McArdle's disease. *Ann Hum Genet* **2004**, *68*, 17-22, doi:10.1046/j.1529-8817.2003.00067.x.

267. Rubio, J.C.; Lucia, A.; Fernandez-Cadenas, I.; Cabello, A.; Blazquez, A.; Gamez, J.; Andreu, A.L.; Martin, M.A.; Arenas, J. Novel mutation in the PYGM gene resulting in McArdle disease. *Arch Neurol* **2006**, *63*, 1782-1784, doi:10.1001/archneur.63.12.1782.

268. McArdle, B. Myopathy due to a defect in muscle glycogen breakdown. *Clin Sci* **1951**, *10*, 13-35.

269. Gonzalez, J.T.; Fuchs, C.J.; Betts, J.A.; van Loon, L.J. Liver glycogen metabolism during and after prolonged endurance-type exercise. *Am J Physiol Endocrinol Metab* **2016**, *311*, E543-553, doi:10.1152/ajpendo.00232.2016.

270. Prats, C.; Graham, T.E.; Shearer, J. The dynamic life of the glycogen granule. *J Biol Chem* **2018**, *293*, 7089-7098, doi:10.1074/jbc.R117.802843.

271. Wojtaszewski, J.F.; Jorgensen, S.B.; Hellsten, Y.; Hardie, D.G.; Richter, E.A. Glycogen-dependent effects of 5-aminoimidazole-4-carboxamide (AICA)-riboside on AMP-activated protein kinase and glycogen synthase activities in rat skeletal muscle. *Diabetes* **2002**, *51*, 284-292, doi:10.2337/diabetes.51.2.284.

272. McClelland, G.B. Fat to the fire: the regulation of lipid oxidation with exercise and environmental stress. *Comp Biochem Physiol B Biochem Mol Biol* **2004**, *139*, 443-460, doi:10.1016/j.cbpc.2004.07.003.

273. Torgan, C.E.; Brozinick, J.T., Jr.; Willems, M.E.; Ivy, J.L. Substrate utilization during acute exercise in obese Zucker rats. *J Appl Physiol (1985)* **1990**, *69*, 1987-1991, doi:10.1152/jappl.1990.69.6.1987.

274. Kirwan, J.A.; Broadhurst, D.I.; Davidson, R.L.; Viant, M.R. Characterising and correcting batch variation in an automated direct infusion mass spectrometry (DIMS) metabolomics workflow. *Anal Bioanal Chem* **2013**, *405*, 5147-5157, doi:10.1007/s00216-013-6856-7.

275. Storey, J.D. A direct approach to false discovery rates. *J Roy Stat Soc B* **2002**, *64*, 479-498, doi:Unsp 1369-7412/02/64479 doi 10.1111/1467-9868.00346.

276. Ward, J.H.; Hook, M.E. Application of an Hierarchical Grouping Procedure to a Problem of Grouping Profiles. *Educ Psychol Meas* **1963**, *23*, 69-81, doi:Doi 10.1177/001316446302300107.

277. Krzanowski, W.J. *Principles of multivariate analysis: a user's perspective*; Oxford University Press, Inc.: 1988.

278. Hastie, T.; Tibshirani, R.; Friedman, J. *The Elements of Statistical Learning: Data Mining, Inference, and Prediction, Second Edition (Springer Series in Statistics)*; 2009.

279. Garratt, M.; Lagerborg, K.A.; Tsai, Y.M.; Galecki, A.; Jain, M.; Miller, R.A. Male lifespan extension with 17-alpha estradiol is linked to a sex-specific metabolomic

response modulated by gonadal hormones in mice. *Aging Cell* **2018**, *17*, e12786, doi:10.1111/acel.12786.

280. Cell Characterization: The XFe24 Analyzer and the XF Real-Time ATP Rate Assay. Available online: https://www.agilent.com/cs/library/usermanuals/public/usermanual-xfe24-cell-characterization-cell-analysis-5994-0370en-agilent.pdf (accessed on 30/10/2022).
281. Perry, C.G.; Kane, D.A.; Herbst, E.A.; Mukai, K.; Lark, D.S.; Wright, D.C.; Heigenhauser, G.J.; Neufer, P.D.; Spriet, L.L.; Holloway, G.P. Mitochondrial creatine kinase activity and phosphate shuttling are acutely regulated by exercise in human skeletal muscle. *J Physiol* **2012**, *590*, 5475-5486, doi:10.1113/jphysiol.2012.234682.
282. Perry, C.G.; Kane, D.A.; Lin, C.T.; Kozy, R.; Cathey, B.L.; Lark, D.S.; Kane, C.L.; Brophy, P.M.; Gavin, T.P.; Anderson, E.J.; et al. Inhibiting myosin-ATPase reveals a dynamic range of mitochondrial respiratory control in skeletal muscle. *Biochem J* **2011**, *437*, 215-222, doi:10.1042/BJ20110366.
283. Belhaj, M.R.; Lawler, N.G.; Hoffman, N.J. Metabolomics and Lipidomics: Expanding the Molecular Landscape of Exercise Biology. *Metabolites* **2021**, *11*, doi:10.3390/metabo11030151.
284. Hargreaves, M.; Spriet, L.L. Skeletal muscle energy metabolism during exercise. *Nat Metab* **2020**, *2*, 817-828, doi:10.1038/s42255-020-0251-4.
285. Howarth, K.R.; Phillips, S.M.; MacDonald, M.J.; Richards, D.; Moreau, N.A.; Gibala, M.J. Effect of glycogen availability on human skeletal muscle protein turnover during exercise and recovery. *J Appl Physiol (1985)* **2010**, *109*, 431-438, doi:10.1152/japplphysiol.00108.2009.
286. Girard, I.; Garland, T., Jr. Plasma corticosterone response to acute and chronic voluntary exercise in female house mice. *J Appl Physiol (1985)* **2002**, *92*, 1553-1561, doi:10.1152/japplphysiol.00465.2001.
287. Garland, P.B.; Yates, D.W.; Haddock, B.A. Spectrophotometric studies of acyl-coenzyme A synthetases of rat liver mitochondria. *Biochem J* **1970**, *119*, 553-564, doi:10.1042/bj1190553.
288. Leonardi, R.; Jackowski, S. Biosynthesis of Pantothenic Acid and Coenzyme A. *EcoSal Plus* **2007**, *2*, doi:10.1128/ecosalplus.3.6.3.4.
289. Watkins, P.A. Fatty acids: Metabolism. In *Encyclopedia of Human Nutrition (Third Edition)*, Caballero, B., Ed.; Academic Press: Waltham, 2013; pp. 220-230.

290. Magnusdottir, S.; Ravcheev, D.; de Crecy-Lagard, V.; Thiele, I. Systematic genome assessment of B-vitamin biosynthesis suggests co-operation among gut microbes. *Front Genet* **2015**, *6*, 148, doi:10.3389/fgene.2015.00148.

291. Yoshii, K.; Hosomi, K.; Sawane, K.; Kunisawa, J. Metabolism of Dietary and Microbial Vitamin B Family in the Regulation of Host Immunity. *Front Nutr* **2019**, *6*, 48, doi:10.3389/fnut.2019.00048.

292. Gominak, S.C. Vitamin D deficiency changes the intestinal microbiome reducing B vitamin production in the gut. The resulting lack of pantothenic acid adversely affects the immune system, producing a "pro-inflammatory" state associated with atherosclerosis and autoimmunity. *Med Hypotheses* **2016**, *94*, 103-107, doi:10.1016/j.mehy.2016.07.007.

293. Nay, K.; Jollet, M.; Goustard, B.; Baati, N.; Vernus, B.; Pontones, M.; Lefeuvre-Orfila, L.; Bendavid, C.; Rue, O.; Mariadassou, M.; et al. Gut bacteria are critical for optimal muscle function: a potential link with glucose homeostasis. *Am J Physiol Endocrinol Metab* **2019**, *317*, E158-E171, doi:10.1152/ajpendo.00521.2018.

294. Robishaw, J.D.; Neely, J.R. Coenzyme A metabolism. *Am J Physiol* **1985**, *248*, E1-9, doi:10.1152/ajpendo.1985.248.1.E1.

295. Whitfield, J.; Harris, R.C.; Broad, E.M.; Patterson, A.K.; Ross, M.L.R.; Shaw, G.; Spriet, L.L.; Burke, L.M. Chronic pantothenic acid supplementation does not affect muscle coenzyme A content or cycling performance. *Appl Physiol Nutr Metab* **2021**, *46*, 280-283, doi:10.1139/apnm-2020-0692.

296. Bihlmeyer, N.A.; Kwee, L.C.; Clish, C.B.; Deik, A.A.; Gerszten, R.E.; Pagidipati, N.J.; Laferrere, B.; Svetkey, L.P.; Newgard, C.B.; Kraus, W.E.; et al. Metabolomic profiling identifies complex lipid species and amino acid analogues associated with response to weight loss interventions. *PLoS One* **2021**, *16*, e0240764, doi:10.1371/journal.pone.0240764.

297. Pavlova, T.; Vidova, V.; Bienertova-Vasku, J.; Janku, P.; Almasi, M.; Klanova, J.; Spacil, Z. Urinary intermediates of tryptophan as indicators of the gut microbial metabolism. *Anal Chim Acta* **2017**, *987*, 72-80, doi:10.1016/j.aca.2017.08.022.

298. Tabone, M.; Bressa, C.; Garcia-Merino, J.A.; Moreno-Perez, D.; Van, E.C.; Castelli, F.A.; Fenaille, F.; Larrosa, M. The effect of acute moderate-intensity exercise on the serum and fecal metabolomes and the gut microbiota of cross-country endurance athletes. *Sci Rep* **2021**, *11*, 3558, doi:10.1038/s41598-021-82947-1.

299. Mach, N.; Moroldo, M.; Rau, A.; Lecardonnel, J.; Le Moyec, L.; Robert, C.; Barrey, E. Understanding the Holobiont: Crosstalk Between Gut Microbiota and Mitochondria During Long Exercise in Horse. *Front Mol Biosci* **2021**, *8*, 656204, doi:10.3389/fmolb.2021.656204.

300. Zhang, H.Z.; Zhao, Z.L.; Zhou, C.H. Recent advance in oxazole-based medicinal chemistry. *Eur J Med Chem* **2018**, *144*, 444-492, doi:10.1016/j.ejmech.2017.12.044.

301. Carter, T.C.; Rein, D.; Padberg, I.; Peter, E.; Rennefahrt, U.; David, D.E.; McManus, V.; Stefanski, E.; Martin, S.; Schatz, P.; et al. Validation of a metabolite panel for early diagnosis of type 2 diabetes. *Metabolism* **2016**, *65*, 1399-1408, doi:10.1016/j.metabol.2016.06.007.

302. Gao, X.; Ke, C.; Liu, H.; Liu, W.; Li, K.; Yu, B.; Sun, M. Large-scale Metabolomic Analysis Reveals Potential Biomarkers for Early Stage Coronary Atherosclerosis. *Sci Rep* **2017**, *7*, 11817, doi:10.1038/s41598-017-12254-1.

303. McGranaghan, P.; Saxena, A.; Rubens, M.; Radenkovic, J.; Bach, D.; Schleussner, L.; Pieske, B.; Edelmann, F.; Trippel, T.D. Predictive value of metabolomic biomarkers for cardiovascular disease risk: a systematic review and meta-analysis. *Biomarkers* **2020**, *25*, 101-111, doi:10.1080/1354750X.2020.1716073.

304. Naz, S.; Moreira dos Santos, D.C.; Garcia, A.; Barbas, C. Analytical protocols based on LC-MS, GC-MS and CE-MS for nontargeted metabolomics of biological tissues. *Bioanalysis* **2014**, *6*, 1657-1677, doi:10.4155/bio.14.119.

305. Saoi, M.; Britz-McKibbin, P. New Advances in Tissue Metabolomics: A Review. *Metabolites* **2021**, *11*, doi:10.3390/metabo11100672.

306. Wu, Z.E.; Kruger, M.C.; Cooper, G.J.S.; Sequeira, I.R.; McGill, A.T.; Poppitt, S.D.; Fraser, K. Dissecting the relationship between plasma and tissue metabolome in a cohort of women with obesity: Analysis of subcutaneous and visceral adipose, muscle, and liver. *FASEB J* **2022**, *36*, e22371, doi:10.1096/fj.202101812R.

307. Belhaj, M.R.; Lawler, N.G.; Hawley, J.A.; Broadhurst, D.I.; Hoffman, N.J.; Reinke, S.N. Metabolomics reveals mouse plasma metabolite responses to acute exercise and effects of disrupting AMPK-glycogen interactions. *Frontiers in Molecular Biosciences* **2022**, *9*, doi:10.3389/fmolb.2022.957549.

308. Yang, H.; Wang, H.; Jaenisch, R. Generating genetically modified mice using CRISPR/Cas-mediated genome engineering. *Nat Protoc* **2014**, *9*, 1956-1968, doi:10.1038/nprot.2014.134.

309. Luttrell, M.J.; Halliwill, J.R. The Intriguing Role of Histamine in Exercise Responses. *Exerc Sport Sci Rev* **2017**, *45*, 16-23, doi:10.1249/JES.0000000000000093.

310. Huang, S.; Wu, H.; Luo, F.; Zhang, B.; Li, T.; Yang, Z.; Ren, B.; Yin, W.; Wu, D.; Tai, S. Exploring the role of mast cells in the progression of liver disease. *Front Physiol* **2022**, *13*, 964887, doi:10.3389/fphys.2022.964887.

311. Sun, B.; Karin, M. Obesity, inflammation, and liver cancer. *J Hepatol* **2012**, *56*, 704-713, doi:10.1016/j.jhep.2011.09.020.

312. Olsen, T.; Sollie, O.; Nurk, E.; Turner, C.; Jerneren, F.; Ivy, J.L.; Vinknes, K.J.; Clauss, M.; Refsum, H.; Jensen, J. Exhaustive Exercise and Post-exercise Protein Plus Carbohydrate Supplementation Affect Plasma and Urine Concentrations of Sulfur Amino Acids, the Ratio of Methionine to Homocysteine and Glutathione in Elite Male Cyclists. *Front Physiol* **2020**, *11*, 609335, doi:10.3389/fphys.2020.609335.

313. Banerjee, R.; Evande, R.; Kabil, O.; Ojha, S.; Taoka, S. Reaction mechanism and regulation of cystathionine beta-synthase. *Biochim Biophys Acta* **2003**, *1647*, 30-35, doi:10.1016/s1570-9639(03)00044-x.

314. Radak, Z.; Chung, H.Y.; Goto, S. Systemic adaptation to oxidative challenge induced by regular exercise. *Free Radic Biol Med* **2008**, *44*, 153-159, doi:10.1016/j.freeradbiomed.2007.01.029.

315. Stipanuk, M.H. Sulfur amino acid metabolism: pathways for production and removal of homocysteine and cysteine. *Annu Rev Nutr* **2004**, *24*, 539-577, doi:10.1146/annurev.nutr.24.012003.132418.

316. Hill, E.E.; Zack, E.; Battaglini, C.; Viru, M.; Viru, A.; Hackney, A.C. Exercise and circulating cortisol levels: the intensity threshold effect. *J Endocrinol Invest* **2008**, *31*, 587-591, doi:10.1007/BF03345606.

317. Ayada, K.; Tadano, T.; Endo, Y. Gnawing behavior of a mouse in a narrow cylinder: a simple system for the study of muscle activity, fatigue, and stress. *Physiol Behav* **2002**, *77*, 161-166, doi:10.1016/s0031-9384(02)00844-2.

318. Gong, S.; Miao, Y.L.; Jiao, G.Z.; Sun, M.J.; Li, H.; Lin, J.; Luo, M.J.; Tan, J.H. Dynamics and correlation of serum cortisol and corticosterone under different physiological or stressful conditions in mice. *PLoS One* **2015**, *10*, e0117503, doi:10.1371/journal.pone.0117503.

319. Huang, Y.M.; Chi, C.W.; Wu, P.S.; Tai, H.C.; Chien, M.N.; Chen, Y.J. Adrenal Gland Irradiation Causes Fatigue Accompanied by Reactive Changes in Cortisol Levels. *J Clin Med* **2022**, *11*, doi:10.3390/jcm11051214.

320. Khandelwal, J.K.; Hough, L.B.; Pazhenchevsky, B.; Morrishow, A.M.; Green, J.P. Presence and measurement of methylimidazoleacetic acids in brain and body fluids. *J Biol Chem* **1982**, *257*, 12815-12819.
321. Guimaraes-Ferreira, L. Role of the phosphocreatine system on energetic homeostasis in skeletal and cardiac muscles. *Einstein (Sao Paulo)* **2014**, *12*, 126-131, doi:10.1590/s1679-45082014rb2741.
322. Maqdasy, S.; Lecoutre, S.; Renzi, G.; Frendo-Cumbo, S.; Rizo-Roca, D.; Moritz, T.; Juvany, M.; Hodek, O.; Gao, H.; Couchet, M.; et al. Impaired phosphocreatine metabolism in white adipocytes promotes inflammation. *Nat Metab* **2022**, *4*, 190-202, doi:10.1038/s42255-022-00525-9.
323. Possik, E.; Al-Mass, A.; Peyot, M.L.; Ahmad, R.; Al-Mulla, F.; Madiraju, S.R.M.; Prentki, M. New Mammalian Glycerol-3-Phosphate Phosphatase: Role in beta-Cell, Liver and Adipocyte Metabolism. *Front Endocrinol (Lausanne)* **2021**, *12*, 706607, doi:10.3389/fendo.2021.706607.
324. O'Neill, H.M.; Holloway, G.P.; Steinberg, G.R. AMPK regulation of fatty acid metabolism and mitochondrial biogenesis: implications for obesity. *Mol Cell Endocrinol* **2013**, *366*, 135-151, doi:10.1016/j.mce.2012.06.019.
325. Zhang, F.; Chen, Y.; Heiman, M.; Dimarchi, R. Leptin: structure, function and biology. *Vitam Horm* **2005**, *71*, 345-372, doi:10.1016/S0083-6729(05)71012-8.
326. Galic, S.; Oakhill, J.S.; Steinberg, G.R. Adipose tissue as an endocrine organ. *Mol Cell Endocrinol* **2010**, *316*, 129-139, doi:10.1016/j.mce.2009.08.018.
327. Hingst, J.R.; Kjobsted, R.; Birk, J.B.; Jorgensen, N.O.; Larsen, M.R.; Kido, K.; Larsen, J.K.; Kjeldsen, S.A.S.; Fentz, J.; Frosig, C.; et al. Inducible deletion of skeletal muscle AMPKalpha reveals that AMPK is required for nucleotide balance but dispensable for muscle glucose uptake and fat oxidation during exercise. *Mol Metab* **2020**, *40*, 101028, doi:10.1016/j.molmet.2020.101028.
328. Ferraro, E.; Giammarioli, A.M.; Chiandotto, S.; Spoletini, I.; Rosano, G. Exercise-induced skeletal muscle remodeling and metabolic adaptation: redox signaling and role of autophagy. *Antioxid Redox Signal* **2014**, *21*, 154-176, doi:10.1089/ars.2013.5773.
329. Qiu, L.Q.; Lai, W.S.; Stumpo, D.J.; Blackshear, P.J. Mouse Embryonic Fibroblast Cell Culture and Stimulation. *Bio Protoc* **2016**, *6*, doi:10.21769/BioProtoc.1859.

Research Portfolio Appendix

List of Publications

Belhaj, M.R., Lawler, N.G., & Hoffman, N.J. (2021). Metabolomics and Lipidomics: Expanding the Molecular Landscape of Exercise Biology. *Metabolites*, 11(3). https://doi.org/10.3390/metabo11030151

This published review article is accessible at the link below.

https://www.mdpi.com/2218-1989/11/3/151

Belhaj, M.R., Lawler, N.G., Hawley, J.A., Broadhurst, D.I., Hoffman, N.J., & Reinke, S.N. (2022). Metabolomics reveals mouse plasma metabolite responses to acute exercise and effects of disrupting AMPK-glycogen interactions. *Front. Mol. Biosci.*, 9. https://doi.org/10.3389/fmolb.2022.957549

This published original research article is accessible at the link below.

https://www.frontiersin.org/articles/10.3389/fmolb.2022.957549/full

Belhaj, M.R., Broadhurst, D.I., Dignan, T., Whitfield, J., Hawley, J.A., Reinke, S.N., & Hoffman, N.J. *In preparation.*

Statement of Contribution of Others

As a requirement from the Australian Catholic University Higher Degree Research policies with regard to the degree of Doctor of Philosophy with Publication, this statement is provided to summarise and clearly identify the nature and extent of the intellectual input by the candidate and any co-authors.

Belhaj, M.R., Lawler, N.G., & Hoffman, N.J. (2021). Metabolomics and Lipidomics: Expanding the Molecular Landscape of Exercise Biology. *Metabolites*, 11(3). https://doi.org/10.3390/metabo11030151

Statement of contribution: MRB performed the literature search and led manuscript conceptualisation, writing and editing. NGL was involved in manuscript conceptualisation and editing. NJH was involved in manuscript conceptualisation, editing and journal correspondence.

I acknowledge that my contribution to the above paper is 75 percent.

Mehdi Belhaj Date: 18/11/2022

I acknowledge that my contribution to the above paper is 10 percent.

Nathan Lawler Date: 18/11/2022

I acknowledge that my contribution to the above paper is 15 percent.

Nolan Hoffman Date: 18/11/2022

Belhaj, M.R., Lawler, N.G., Hawley, J.A., Broadhurst, D.I., Hoffman, N.J., & Reinke, S.N. (2022). Metabolomics reveals mouse plasma metabolite responses to acute exercise and effects of disrupting AMPK-glycogen interactions. *Front. Mol. Biosci.*, 9. https://doi.org/10.3390/metabo11030151

Statement of contribution: MRB was involved in study conceptualisation and led the experimental design, mouse colony management, data collection, data processing and analysis, data interpretation, and writing and editing the manuscript. JAH was involved in study conceptualisation, experimental design, data interpretation, and editing the manuscript. NGL was involved in data collection, data processing, and writing and editing the manuscript. DIB was involved in study conceptualisation, experimental design, data processing and analysis, data interpretation and writing and editing the manuscript. NJH was involved in study conceptualisation, experimental design, acquisition of animal ethics approval, mouse colony management, data collection, data analysis, data interpretation, writing and editing the manuscript, and journal correspondence. SNR was involved in experimental design, data collection, data processing and analysis, data interpretation, writing and editing the manuscript, and journal correspondence.

I acknowledge that my contribution to the above paper is 55 percent.

Mehdi Belhaj Date: 18/11/2022

I acknowledge that my contribution to the above paper is 5 percent.

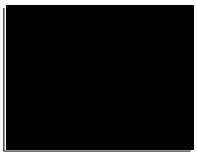

Nathan Lawler Date: 18/11/2022

I acknowledge that my contribution to the above paper is 5 percent.

John Hawley Date: 18/11/2022

I acknowledge that my contribution to the above paper is 10 percent.

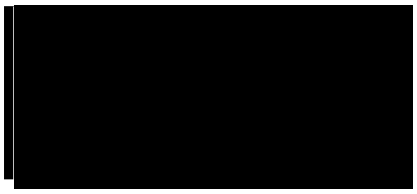

David Broadhurst Date: 18/11/2022

I acknowledge that my contribution to the above paper is 10 percent.

Nolan Hoffman Date: 18/11/2022

I acknowledge that my contribution to the above paper is 15 percent.

Stacey Reinke Date: 18/11/2022

Belhaj, M.R., Broadhurst, D.I., Dignan, T., Whitfield, J., Hawley, J.A., Reinke, S.N., & Hoffman, N.J. *In preparation.*

Statement of contribution: MRB was involved in study conceptualisation and led the experimental design, mouse colony management, data collection, data processing and analysis, data interpretation, and writing and editing the manuscript. DIB was involved in study conceptualisation, experimental design, data processing and analysis, data interpretation, writing and editing the manuscript. TD was involved in data collection, data processing, and writing and editing the manuscript. JW was involved in data collection, data analysis, data interpretation, and writing and editing of the manuscript. JAH was involved in study conceptualisation, experimental design, data interpretation, and editing the manuscript. SNR was involved in experimental design, data collection, data processing and analysis, data interpretation, writing and editing the manuscript, and journal correspondence. NJH was involved in conceptualisation, experimental design, acquisition of ethics approval, mouse colony management, data collection, data analysis, data interpretation, writing and editing the manuscript, and journal correspondence.

I acknowledge that my contribution to the above paper is above 55 percent.

Mehdi Belhaj Date: 18/11/2022

I acknowledge that my contribution to the above paper is 10 percent.

David Broadhurst Date: 18/11/2022

I acknowledge that my contribution to the above paper is 5 percent.

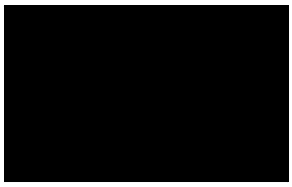

Thomas Dignan Date: 18/11/2022

I acknowledge that my contribution to the above paper is 5 percent.

Jamie Whitfield Date: 18/11/2022

I acknowledge that my contribution to the above paper is 5 percent.

John Hawley Date: 18/11/2022

I acknowledge that my contribution to the above paper is 10 percent.

Stacey Reinke Date: 18/11/2022

I acknowledge that my contribution to the above paper is 10 percent.

Nolan Hoffman Date: 18/11/2022